

Obtaining well-posedness in mathematical modelling of fluvial morphodynamics

Chavarrias Borrás, Victor

DOI

[10.4233/uuid:f741b590-8cd7-4e52-9641-b471954db5b2](https://doi.org/10.4233/uuid:f741b590-8cd7-4e52-9641-b471954db5b2)

Publication date

2019

Document Version

Final published version

Citation (APA)

Chavarrias Borrás, V. (2019). *Obtaining well-posedness in mathematical modelling of fluvial morphodynamics*. [Dissertation (TU Delft), Delft University of Technology].
<https://doi.org/10.4233/uuid:f741b590-8cd7-4e52-9641-b471954db5b2>

Important note

To cite this publication, please use the final published version (if applicable).
Please check the document version above.

Copyright

Other than for strictly personal use, it is not permitted to download, forward or distribute the text or part of it, without the consent of the author(s) and/or copyright holder(s), unless the work is under an open content license such as Creative Commons.

Takedown policy

Please contact us and provide details if you believe this document breaches copyrights.
We will remove access to the work immediately and investigate your claim.

Obtaining well-posedness in mathematical modelling of fluvial morphodynamics

Obtaining well-posedness in mathematical modelling of fluvial morphodynamics

Proefschrift

ter verkrijging van de graad van doctor
aan de Technische Universiteit Delft,
op gezag van de Rector Magnificus Prof. dr. ir. T.H.J.J. van der Hagen,
voorzitter van het College voor Promoties,
in het openbaar te verdedigen op donderdag 14 november 2019 om 12:30 uur

door

Víctor CHAVARRÍAS BORRÀS

Ingeniero de Caminos, Canales y Puertos,
Universitat Politècnica de Catalunya, Barcelona, Spanje,
geboren te Barcelona, Spanje.

Dit proefschrift is goedgekeurd door de

promotor: Dr. ir. A. Blom

promotor: Prof. dr. ir. W.S.J. Uijttewaal

Samenstelling promotiecommissie:

Rector Magnificus,

voorzitter

Dr. ir. A. Blom,

Technische Universiteit Delft, promotor

Prof. dr. ir. W.S.J. Uijttewaal,

Technische Universiteit Delft, promotor

Onafhankelijke leden:

Prof. dr. M.J. Franca,

IHE, Technische Universiteit Delft

Prof. dr. A. Doelman,

Universiteit Leiden

Prof. dr. ir. A.J.H.M. Reniers,

Technische Universiteit Delft

Prof. dr. ir. A.W. Heemink,

Technische Universiteit Delft

Overige leden:

Dr. A. Siviglia,

Eidgenössische Technische Hochschule Zürich



Front & Back: Tribute to all the old reports that inspired this thesis.

Copyright © 2019 by V. Chavarrías

ISBN 978-94-6384-063-7

An electronic version of this dissertation is available at
<http://repository.tudelft.nl/>.

Bagatelle No. 25

Contents

Summary	xiii
Samenvatting	xv
Preface	xix
1 Introduction	1
1.1 Context	2
1.2 The Problem of Ill-Posedness	7
1.3 Ill-posedness in River Morphodynamics	11
1.4 Objectives and Research Questions	13
1.5 Methodology	14
2 Ill-posedness in Modelling Mixed-Sediment River Morphodynamics	15
2.1 Introduction	17
2.2 Model Equations	20
2.2.1 Flow Equations	20
2.2.2 Adapted Active Layer Model Equations	20
2.2.3 Simplified Vertically Continuous Model Equations	21
2.2.4 Closure Relations	22
2.2.5 Matrix Formulation	23
2.3 Characterization of the Mathematical Models	25
2.3.1 Steady Active Layer Model Consisting of Two Size Fractions	25
2.3.2 Steady Vertically Continuous Model Consisting of Two Size Fractions	27
2.4 Active Layer Model Parameter Study	28
2.4.1 Hiding	28
2.4.2 Aggradational Flux to the Substrate	29
2.4.3 Prefactor in a Sediment Transport Relation and Morphodynamic Factor	31
2.4.4 Exponent and Critical Shields Stress in a Sediment Transport Relation	31
2.4.5 Active Layer Thickness	32
2.5 Consequences of Ill-Posedness	32
2.5.1 Numerical Examples	32
2.5.2 Sensitivity Analysis	35

2.6	Implications of Considering More than Two Size Fractions or an Unsteady Active Layer Thickness	38
2.6.1	Ill-Posed Domain of a Three-Size-Fractions Case	39
2.6.2	Effect of an Unsteady Active Layer Thickness in the Ill-Posed Domain	42
2.7	Conclusions	42
3	Ill-posedness in Modelling Two-Dimensional Morphodynamic Problems: Effects of Bed Slope and Secondary Flow	45
3.1	Introduction	47
3.2	Mathematical Model	48
3.2.1	Primary Flow Equations	49
3.2.2	Secondary Flow Equations	50
3.2.3	Morphodynamic Equations	52
3.2.4	Linearised System of Equations	53
3.3	Instability, Hyperbolicity, and Ill-Posedness	56
3.4	Stability Analysis	63
3.4.1	Ill-Posedness Due to Secondary Flow	63
3.4.2	Ill-Posedness Due to Bed Slope Effect	65
3.5	Application	71
3.5.1	Secondary Flow	71
3.5.2	Bed Slope Effect	71
3.6	Discussion	74
3.7	Conclusions	77
4	A Regularization Strategy for Modelling Mixed-Sediment River Morphodynamics	79
4.1	Introduction	81
4.2	Overview of Regularization Techniques	82
4.3	Regularization Strategy for the Active Layer Model	84
4.3.1	Modified System of Equations	84
4.3.2	Derivation of the Regularization Coefficients	85
4.3.3	Validity under Unsteady Flow Conditions	87
4.3.4	Validity under Multiple Size Fractions Conditions	88
4.3.5	Implementation	90
4.4	Laboratory Experiments	91
4.4.1	Experimental Plan and Measurements	91
4.4.2	Results	93
4.5	Numerical Modeling	98
4.5.1	Modeling of our Laboratory Experiments	98
4.5.2	Comparison between Ribberink's (1987) Two-Layer Model and the Regularized Model	105
4.6	Discussion	107
4.6.1	Physical Interpretation of the Regularization Strategy	107
4.6.2	Alternatives to the Regularization Strategy	108
4.7	Conclusions	109

5	A Well-posed Alternative to the Hirano Active Layer Model for Mixed-Size Sediment Rivers	111
5.1	Introduction	113
5.2	The SILKE model	115
5.2.1	Conservation Equations	115
5.2.2	Closure Relations	118
5.2.3	Numerical Solution	121
5.3	Instability, Well-Posedness, and Dispersion	122
5.3.1	Linear Model	122
5.3.2	Instability Mechanism	123
5.3.3	Well-Posedness	128
5.3.4	Tracer Sediment Dispersion	128
5.4	Model Application	130
5.4.1	Tracer Propagation Without Temporary Burial	131
5.4.2	Tracer Propagation With Temporary Burial	132
5.4.3	Ill-posed Conditions Assuming Constant Active Layer Thickness	137
5.4.4	Ill-posed Conditions Assuming Variable Active Layer Thickness	141
5.5	Discussion	143
5.5.1	Physical Reasoning of the Well-Posedness of the Model	143
5.5.2	Limitations of the SILKE Model	143
5.5.3	Limitations of the Interpretation of the Model Instability	145
5.5.4	Modelling of the Experiment by Blom et al. (2003)	146
5.6	Conclusions	146
6	Discussion	149
6.1	The Problem of Ill-Posedness	150
6.2	Extending the Regularization Strategy	151
6.3	Extending the SILKE model	152
6.4	Selecting a Solution to Account for Mixed-Size Sediment	153
6.5	Solution to Ill-posedness due to Accounting for Secondary Flow and Bed Slope Effect	156
6.6	Ill-posedness in Other Topics and Remaining Challenges	157
7	Conclusions and Recommendations	159
7.1	Conclusions	160
7.1.1	Ill-Posedness due to Accounting for Mixed-Size Sediment	160
7.1.2	Ill-Posedness due to Two-Dimensional Effects	161
7.1.3	Regularization of the Active Layer Model	162
7.1.4	Development of a New Model to Account for Mixed-Size Sediment Morphodynamics	163
7.2	Recommendations	164
	References	167
	Epilogue	201
	Acknowledgements	203

Appendices	211
A Supplementary material to Chapter 2	213
A.1 Flow Equations	214
A.2 Active Layer Equations	214
A.3 Sediment Transport Closure Relation	216
A.4 System of Equations of the Steady Vertically Continuous Model Consisting of Two Size Fractions	217
A.5 Perturbation Analysis	218
A.6 Effect of Grain Size Distribution of the Aggradational Flux to the Substrate on the Elliptic Domain	219
A.7 Results of all Simulations of the Sensitivity Analysis.	221
A.8 Implications of an Unsteady Active Layer Thickness in the Ill-posed Domain	223
B Supplementary material to Chapter 3	227
B.1 Eddy Viscosity.	228
B.2 Magnitude of the Sediment Transport Rate	228
B.3 Proof of Ill-posedness Due to Secondary Flow without Diffusion	229
B.4 Proof of Ill-posedness Due to Lack of Bed Slope Effect under Unisize Conditions	230
B.5 Well-Posed Domain under Mixed-Size Sediment Conditions.	231
C Supplementary material to Chapter 4	235
C.1 Model Equations.	236
C.1.1 Flow Equations	236
C.1.2 Active Layer Model	237
C.1.3 Simplified Active Layer Model.	238
C.1.4 Closure Relations	239
C.1.5 Matrix Formulation	240
C.2 Mass Conservation of the Modified System	242
C.3 Parameters of the Numerical Simulation of the Thought Experiment	242
C.4 Proof of Positive Regularized Eigenvalues	243
C.5 Numerical Solution of the System of Equations	244
C.5.1 Model Equations.	244
C.5.2 Solution Procedure	245
C.5.3 Flow Solver	246
C.5.4 Bed Elevation Solver.	247
C.5.5 Substrate Solver	247
C.5.6 Active Layer Solver	248
C.6 Preparatory Experiments	251
C.7 Calibration of the Numerical Model.	255
C.8 Predicted Propagation Speed of Tracer Sediment under Normal Flow Conditions.	257

D Supplementary material to Chapter 5	259
D.1 Matrices of the Linear Model	260
D.2 Eigenvalues of the Linear Model	261
D.3 Advection-Diffusion Behavior at Long Time Scales	264
D.4 Conditions of the Experiment by Chavarrías et al. (2019)	267
D.5 Conditions, Results, and Model Calibration of the Experiment by Sayre and Hubbell (1965).	268
D.6 Conditions of the Experiment by Blom et al. (2003).	271
List of Figures	273
List of Tables	283
About the author	285
List of Publications	287

Summary

In guaranteeing the supply of fresh water, navigable rivers, or flood safety, humans intervene rivers, among others, by constructing dams, supplying sediment, or constructing groynes. Interventions cause changes to the river system in the short term (days, months), as well as in the long term (years, centuries). For instance, the construction of a dam immediately changes the flow regime downstream from the dam. Moreover, by disrupting the sediment course, it also causes a lowering and coarsening of the bed surface. The success of such interventions depends, at least partially, on our ability to predict the river response to the interventions. We essentially aim to answer questions such as: How fast will the bed degrade? How much sediment should I supply to avoid degradation? Which grain size should the supplied sediment have?

Mathematical models are used to answer such questions. A mathematical model sets the relations between variables representing physical quantities such as the flow depth, the bed elevation, or the mass of sediment of a certain grain size at the bed surface. The relations between variables (i.e., the model equations) are derived from physical principles such as mass and momentum conservation and explain the rate at which variables change with time. Hence, given an initial condition (e.g., the river state before a dam is constructed) and the conditions at the boundaries of the domain of interest (e.g., the water and sediment discharge far upstream of the dam), the solution of the model describes the evolution of the river.

A crucial requirement to a mathematical model is the fact it needs to be well-posed to be useful. Well-posedness implies that the model must have a unique solution which depends continuously on the initial and boundary conditions. The fact that models describe a simplified version of reality causes that models may not always be well-posed. When key physical processes are not well represented by a model, this may be ill-posed. Ill-posed models are characterized by developing spurious oscillations in the solution and, essentially, useless results.

The first and second parts of this study investigate the conditions in which fluvial models are ill-posed. First, we focus on ill-posedness due to accounting for changes in the bed surface texture. For some applications, it is sufficient to consider that the river sediment is of the same size. Yet, other questions are related to the grain size distribution of the bed surface sediment. For the latter cases, the standard model for predicting changes in bed surface grain size distribution is the active layer model (*Hirano, 1971*). It successfully predicts river morphodynamics with mixed-size sediment under a wide range of conditions. Yet, it may be ill-posed. We conduct an analytical study that yields a methodology to determine whether the model is well-posed. The study shows that the active layer model is ill-posed under a wider range of conditions than was previously known. Moreover, we find that an alternative model that omits the discretized nature of the active layer model may also be ill-posed.

The first part of the study accounts for changes of the variables in the streamwise

direction only. The second part includes the changes in the transverse direction. In particular, we study ill-posedness due to accounting for secondary flow and bed slope effects. Secondary flow is the circular motion that occurs in the transverse direction due to the curvature of the streamlines of the primary flow (i.e., due to bends). Secondary flow causes the outer part of bends to become deeper than the inner part. This effect is counteracted by the effect of the (transverse) bed slope, which causes sediment to be transported to the outer part of the bend. Our analysis shows that the models of secondary flow and bed slope effect may yield an ill-posed model.

The third and fourth part of this study focus on solving the problem of ill-posedness due to accounting for changes in the bed surface texture (i.e., caused by the active layer model), which appears to be the most essential problem. The active layer model is well-posed over a wide range of conditions, it is computationally cheap, widely applied in practice, and has been implemented in engineering software. For this reason, the first proposed solution aims at obtaining a well-posed model without modifying the essence of the active layer model. The core idea behind the strategy is that the active layer model is ill-posed when the predicted time scale of mixing processes is physically unrealistic. We devise a regularization strategy that, by modifying the time scale of the mixing processes, guarantees well-posedness of the active layer model. A limitation of the strategy is that it can only be applied to conditions in which the active layer thickness is constant with time. This limitation hinders accounting for mixing of sediment due to, for instance, dune growth.

We conduct a set of laboratory experiments to test the regularization strategy. The experiments are conducted under conditions in which the active layer model is ill-posed. In the experiments, we reproduce degradational conditions in which the bed surface sediment is coarser than the substrate sediment. We observe that the entrainment of fine sediment occurs in cycles. Fine sediment is exposed and entrained, causing a degradational wave. Subsequently, coarse sediment from upstream fills the space left by the degradational wave. Degradation continues until fine sediment is exposed again. The regularization strategy captures the changes in bed elevation and bed surface texture averaged over the passage of several bedforms and entrainment cycles, but does not capture the instability mechanism observed in the experiments.

The second proposed solution to the problem of ill-posedness overcomes the limitations of the regularization strategy. We derive an alternative model to the active layer model that is unconditionally well-posed, can be applied to conditions in which the active layer thickness changes with time, and captures the instability mechanism observed in the laboratory experiments. The crucial element of the model is the fact that it accounts for the physical processes occurring at the small time and spatial scales. This is done by relaxing the assumption that the sediment transport rate is at capacity.

The alternative model satisfactorily reproduces the new set of laboratory experiments and an existing data set in which sediment mixing occurs due to an increase in dune height. It also reproduces the dynamics of tracer dispersion when temporary burial of sediment due to bedforms is negligible. However, when temporary burial of sediment becomes an important mechanism, the results appear to be less satisfactory.

Overall, we find ill-posedness to be ubiquitous. We expect modelling of other processes than the ones we have studied to have a yet unknown domain of ill-posedness.

Samenvatting

Mensen grijpen in in rivieren om de zoetwatervoorziening, bevaarbaarheid, en overstromingsveiligheid te garanderen. Voorbeelden zijn de aanleg van dammen, suppletie van sediment en kribben. Dergelijke interventies veroorzaken veranderingen in het riviersysteem op korte termijn (dagen, maanden), maar ook op de lange termijn (jaren, eeuwen). Een dam verandert bijvoorbeeld onmiddellijk de hydrograaf stroomafwaarts van de dam. Bovendien veroorzaakt een dam, door de sedimenttransport te verstoren, ook vaak beddingerosie en vergroving van de rivierbedding. Het succes van interventies hangt, althans gedeeltelijk, af van ons vermogen om de veranderingen die de interventies veroorzaken te voorspellen. Vragen die we daarbij willen beantwoorden zijn bijvoorbeeld: Hoe snel daalt de bodem? Hoeveel sediment moeten we suppleren om bodemerosie te stoppen? Welke korrelgrootte moet het gesuppleerde sediment hebben?

Wiskundige modellen worden gebruikt om dergelijke vragen te beantwoorden. Een wiskundig model beschrijft de relaties tussen fysieke grootheden, zoals de waterdiepte, het bodemniveau, en de samenstelling van het sediment aan het beddingoppervlak. De relaties tussen variabelen (d.w.z. de modelvergelijkingen) zijn afgeleid van fysische principes zoals massabehoud en impulsbehoud, en beschrijven de snelheid waarmee deze variabelen veranderen. De oplossing van het model beschrijft de respons van de rivier op de interventie(s), gegeven een initiële situatie (bijvoorbeeld de toestand van de rivier voordat de dam werd gebouwd) en de omstandigheden aan de grenzen van het interessegebied (bijvoorbeeld de hydrograaf en sedimentaanvoer ver stroomopwaarts van de dam).

Een cruciaal punt hierbij is dat het wiskundige model alleen van nut is als het goed gesteld is. Goedgesteldheid impliceert dat het model een unieke oplossing heeft die continu afhankelijk is van de begin- en randvoorwaarden. Het feit dat modellen een vereenvoudigde versie van de werkelijkheid beschrijven, zorgt ervoor dat modellen niet altijd goed gesteld zijn. Wanneer belangrijke fysische processen niet goed worden weergegeven door een model, kan het model slecht gesteld zijn. Slecht gestelde modellen worden gekenmerkt door het ontwikkelen van niet-fysische oscillaties in de oplossing en, in wezen, nuttelose resultaten.

Het eerste en tweede deel van dit onderzoek analyseren we de omstandigheden waarin riviermodellen slecht gesteld zijn. Als eerste richten we ons hierbij op slechtgesteldheid als gevolg van veranderingen in de samenstelling van het beddingoppervlak. Soms volstaat de aanname dat de korrelgrootte van het beddingsediment uniform en constant is. Andere vragen hebben betrekking op veranderingen (in ruimte en tijd) van de samenstelling van het beddingsediment. Voor deze laatste categorie is het actieve laagmodel (*Hirano, 1971*) het standaardmodel. Het actieve laagmodel beschrijft met succes riviermorfodynamica in situaties met gemengd sediment onder een breed scala aan omstandigheden. Toch kan het model slecht gesteld zijn. Onze analytische analyse levert een methode om te bepalen of het model goed is gesteld. We laten zien dat het actieve laagmodel slecht gesteld is onder een bredere range aan omstandigheden dan voorheen bekend was. Bovendien vinden we

dat een alternatief model dat de discretisatie van het actieve laagmodel vermijdt, ook slecht gesteld kan zijn.

Het eerste deel van het onderzoek beperkt zich tot veranderingen van variabelen in slechts de stroomrichting. Het tweede deel omvat ook veranderingen van variabelen in de dwarsrichting van de rivier. We richten ons hier met name op de modellering van secundaire stroming en bodemhellingseffecten. Secundaire stroming is de cirkelvormige beweging die optreedt in de dwarsrichting van de rivier als gevolg van de kromming van de stroomlijnen van de primaire stroming (d.w.z. in rivierbochten). Deze secundaire stroming zorgt ervoor dat de buitenbocht dieper is dan de binnenbocht. Dit effect wordt tegengegaan door het effect van de (dwars)bodemhelling. Onze analyse toont aan dat de deelmodellen voor secundaire stroming en het bodemhellingseffect een slecht gesteld model kunnen opleveren.

Het derde en vierde deel van deze studie richt zich op het oplossen van het probleem van het slecht gesteld zijn, als gevolg van het modelleren van veranderingen in de bodemsamenstelling (d.w.z. gerelateerd het actieve laagmodel), wat de meest essentiële oorzaak van het slecht gesteld zijn lijkt te zijn. Het actieve laagmodel is goed gesteld over een breed scala aan omstandigheden, het is rekentechnisch efficiënt, wordt in de praktijk breed toegepast, en het is geïmplementeerd in grootschalig software. Om deze reden beoogt onze eerste oplossing een goed gesteld model te verkrijgen zonder de essentie van het actieve laagmodel te wijzigen. De gedachte achter deze regularisatiestrategie is dat het actieve laagmodel slecht is gesteld wanneer de voorspelde tijdschaal van sedimentmenging fysisch onrealistisch is. De regularisatiestrategie garandeert een goed gesteld actieve laagmodel door de tijdschaal van het proces van sedimentmenging te wijzigen. Een beperking van de strategie is dat deze alleen kan worden toegepast op omstandigheden waarbij de actieve laagdikte in de tijd constant is. Deze beperking belet het modelleren van sedimentmenging als gevolg van bijvoorbeeld duingroei.

We voeren een serie laboratoriumexperimenten uit om de regularisatiestrategie te testen. De experimenten zijn uitgevoerd onder omstandigheden waarbij het actieve laagmodel slecht gesteld is. In de experimenten reproduceren we omstandigheden met bodemerosie waarin het bodemoppervlak grover is dan het substraat. We zien dat de opname van fijn sediment plaatsvindt in cycli. Fijn sediment wordt opgenomen, waardoor een erosiegolf ontstaat. Vervolgens vult grof sediment dat van stroomopwaarts wordt aangevoerd de ruimte die is achtergelaten door de erosiegolf. De voortgaande beddingerosie maakt dat fijn sediment weer beschikbaar komt aan het bodemoppervlak. De regularisatiestrategie beschrijft de veranderingen van bodemniveau en samenstelling gemiddeld over de cycli, maar beschrijft het instabiliteitsmechanisme dat we hebben gezien in de experimenten niet.

Onze tweede oplossing voor het slecht gesteld zijn kent de beperkingen van de regularisatiestrategie niet. We leiden een alternatief model af dat onvoorwaardelijk goed gesteld is, kan worden toegepast op omstandigheden waarin de actieve laagdikte verandert in de tijd, en beschrijft het instabiliteitsmechanisme dat in de experimenten is waargenomen. Het cruciale element van het model is het feit dat het rekening houdt met de fysische processen die op kleine tijd- en ruimteschaal plaatsvinden. Dit doen we door het loslaten van de aanname dat het sedimenttransport op capaciteit is.

Het alternatieve model reproduceert op bevredigende wijze zowel de nieuwe labo-

ratoriumexperimenten als laboratoriumexperimenten waarin sedimentmenging optreedt als gevolg van duingroei. Het reproduceert ook tracerdispersie, mits tijdelijke bedekking door bodemvormen verwaarloosbaar is. In het laatste geval zijn de resultaten nog niet bevredigend.

We vinden we dat het probleem van slechtgesteldheid alomtegenwoordig is. Het modelleren van andere processen dan die we hebben bestudeerd hebben een nog onbekend domein van slechtgesteldheid.

Preface

You are holding in your hands the result of a journey in which I have learned as much about rivers and science as about myself. As in a Greek epic poem, along this journey I have experienced happiness, sadness, despair, confidence, relief, curiosity, joy, pain, tiredness, and euphoria. Luck is always part of great journeys. The lucky event that brought me until here occurred on the 6th of June of 2012. By then, I was certain I liked river engineering and morphodynamics. I had applied for conducting the last year of my studies in Delft University of Technology and, although I only intended to do courses, the regulation of the exchange program made me to do a research project too. How could I find in a matter of days a supervisor and a project in a university I have never attended? In despair, I went to the office of Prof. Dr. Juan Pedro Martín Vide. He opened the proceedings of the RCEM conference of 2011 saying “I remember a researcher from Delft University of Technology...”, and fortunately found the email address he was looking for. Within just a few minutes, I received a reply from Dr. Astrid Blom, who offered me a project, a flume, and her supervision.

In that research project, I conducted laboratory experiments dealing with flow and sediment of different sizes. When modelling the laboratory experiments, I found some wiggles in the solution that I could not understand. These wiggles triggered the research project that culminates in this book. This book will explain you why wiggles occur, why they are undesired, and how we can prevent them.

You may be reading this text for several reasons. Maybe you have a personal connection with me and no background in rivers, models, and equations. The book is inevitably technical, but you may want to read the introduction. I thought about you when writing it. Specifically for you, I also cite this poem about the Mississippi River that perfectly summarizes what a river is:

I do not know much about gods; but I think that the river
Is a strong brown god—sullen, untamed and intractable,
Patient to some degree, at first recognized as a frontier;
Useful, untrustworthy, as a conveyor of commerce;
Then only a problem confronting the builder of bridges.
The problem once solved, the brown god is almost forgotten
By the dwellers in cities—ever, however, implacable,
Keeping his seasons and rages, destroyer, reminder
Of what men choose to forget. Unhonoured, unpropitiated
By worshippers of the machine, but waiting, watching and waiting.

*T. S. Eliot, part of Section 1 of *The Dry Salvages* in *The Four Quartets*.*

After you have read the introduction, jump directly to the acknowledgments section. Ask me to explain you the topic if you are really interested. I will be glad to talk for hours about it.

A reader learned in science, morphodynamics, rivers, flow, and equations, may want to directly read Chapters 2-5, in which the core research is presented. The chapters are presented in what I consider a logical order, but they can be read independently of each other, as each chapter is structured as a journal article.

In writing this book, I have tried to conduct the “most appropriate charitable work of our time: not to publish superfluous books” (*Ortega y Gasset*, 1937). For this reason, I hope that you enjoy it, even if you only read the acknowledgments, skim through the text, check a figure, or use it to fill your bookshelf.

Víctor CHAVARRÍAS BORRÀS
Delft, January 2019

1

Introduction

*The greatest scientific discovery
was the discovery of ignorance.*

Harari (2016)

*Under various names, I have praised only you, rivers.
You are milk and honey and love and death and dance.*

Miłosz (1988)

1.1. Context

Humankind has intervened in rivers for millennia. An impressive example is the Quatinah Barrage on the Oronte River (Syria), which is a dam built between 1319–1304 BC during the reign of the Egyptian Pharaoh Sethi, and still in use (*Chen, 2015*). The rise of the Roman Empire was accompanied by the rise of innovative systems of hydraulic structures to provide drinking water, irrigate, and for sanitary purposes (*Mays, 2010*). Emerita Augusta (the modern city of Mérida, Spain) is an example of such a system of structures. The Romans built the Proserpina and Cornalvo dams (Figure 1.1), which impounded the Las Pardillas and Albarregas rivers, two tributaries of the Guadiana River. They dug channels and constructed several aqueducts to transport water. This intervention has affected the Guadiana basin for almost 2000 years.



Figure 1.1: Proserpina dam, Mérida (Spain). Picture by Alonso de Mendoza (CC BY-SA4.0).

Compared to the long experience intervening the flow of rivers, the understanding of the consequences of the interventions and, more specifically, the understanding of the dynamics of rivers has always lagged behind. Before the Scientific Revolution, which started in Europe in the XVIth century (*Hall, 1954*), the dynamics of rivers were mainly explained by the will of the gods such as Sobek in Egypt (Figure 1.2), Achelous in Greece, Yami in India, or Yamata no Orochi in Japan (*Gad, 2008; Lee, 2006; Warrior, 2014; Owwehand, 1958*). The empowerment of human reason within the Scientific Revolution brought a more systematic approach to understanding the dynamics of rivers. However, interventions were still largely based on empirical knowledge, experience, and previous successes and failures. Examples can be found in the activities of Rijkswaterstaat, the Dutch national water management authority since 1798, during the XIXth century. The engineers of Rijkswaterstaat achieved challenging tasks such as the compilation of a river atlas and the introduction a national water gauge system. Yet, they were unable to arrive at a consensus regarding river interventions due to, in part, a lack of understanding of the river



Figure 1.2: Relief of Sobek in the temple of Kom Ombo (Egypt). Picture by Hedwig Storch (CC BY-SA3.0).

dynamics (Bosch, 2014).

A new paradigm arose with the use of scale models to help in the design of interventions. The work by *Fargue* (1894) was an early example of the use of scale models. *Fargue* (1894) conducted 21 mobile bed experiments in an approximately 60 m long outdoor curved flume to generalize the observations he had done on the Garonne river as regards to flow in bends (see also *Hager* (2003)). In the Netherlands the increase in use of laboratory experiments occurred hand in hand with the foundation of the *Waterloopkundig Laboratorium* (WL | Delft Hydraulics) by Dr. Johannes Th. Thijsse (1893–1984) in 1927 (*Vreugdenhil et al.*, 2001). An example is the scale model of the Dutch Rhine-Meuse branches constructed in the centre of Delft in the 1950's (Figure 1.3). The insight from these scale experiments was crucial in providing understanding of the processes underlying fluvial dynamics as well as engineering solutions to water problems (e.g. *Disco and Toussaint*, 2014). Drawbacks of scale experiments are the cost in terms of space, time, and labor, and the fact that scale models cannot easily be modified. More importantly, a scale model generally suffers from scale effects, as it is technically difficult to keep all ratios between the relevant forces in the prototype (e.g., inertia, gravity, viscosity, surface tension, pressure, *et cetera*) equal to the equivalent ratios in the scale model. Furthermore, when the same fluid is used in the model and in the prototype, as usually occurs in morphodynamic laboratory experiments, only one ratio between forces can be identical and scale effects are unavoidable (*Heller*, 2011).

A second revolution, the one related to information and communication technology, laid the groundwork for a paradigm change in river hydraulics. Mathematical models explaining the flow of water, such as the *Saint-Venant* (1871) equations describing depth-averaged one-dimensional flow, existed already in the XIXth century. Yet, the ability to



Figure 1.3: Picture of the scale model of the Dutch Rhine-Meuse branches built by the *Waterloopkundig Laboratorium* in the centre of Delft in 1950. The model was built in the Schuttersveld and the picture was taken from Het Raam. The church on the top right corner is the Lutherse Kerk (also known as Saint George's Chapel) and the windmill on the top left is Molen de Roos. Flow goes from bottom to top. The right-hand branch is the Lek. The second branch starting to count from the right is the Waal. The third one is the Meuse. The upstream boundary is approximately at Wijk bij Duurstede and Tiel. The Biesbosch is visible in the centre of the domain on the left. Picture courtesy of Deltares.

solve the equations was limited due to their complexity. Almost half a century after the *Saint-Venant* (1871) equations were formulated, the Nobel laureate Dr. Hendrik A. Lorentz (1853–1928) started leading a committee to study the hydrodynamic changes in the Dutch Wadden Sea due to the closure of the Zuiderzee (now the IJsselmeer). There were contradictory opinions on the effect of the closure on the tidal motions in the Wadden Sea. While Cornelis Lely (1854–1929), one of the engineers advocating for the closure,

stated that the effects were going to be negligible (Mazure, 1963), Rijkswaterstaat Engineer H. E. de Bruijn (1841–1915) said that the high tide water level would double (De Bruijn, 1911). The opinions were not based on experimental work or on calculations. As De Bruin mentioned, “one has to sense it, as it were, based on experience gained elsewhere and on relevant research” (Disco and Van den Ende, 2003). To properly assess the effect of the closure on the tidal motion, Lorentz (1926) discretized the Wadden Sea considering one-dimensional channels connected at nodes (Figure 1.4) and computed the flow solving the *Saint-Venant* (1871) equations (Figure 1.5). The computations were done by hand and the equations were simplified (linearizing the quadratic friction term) to obtain a manageable problem. They predicted that the rise in the tidal range would be about 0.7 m (see also Van Houweninge and De Graauw, 1982). The computations resulted to be very accurate, as the error turned out to be a few centimeters only (Van den Ende, 1992). However, it took the committee 8 years to find the answer (1918–1926), which was 3 years longer than the construction of the 30 km long dike closing the Zuiderzee (1927–1932).

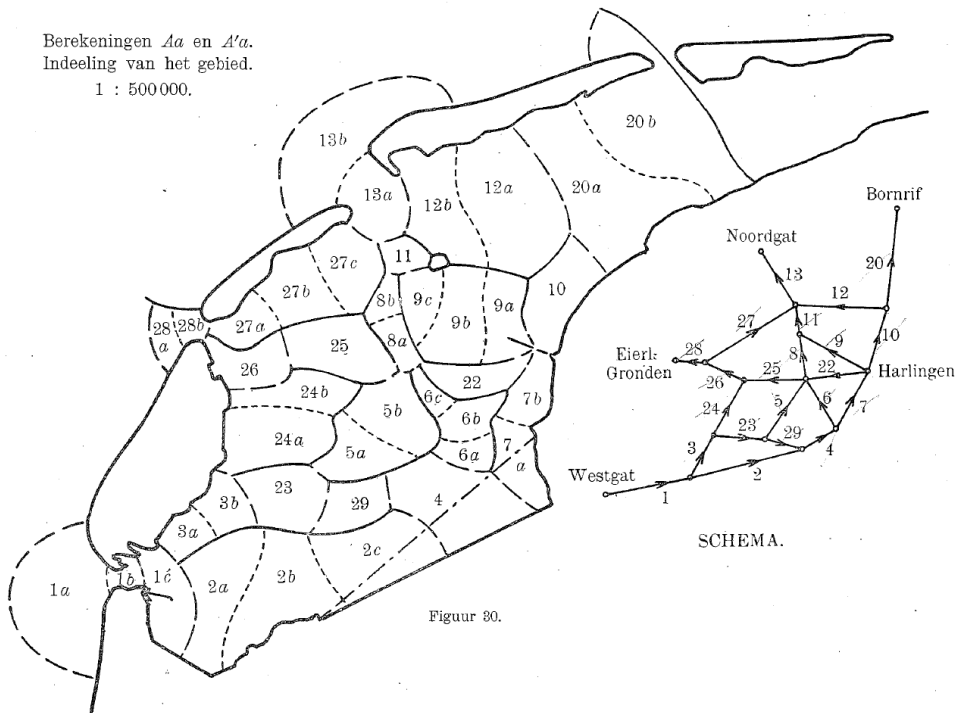


Figure 1.4: Numerical discretization of the Wadden Sea to compute the tide after closure of the Zuiderzee by the Afsluitdijk (the straight line on the bottom part of domains 2c and 4). The subplot on the right indicates the nodes and the channels that divide the domain. The general plot shows the area represented by each channel. Some channels are subdivided (e.g. 1a, 1b, and 1c) as the properties along the channel change significantly although there is no connection (node) with another channel. This image is reproduced from the original in Lorentz (1926).

World War II illustrated the power of computers in solving systems of equations and

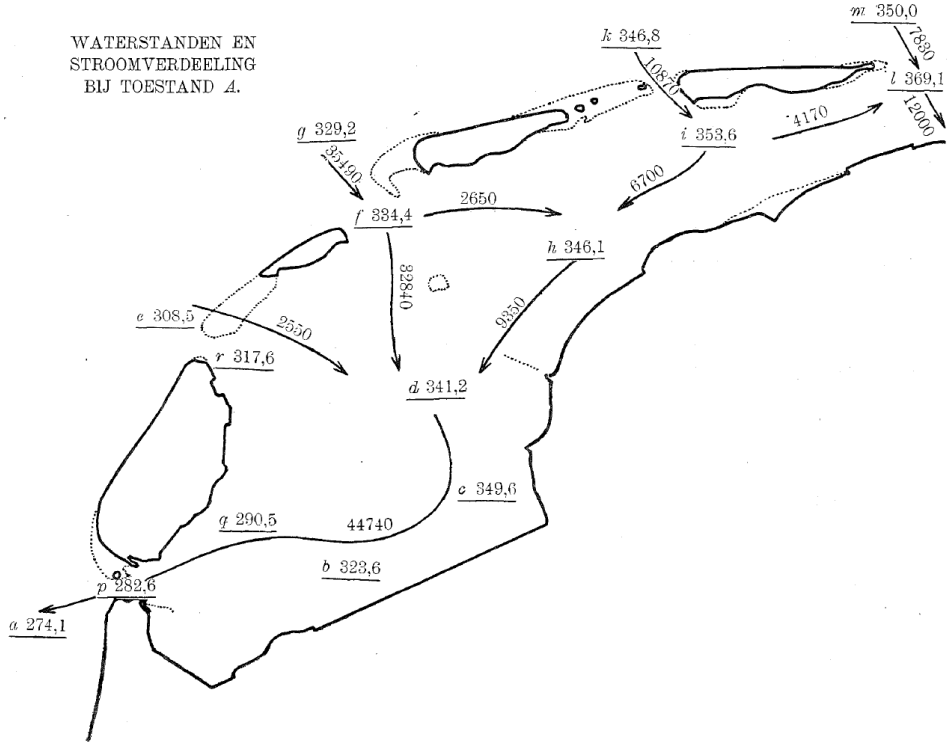


Figure 1.5: Predicted water level and water discharge division after closure of the Zuiderzee for the conditions of the storm of 1894. The figure presents the prediction for the conditions on the 23rd of December of 1894 between 3 and 4 am. Water level values (in centimeters) are underlined. Water flow direction is shown using arrows and discharge values (in cubic meters per second) are on the arrows. This image is reproduced from the original in *Lorentz (1926)*.

mathematical models in projects such as the Manhattan Project (see e.g. *Anderson, 1986*) or in deciphering enemy coded messages (*Booß-Bavnbek and Høyrup, 2003*). Computer power was first used for hydraulic purposes in the United States. *Isaacson et al. (1954)* numerically solved the *Saint-Venant (1871)* equations to predict flood propagation in the Ohio River. In Europe the first use of computer power for hydraulic purposes occurred in 1961 (*Cunge and Hager, 2015*). Dr. Alexander Preissmann (1916–1990) developed the famous numerical scheme bearing his name to build a numerical model of the Mekong Delta. The numerical model that efficiently solved the *Saint-Venant (1871)* equations was the preferred option by UNESCO over a scale model proposed by WL | Delft Hydraulics. With the increase in computer power, the use of mathematical models in solving river related questions has become ubiquitous (Figure 1.6).

However, mathematical models are not all powerful. As a model represents a simplified version of the actual physical processes, it can be applied to reproduce processes at a certain scale only. The range of applicability of different mathematical models depends on the simplifications and assumptions considered to derive them. For instance, the flow

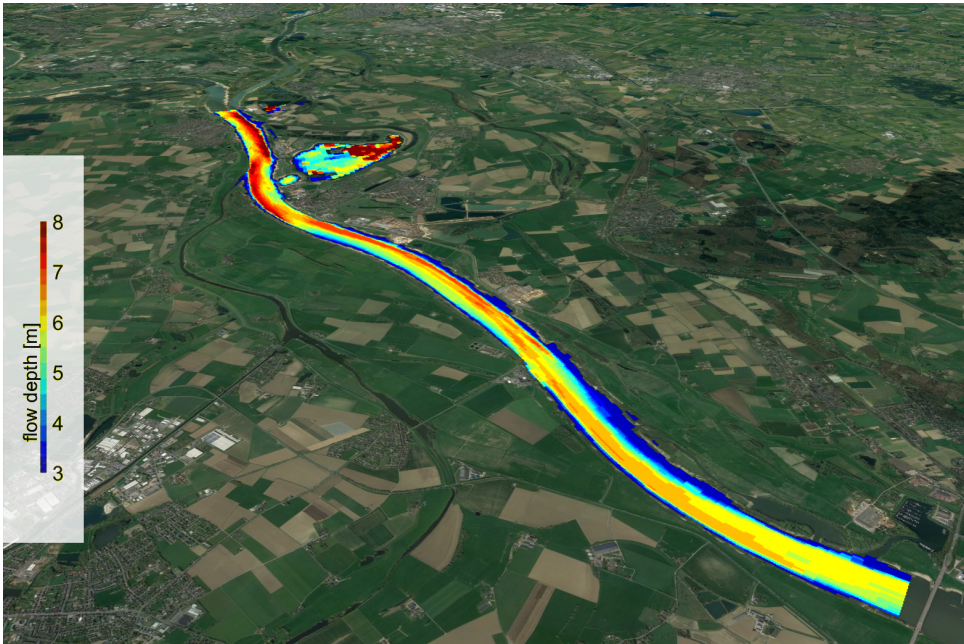


Figure 1.6: Morphodynamic simulation of the Bovenrijn between Emmerich (Germany), Rhine-kilometer 852.3, and the bifurcation near Pannerden (the Netherlands), Rhine-kilometer 866.0 (Ottevanger *et al.*, 2015). The Rhine bridge at Emmerich is seen in the lower right-hand corner. The flow discharge is equal to $2251 \text{ m}^3/\text{s}$. The simulation is made using Delft3D. Data represents the river in 2015. Satellite data from Google Earth[®].

is assumed to be hydrostatic in the derivation of the *Saint-Venant* (1871) equations. For this reason, these equations can represent phenomena occurring over length scales significantly longer than the flow depth such as the propagation of a flood wave (Battjes and Labeyrie, 2017), but cannot model flow recirculation occurring downstream of a dune (Best, 2005). Flow recirculation is a strongly three-dimensional process not resolved by the *Saint-Venant* (1871) equations.

The simplification of the physical processes causes models to be applicable under certain conditions only. As we will see in this thesis, when key assumptions used in deriving a model are invalid, the model is incapable of reproducing the physical processes. In this thesis we will deal with the problem of invalid assumptions in modelling river morphodynamic processes. In the following section we will introduce these topics.

1.2. The Problem of Ill-Posedness

In this section we will focus on the problem of invalid assumptions and the consequences that this has for mathematical models.

An accepted framework to mathematically describe fluvial processes (and any physical process in general) is to set up a system of partial differential equations that stem from physical principles such as mass and momentum conservation. Each equation relates the temporal rate of change of a variable to temporal and spatial changes of other

variables. For instance, the *Saint-Venant* (1871) equations are a set of two partial differential equations relating the mean flow velocity and mean flow depth, which are obtained considering conservation of mass and momentum within a control volume. The *Exner* (1920) equation describes conservation of mass of bed sediment and allows for modelling bed elevation change.

When modelling change with time we need to prescribe initial conditions (e.g., the river bathymetry), as well as boundary conditions (e.g., the water and sediment discharge at the upstream end of the domain and the water surface elevation at the downstream end). For the model to be representative of the physical processes, a unique solution to the mathematical problem needs to exist, and the solution needs to depend continuously on the data (*Hadamard*, 1923). In mathematical terms this means that the model needs to be well-posed.

The fact that a solution to the problem needs to exist and has to be unique is relatively trivial. The fact that the solution needs to depend continuously on the initial and boundary conditions is less evident. To explain the relevance of this condition we consider the propagation with time of small waves on a string. The equation that models this physical process is (*Haberman*, 2004):

$$\frac{\partial^2 f}{\partial t^2} - \gamma \frac{\partial^2 f}{\partial x^2} = 0, \quad (1.1)$$

where $f(x, t)$ [m] is the vertical displacement of the string (Figure 1.7a), t [s] represents time, x [m] space, and γ [m^2/s^2] is a constant that depends on the properties of the string. When the initial displacement and its derivative are equal to 0 (i.e., $f(x, 0) = 0$ and $\partial f / \partial t|_{(x,0)} = 0 \forall x$), the string remains static (i.e., $f(x, t) = 0 \forall x, t$). This is the equilibrium solution.

As in reality the initial displacement and its derivative are never exactly equal to 0, we consider a situation in which the initial displacement is equal to 0 and its derivative is close to 0 but not exactly equal to 0. We represent the disturbance in the derivative as a wave-like perturbation:

$$\left. \frac{\partial f}{\partial t} \right|_{(x,0)} = \frac{\nu}{k} \sin(kx) \forall x, \quad (1.2)$$

where k [rad/m] is the wave number of the disturbance and ν [rad/s] a constant. Parameter ν provides the right dimensions to the equation and we arbitrarily set it equal to 1 rad/s without loss of generality. The solution to this problem (Equations (1.1), (1.2), and $f(x, 0) = 0$) exists and is unique:

$$f(x, t) = \frac{\nu}{k^2 \sqrt{\gamma}} \sin(k \sqrt{\gamma} t) \sin(kx) \forall (x, t). \quad (1.3)$$

In Figures 1.7b-c we show the displacement f as a function of space and time for a case in which $\gamma = 1 \text{ m}^2/\text{s}^2$ and k equals 10 rad/m and 20 rad/m, respectively. Waves propagate with time and a larger value of k creates perturbations of a smaller amplitude. As k tends to infinity, the disturbance tends to 0 and the solution tends to the equilibrium solution. This implies that the solution depends continuously on the initial condition. For this reason, the problem is well-posed. Moreover, as observed in nature, ever smaller perturbations have an ever smaller effect. We conclude that the model is physically realistic.

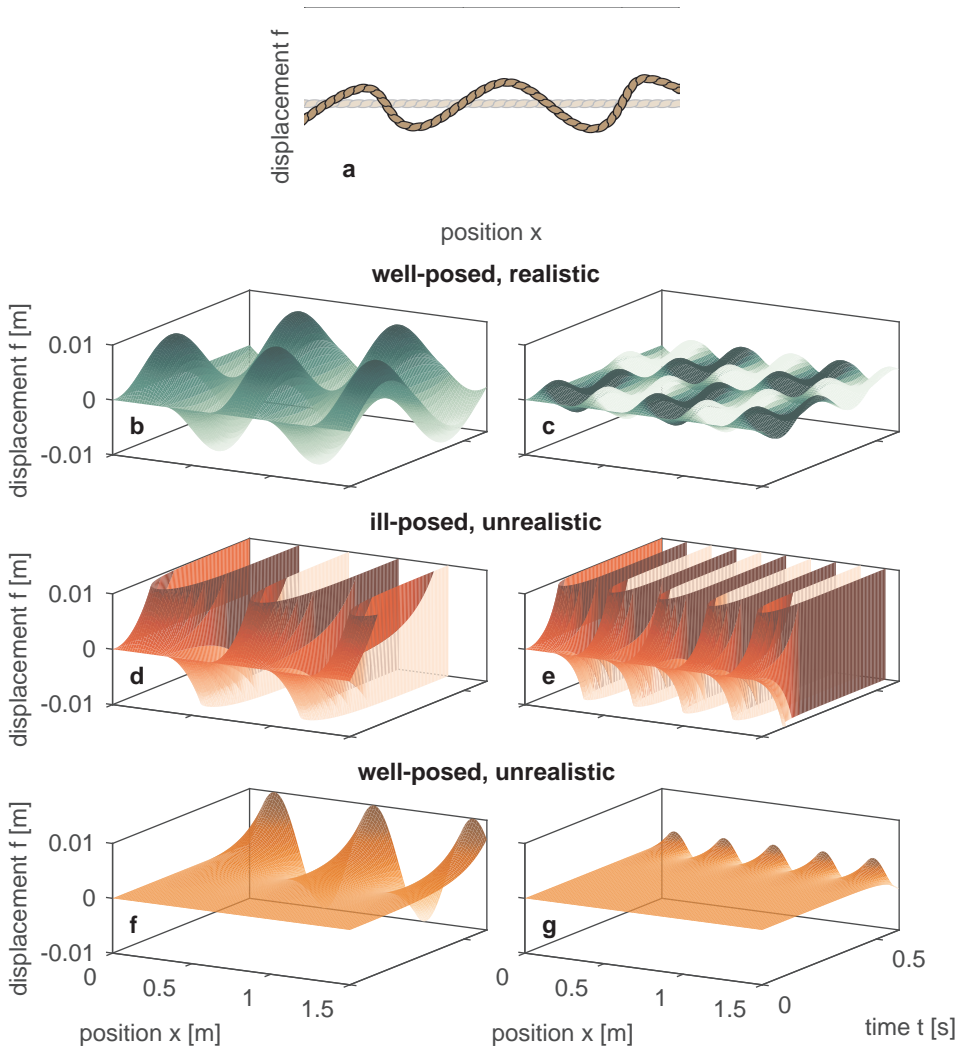


Figure 1.7: Solutions of the model representing the propagation of waves on a string. In panel a we show the model sketch. The transparent string represents the equilibrium solution. The solutions in panels b-c are found considering $\gamma = 1 \text{ m}^2/\text{s}^2$ and imposing an initial conditions. In panels d-e we consider $\gamma = -1 \text{ m}^2/\text{s}^2$ and we impose an initial condition. In panels f-g, we consider a value of $\gamma = -1 \text{ m}^2/\text{s}^2$ and we impose a future condition at $\tau = 0.6 \text{ s}$. The value of k is equal to 10 rad/m in panels b, d, and f and it is equal to 20 rad/m in panels c, e, and g.

We consider the same situation except for the fact that $\gamma < 0$. Just as in the previous case, a solution exists and it is unique:

$$f(x, t) = \frac{v}{k^2 \sqrt{-\gamma}} \sinh(k \sqrt{-\gamma} t) \sin(kx) \forall (x, t). \tag{1.4}$$

In Figures 1.7d-e we show cases that are equivalent to the ones in Figures 1.7b-c except for the fact that $\gamma = -1 \text{ m}^2/\text{s}^2$. As k tends to infinity, the disturbance tends to 0, but the solution for the displacement tends to infinity. This is because, as k increases, $1/k^2$ tends to 0, but the hyperbolic sine tends to infinity in a faster way (exponentially). The solution for the disturbance tending to 0 is different from the equilibrium solution. The problem is ill-posed, as the solution does not depend continuously on the data. The solution is physically unrealistic, as it is unreasonable that a negligible disturbance causes infinitely fast growth of perturbations. This model cannot represent physical processes.

The conclusion that the model for $\gamma < 0$ cannot represent physical processes can be reached without finding and analyzing the solution. When deriving the model (Equation (1.1)), one finds that $\gamma = T/\rho$ where T [N] is the magnitude of the tension in the string and ρ [kg/m] is the mass per unit length of the string (Haberman, 2004). As neither the mass nor the tension can be negative, no physical interpretation exists for a value of $\gamma < 0$. We conclude that the case of $\gamma < 0$ is a mathematical example of ill-posedness which has no physical significance.

Alternatively, we reach the conclusion that the case for a value of $\gamma < 0$ cannot represent a physical process from the perspective of the conditions to the equation rather than the model parameter. Considering a value of $\gamma < 0$ we solve Equation (1.1) assuming that the perturbation at a certain time τ [s] is:

$$\left. \frac{\partial f}{\partial t} \right|_{(x,\tau)} = \frac{v}{k} \sin(kx) \quad \forall x. \quad (1.5)$$

In this case the unique solution is:

$$f(x, t) = \frac{v}{k^2 \sqrt{-\gamma} \cosh(k \sqrt{-\gamma} \tau)} \sinh(k \sqrt{-\gamma} t) \sin(kx) \quad \forall (x, t). \quad (1.6)$$

Just as in the case of $\gamma > 0$, an increase in k causes the perturbation to tend to 0 and we find that the solution tends to the equilibrium solution (Figures 1.7f-g). For this reason, this case is well-posed. However, the model is physically unrealistic, as we have imposed a future condition. It is physically impossible to prescribe the entire solution at a certain future time. Worded differently, a case in which $\gamma < 0$ would be well-posed if we would impose the solution in the future. We conclude that this model cannot describe the propagation of disturbances in a string.

Ill-posedness is a symptom of the fact that there are key physical processes that are not captured by the model (Joseph and Saut, 1990; Fowler, 1997). In other words, ill-posedness can appear when one tries to apply a model under conditions in which the assumptions used in deriving it are not valid. In the case of small waves on a string we have seen that when using the right data (i.e., an initial condition rather than a future condition) and a physically realistic value of the model parameter (i.e., $\gamma > 0$), the model is always well-posed. Under these conditions the model is a fair simplification of the physical processes. In more complex models the change of behavior from being well-posed to ill-posed is set by a combination of parameters that may be physically realistic. An example is the model of two superimposed inviscid shallow-flow layers used to represent, for instance, stratified flow in the ocean or the atmosphere. When the difference between the velocity

of the upper and lower layers exceed a certain threshold, the model becomes ill-posed (Long, 1956; Armi, 1986; Pelanti *et al.*, 2008). Under this condition, the model lacks a key physical process. If, rather than assuming that the flow is inviscid, the forces at the interface between the layers are accounted for, the domain in which the model is ill-posed decreases (Travis *et al.*, 1976; Lyczkowski *et al.*, 1978; Abgrall and Karni, 2009). The range of conditions over which the model is valid increases by an improved representation of the physical processes.

For the simple model of small waves on a string there exists an analytical solution. For more complex models we need to approach the problem numerically. Numerical solutions of ill-posed problems typically show an oscillatory component: a growing wavy pattern (e.g. Castro Díaz *et al.*, 2011; Barker and Gray, 2017; Toro *et al.*, 2018). However, wave growth is certainly not a synonym of ill-posedness. The classical example of wave growth in river morphodynamics is the growth of bars, which can be predicted using a model that combines the Shallow Water Equations for two-dimensional flow with the Exner (1920) equation. The model shows that long perturbations (in the streamwise and transverse direction) superimposed to an initially flat state grow and short perturbations decay. This implies that, as observed in nature, a narrow channel is stable but above a certain value of width-to-depth ratio perturbations to an initially flat state grow and bars form (Callander, 1969; Engelund and Skovgaard, 1973; Fredsøe, 1978; Colombini *et al.*, 1987). The existence of a lower limit of wave length for waves to grow is a property characteristic of well-posed models.

Growth of *short* waves characterizes ill-posedness. In an ill-posed model there is no lower limit to the wave length of growing perturbations. All perturbations grow independently of the wave length. This causes the numerical solution of an ill-posed model to continue to change as the grid is refined (Kabanikhin, 2008). The discretization of a spatial domain into cells limits the smallest wave that the model resolves. Ever smaller cells resolve ever shorter waves and, since all grow, the solution continues to change. In numerical terms, one says that the solution does not converge with the grid. Certainly, grid convergence is a property necessary for a model to be useful. Moreover, as the growth rate increases for decreasing wave length (e.g. Joseph and Saut, 1990), a refinement of the mesh may lead to failure of the numerical solver.

Chaotic models and ill-posed models share the property that perturbations to the initial and boundary conditions yield divergent solutions. There are, however, two essential differences between chaos and ill-posedness. The solution of a chaotic model may be sensitive to the data but remains valid in statistical terms (Devaney, 1989). Second, there is a certain initial period of time in which the solution of a chaotic model is valid, as perturbations to the data remain bounded for a sufficiently short time (Banks *et al.*, 1992). The solution of an ill-posed model has no period of time over which it is valid. In the example above (Equation (1.4)), for *any* fixed value of time the solution tends to infinity for a sufficiently small perturbation (i.e., for a sufficiently large value of parameter k).

1.3. Ill-posedness in River Morphodynamics

After having introduced the problem of ill-posedness in general terms, here we will focus on the problem of ill-posedness in river morphodynamic modelling.

Cordier et al. (2011) studied the well-posedness of the one-dimensional river morphodynamic model formed by the *Saint-Venant* (1871) equations and the *Exner* (1920) equation. Assuming a Chézy-type friction they found that the model is always well-posed.

In their model, the sediment is represented by a single grain size. This limits the applicability of the model to conditions where sediment sorting does not play a significant role. Several important phenomena in rivers are intrinsically related to the fact that sediment consists of a range of grain sizes. One needs to account for mixed-size sediment to, for instance, explain the typical downstream fining that characterizes rivers (*Sternberg*, 1875; *Blom et al.*, 2016), the existence of a zone in which a gravel river suddenly changes into a sand river (*Yatsu*, 1955; *Blom et al.*, 2017a), the fact that the bed surface sediment is typically coarser than the substrate sediment (*Parker and Klingeman*, 1982), and the fact that sediment in the outer part of a bend is usually coarser than in the inner side (*Parker and Andrews*, 1985).

Hirano (1971) formulated the active layer model to be able to predict such mixed-size sediment phenomena. In the active layer model sediment is composed of several grain size fractions that are each characterized by a representative grain size. The bed is discretized into two layers. The top layer (i.e., the active layer) interacts with the flow, which implies that sediment can be entrained from the active layer only and sediment is deposited in the active layer only. The active layer is assumed to be homogeneous (i.e., sediment in this layer is mixed). Contrary to the active layer, the substrate may be stratified. The active layer model has successfully reproduced a large number mixed-size sediment phenomena (including the processes above mentioned) over half a century. It is implemented in software packages such as *Delft3D* (*Sloff and Mosselman*, 2012), *BASEMENT* (*Vetsch et al.*, 2006) and *Telemac* (*Villaret et al.*, 2013). Unfortunately, the active layer model may suffer from ill-posedness, which was first found by *Ribberink* (1987) using a simplified version of the active layer model. He found that, under degradational conditions when the mean grain size of the sediment in the active layer is coarser than that in the substrate, the model may become ill-posed.

Several researchers have proposed alternatives to the active layer model. *Ribberink* (1987) included an exchange layer in between the active layer and the substrate to account for mixing due to dunes substantially higher than the average dune height. The model by *Ribberink* (1987) reduces the likelihood that the model becomes ill-posed, but does not exclude the possibility (*Sieben*, 1994). The most notable alternative is the framework for conservation of sediment mass in which the bed is treated in a probabilistic manner (*Parker et al.*, 2000). This implies that there is no discrete distinction between the active and the inactive sediment. The probability of entrainment weights the contribution to the river dynamics of the sediment at each location in the vertical direction. This framework was used by *Blom and Parker* (2004) and *Blom et al.* (2006, 2008) to derive a model that accounts for vertical mixing due to dunes and by *Viparelli et al.* (2017) to model the dynamics of a gravel bed river. Although the vertically continuous framework is more realistic than a discrete representation, its well-posedness has never been studied. Moreover, the simplified character of the model by *Viparelli et al.* (2017) and the limited range of applicability of the model by *Blom and coauthors* due to the small time step needed in solving it have resulted in the fact that the active layer model is still the main formulation accounting for mixed-size sediment river morphodynamics.

When considering river morphodynamics in two-dimensional problems, we need to account for two physical processes not present in one-dimensional models: (1) secondary flow and (2) the effect of the bed slope on the direction of the sediment transport. In a bend, the fact that the flow velocity varies along the vertical direction due to bed friction, causes the formation of a circular motion in the plane perpendicular to main flow direction (*Van Bendegom, 1947; Rozovskii, 1957*). The upper part of the flow is directed outwards and the part close to the bed is directed inwards. For this reason, secondary flow causes sediment to be transported to the inner side of a bend creating a shallow inner side and deep outer side, as first observed by *Thomson (1876)*. This effect is counteracted by gravity, which tends to move sediment downslope to the outer side of the bend. The consequences of two-dimensional effects regarding the well-posedness of morphodynamic models has never been assessed.

In the present study we further investigate the problem of ill-posedness in river morphodynamic models. The results will provide insight into solutions to the problem of ill-posedness.

1.4. Objectives and Research Questions

Our objective is to assess the problem of ill-posedness in river morphodynamic modeling and to provide solutions to it. We aim at gaining insight into the origin of ill-posedness in one-dimensional as well as two-dimensional cases. As the active layer model has proven its validity in representing an ample spectrum of phenomena, we aim to find a first solution that preserves the essential dynamics of the active layer model. Yet, as the origin of ill-posedness is an inaccurate representation of the physics, we aim to find a second solution that solves the problem of ill-posedness from a physical perspective. To this end we will focus on the following research questions:

1. Under which conditions are current models accounting for mixed-size sediment mechanisms ill-posed?
 - (a) How can we determine whether the active layer model is ill-posed?
 - (b) What is the role of the active layer thickness as well as other model parameters in the domain of ill-posedness of the active layer model?
 - (c) How do we recognize ill-posed numerical simulations?
 - (d) Under which conditions does a vertically continuous representation of the bed yield an ill-posed model?
2. What is the role of two-dimensional effects with respect to model well-posedness?
 - (a) How does the formulation accounting for the secondary flow affect model well-posedness?
 - (b) How does the formulation accounting for the transverse bed slope affect model well-posedness?
3. How can we prevent the active layer model from being ill-posed?

- (a) Which possible strategies can we follow to avoid ill-posedness of the active layer model?
 - (b) How physically realistic are the results applying the strategy to avoid ill-posedness?
4. How can we obtain a new model describing mixed-size sediment river morphodynamics that avoids ill-posedness?
- (a) Which physical mechanisms need to be considered in the new model to guarantee its well-posedness?
 - (b) How physically realistic are the results of the new model?

1.5. Methodology

In order to answer Research Question 1 we will conduct a mathematical analysis of the system of equations used to model mixed-size sediment river morphodynamics in one-dimensional cases (Chapter 2). We will analyze the active layer model and we will study the role of the model parameters. By means of numerical simulations we will gain insight into the consequences of ill-posedness. A similar analysis will be conducted regarding the simplified vertically continuous formulation of the bed processes developed by *Viparelli et al.* (2017).

We will extend the analysis to two-dimensional cases to answer Research Question 2 (Chapter 3). We will consider the effect of accounting for secondary flow on the well-posedness of a two-dimensional model. We will also assess the role of the different relations to account for the effect of the bed slope on the sediment transport direction.

In Chapter 4 we will survey possible strategies for preventing the active layer model from being ill-posed (Research Question 3). We will develop a regularization strategy that prevents the active layer model from being ill-posed, while retaining the core of the active layer model. The results of the regularization strategy cannot be compared to the results of the active layer model, as the active layer model is not applicable under the conditions for which the regularization strategy is applied. For this reason we compare the results of the regularization strategy to measured data of situations in which the active layer model is ill-posed. We find that there is no data set to which we can compare the results of the regularization strategy. For this reason, we will conduct a set of laboratory experiments that allows for testing the regularization strategy.

Research Question 4 will be addressed in Chapter 5. In deriving a new model we will first study which physical mechanisms need to be included to guarantee that the model is well-posed. We will analyze the new set of conservation equations to prove its well-posedness. The results of the new model will be compared to the above experimental data. We also consider its applicability at larger spatial and temporal scales by modelling a field case.

2

Ill-posedness in Modelling Mixed-Sediment River Morphodynamics

*We may regard the present state of the universe
as the effect of its past and the cause of its future.*

Laplace (1814)

The sediments are a sort of epic poem of the Earth.

Carson (1951)

In this chapter we analyze the Hirano active layer model used in mixed sediment river morphodynamics concerning its ill-posedness. Ill-posedness causes the solution to be unstable to short-wave perturbations. This implies that the solution presents spurious oscillations, the amplitude of which depends on the domain discretization. Ill-posedness not only produces physically unrealistic results but may also cause failure of numerical simulations. By considering a two-fraction sediment mixture we obtain analytical expressions for the mathematical characterization of the model. Using these we show that the ill-posed domain is larger than what was found in previous analyses, not only comprising cases of bed degradation into a substrate finer than the active layer but also in aggradational cases. Furthermore, by analyzing a three-fraction model we observe ill-posedness under conditions of bed degradation into a coarse substrate. We observe that oscillations in the numerical solution of ill-posed simulations grow until the model becomes well-posed, as the spurious mixing of the active layer sediment and

This chapter has been published in *Advances in Water Resources* 114, (2018) 219–235.

substrate sediment acts as a regularization mechanism. Finally we conduct an eigenstructure analysis of a simplified vertically continuous model for mixed sediment for which we show that ill-posedness occurs in a wider range of conditions than the active layer model.

2.1. Introduction

The mixed character of the sediment is a property necessary to explain physical phenomena such as downstream fining (*Sternberg, 1875; Blom et al., 2016*), the gravel sand transition zone (*Yatsu, 1955; Blom et al., 2017a*), the formation of bedload sheets (*Seminara et al., 1996*), or bed surface armoring (*Parker and Klingeman, 1982*). *Hirano (1971)* was the first to develop a mass conservation model for mixed-size sediment. The model assumes that the topmost part of the bed, i.e. the active layer, interacts with the flow and is instantaneously mixed. Below the active layer lies the substrate which can have vertical stratification. In this schematic representation of the morphodynamic processes only the active layer sediment is affected by entrainment and depositional processes. A vertical flux of sediment originates from changes in elevation of the interface between the active layer and the substrate.

One of the critical aspects of the active layer model is the fact that the vertical extent of the active layer, or active layer thickness, shall be a priori assigned. However, it cannot be physically measured, as it stems from the above schematic representation (*Siviglia et al., 2017; Church and Haschenburger, 2017*). The active layer thickness is related to the time scale of the process under consideration (*Bennett and Nordin, 1977; Rahuel et al., 1989; Sieben, 1997; Wu, 2007*). In plane bed conditions and short time scales the active layer thickness is assumed to be proportional to the size of a characteristic coarse fraction in the bed, for instance, D_{84} or D_{90} (e.g., *Petts et al., 1989; Rahuel et al., 1989; Parker and Sutherland, 1990*). If bed forms are predominant and the time scale under consideration involves the mixing induced by the passage of several bed forms, the active layer thickness is typically related to a characteristic bed form height (e.g., *Deigaard and Fredsøe, 1978; Lee and Odgaard, 1986; Armanini and Di Silvio, 1988*). The active layer thickness may vary over space and time, although often it is assumed to be a uniform constant.

The active layer modeling framework has proven to be able to represent a wide variety of physical phenomena such as bed surface armoring (e.g., *Park and Jain, 1987*) and the morphodynamics of gravel-bed rivers (e.g., *Vogel et al., 1992*) and tidal basins (e.g., *Carniello et al., 2012*). Moreover, it is implemented in a large amount of software packages such as Telemac (*Villaret et al., 2013*), Delft3D (*Sloff and Mosselman, 2012*), and BASEMENT (*Vetsch et al., 2006*).

The mathematical representation of river morphodynamics should be well-posed. This means that the mathematical problem must have a unique solution which depends continuously on the data (*Hadamard, 1923*). If the solution does not depend continuously on the data, the model is unfit to represent the corresponding physics.

Despite its widespread use, the active layer model has one major mathematical shortcoming: the model can change its mathematical character under some parameter settings. Therefore the mathematical problem that represents the physics of river morphodynamics can become ill-posed. This fact was first recognized by *Ribberink (1987)*. To this end he simplified the active layer model by considering an equation for the mean grain size of the active layer sediment rather than one active layer equation for each grain size fraction. He found that under aggradational conditions the problem is unconditionally well-posed and the system may become ill-posed under degradational conditions if the substrate is finer than the active layer (i.e. degradation in an armored river). *Ribberink (1987)* included a third layer between the active layer and the substrate to model the effects of dunes excep-

tionally larger than the average dune height. Although this model includes more physical mechanisms and improves the prediction of mixed sediment processes in dune-dominated cases, it may still become ill-posed (*Sieben, 1994*).

To understand the conditions in which the active layer model becomes ill-posed we focus on how information propagates along a river. We first consider a certain reach characterized by normal flow and immobile sediment. A perturbation of the flow propagates along the river in the form of two waves traveling at speeds equal to $u \pm \sqrt{gh}$ where u [m/s] denotes the mean flow velocity, h [m] the flow depth, and g [m/s²] is the acceleration due to gravity. If sediment is mobile, yet uniform, a perturbation in bed elevation (e.g., a sediment hump) will propagate with a speed that is termed the “bed celerity” (*De Vries, 1965; Lyn and Altinakar, 2002; Stecca et al., 2014*). As the bed elevation affects the flow, the bed elevation perturbation also induces a perturbation of the flow. Thus, under unisize sediment conditions, a perturbation of the bed elevation leads to three waves (Figure 2.1a). Although each of the waves perturb both bed elevation and flow, two of the waves perturb mainly the flow without much change in bed level if the Froude number ($Fr = u/\sqrt{gh}$) is sufficiently small (*De Vries, 1973; Needham, 1990; Zanré and Needham, 1994*).

The consideration of mixed sediment (of two size fractions to simplify the example) introduces another celerity which is termed the “sorting celerity” (*Suzuki, 1976; Ribberink, 1987; Stecca et al., 2014*). Thus, under mixed sediment conditions (with two grain sizes), a perturbation of bed elevation causes four waves. Although each wave perturbs the flow, bed elevation, and surface grain size distribution, two of these perturb mainly the flow, one mainly the bed level, and one mainly the surface grain size distribution (*Ribberink, 1987; Stecca et al., 2014*) (Figure 2.1b).

Sieben (1994) identified a region of parameters where, for a sediment mixture consisting of two grain size classes under bed degradation into a substrate finer than the active layer, the model is unconditionally ill-posed. This occurs when the “sorting celerity” equals the “bed celerity”. This was confirmed by *Stecca et al. (2014)*, who observed, through numerical computation of the system eigenvalues, such model behavior also in case of more than two sediment fractions.

Furthermore, *Stecca et al. (2014)* analytically confirmed the outcomes of *Ribberink’s* analysis using a more realistic unsteady model for two sediment size fractions. They considered grain size selectivity of the bedload but hiding in a limited manner. Hiding accounts for the fact that grain size fractions finer than a characteristic mean grain size of the mixture hide behind larger grains and so they experience a larger critical bed shear stress compared to the unisize case (*Einstein, 1950; Komar, 1987a,b*). The opposite happens for coarse sediment fractions, which experience a larger exposure to the flow than in a unisize case. In their analysis *Stecca et al. (2014)* showed that the model can become ill-posed under degradational conditions if and only if the substrate is finer than a reference grain size distribution which is related to the grain size distribution of the bedload, instead of the active layer (as in *Ribberink (1987)* analysis).

To overcome the problem of setting the active layer thickness, *Parker et al. (2000)* developed a stochastic framework without the need for a distinction between the active and inactive parts of the bed. *Blom and Parker (2004)*, *Blom et al. (2006)*, and *Blom et al. (2008)* developed a model that accounts for dune sorting and the variability of bed ele-

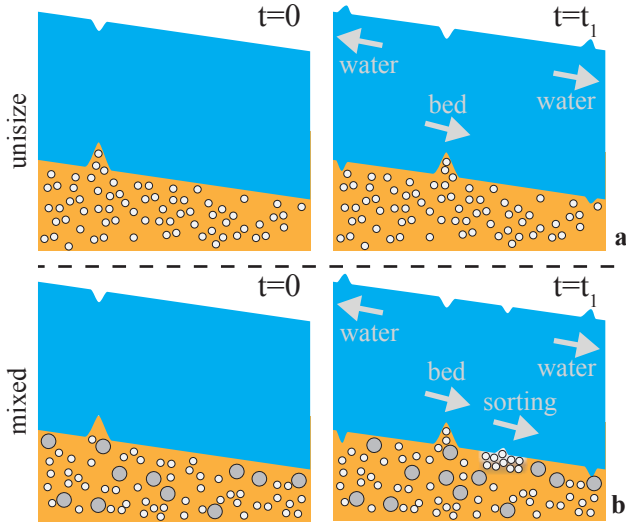


Figure 2.1: Schematic of the effect of a perturbation in bed elevation in (a) a unisize sediment case and (b) a mixed sediment case. In the latter case, a perturbation in bed elevation introduces another wave, which is mainly related to the bed surface grain size distribution. Yet, each wave perturbs the flow, bed elevation, and bed surface grain size distribution. The arrows indicate the direction of propagation of the perturbations under subcritical flow conditions. The words “water”, “bed”, and “sorting” refer to a perturbation in water flow, bed level, and surface grain size distribution, respectively.

variation based on the stochastic framework developed by *Parker et al.* (2000). The model associates a probability of grain size selective entrainment to all elevations within the bed, and hence allows for sediment at any elevation to be entrained and contribute to the bed-load discharge. *Viparelli et al.* (2017) developed a simplified vertically continuous model assuming slow changes in bed elevation and a steady probability distribution of entrainment, deposition, and bed elevation, which make their model suitable for large space and time domains. So far the well-posedness of the continuous model has never been assessed.

Our main objective is to analyze the problem of ill-posedness of the active layer model used for mixed sediment morphodynamics. The present chapter provides four key improvements with respect to presently available knowledge: (i) we obtain analytical expressions to characterize a simplified model (i.e., to find whether it is ill-posed or well-posed) when only two sediment fractions are composed, (ii) we study the effect of model parameter choice on ill-posedness, (iii) we find new (previously neglected) ill-posedness domains, and (iv) we study the consequences of ill-posedness in numerical simulations. Our second objective is to mathematically characterize the vertically continuous model developed by *Viparelli et al.* (2017). In the next section we present the general set of equations for modeling mixed sediment river morphodynamics using (a) the active layer model and (b) the vertically continuous model developed by *Viparelli et al.* (2017). The models are simplified and analyzed in Section 2.3. We analyze the effect of model parameters on the ill-posedness of the active layer model in Section 2.4. In Section 2.5 we study the consequences of ill-posedness using numerical runs. In Section 2.6 we relax and study the simplifications of our analysis.

2.2. Model Equations

In this section we present the equations used to model river morphodynamics. These equations represent one-dimensional hydrostatic flow over a mobile bed composed of an arbitrary number N of non-cohesive sediment fractions characterized by a grain size d_k [m], where the subscript k identifies each fraction in increasing size (i.e., $d_1 < d_2 < \dots < d_N$).

In the following section we describe the flow equations. As previous research has clarified (Ribberink, 1987; Stecca et al., 2014), a key parameter in determining well-posedness of the active layer model is the active layer thickness. In this chapter we both consider a model with constant, and with unsteady (time-varying) active layer thickness. While the well-posedness of the model with constant active layer thickness has been analyzed in previous work (Ribberink, 1987; Stecca et al., 2014), to our knowledge no analysis of the well-posedness of the model with unsteady active layer thickness is available, although use of such a model is documented in the literature (e.g. Karim et al., 1983). The equations of the adapted active layer model are presented in Section 2.2.2. In Section 2.2.3 we present the vertically continuous model derived by Viparelli et al. (2017). The closure relations for both models are treated in Section 2.2.4. In Section 2.2.5 we present a compact matrix formulation of the model equations.

2.2.1. Flow Equations

The flow is described by the 1D Shallow Water Equations (i.e., the *Saint-Venant* equations (Saint-Venant, 1871)) considering constant width. Assuming steady flow conditions the water discharge is uniform and conservation of momentum reduces to the so-called backwater equation (A.1). When assuming steady flow over a movable bed composed of sediment of different sizes we implicitly assume that the flow adapts instantaneously to perturbations in bed elevation and grain size distribution. Worded differently, we assume that flow perturbations propagate infinitely fast relative to perturbations in bed elevation and surface grain size distribution. This assumption is referred to in literature as the “quasi-steady flow assumption” (De Vries, 1965; Zhang and Kahawita, 1987, 1990; Cao and Carling, 2002a). The quasi-steady flow assumption is acceptable provided that the Froude number is sufficiently small, $1 - Fr^2 = \mathcal{O}(1)$ (De Vries, 1973; Sieben, 1999; Lyn and Altinakar, 2002). Note that in this context the term “quasi-steady” has a meaning different from, for instance, its use in the modeling of flood waves where “quasi-steady” refers to negligible inertia in the momentum balance.

2.2.2. Adapted Active Layer Model Equations

The conservation of the total amount of sediment in the bed is formulated by the *Exner* equation (Exner, 1920). The active layer equation describes mass conservation for each size fraction (Hirano, 1971). A.2 presents the details of the active layer model.

To analyze the model with unsteady active layer thickness, we first need to set a closure relation expressing the thickness change in time. We consider an empirical power relation between dune height H [m] and flow depth h [m] (Yalin, 1964; Gill, 1971):

$$H = a_L b^{b_L}, \quad (2.1)$$

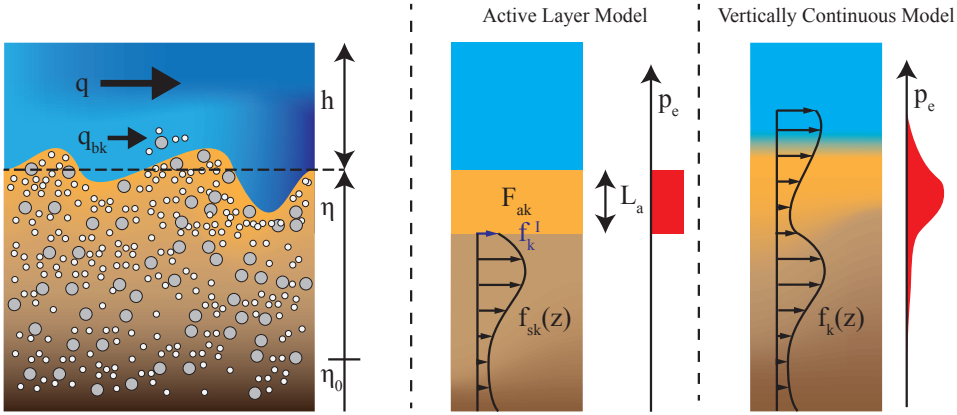


Figure 2.2: Representation of the main variables of the active layer model (Hirano, 1971) and the vertically continuous model proposed by Viparelli et al. (2017).

where a_L [m^{1-b_L}] and b_L [–] are constants. Allen (1968a,b) proposed values of $a_L = 0.1 \sim 0.2 m^{1-b_L}$ and $b_L = 0.9 \sim 1.2$ (with b in [m]). Assuming that the active layer thickness L_a [m] is equal to the mean dune height (Blom, 2008), we relate the active layer thickness to the flow depth as follows:

$$L_a = a_L b^{b_L}. \quad (2.2)$$

To obtain an equation for the active layer thickness variation we differentiate the constitutive law, Equation (2.2), with respect to time and then substitute the continuity equation (A.1) in it:

$$\frac{\partial L_a}{\partial t} = -a_L b_L b^{b_L-1} \frac{\partial q}{\partial x}. \quad (2.3)$$

Substitution of Equation (2.3) into the active layer equation (A.5) yields the following adapted active layer equation:

$$\frac{\partial M_{ak}}{\partial t} - f_k^I \frac{\partial q_b}{\partial x} + f_k^I a_L b_L b^{b_L-1} \frac{\partial q}{\partial x} + \frac{\partial q_{bk}}{\partial x} = 0, \quad (2.4)$$

where t [s] denotes the time coordinate, x [m] the streamwise coordinate, $q = ub$ [m^2/s] the water discharge per unit width, q_b [m^2/s] is the sediment transport rate per unit width multiplied by $1/(1-p)$ where p [–] is the bed porosity (i.e., the sediment transport rate q_b accounts for pores), q_{bk} [m^2/s] is the sediment transport rate per size fraction, M_{ak} [m] is the volume of sediment of size fraction k in the active layer per unit of bed area, and f_k^I [–] is the volume fraction content of size fraction k at the interface between the active layer and the substrate. In Figure 2.2 we show a schematic representation of the main variables of the active layer model.

2.2.3. Simplified Vertically Continuous Model Equations

The conserved quantity in the vertically continuous model (similar to M_{ak} in the active layer model) is the product of the cumulative probability of bed elevation (P_e [–]) and the

volume fraction content of a specific grain size class k (f_k [—]) (Parker et al., 2000; Pelosi et al., 2014). The vertical coordinate is z [m]. To simplify the problem, the probability distribution depends on a second vertical coordinate $y = z - \eta$ which is centered at the mean bed elevation. Assuming slow changes in mean bed elevation and a constant (in time and space) probability distribution of bed elevation, Viparelli et al. (2017) obtain an equation for the change in time of the volume fraction content, f_k :

$$P_c \frac{\partial f_k}{\partial t} = -p_c \frac{\partial q_{bk}}{\partial x} - \frac{\partial q_b}{\partial x} \frac{\partial f_k P_c}{\partial y}, \quad (2.5)$$

where p_c [m^{-1}] is the probability density function of bed elevation (Figure 2.2).

As in the active layer model, information is only advected in streamwise direction, i.e., the conservation equation does not include divergence terms in the y direction and the only independent variable in space is x . In contrast to the active layer model, there is no inactive substrate and sediment at all elevations plays a role. This is illustrated by the dependence of the probability function on the y coordinate and the gradient in the y direction in Equation (2.5). Thus, although the system of equations is one-dimensional, the mathematical character of the model is a property depending not only on the streamwise coordinate x but also on the vertical coordinate y .

2.2.4. Closure Relations

We apply the Chézy law for the friction slope. Thus, the friction slope is proportional to the square of the mean flow velocity divided by the flow depth, $S_f = C_f u^2 / (g b)$, where C_f [—] is a nondimensional friction coefficient. For simplicity, we assume a constant nondimensional friction coefficient that is independent of the flow and bed parameters.

We apply a generalized form of the Meyer-Peter and Müller (1948) transport relation, in which the sediment transport rate is a power function of the excess bed shear stress:

$$q_{bk}^* = A [\max(\theta_k - \xi_k \theta_c, 0)]^B, \quad (2.6)$$

where q_{bk}^* [—] is a nondimensional sediment transport rate (A.3), A [—] and B [—] are nondimensional parameters, θ_k [—] is the nondimensional bed shear stress of size fraction k , also known as Shields (1936) parameter, θ_c [—] is the nondimensional critical bed shear stress, and ξ_k [—] is the hiding coefficient. Table 2.1 summarizes appropriate values of A , B , and θ_c according to several authors.

A common hiding function is the one due to Egiazaroff (1965) (A.3). A simpler relation was developed by Parker et al. (1982):

$$\xi_k = \left(\frac{D_m}{d_k} \right)^b, \quad (2.7)$$

where D_m [m] is a characteristic mean grain size and b is a nondimensional parameter. A value of $b > 1$ (Dhamotharan et al., 1980; Misri et al., 1984; Kubhle, 1993) implies that hiding is so strong that the coarser fraction(s) in the mixture is (are) more mobile than the finer one(s), i.e., reverse mobility (Solari and Parker, 2000).

A final closure relation is required (only for the active layer model) for the volume fraction content of sediment of size fraction k at the interface between the active layer

Author	A [—]	B [—]	θ_c [—]
<i>Meyer-Peter and Müller</i> (1948)	8	1.5	0.047
<i>Engelund and Hansen</i> (1967)	$0.05/C_f$	2.5	0
<i>Fernandez-Luque and Van Beek</i> (1976)	5.7	1.5	0.037 - 0.0455
<i>Wong and Parker</i> (2006a) (1)	4.93	1.6	0.047
<i>Wong and Parker</i> (2006a) (2)	3.97	1.5	0.0495

Table 2.1: Values of parameters in Equation (2.6) according to several authors.

and the substrate, f_k^I . When the interface lowers the texture at the interface is equal to that at the topmost part of the substrate. When the interface elevation increases various relations can be applied for f_k^I . *Hirano* (1971) proposed that during aggradation the grain size distribution at the interface is equal to the one of the active layer. According to *Parker* (1991) also the bedload sediment plays a role in the aggradational flux to the substrate. *Hoey and Ferguson* (1994) combined both concepts in one parameter α [—] spanning the range [0,1] that describes the contribution of the active layer relative to the one of the bedload:

$$f_k^I = \begin{cases} f_{sk}(z = \eta - L_a) & \text{if } \frac{\partial(\eta - L_a)}{\partial t} < 0 \\ \alpha F_{ak} + (1 - \alpha) p_k & \text{if } \frac{\partial(\eta - L_a)}{\partial t} > 0 \end{cases}, \quad (2.8)$$

where $p_k = q_{bk}/q_b$ [—] is the fraction of sediment transport rate of size fraction k .

2.2.5. Matrix Formulation

In this section we introduce a matrix formulation to assess the well-posedness of the system of equations.

A system of partial differential equations (PDEs) can be mathematically classified as being of a hyperbolic, elliptic, or mixed type (e.g., *Courant and Hilbert*, 1989). To this end we write the problem in matrix-vector form (e.g., *Toro*, 2001):

$$\frac{\partial \mathbf{Q}}{\partial t} + \mathbf{A} \frac{\partial \mathbf{Q}}{\partial x} = \mathbf{S}. \quad (2.9)$$

This equation is the one-dimensional quasi-linear non-conservative form of the advection equation. \mathbf{Q} is the vector of dependent variables, \mathbf{A} is the system matrix, and \mathbf{S} is the vector of source terms.

A system is hyperbolic at a point (x, t) if all the eigenvalues of matrix \mathbf{A} are real. Physical propagation problems are modeled with hyperbolic systems of equations. If all eigenvalues are complex, the system is termed elliptic. Elliptic systems model equilibrium physical problems. If matrix \mathbf{A} has both real and complex eigenvalues it is a mixed-type system.

A space-time dependent problem, in which we prescribe boundary conditions as a function of time and an initial condition (as is the case in modeling river morphodynamics), governed by an elliptic set of equations is ill-posed (*Hadamard*, 1923; *Joseph and Saut*, 1990; *Kabanikhin*, 2008). This is confirmed by a perturbation analysis that shows that, if

and the vector of source terms is:

$$\mathbf{S}_{vc} = [0, -g h S_f, 0, 0]^T. \quad (2.15)$$

2.3. Characterization of the Mathematical Models

In this section we analyze the mathematical character of the models described in Section 2.2. Eigenvalues computed numerically can be obtained for an unlimited number of fractions. Here we study a simple case assuming steady flow and two size fractions to obtain analytical expressions of the eigenvalues.

As in our case the temporal change of the active layer thickness depends on the spatial gradient of the water discharge per unit width, Equation (2.3), the steady flow assumption implies a constant active layer thickness. Yet, in a numerical simulation where the steady flow assumption is used but the upstream discharge varies with time (i.e., alternating steady flow), the active layer thickness may vary with time. However, in such a case the perturbations due to a change in active layer thickness propagate infinitely fast relative to the perturbations in bed elevation and surface grain size distribution.

The implications of more than two sediment size fractions and an active layer thickness as a function of the flow depth are studied in Section 2.6.

2.3.1. Steady Active Layer Model Consisting of Two Size Fractions

Substitution of the backwater equation, (A.3), in the *Exner* equation, (A.4), and the active layer equation, (A.5), allows us to obtain a reduced model where the vector of dependent variables (\mathbf{Q}_{alS_2}) is:

$$\mathbf{Q}_{alS_2} = [\eta, M_{a1}]^T, \quad (2.16)$$

the vector of source terms (\mathbf{S}_{alS_2}) reads:

$$\mathbf{S}_{alS_2} = -S_f \frac{u \psi}{1 - Fr^2} [1, \gamma_1]^T, \quad (2.17)$$

and the system matrix (\mathbf{A}_{alS_2}) is:

$$\mathbf{A}_{alS_2} = u \begin{bmatrix} \frac{\psi}{1 - Fr^2} & \chi_1 \\ \frac{\psi}{1 - Fr^2} \gamma_1 & \chi_1 \mu_{1,1} \end{bmatrix}. \quad (2.18)$$

We define $\psi [-]$ as:

$$\psi = \frac{\partial q_b}{\partial q}, \quad (2.19)$$

which is a parameter related to the intensity of total bedload in the flow and ranges between 0 (null sediment discharge, i.e., fixed bed) and $\mathcal{O}(10^{-2})$ (high sediment discharge), (e.g., *De Vries* (1965); *Lyn and Altinakar* (2002); *Stecca et al.* (2014)).

The parameter $\gamma_1 [-]$ is a measure of the fraction content of sediment in transport relative to the fraction content of sediment at the interface between the active layer and

the substrate (*Stecca et al.*, 2014):

$$\gamma_1 = c_1 - f_1^I, \quad (2.20)$$

where $c_1 \in [0, 1]$ [–] is a parameter expressing the increase in the sediment transport intensity of the fine fraction relative to the total sediment transport intensity (*Stecca et al.*, 2014):

$$c_1 = \frac{1}{\psi} \frac{\partial q_{b1}}{\partial q}. \quad (2.21)$$

We now introduce the parameter χ_1 [–] which is a nondimensional measure of the derivative of the total sediment transport rate with respect to the volume of fine sediment in the active layer:

$$\chi_1 = \frac{1}{u} \frac{\partial q_b}{\partial M_{a1}}. \quad (2.22)$$

The parameter $\mu_{1,1}$ [–] is defined as:

$$\mu_{1,1} = d_{1,1} - f_1^I, \quad (2.23)$$

where $d_{1,1}$ [–] is a nondimensional measure of the derivative of the sediment transport rate of the fine fraction with respect to the volume of fine sediment in the active layer:

$$d_{1,1} = \frac{1}{u\chi_1} \frac{\partial q_{b1}}{\partial M_{a1}}. \quad (2.24)$$

We obtain the eigenvalues of the system matrix finding the roots of its second degree characteristic polynomial. The eigenvalues are nondimensionalized dividing by the flow velocity:

$$\lambda_{\text{alS}2i} = \frac{1}{2} \left[\lambda_b + \lambda_{s1} \pm \sqrt{\Delta_{\text{alS}2}} \right] \quad \text{for } i = 1, 2, \quad (2.25)$$

where the discriminant is:

$$\Delta_{\text{alS}2} = (\lambda_b - \lambda_{s1})^2 + 4\lambda_b\lambda_{s1} \frac{\gamma_1}{\mu_{1,1}}. \quad (2.26)$$

The eigenvalues of the system carry coupled information on both the bed elevation and the surface grain size distribution which shows that a perturbation in bed elevation causes a perturbation in surface grain size distribution and vice versa (Section 2.1). Yet, we identify two nondimensional celerities that approximate the changes in bed elevation (λ_b) and in surface grain size distribution (λ_{s1}) independently.

The bed celerity, which is independent of the active layer thickness, was first derived by *De Vries* (1965) for unisize sediment:

$$\lambda_b = \frac{\psi}{1 - \text{Fr}^2}. \quad (2.27)$$

We define the nondimensional sorting celerity as:

$$\lambda_{s1} = \chi_1 \mu_{1,1}. \quad (2.28)$$

This sorting celerity differs from the one of *Ribberink* (1987) as he considered a perturbation in the mean grain size while here the sorting celerity relates to a perturbation in the volume fraction content of each grain size fraction individually. The proposed expression for the sorting celerity in Equation (2.28) is a generalization of the expression proposed by *Stecca et al.* (2014), as we have relaxed *Stecca et al.*'s assumption of limited hiding.

The mathematical character of the model depends on the sign of the discriminant Δ_{alS_2} , Equation (2.26). If $\Delta_{\text{alS}_2} > 0$ the two eigenvalues are real and the system is hyperbolic. If $\Delta_{\text{alS}_2} < 0$ the eigenvalues are complex and the system is elliptic. A large difference between the bed celerity and sorting celerity reduces the likelihood that the model becomes elliptic. Hyperbolicity is guaranteed if $\gamma_1 > 0$. If $\gamma_1 < 0$ and the bed and sorting celerities are equal, ellipticity is guaranteed (*Sieben*, 1994; *Stecca et al.*, 2014).

Assuming that reverse mobility does not occur (Section 2.2.4), c_1 is larger than the volume fraction content of fine sediment in the active layer (F_{a1}) due to the grain size selectivity of the sediment transport relation (*Stecca et al.*, 2014). If we also assume that the sediment transferred to the substrate in aggradational conditions has the same grain size distribution as the active layer (*Hirano*, 1971), then the parameter γ_1 is always positive in aggradational conditions. Only a substrate finer than the active layer yields a negative value of the parameter γ_1 . Thus, a two-fraction active layer model can only be ill-posed if the bed degrades into a substrate that is finer than the active layer (a result also found by *Stecca et al.* (2014) considering unsteady flow).

In Sections 2.4.1 and 2.4.2 we assess the relaxation of the assumptions that reverse mobility does not occur and that the aggradational flux to the substrate has the same grain size distribution as the active layer.

2.3.2. Steady Vertically Continuous Model Consisting of Two Size Fractions

We apply the same procedure used to analyze the active layer model to the vertically continuous model (Section 2.2.3). In this manner we obtain the discriminant of the eigenvalues (A.4):

$$\Delta_{\text{vcS}_2} = (\lambda_{\text{b}} - \lambda_{\text{sc1}})^2 + 4\lambda_{\text{b}}\lambda_{\text{sc1}}\frac{g_1}{m_{1,1}}, \quad (2.29)$$

where λ_{sc1} , g_1 , and $m_{1,1}$ are the equivalents to λ_{s1} , γ_1 , and $\mu_{1,1}$ of the active layer model (A.4).

Similar to the active layer model (Section 2.3.1), the continuous model is hyperbolic and well-posed if $\Delta_{\text{vcS}_2} > 0$ and vice versa. Although the expression of the discriminant of the vertically continuous model, Equation (2.29), is similar to the one of the active layer model, Equation (2.26), there is an essential difference between the two. In the active layer model the discriminant is a function of the streamwise position, $\Delta_{\text{alS}_2}(x)$, yet in the continuous model the discriminant is also a function of the vertical coordinate, $\Delta_{\text{vcS}_2}(x, y)$. Thus, ellipticity or hyperbolicity is a property not only of the streamwise coordinate but also of the elevation in the bed (Section 2.2.3). Hyperbolicity is guaranteed if $g_1 > 0$ but, contrary to the active layer model, this parameter can be negative both under aggradational and degradational conditions.

Due to grain size selective transport we can assure that, if reverse mobility conditions do not prevail, the concentration c_1 is larger than the volume fraction content representative of the bed surface F_{b1} , Equation (A.14). However, F_{b1} is a weighted average of all sediment and for this reason there is no guarantee that for all bed elevations the average volume fraction content (F_{b1}) is larger than the local volume fraction content in the bed sediment (f_1). Moreover, as there is no distinction between aggradational and degradational cases, the domain in which the model is likely to be ill-posed is larger than for the active layer model. The presence of fine sediment at the locations having larger probability of entrainment in combination with a “smooth” vertical variation (small derivative) of the volume fraction content of fine sediment reduces the likelihood of the model becoming elliptic.

2.4. Active Layer Model Parameter Study

In this section we assess the effects of various model parameters on the mathematical character of the active layer model. To this end we study the analytical expressions of the eigenvalues of the steady model considering two sediment size fractions obtained in Section 2.3.1.

2.4.1. Hiding

Given the fact that ill-posedness arises when considering different grain sizes in the mixture and that a larger difference between grain sizes increases the ill-posed domain, intuitively hiding should reduce the likelihood of ill-posedness. Its effect, however, is opposite as we will show here.

To explain this counter-intuitive result we analyze the term in the characteristic polynomial intrinsically related to hiding. This term is the derivative of the sediment transport rate of fine and coarse sediment with respect to the volume of fine sediment in the active layer ($\partial q_{bk} / \partial M_{a1}$). It can be considered as the summation of two terms:

$$\frac{\partial q_{bk}}{\partial M_{a1}} = \frac{1}{L_a} \left(\underbrace{\frac{\partial F_{ak}}{\partial F_{a1}} Q_{bk}}_{\text{presence}} + F_{ak} \underbrace{\frac{\partial Q_{bk}}{\partial F_{a1}}}_{\text{hiding}} \right) \quad \text{for } k = 1, 2. \quad (2.30)$$

We name the first and second terms on the right-hand side the “presence term” and the “hiding term”, respectively. The “presence term” explains that an increase in the volume fraction content of the fine sediment in the active layer implies both (1) an increase of the sediment transport rate of the fine fraction as its presence at the bed surface is larger, and (2) a consequent decrease of the sediment transport rate of the coarse fraction because its presence at the bed surface decreases. The “hiding term” indicates the fact that a variation of the volume fraction content of the fine sediment changes the sediment transport rate of both fine and coarse fractions due to a change in the mean grain size of the sediment mixture. The “presence term” is positive for the fine fraction and negative for the coarse fraction. The “hiding term” is always positive.

In a situation where hiding is negligible, an increase of the characteristic size of the coarse fraction or decrease of the fine fraction, which is associated with a larger likeli-

F_{a1} [-]	f_1^1 [-]	d_1 [m]	d_2 [m]	C_f [-]	u [m/s]	b [m]	L_a [m]
0	0.6	0.002	0.004	0.015	0.68	0.20	0.01

Table 2.2: Values of the reference case. For these values the active layer thickness can be seen as representative of plane bed conditions ($L_a \approx 2.5D_{90}$) as well as bedform dominated conditions ($L_a \approx a_1 b^{b_1}$).

hood that the model is elliptic, causes an increase of the “presence term” and thus of $\partial q_{bk}/\partial M_{a1}$. With respect to such a situation, hiding decreases the “presence term” of both fine and coarse sediment (reducing the likelihood of ellipticity) but introduces the positive contribution of the “hiding term”. Overall, the “hiding term” may dominate, which increases the value of $\partial q_{bk}/\partial M_{a1}$ and thus of the likelihood of ellipticity.

Interestingly, in degradational conditions into a fine substrate (a situation prone to be elliptic) the hiding term dominates. Thus, hiding increases the likelihood that the model is elliptic in degradational conditions into a substrate finer than the active layer.

In Figure 2.3a we show the effect of hiding on the discriminant of the steady active layer model considering two size fractions, Equation (2.26). We consider the reference case described in Table 2.2. The sediment transport rate is computed using the relation derived by *Meyer-Peter and Müller* (1948). To obtain different values of hiding we vary parameter b in the power law hiding function in Equation (2.7) between 0 and 1 (purple line in Figure 2.3a). The yellow line in Figure 2.3a is obtained varying the characteristic grain size of the fine fraction between 0.001 m and 0.004 m using the *Egiazaroff* hiding relation, Equation (A.15). The discriminant decreases for increasing hiding independent from the hiding function.

Besides these cases under degradational conditions, we may encounter problems even under aggradation. In fact, if hiding is so strong that reverse mobility is induced, then one of the assumptions of the analysis by *Stecca et al.* (2014), may not be fulfilled. In detail, it may happen that the reference content c_1 related to the fine sediment in the bedload, Equation (2.21), is not greater than the content of fines in the active layer F_{a1} , which was their assumption under grain size selective transport. When reverse mobility instead determines conditions such that $c_1 < F_{a1}$, then the discriminant, Equation (2.26), may be negative, and the model may become elliptic even under aggradational conditions.

2.4.2. Aggradational Flux to the Substrate

The sediment transferred to the substrate under aggradational conditions using the model by *Hoey and Ferguson* (1994) (Section 2.2.4) is always finer than the sediment in the active layer. This is because the bedload is finer than the bed surface due to grain size selective processes (provided that reverse mobility does not dominate). Thus, application of the model by *Hoey and Ferguson* (1994) implies that under aggradational conditions the interface between the active layer and the substrate is finer than the active layer. This means that the condition $\gamma_1 > 0$ (Section 2.3.1) may not be fulfilled under aggradational conditions, which implies that the model may become ill-posed. Therefore, a larger contribution of the bedload to the aggradational flux to the substrate (smaller value of the parameter α in Equation (2.8)) implies a larger likelihood of the model becoming elliptic

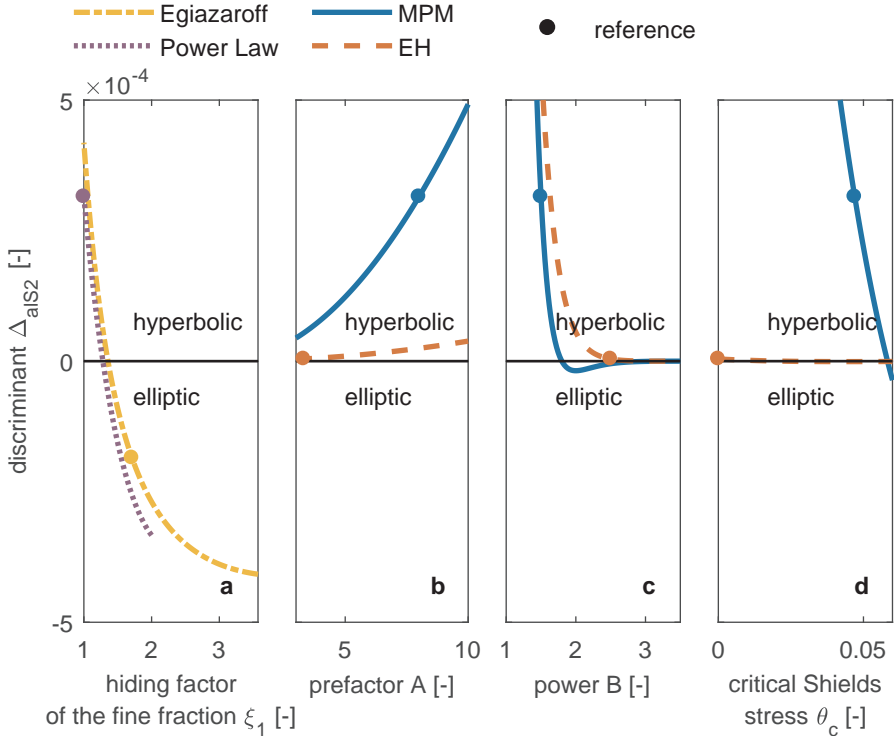


Figure 2.3: Discriminant Δ_{ais2} , Equation 2.26, as a function of: (a) the hiding relation for the fine fraction ξ_1 , (b) the prefactor of the sediment transport formula A , (c) the power B , and (d) the critical Shields stress θ_c . The blue line is obtained varying the parameters from the reference state using the *Meyer-Peter and Müller* (1948) (MPM) sediment transport relation. The red line is obtained using the *Engelund and Hansen* (1967) (EH) relation. The yellow line is obtained by varying the characteristic grain size of the fine fraction using the hiding relation by *Égiazaroff* (1965), Equation (A.15), in combination with the MPM relation, the purple line by varying the coefficient b of the power law function by *Parker et al.* (1982), Equation (2.7), in combination with the MPM relation. The dots represent the reference situation described in Table 2.2. Note that there is a different reference situation depending on the sediment transport relation.

(Appendix A.6).

However, in a hypothetical aggrading case in which the grain size distribution transferred to the substrate is fully composed of bedload sediment ($\alpha = 0$), the relative content of the fine fraction in the vertical sediment flux, γ_1 (Equation (2.20)), that controls the size of the ill-posed domain (Section 2.3.1), is still not as small as it can be found under degradational cases (Appendix A.6). Thus, ill-posed cases are expected to occur primarily under degradational conditions into a fine substrate.

2.4.3. Prefactor in a Sediment Transport Relation and Morphodynamic Factor

The discriminant (Δ_{als_2}) of the steady active layer model for two size fractions, Equation (2.26), can be written as $\Delta_{\text{als}_2} = A^2 \widehat{\Delta}_{\text{als}_2}$, where $\widehat{\Delta}_{\text{als}_2}$ is the discriminant for a unit prefactor (i.e., $A = 1$). The prefactor A increases or decreases the discriminant but does not change its sign, and so it does not change the character of the mathematical system. This is confirmed by Figure 2.3b, which shows the effect of varying the prefactor A in the reference case described in Section 2.4.1.

Since morphodynamic time scales are usually several orders of magnitude larger than the time scales of the flow (Section 2.2.1), computations usually cover a significant number of years. The computational time is sometimes reduced using a morphodynamic factor that multiplies the divergence of the sediment transport rate (Latteux, 1995; Roelvink, 2006; Ranasinghe et al., 2011). This factor can also be considered as a multiplication of the sediment transport rate and therefore has the same effect as the prefactor A . Thus, the use of a morphodynamic factor does not change the mathematical character of the model.

This result is obtained assuming quasi-steady flow. While the prefactor in the sediment transport relation rarely varies by more than an order of magnitude, simulations may be run with morphodynamic acceleration factors $\mathcal{O}(10^2)$. In these latter cases, the quasi-steady flow assumption may not be acceptable, which limits the extension of our analysis.

2.4.4. Exponent and Critical Shields Stress in a Sediment Transport Relation

The discriminant, Equation (2.26), tends to 0^- with increasing values of B if the effective Shields stress for all sediment fractions is smaller than 1, or to ∞ if the effective Shields stress is larger than 1 for at least one fraction. Thus, it is difficult to generalize the effect of the exponent. Its variation from a reference situation can both make the system hyperbolic if the reference situation is elliptic or vice versa. In Figure 2.3c we show the discriminant as a function of B for the same reference cases as in Section 2.4.3. The hyperbolic situation when using Meyer-Peter and Müller (1948) becomes elliptic if the value of the exponent B increases towards the value in Engelund and Hansen (1967).

The effect of the critical Shields stress, θ_c in Equation (2.6), on the discriminant is similar to the effect of the exponent, as its variation can both make a previously hyperbolic case elliptic or vice versa. Figure 2.3d shows how a decrease of the critical shear stress when using the sediment transport relation by Meyer-Peter and Müller (1948) increases the discriminant reducing the likelihood of elliptic behavior.

2.4.5. Active Layer Thickness

The discriminant of the eigenvalues, Equation (2.26), can be written as a second degree polynomial of the inverse of the active layer thickness, i.e., $\Delta_{\text{alS}_2} = a_1(1/L_a)^2 + a_2(1/L_a) + a_3$ where $a_1 > 0$, a_2 , and a_3 are coefficients independent of the active layer thickness. This implies that: (1) the model is well-posed for a sufficiently thin active layer, (2) the model is well-posed for a sufficiently thick active layer, and (3) there exists one ill-posed domain only (regarding the active layer thickness). These results of the two-fractions model confirm previous results based on the simplified active layer model (Ribberink, 1987; Sieben, 1994).

The inverse of the roots of the second degree polynomial are the limit values of the active layer thickness that ensure that the model is well-posed:

$$L_a^\pm = \frac{\widehat{\lambda}_{s1}}{\widehat{\lambda}_b} \left(1 - 2 \frac{\widehat{\gamma}_1}{\widehat{\mu}_{1,1}} \pm \sqrt{\left(2 \frac{\widehat{\gamma}_1}{\widehat{\mu}_{1,1}} - 1 \right)^2 - 1} \right)^{-1}, \quad (2.31)$$

where we have used the notation $\widehat{(\)}$ for the variables with unit active layer thickness (i.e., $L_a = 1$ m). Given the facts that the active layer thickness is one of the most empirical parameters of the system of equations (Section 2.1) and that river morphodynamic models often require calibration (e.g., Cao and Carling, 2002b), Equation (2.31) can be applied to select a certain value for the active layer thickness to avoid a situation that is prone to be ill-posed.

2.5. Consequences of Ill-Posedness

In this section we analyze the consequences of ill-posedness using numerical simulations. Our aim is to provide modellers with the tools to detect occurrence of ill-posedness in their results and understand how the observed unrealistic model behavior changes with parameter and model choices. First we make numerical runs to qualitatively observe the consequences of the non-linear effects that are neglected in the perturbation analysis (Section 2.5.1). In Section 2.5.2 we conduct a sensitivity analysis to generalize the consequences observed in the previous section.

2.5.1. Numerical Examples

The linear perturbation analysis shown in Section 2.2.5 indicates that perturbations grow unboundedly if the model is elliptic. In this section we run four numerical simulations at flume scale to analyze the effects of the neglected non-linear terms. The simulations are one-dimensional for the flow and are computed using the Delft3D software package (Lesser et al., 2004), which solves the unsteady Shallow Water Equations in combination with the active layer model. For simplicity the active layer thickness is assumed constant. Under aggradational conditions the sediment transferred to the substrate is composed of only the active layer sediment (i.e., $\alpha = 1$ in Equation (2.8)). Substrate stratigraphy is stored using a bookkeeping system (Viparelli et al., 2010; Stecca et al., 2016). All simulations start from equilibrium conditions under coarse sediment feeding. A lowering of the base level is imposed, which causes degradation into a fine substrate. We consider a well-posed reference case (Simulation 1) that (initially) has the same parameters as the reference case

Simulation	L_a [m]	hiding	M_f [–]	F_{s1}	Δz	Math. character
1	0.010	no	1	0.6	0.10	hyperbolic
2	0.025	no	1	0.6	0.10	elliptic
3	0.010	yes	1	0.6	0.10	elliptic
4	0.010	yes	2	0.6	0.10	elliptic
5	0.010	no	1	0.6	0.01	hyperbolic
6	0.010	no	1	1.0	0.10	elliptic
7	0.010	no	1	1.0	0.01	elliptic

Table 2.3: Overview of the simulations. Only the parameters that are different between simulations are shown.

L [m]	B [m]	q_{b1} [m ² /s]	q_{b2} [m ² /s]	q [m ² /s]
100	1	0	1×10^{-4}	0.14

T [h]	low. rate [m/h]	Δx [m]	Δt [s]
2	0.03/2	0.1	0.2

Table 2.4: Domain definition, boundary conditions, and numerical parameters. The symbols not defined in the text are: reach length (L), channel width (B), simulation time (T), lowering rate of the downstream water level (low. rate), horizontal discretization length (Δx), and time step (Δt).

of the parameter study of Section 2.4 (Table 2.2). Then, the active layer thickness is changed (Simulation 2) and hiding is considered (Simulation 3). Simulation 4 is equal to Simulation 3 except for its morphodynamic factor. Table 2.3 summarizes the differences between the four simulations. The boundary conditions that are in equilibrium with the initial condition (*Blom et al.*, 2016) as well as other parameters are described in Table 2.4.

In Figure 2.4a we plot the discriminant of the eigenvalues of the quasi-steady active layer model, Equation (2.26), at the initial time as a function of the active layer thickness. Note that the conditions of Simulation 1 yield a well-posed model ($\Delta_{\text{alS}_2} > 0$) while the conditions of Simulation 2 yield an ill-posed model ($\Delta_{\text{alS}_2} < 0$). In Figure 2.4d-e we show the evolution of the bed elevation for Simulations 1 and 2, respectively. The ill-posed Simulation 2 shows an oscillatory behavior that is not present in the well-posed Simulation 1. We have not imposed any initial perturbation, which implies that numerical noise is sufficient to trigger the oscillatory behavior.

Simulation 3 is the same as Simulation 1, yet the sediment transport rate now accounts for hiding using the *Parker et al.* (1982) function, Equation (2.7), with exponent b equal to 0.8. Simulation 3 is ill-posed (Figure 2.4b) and the solution shows oscillations (Figure 2.4f) just as in the ill-posed Simulation 2.

Simulation 4 is the same as Simulation 3 except for its morphodynamic factor equal to two, which decreases the value of the discriminant (Figure 2.4c), causing oscillations to develop faster (Figure 2.4g).

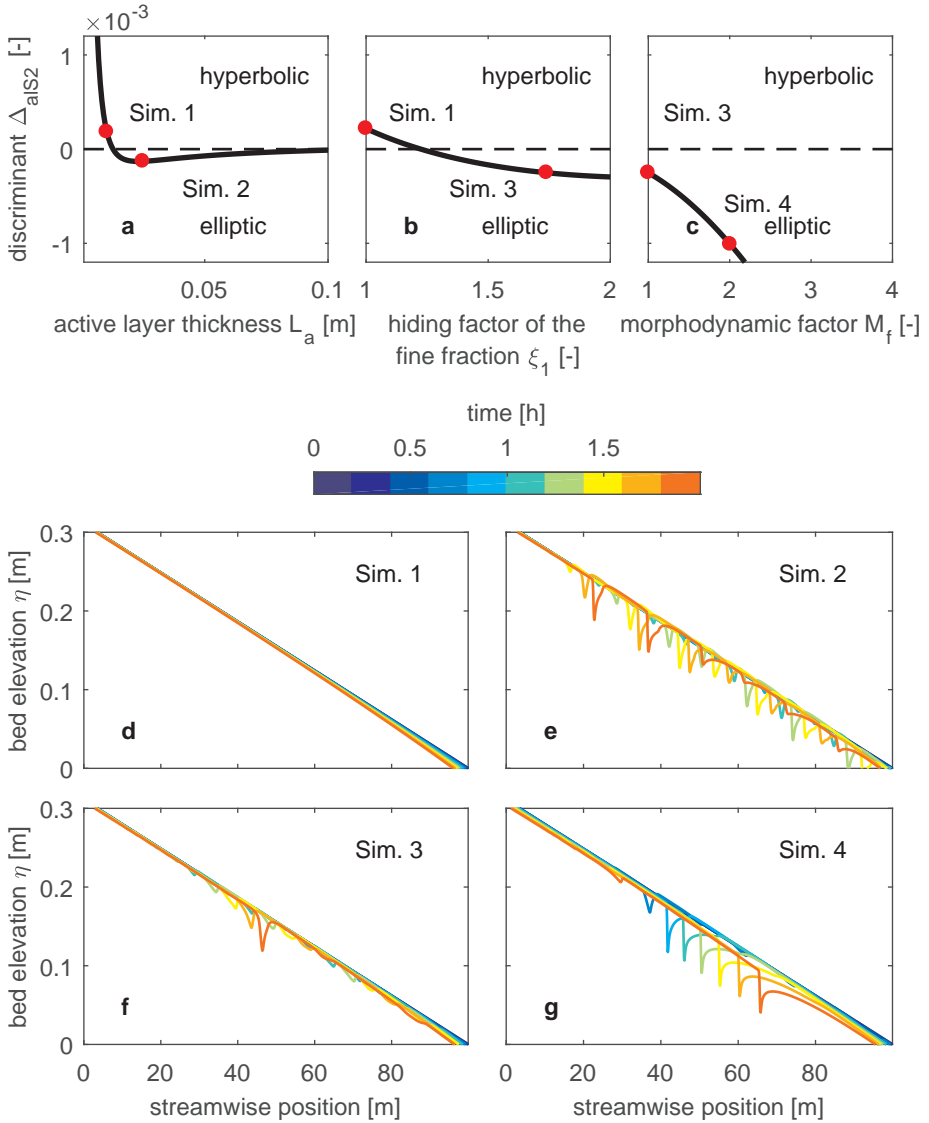


Figure 2.4: Discriminant Δ_{alS2} , Equation 2.26, as a function of (a) the active layer thickness L_a , (b) the hiding function of the fine fraction ξ_1 , and (c) the morphological factor M_f . Numerical solutions of (d) Simulation 1, (e) Simulation 2, (f) Simulation 3, and (g) Simulation 4. See Table 2.3 for the parameters definition.

	parameter	values
physical	d_1 [m]	0.0005, 0.001, 0.002
	d_2 [m]	0.002, 0.003, 0.004
	L_a [m]	0.010, 0.015, 0.020, 0.050
	f_{s1} [-]	0.6, 0.8, 1.0
numerical	Δx [m]	0.1, 0.2
	Δz [m]	0.01, 0.02, 0.05, 0.10

Table 2.5: Values of the physical and numerical parameters varied in the sensitivity analysis.

For all cases oscillations do not occur at the upstream end of the domain. This is because oscillations require time (and so space) to grow. In all cases oscillations grow until a maximum amplitude is reached and then propagate downstream. This maximum amplitude is such that the conditions are at the brink of ill-posedness and well-posedness. Worded differently, downstream from the location where the amplitude is maximum the model is ill-posed and it is well-posed upstream from it.

The oscillations are associated with degradation and subsequent aggradation. The deposited sediment has the same grain size distribution as the active layer (which is coarser than the initial substrate), so the overall effect of an oscillation is a coarsening of the topmost part of the substrate. This coarsening acts as a regularization mechanism, which not only restores hyperbolicity but also dampens oscillations that arrive from upstream by limiting the source of fine material.

It is likely that, because of the regularization mechanism, computations do not crash. As a result the extent and likelihood of ellipticity may in practice be underestimated. Yet, the results are physically unrealistic and implementing an automated check of the eigenvalues would be good practice for software developers and users.

2.5.2. Sensitivity Analysis

The previous section has shown that, due to the non-linearity of the system, an ill-posed simulation generates non-physical oscillations that propagate downstream and grow until a certain maximum amplitude at which the mathematical problem is at the brink of ill-posedness and well-posedness. In this section we run a sensitivity analysis to generalize those results.

To this end, we vary 4 physical parameters and 2 parameters related to the domain discretization, using Simulation 1 as a reference case. Table 2.5 summarizes the parameter values used in the sensitivity analysis.

As we are interested in studying the behavior of simulations under ill-posed conditions we exclude from the analysis those simulations in which the combination of parameters yield a well-posed model. As we have observed that the oscillations need space to grow until a maximum value (Section 2.5.1), we exclude those simulations in which the domain is not long enough to develop an oscillation that travels with a constant amplitude. A set

of 173 out of 256 simulations fulfills these two requirements.

In Figure 2.5a we plot the maximum flow depth (h_{\max}) nondimensionalized with the normal flow depth (h_n), as a function of the discriminant, Equation (2.26). For the sake of clarity we plot the results of the simulations with a horizontal discretization length (Δx) equal to 0.1 m and a thickness of the substrate layers equal to 0.01 m and 0.10 m (see Appendix A.7 for the results of all simulations). The parameters used to evaluate the discriminant are those at the start of the simulation (normal flow). The vertical black lines join simulations with the same physical parameters (i.e., they only differ regarding numerical parameters) and the color of each dot is related to the thickness of the substrate layer. The linear analysis has shown that the growth rate depends on the discriminant (Section 2.2.5), however there is only mild correlation between the discriminant and the maximum amplitude of the oscillations.

A thinly discretized substrate is associated with a larger amplitude of the oscillations (Figure 2.5a). This effect can be seen only empirically since it is not a parameter of the system of equations nor does it appear in the linear stability analysis.

For all simulations we compute the flow depth that yields a value of the discriminant at the initial condition equal to 0 (i.e., at the brink between ellipticity and hyperbolicity). This is done numerically finding the root of $\Delta_{\text{als}_2}(b)$, Equation (2.26), considering the water discharge and volume of sediment in the active layer and at the substrate of the initial condition. We term this flow depth the hyperbolic flow depth (h_{hyp}), which is independent of the numerical parameters of the simulation and depends on physical parameters only. In Figure 2.5b we compare the measured maximum flow depth and the hyperbolic flow depth. The grey line represents the situation in which $h_{\max} = h_{\text{hyp}}$. We see that the hyperbolic flow depth can be used as a rough estimate of the maximum flow depth that will occur in an elliptic simulation. One important source of scatter is the fact that the hyperbolic flow depth depends on the initial condition only, whereas the maximum flow depth also depends on the evolution of the solution as the oscillations interact with each other.

In Figure 2.5c we plot the nondimensional maximum flow depth as a function of the streamwise location where the maximum flow depth occurs (nondimensionalized with the total length of the domain). For the sake of clarity we plot the results of the simulations with a thickness of the bookkeeping layers (Δz) equal to 0.01 m (see Appendix A.7 for the results of all simulations). In the thinly discretized simulations we find the maximum amplitude more upstream compared to the coarsely discretized simulations. The location where the maximum amplitude of the oscillations is found is related to its growth rate since a faster growing oscillation develops its maximum amplitude in less distance than a slower one. This result confirms the findings of linear stability analysis (Section 2.2.5).

Also the maximum flow depth and the domain discretization are mildly correlated. Similar to the vertical discretization, smaller cells yield a larger maximum flow depth but this effect can be seen only empirically.

The discretization of the substrate affects also the duration of the elliptic behavior. Figure 2.6 shows the longitudinal profile of four simulations from the sensitivity analysis at the end of the run (Simulations 1, 5, 6, and 7, see Table 2.3). The substrate of the well-posed simulations at the end of the runs is unaltered, whereas it has coarsened in the

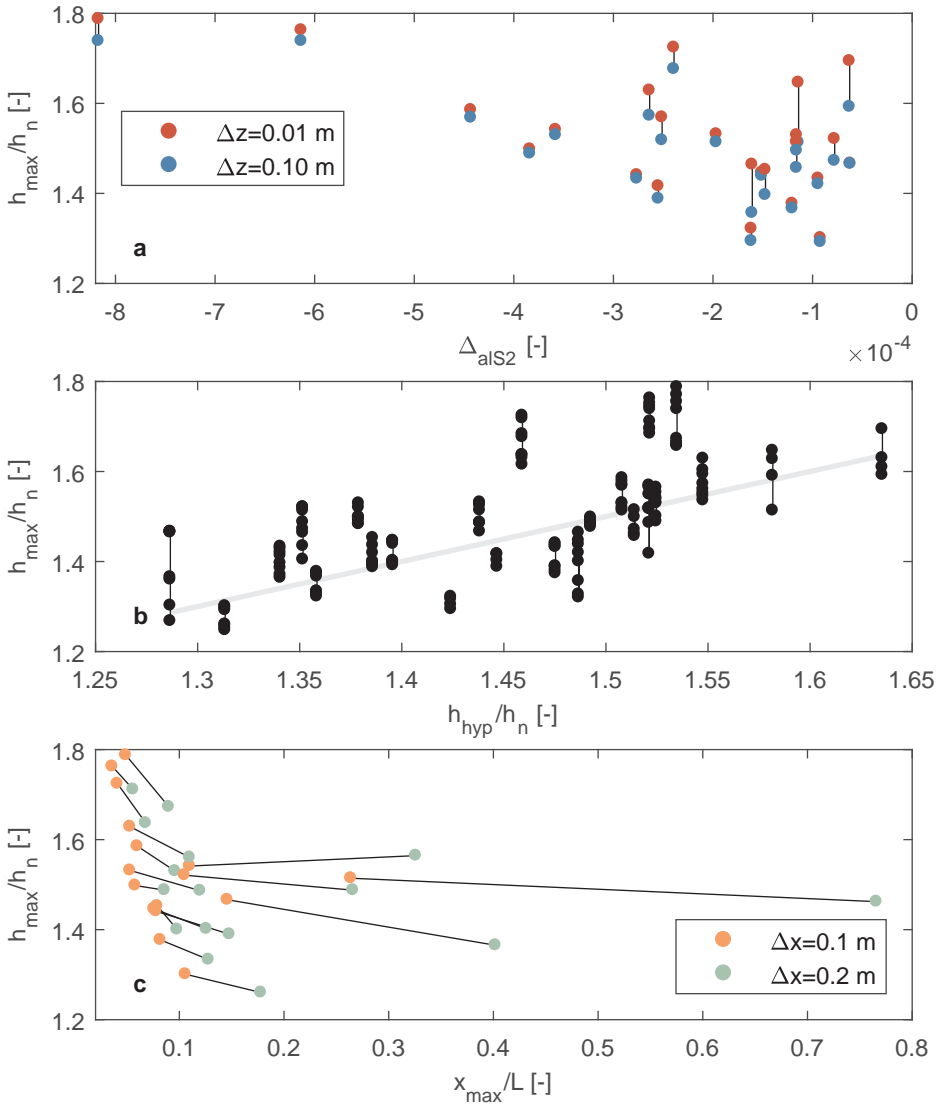


Figure 2.5: Maximum flow depth h_{\max} (nondimensionalized by the normal flow depth h_n) that develops as a consequence of ellipticity. In (a) the maximum flow depth is plotted against the discriminant $\Delta_{\text{als}2}$ for a horizontal discretization length (Δx) equal to 0.1 m and for a thickness of the bookkeeping layers (Δz) equal to 0.01 m (red dots) and 0.10 m (blue dots). The vertical black lines connect two simulations in which all parameters but Δz are the same. In (b) the maximum flow depth is plotted against the hyperbolic flow depth (h_{hyp}) nondimensionalized with the normal flow depth. Each black dot is the result of a simulation. The black lines connect simulations with the same physical parameters and the grey line is the perfect agreement. In (c) the maximum flow depth is plotted against the distance from upstream at which the maximum flow depth occurs (x_{\max}) nondimensionalized with the length of the domain (L) for a thickness of the bookkeeping layers (Δz) equal to 0.01 m and for a horizontal discretization length equal to 0.1 m (orange dots) and 0.2 m (green dots). The black lines connect two simulations in which all parameters but Δx are the same.

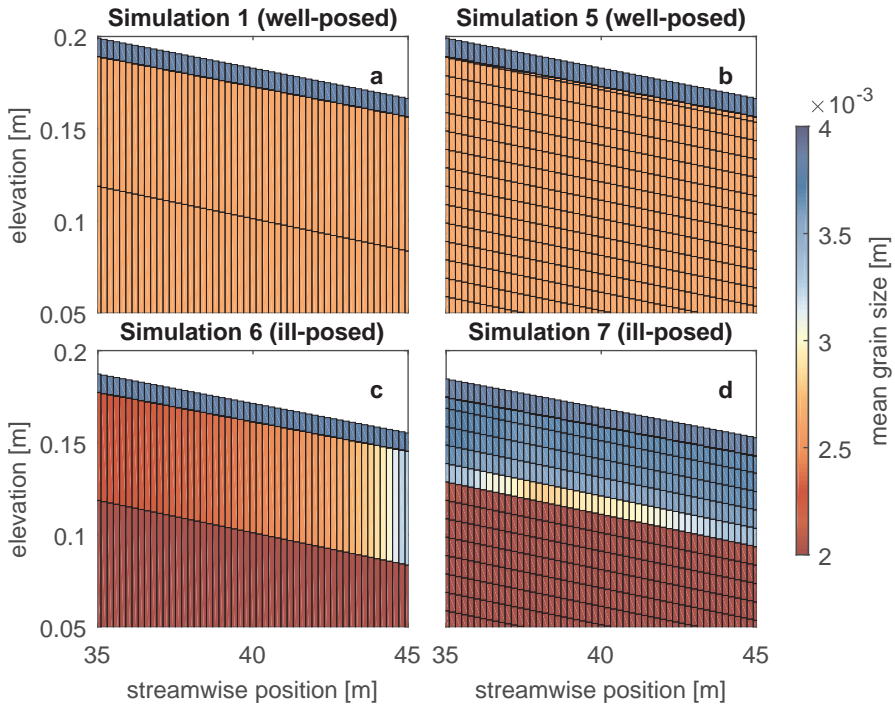


Figure 2.6: Grain size stratification at the end of: (a) Simulation 1, (b) Simulation 5, (c) Simulation 6, and (d) Simulation 7. The substrate of the ill-posed simulations coarsens unrealistically.

ill-posed cases due to the oscillatory behavior, which acts as a regularization mechanism (Section 2.5.1). A thinly discretized substrate enhances the regularization mechanism as one full layer is created with the grain size distribution of the (coarse) active layer during the aggrading phase of the oscillation. If the bed is discretized into thick layers the material transferred to the substrate will be averaged with the sediment already present in the top substrate layer. The resulting grain size distribution of the substrate may not be sufficiently coarse to prevent the model from being ill-posed.

2.6. Implications of Considering More than Two Size Fractions or an Unsteady Active Layer Thickness

To obtain an analytical expression of the eigenvalues we have restricted our analysis to mixtures of sediment composed of two size fractions and steady flow. In this section we explore the consequences of relaxing these assumptions.

2.6.1. Ill-Posed Domain of a Three-Size-Fractions Case

A model for three sediment size fractions is too complex to obtain analytical expressions of the eigenvalues. We therefore first attempt to provide insight addressing a specific case based on the results of the case for two size fractions.

The concept of a finer or coarser active layer relative to the substrate is unequivocally applicable in the case of two size fractions. However, this concept is not as straightforward for three size fractions, as it requires the definition of a mean grain size. As an extension of the results for the two size fractions case where the model can only be ill-posed in degradational conditions into a substrate finer than the active layer (assuming certain conditions on the closure relations, Section 2.3.1), we consider a situation with three size fractions which, regardless of the method to compute the mean grain size, is governed by degradation into a substrate coarser than the active layer. This happens, for instance, if the volume fraction contents in the active layer of the fine, medium, and coarse size fractions are 0.5, 0.5, and 0, respectively; and at the interface are 0.5, 0, and 0.5.

We consider a sediment mixture with the above volume fraction contents and characteristic grain sizes of the fine, medium, and coarse fraction equal to 0.001 m, 0.003 m and 0.005 m. All the other parameters are equal to the reference case (Table 2.2). This situation is elliptic as two of the eigenvalues of the system matrix are complex. Thus, in a three size fractions case the mean grain size of the sediment in the active layer relative to that at the interface is not a valid discriminant of the mathematical character of the system of equations.

Figure 2.7 shows the results of a numerical simulation based on the above parameters. The solution presents oscillations as in the previous ill-posed cases. However, the amplitude of these oscillations is now significantly smaller (compare Figure 2.7a to Figure 2.4e). A relatively large oscillation appears after approximately 3 h which entrains coarse sediment from the substrate (Figure 2.7b). During the aggradational phase of the oscillations fine sediment from the active layer is transferred to the substrate. Thus, at the end of the simulation the top part of the substrate is finer than initially (Figure 2.7c).

To illustrate the implications of this result we study the effects of discretizing the same sediment mixture into two or three sediment fractions. To discretize the sample into three sediment fractions we use characteristic grain sizes equal to 0.001 m, 0.003 m and 0.005 m and to discretize it into two sediment fractions we use 0.002 m and 0.004 m. The volume fraction content in the medium size of the three fraction mixture is equally split between the fine and coarse bins of the two fraction mixture. We vary all volume fraction contents between 0 and 1 to obtain different sediment mixtures and the flow depth (keeping the water discharge per unit width constant) between 0.15 m and 1.5 m to obtain different flow conditions. All other parameters are equal to the reference case.

Figure 2.8a-b shows the elliptic domain when the mixture is discretized into two and three size fractions, respectively. On the vertical axis we plot the difference between the mean grain size of the sediment in the active layer (D_{ma} [m]) and at the interface between the active layer and the substrate (D_{mi} [m]). Note that some situations that are well-posed when the mixture is discretized into two fractions are ill-posed when it is discretized into three fractions.

We cannot prove that the eigenvalues of the system matrix for three size fractions are always real under aggradational conditions due to the complexity of the expressions.

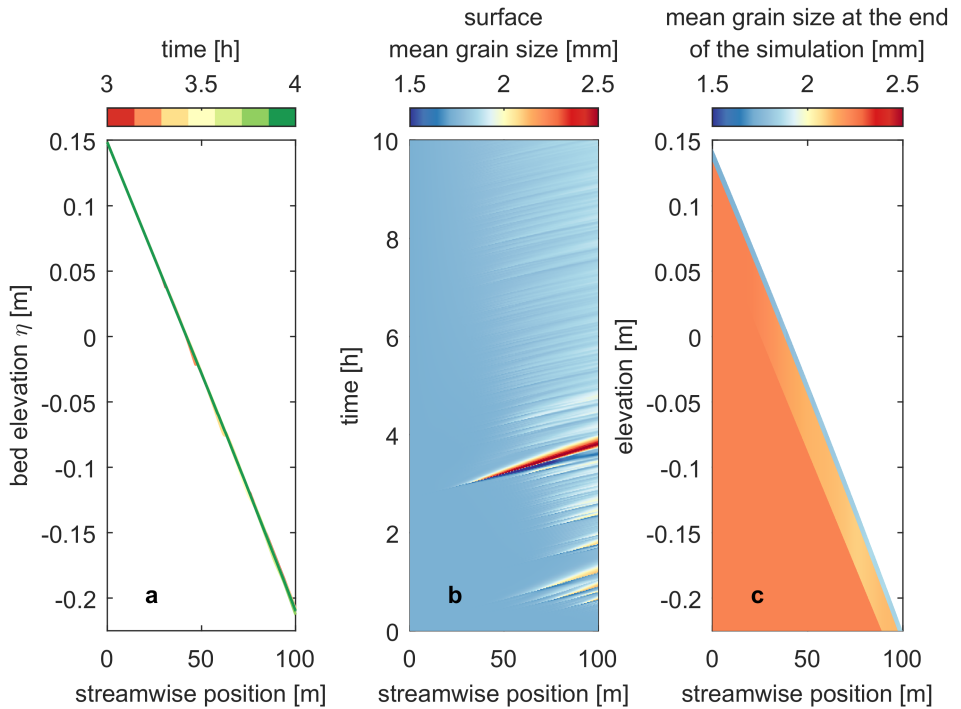


Figure 2.7: Results of an ill-posed simulation with 3 grain size fractions under degradational conditions into a substrate coarser than the active layer: (a) bed elevation at selected times, (b) surface mean grain size with time, and (c) grain size stratification at the end of the simulation.

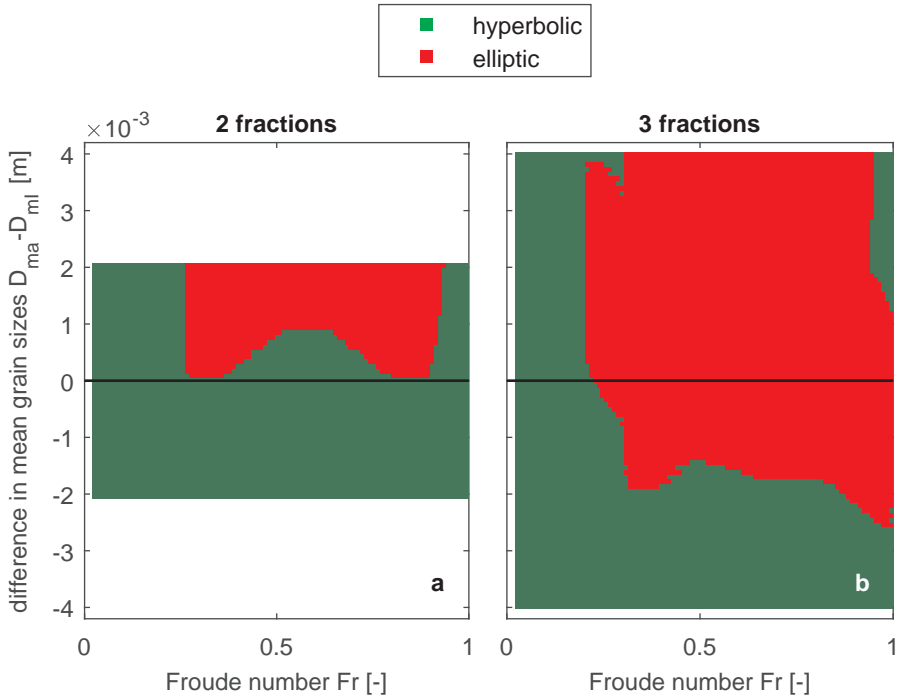


Figure 2.8: Ill-posed domain for degradational cases in which the sediment mixture is discretized into (a) two and (b) three size fractions as a function of the Froude number (Fr) and the difference between the mean grain size of the sediment in the active layer (D_{ma}) and at the interface between the active layer and the substrate (D_{ml}). When the mixture is discretized into three size fractions the model may be ill-posed under degradational conditions into a substrate coarser than the active layer.

Nevertheless, we have not obtained a single complex value in any of the aggradational tests we have conducted.

2.6.2. Effect of an Unsteady Active Layer Thickness in the Ill-Posed Domain

In this section we analyze the implications of considering a variable active layer thickness with respect to the ill-posedness of the system of equations. The flow needs to be considered unsteady to study the variability of the active layer thickness if it is related to dune growth (Section 2.3). We simplify the system assuming two sediment size fractions and negligible hiding (*Stecca et al.* (2014) and Appendix A.8).

We obtain the characteristic polynomial of the system matrix, Equation (2.11). We prove that in aggradational and degradational conditions into a substrate coarser than the active layer the characteristic polynomial has 5 real roots (Appendix A.8). Therefore the model is well-posed regardless of the unsteady active layer thickness. Regarding degradational conditions into a substrate finer than the active layer we prove that if $\lambda_b > \lambda_{s1} F_{a1} / f_1^I$, considering a variable active layer thickness increases the likelihood of the model becoming elliptic. Note that, assuming a similar order of magnitude of the bed and sorting celerities, in conditions prone to be elliptic (i.e., degradation into a substrate significantly finer than the active layer) a variable active layer thickness increases the domain in which the active layer model is elliptic. We numerically test several sets of parameters and we find no case where the model is hyperbolic if the active layer is unsteady but elliptic if it is constant (Appendix A.8). This suggests that, although we do not provide a formal proof, an unsteady active layer thickness always increases the likelihood of the model being ill-posed.

2.7. Conclusions

We have assessed the well-posedness of the equations used to model mixed sediment river morphodynamics. In particular we have studied the system formed by the flow equations (*Saint-Venant*, 1871) together with the active layer model (*Hirano*, 1971) and a simplified vertically continuous model (*Viparelli et al.*, 2017). Our findings are the following:

- Considering two size fractions and the quasi-steady flow assumption we obtain an analytical expression for the discriminant that determines whether the active layer and continuous models are ill-posed.
- Assuming (i) two size fractions, (ii) steady flow, (iii) no reverse mobility, and (iv) that under aggradational conditions the depositional flux of sediment to the substrate is entirely composed of active layer sediment, the active layer model can be ill-posed under degradational conditions into a substrate finer than the active layer only.
- The use of a hiding factor increases the likelihood of ill-posedness. Strong hiding that causes reverse mobility may cause ill-posedness also in aggradational conditions.

- Aggradational cases may be ill-posed if the depositional flux of sediment to the substrate includes bedload sediment (*Hoey and Ferguson, 1994*).
- The active layer model may be ill-posed in degradational conditions into a substrate coarser than the active layer if more than two size fractions are considered.
- Considering a variable active layer thickness associated with dune growth increases the likelihood that the active layer model is ill-posed.
- The simplified vertically continuous model can be ill-posed under both aggradational and degradational conditions. A small vertical gradient of the probability of bed elevation and volume fraction content decreases the likelihood of the model being ill-posed.
- Ill-posedness results in non-physical oscillations that grow until a maximum amplitude is reached, at which the model recovers its hyperbolic character (and becomes well-posed). The non-physical oscillations itself act as a regularizing mechanism by coarsening the substrate.

The numerical solution of an ill-posed problem may be reliable if perturbations do not have space and/or time to grow or if the consequences of the perturbations are negligible compared to the accuracy of the problem data. However, the reliability of the solution becomes subjective. This implies that it is up to the modeller to decide whether a solution is representative of the physical phenomenon under consideration.

In a well-posed model a finer grid provides more accurate results. This is opposite in ill-posed models as the growth rate of oscillations decreases with grid size. Thus, if a model is ill-posed, one may be tempted to use a larger grid size such that oscillations do not have space to grow and numerical viscosity is sufficient to suppress the consequences of ill-posedness. We do not recommend to follow this strategy because of the subjectivity of the solution.

We do not recommend discarding the active layer and vertically continuous models for modeling mixed sediment river morphodynamics. The former has proven its validity over a large range of situations (Section 2.1) and the latter is yet a simplified version of a continuous sediment conservation model. Moreover, both models are well-posed for a vast range of situations.

The ill-posedness of the system of equations is a fundamental mathematical problem independent of the numerical solver. It can only be solved by an improved set of equations that represents physical processes in a better way than existing models do. In this regard we are currently conducting laboratory experiments to investigate the physical mechanisms that are relevant under conditions in which the active layer model is ill-posed. One may want to introduce minimal changes to the active layer model to regularize it (i.e., to ensure that the model is always well-posed). In this case, the most straightforward solution is to check whether the model is ill-posed and to change the active layer thickness to a value that provides a well-posed model. One needs to be aware that this approach is not simply a numerical trick, as it implies a change of the time scale of the physical processes under consideration. Moreover, it implies a temporal change of the active layer thickness which may be relatively large and local. Preliminary simulations show that this solution

is not always stable. Another possibility may be to artificially modify the celerities without changing the actual thickness of the active layer. A similar approach has been used by *Zanotti et al.* (2007) to regularize the ill-posed two-layer shallow water model. Current work by the authors builds on this idea.

3

Ill-posedness in Modelling Two-Dimensional Morphodynamic Problems: Effects of Bed Slope and Secondary Flow

The purpose of computing is insight, not numbers.

Hamming (1962)

Rivers are like stories.

*They have a beginning, a middle, and an end.
In between, they flow. Or would flow, if we let them.*

Hass (2000)

A two-dimensional model describing river morphodynamic processes under mixed-size sediment conditions is analysed with respect to its well-posedness. Well-posedness guarantees the existence of a unique solution continuously depending on the problem data. When a model becomes ill-posed, infinitesimal perturbations to a solution grow infinitely fast. Apart from the fact that this behaviour cannot represent a physical process, numerical simulations of an

This chapter has been published in *Journal of Fluid Mechanics* **868**, (2019) 461–500.

ill-posed model continue to change as the grid is refined. For this reason, ill-posed models cannot be used as predictive tools. One source of ill-posedness is due to the simplified description of the processes related to vertical mixing of sediment. The current analysis reveals the existence of two additional mechanisms that lead to model ill-posedness: secondary flow due to the flow curvature and the gravitational pull on the sediment transport direction. When parametrising secondary flow, accounting for diffusion in the transport of secondary flow intensity is a requirement for obtaining a well-posed model. When considering the theoretical amount of diffusion, the model predicts instability of perturbations that are incompatible with the shallow water assumption. The gravitational pull is a necessary mechanism to yield a well-posed model, but not all closure relations to account for this mechanism are valid under mixed-size sediment conditions. Numerical simulations of idealised situations confirm the results of the stability analysis and highlight the consequences of ill-posedness.

3.1. Introduction

Modelling of fluvial morphodynamic processes is a powerful tool not only to predict the future state of a river after, for instance, an intervention or a change in the discharge regime (*Blom et al.*, 2017b), but also as a source of understanding of the processes responsible for patterns such as dunes, meanders, and bars (*Callander*, 1969; *Seminara*, 2006; *Colombini and Stocchino*, 2012). A framework for modelling the morphodynamic development of alluvial rivers is composed of a system of partial differential equations for modelling the flow, change in bed elevation, and change in the bed surface texture. The *Saint-Venant* (1871) equations account for conservation of water mass and momentum and enable modelling processes with a characteristic length scale significantly longer than the flow depth in one-dimensional cases. The Shallow Water Equations describe the depth-averaged flow in two-dimensional cases. Conservation of unisize bed sediment is typically modelled using the *Exner* (1920) equation and, under mixed-size sediment conditions, the active layer model (*Hirano*, 1971) accounts for mass conservation of bed sediment of each grain size.

Although widely successful in predicting river morphodynamics, a fundamental problem arises when using the above framework. Under certain conditions the description of the phenomena is not captured by the system of equations, which manifests as an ill-posed model. Models describe a simplified version of reality, which allows us to understand the key elements playing a major role in the dynamics of the system one studies (*Paola and Leeder*, 2011). Major simplifications such as reducing streamwise morphodynamic processes to a diffusion equation allow for insight on the creation of stratigraphic records and evolution on large spatial scales (*Paola et al.*, 1992; *Paola*, 2000; *Paola and Leeder*, 2011). There is a difference between greatly simplified models and models that do not capture the physical processes. A simplified model reproduces a reduced-complexity version of reality (*Murray*, 2007) and it is mathematically well-posed, as a unique solution exists that depends continuously on the data (*Hadamard*, 1923; *Joseph and Saut*, 1990). An ill-posed model lacks crucial physical processes that cause the model to be unsuitable to capture the dynamics of the system (*Fowler*, 1997). An ill-posed model is unrepresentative of a physical phenomenon, as the growth rate of infinitesimal perturbations to a solution (i.e., negligible noise from a physical perspective) tends to infinity (*Kabanikhin*, 2008). This is different from chaotic systems, in which noise similarly causes the solution to diverge but not infinitely fast (*Devaney*, 1989; *Banks et al.*, 1992).

An example of an ill-posed model is the one describing the dynamics of granular flow. The continuum formulation of such a problem depends on deriving a model for the granular viscosity. *Jop et al.* (2005, 2006) relate viscosity to a dimensionless shear rate. The model captures the dynamics of granular flows if the dimensionless shear rate is within a certain range, but otherwise the model is ill-posed and loses its predictive capabilities (*Barker et al.*, 2015). A better representation of the physical processes guaranteeing that viscosity tends to 0 when the dimensionless shear rate tends to 0 extends the domain of well-posedness (*Barker and Gray*, 2017).

Under unisize sediment and one-dimensional flow conditions, the Saint-Venant-Exner model may be ill-posed when the Froude number is larger than 6 (*Cordier et al.*, 2011). As most flows of interest are well below this limit, we can consider modelling of fluvial problems under unisize sediment conditions to be well-posed. This is not the case when

considering mixed-size sediment. Using the active layer model we assume that the bed can be discretised into two layers: the active layer and the substrate. The sediment transport rate depends on the grain size distribution of the active layer. A vertical flux of sediment occurs between the active layer and the substrate if the elevation of the interface between the active layer and the substrate changes. The active layer is well-mixed, whereas the substrate can be stratified. The above simplification of the physical processes responsible for vertical mixing causes the active layer model to be ill-posed (Ribberink, 1987; Stecca *et al.*, 2014; Chavarrías *et al.*, 2018a). In particular, the active layer is prone to be ill-posed under degradational conditions into a substrate finer than the active layer (i.e., an armoured bed (Parker and Sutherland, 1990)) for any value of the Froude number.

Previous analyses of river morphodynamic models regarding their well-posedness have been focused on conditions of one-dimensional flow (Ribberink, 1987; Cordier *et al.*, 2011; Stecca *et al.*, 2014; Chavarrías *et al.*, 2018a). Our objective is to extend these analyses to conditions of two-dimensional flow. More specifically we include the secondary flow and the bed slope effect in the analysis of the well-posedness of the system of equations.

As the flow is intrinsically three-dimensional, the depth-averaging procedure eliminates an important flow component: the secondary flow (Van Bendegom, 1947; Rozovskii, 1957). The secondary flow causes, for instance, an increase in the amplitude of meanders (Kitanidis and Kennedy, 1984) and plays an important role in bar development (Olesen, 1982). To understand the morphology of two-dimensional features, it is necessary to account for the fact that the sediment transport direction is affected by the gravitational pull when the bed slope in the transverse direction is significant (Dietrich and Smith, 1984; Seminara, 2006). This is usually done using a closure relation that sets the angle between the flow and the sediment transport directions as a function of the flow and sediment parameters (Van Bendegom, 1947; Engelund, 1974; Talmon *et al.*, 1995; Seminara *et al.*, 2002; Parker *et al.*, 2003; Francalanci and Solari, 2007, 2008; Baar *et al.*, 2018).

In this chapter we show that combining these two effects, secondary flow and sediment deflection by the bed slope, leads in some cases to an ill-posed system of equations. The chapter is organised as follows. In Section 3.2 we present the model equations describing the primary and secondary flow, as well as changes in bed elevation and surface texture. In Section 3.3 we extend the explanation of ill-posedness and relate it to growth of perturbations. We subsequently conduct a stability analysis of the equations, which indicates the conditions under which the secondary flow model and the closure relation for the bed slope effect yield an ill-posed model (Section 3.4). In Section 3.5 we run numerical simulations of idealised cases to test the validity of the analytical results and study the consequences of ill-posedness.

3.2. Mathematical Model

In this section we present the two-dimensional mathematical model of flow, accounting for secondary flow, coupled to a morphodynamic model for mixed-size sediment. We subsequently introduce the equations describing the primary flow (Section 3.2.1), the secondary flow (Section 3.2.2), and morphodynamic change (Section 3.2.3). In Section 3.2.4 we linearise the system of equations to study the stability of perturbations.

3.2.1. Primary Flow Equations

The primary flow is described using the depth-averaged Shallow Water Equations (e.g. *Vreugdenhil, 1994*):

$$\frac{\partial h}{\partial t} + \frac{\partial q_x}{\partial x} + \frac{\partial q_y}{\partial y} = 0, \quad (3.1)$$

$$\begin{aligned} & \frac{\partial q_x}{\partial t} + \frac{\partial (q_x^2/h + gh^2/2)}{\partial x} + \frac{\partial \left(\frac{q_x q_y}{h} \right)}{\partial y} + gh \frac{\partial \eta}{\partial x} - F_{sx} = \\ & = 2 \frac{\partial}{\partial x} \left(\nu h \frac{\partial \left(\frac{q_x}{h} \right)}{\partial x} \right) + \frac{\partial}{\partial y} \left(\nu h \left(\frac{\partial \left(\frac{q_x}{h} \right)}{\partial y} + \frac{\partial \left(\frac{q_y}{h} \right)}{\partial x} \right) \right) - gh S_{fx}, \end{aligned} \quad (3.2)$$

$$\begin{aligned} & \frac{\partial q_y}{\partial t} + \frac{\partial (q_y^2/h + gh^2/2)}{\partial y} + \frac{\partial \left(\frac{q_x q_y}{h} \right)}{\partial x} + gh \frac{\partial \eta}{\partial y} - F_{sy} = \\ & 2 \frac{\partial}{\partial y} \left(\nu h \frac{\partial \left(\frac{q_y}{h} \right)}{\partial y} \right) + \frac{\partial}{\partial x} \left(\nu h \left(\frac{\partial \left(\frac{q_y}{h} \right)}{\partial x} + \frac{\partial \left(\frac{q_x}{h} \right)}{\partial y} \right) \right) - gh S_{fy}, \end{aligned} \quad (3.3)$$

where (x, y) [m] are Cartesian coordinates and t [s] is the time coordinate. The variables $(q_x, q_y) = (uh, vh)$ [m²/s] are the specific water discharges in the x and y direction, respectively, where h [m] is the flow depth and u [m/s] and v [m/s] are the depth-averaged flow velocities. The variable η [m] is the bed elevation and g [m/s²] the acceleration due to gravity. The friction slopes are (S_{fx}, S_{fy}) [–] and the diffusion coefficient ν [m²/s] is the horizontal eddy viscosity. The depth-averaging procedure of the equations of motion introduces terms that originate from the difference between the actual velocity at a certain elevation in the water column and the depth-averaged velocity. We separate the contributions due to turbulent motion and secondary flow caused by the flow curvature. The contribution due to turbulent motion is accounted for by the diffusion coefficient. *Elder (1959)* derived an expression for the diffusion coefficient that accounts for the effect of turbulent motion on the depth-averaged flow assuming a logarithmic profile for the primary flow and negligible effect of molecular viscosity:

$$\nu_E = \frac{1}{6} \kappa h u^*, \quad (3.4)$$

where $\kappa = 0.41$ [–] is the von Kármán constant and $u^* = \sqrt{C_f} Q/h$ [m/s] is the friction velocity. Parameter C_f [–] is a nondimensional friction coefficient, which we assume to be constant (*Ikedo et al., 1981; Schielen et al., 1993*) and $Q = \sqrt{q_x^2 + q_y^2}$ [m²/s] is the module of the specific water discharge. In the numerical simulations we will assume the eddy viscosity to be a constant equal to the value given by ν_E in a reference state (e.g. *Falconer, 1980; Lien et al., 1999*). Appendix B.1 presents the limitations of the coefficient derived by *Elder (1959)*.

The terms (F_{sx}, F_{sy}) [m²/s²] account for the effect of secondary flow. These terms are responsible for a transfer of momentum that shifts the maximum velocity to the outer bend (*Kalkwijk and De Vriend, 1980*), as well as for a sink of energy in the secondary

circulation (Flokstra, 1977; Begnudelli et al., 2010). We deal with these terms in Section 3.2.2.

We assume a Chézy-type friction:

$$S_{fx} = \frac{C_f q_x Q}{g b^3}, \quad S_{fy} = \frac{C_f q_y Q}{g b^3}. \quad (3.5)$$

One underlying assumption of the system of equations presented above is that the vertical length and velocity scales are negligible with respect to the horizontal ones. Another assumption is the fact that the concentration of sediment (the ratio between the solid and liquid discharge) is small (below 6×10^{-3} (Garegnani et al., 2011, 2013)), such that we apply the clear water approximation.

3.2.2. Secondary Flow Equations

This section describes the equations that model secondary flow (i.e., formulations for F_{sx} and F_{sy} in equations (3.2) and (3.3)). The secondary flow velocity profile u^s [m/s] (i.e., the vertical profile of the velocity component perpendicular to the primary flow) is assumed to have a universal shape as a function of the relative elevation in the water column $\zeta = (z - \eta)/b$ [–], where z [m] is the vertical Cartesian coordinate perpendicular to x and y increasing in upward direction (Rozovskii, 1957; Engelund, 1974; De Vriend, 1977, 1981; Booij and Pennekamp, 1984). Worded differently, the vertical profile of the secondary flow is parametrised by a single value representing the intensity of the secondary flow I [m/s], such that $u^s = f(\zeta)I$. The secondary flow intensity I is the integral of the absolute value of the secondary flow velocity profile (De Vriend, 1981). Among others, Rozovskii (1957), Engelund (1974), and De Vriend (1977), derive equilibrium profiles of the secondary flow that differ in the description of the eddy viscosity, vertical profile of the primary flow, and the boundary condition of the flow at the bed. Following De Vriend (1977), we assume a logarithmic profile for the primary flow (i.e., a parabolic distribution of the eddy viscosity) and vanishing velocity close to the bed at $\zeta = \exp(-1 - 1/\alpha)$ where $\alpha = \frac{\sqrt{C_f}}{x} < 0.5$.

The depth-averaging procedure yields the integral value (along z) of the force per unit mass that the secondary flow exerts on the primary flow (De Vriend, 1977; Kalkwijk and De Vriend, 1980):

$$F_{sx} = \frac{\partial T_{xx}}{\partial x} + \frac{\partial T_{xy}}{\partial y}, \quad (3.6)$$

$$F_{sy} = \frac{\partial T_{yx}}{\partial x} + \frac{\partial T_{yy}}{\partial y}, \quad (3.7)$$

where T_{lm} [m³/s²] is the integral shear stress per unit mass in the direction l - m . Assuming a large width-to-depth ratio (i.e., $B/b \gg 1$, where B [m] is the characteristic channel width) and a mild curvature (i.e., $b/R_s \ll 1$, where R_s [m] is the radius of curvature of the streamlines), the shear stress terms are:

$$T_{xx} = -2 \frac{\beta^* I}{Q} q_x q_y, \quad (3.8)$$

$$T_{xy} = T_{yx} = \frac{\beta^* I}{Q} (q_x^2 - q_y^2), \quad (3.9)$$

$$T_{yy} = T_{yy} = 2 \frac{\beta^* I}{Q} q_x q_y, \quad (3.10)$$

where $\beta^* = 5\alpha - 15.6\alpha^2 + 37.5\alpha^3$.

The simplest strategy to account for secondary flow assumes that the secondary flow is fully developed. This is equivalent to saying that the secondary flow intensity is equal to the equilibrium value $I_c = Q/R_s$ [m/s] found in an infinitely long bend (Rozovskii, 1957; Englund, 1974; De Vriend, 1977, 1981; Booij and Pennekamp, 1983). A change in channel curvature leads to the streamwise adaptation of secondary flow to the equilibrium value (De Vriend, 1981; Ikeda and Nishimura, 1986; Johannesson and Parker, 1989; Seminara and Tubino, 1989). Booij and Pennekamp (1984) and Kalkwijk and Booij (1986) not only account for the spatial adaptation but also the temporal adaptation of the secondary flow associated with a variable discharge or tides. Here we adopt the latter strategy, which has been applied, for instance, in modelling the morphodynamics of braided rivers (Javernick et al., 2016; Williams et al., 2016; Javernick et al., 2018). The spatial and temporal adaptation of secondary flow is expressed by (Jagers, 2003):

$$\frac{\partial I}{\partial t} + \frac{q_x}{h} \frac{\partial I}{\partial x} + \frac{q_y}{h} \frac{\partial I}{\partial y} - \frac{\partial}{\partial x} \left(\nu \frac{\partial I}{\partial x} \right) - \frac{\partial}{\partial y} \left(\nu \frac{\partial I}{\partial y} \right) = S_s, \quad (3.11)$$

where S_s [m/s²] is a source term which depends on the difference between the local secondary flow intensity and its equilibrium value:

$$S_s = -\frac{I - I_c}{T_1}, \quad (3.12)$$

where T_1 [s] is the adaptation time scale of the secondary flow:

$$T_1 = \frac{L_1 b}{Q}, \quad (3.13)$$

where $L_1 = L_1^* b$ [m] is the adaptation length scale of the secondary flow, which depends on the nondimensional length scale $L_1^* = \frac{1-2\alpha}{2x^2\alpha}$ (Kalkwijk and Booij, 1986).

The radius of curvature of the streamlines is defined as (e.g. Legleiter and Kyriakidis, 2006):

$$\frac{1}{R_s} = \frac{\frac{dx}{dt} \frac{d^2y}{dt^2} - \frac{dy}{dt} \frac{d^2x}{dt^2}}{\left(\left(\frac{dx}{dt} \right)^2 + \left(\frac{dy}{dt} \right)^2 \right)^{3/2}}, \quad (3.14)$$

assuming steady flow and in terms of water discharge we obtain:

$$\frac{1}{R_s} = \frac{-q_x q_y \frac{\partial q_x}{\partial x} + q_x^2 \frac{\partial q_y}{\partial x} - q_y^2 \frac{\partial q_x}{\partial y} + q_x q_y \frac{\partial q_y}{\partial y}}{(q_x^2 + q_y^2)^{3/2}}. \quad (3.15)$$

The secondary flow model described in this section closes the primary flow model described in Section 3.2.1 given a certain bed elevation. In the following section we describe the model equations that describe changes in bed elevation as a function of the primary and secondary flow.

3.2.3. Morphodynamic Equations

We consider an alluvial bed composed of an arbitrary number N of non-cohesive sediment fractions characterised by a grain size d_k [m], where the subscript k denotes the grain size fraction in increasing order (i.e., $d_1 < d_2 < \dots < d_N$). Bed elevation change depends on the divergence of the sediment transport rate (*Exner, 1920*):

$$\frac{\partial \eta}{\partial t} + \frac{\partial q_{bx}}{\partial x} + \frac{\partial q_{by}}{\partial y} = 0, \quad (3.16)$$

where $q_{bx} = \sum_{k=1}^N q_{bxk}$ [m²/s] and $q_{by} = \sum_{k=1}^N q_{byk}$ [m²/s] are the total specific (i.e., per unit of differential length) sediment transport rates including pores in the x and y direction, respectively. The variables q_{bxk} [m²/s] and q_{byk} [m²/s] are the specific sediment transport rates of size fraction k including pores. For simplicity we assume a constant porosity and density of the bed sediment. The sediment transport rate is assumed to be locally at capacity, which implies that we do not model the temporal and spatial adaptation of the sediment transport rate to capacity conditions (*Bell and Sutherland, 1983; Phillips and Sutherland, 1989; Jain, 1992*).

Changes in the bed surface grain size distribution are accounted for using the active layer model (*Hirano, 1971*). For simplicity, we assume a constant active layer thickness L_a [m]. Conservation of sediment mass of size fraction k in the active layer reads:

$$\frac{\partial M_{ak}}{\partial t} + f_k^I \frac{\partial \eta}{\partial t} + \frac{\partial q_{bxk}}{\partial x} + \frac{\partial q_{byk}}{\partial y} = 0 \quad k \in \{1, N-1\}, \quad (3.17)$$

and in the substrate (*Chavarrías et al., 2018a*):

$$\frac{\partial M_{sk}}{\partial t} - f_k^I \frac{\partial \eta}{\partial t} = 0 \quad k \in \{1, N-1\}, \quad (3.18)$$

where $M_{ak} = F_{ak} L_a$ [m] and $M_{sk} = \int_{\eta_0}^{\eta_0 + \eta - L_a} f_{sk}(z) dz$ [m] are the volume of sediment of size fraction k per unit of bed area in the active layer and the substrate, respectively. Parameter η_0 [m] is a datum for bed elevation. Parameters $F_{ak} \in [0, 1]$, $f_{sk} \in [0, 1]$, and $f_k^I \in [0, 1]$ are the volume fraction content of sediment of size fraction k in the active layer, substrate, and at the interface between the active layer and the substrate, respectively. By definition, the sum of the volume fraction content over all size fractions equals 1:

$$\sum_{k=1}^N F_{ak} = 1, \quad \sum_{k=1}^N f_{sk}(z) = 1, \quad \sum_{k=1}^N f_k^I = 1. \quad (3.19)$$

Under degradational conditions, the volume fraction content of size fraction k at the interface between the active layer and the substrate is equal to that at the top part of the

substrate ($f_k^I = f_{sk}(z = \eta - L_a)$ for $\partial\eta/\partial t < 0$). This allows for modelling of arbitrarily abrupt changes in grain size due to erosion of previous deposits. Under aggradational conditions the sediment transferred to the substrate is a weighted mixture of the sediment in the active layer and the bed load (Parker, 1991; Hoey and Ferguson, 1994; Toro-Escobar et al., 1996). Here we simplify the analysis and we assume that the contribution of the bed load to the depositional flux is negligible (i.e., $f_k^I = F_{ak}$ for $\partial\eta/\partial t > 0$) (Hirano, 1971).

The magnitude of the sediment transport rate is assumed to be a function of the local bed shear stress. We apply the sediment transport relation by Engelund and Hansen (1967) in a fractional manner (Blom et al., 2016, 2017b) as well as the one by Ashida and Michiue (1971) (Appendix B.2).

The direction of the sediment transport (φ_{sk} [rad]) is affected by the secondary flow and the bed slope (Van Bendegom, 1947):

$$\tan \varphi_{sk} = \frac{\sin \varphi_\tau - \frac{1}{g_{sk}} \frac{\partial \eta}{\partial y}}{\cos \varphi_\tau - \frac{1}{g_{sk}} \frac{\partial \eta}{\partial x}} \quad k \in \{1, N\}, \quad (3.20)$$

where g_{sk} [—] is a function that accounts for the influence of the bed slope on the sediment transport direction and φ_τ [rad] is the direction of the sediment transport accounting for the secondary flow only:

$$\tan \varphi_\tau = \frac{q_y - h\alpha_1 \frac{q_x}{Q} I}{q_x - h\alpha_1 \frac{q_y}{Q} I}. \quad (3.21)$$

Assuming a mild curvature, uniform flow conditions, and a logarithmic profile of the primary flow, the constant α_1 [—] is (De Vriend, 1977):

$$\alpha_1 = \frac{2}{\chi^2} (1 - \alpha). \quad (3.22)$$

The effect of the bed slope on the sediment transport direction depends on the grain size (Parker and Andrews, 1985). We account for this effect setting:

$$g_{sk} = A_s \theta_k^{B_s} \quad k \in \{1, N\}, \quad (3.23)$$

where A_s [—] and B_s [—] are nondimensional parameters and θ_k [—] is the Shields (1936) stress (Appendix B.2). Different values of the coefficients A_s and B_s have been proposed (for a recent review, see Baar et al. (2018)). We consider two possibilities: (1) $A_s = 1$, $B_s = 0$ (Schielen et al., 1993) and (2) $A_s = 1.70$ and $B_s = 0.5$ (Talmon et al., 1995). In the first and simpler case, the bed slope effect is independent from the bed shear stress (Engelund and Skovgaard, 1973; Engelund, 1975). In the second, more complex, case, the bed slope effect is assumed to be dependent on the fluid drag force on the grains, which is assumed to depend on the Shields stress (Koch and Flokstra, 1981).

3.2.4. Linearised System of Equations

The system of equations describing the flow, change of bed level, and change of the bed surface texture is highly non-linear. Here we linearise the system of equations to provide

insight into the fundamental properties of the model and to study the stability of perturbations. To this end we consider a reference state that is a solution to the system of equations. The reference state is a steady uniform straight flow in the x direction over an inclined plane bed composed of an arbitrary number of size fractions. Mathematically: $h_0 = \text{ct.}$, $q_{x0} = \text{ct.}$, $q_{y0} = 0$, $I_0 = 0$, $\frac{\partial \eta}{\partial x} = \text{ct.} = \frac{-C_t q_{x0}^2}{g b_0^3}$, $\frac{\partial \eta}{\partial y} = 0$, $M_{ak0} = \text{ct.} \forall k \in \{1, N-1\}$, where ct. denotes a constant different from 0 and subscript 0 indicates the reference solution.

3

We add a small perturbation to the reference solution denoted by $'$ and we linearise the resulting system of equations. After substituting the reference solution we obtain a system of equations of the perturbed variables:

$$\frac{\partial \mathbf{Q}'}{\partial t} + \mathbf{D}_{x0} \frac{\partial^2 \mathbf{Q}'}{\partial x^2} + \mathbf{D}_{y0} \frac{\partial^2 \mathbf{Q}'}{\partial y^2} + \mathbf{A}_{x0} \frac{\partial \mathbf{Q}'}{\partial x} + \mathbf{A}_{y0} \frac{\partial \mathbf{Q}'}{\partial y} + \mathbf{B}_0 \mathbf{Q}' = 0, \quad (3.24)$$

where the vector of dependent variables is:

$$\mathbf{Q}' = [h', q'_x, q'_y, I', \eta', [M'_{ak}]]^T, \quad (3.25)$$

where the square bracket indicates the vector character.

The diffusive matrix in x direction is:

$$\mathbf{D}_{x0} = \begin{bmatrix} 0 & 0 & 0 & 0 & 0 & 0 \\ 2\nu \frac{q_{x0}}{b_0} & -2\nu & -\nu & 0 & 0 & 0 \\ 0 & 0 & -\nu & 0 & 0 & 0 \\ 0 & 0 & 0 & -\nu & 0 & 0 \\ 0 & 0 & 0 & 0 & 0 & 0 \\ 0 & 0 & 0 & 0 & 0 & 0 \end{bmatrix}, \quad (3.26)$$

where 0 denotes the zero matrix. The diffusive matrix in y direction is:

$$\mathbf{D}_{y0} = \begin{bmatrix} 0 & 0 & 0 & 0 & 0 & 0 \\ \nu \frac{q_{x0}}{b_0} & -\nu & 0 & 0 & 0 & 0 \\ \nu \frac{q_{x0}}{b_0} & -\nu & -2\nu & 0 & 0 & 0 \\ 0 & 0 & 0 & -\nu & 0 & 0 \\ 0 & 0 & 0 & 0 & \frac{\partial q_{by}}{\partial \frac{\partial \eta}{\partial y}} & 0 \\ 0 & 0 & 0 & 0 & \left[\frac{\partial q_{byk}}{\partial \frac{\partial \eta}{\partial y}} \right]_0 & -f_{k0} \left[\frac{\partial q_{by}}{\partial \frac{\partial \eta}{\partial y}} \right]_0 \end{bmatrix}. \quad (3.27)$$

The advective matrix in x direction is:

$$\mathbf{A}_{x0} = \begin{bmatrix} 0 & 1 & 0 & 0 & 0 & 0 \\ g h_0 - \left(\frac{q_{x0}}{h_0}\right)^2 & 2\frac{q_{x0}}{h_0} & 0 & 0 & g h_0 & 0 \\ 0 & 0 & \frac{q_{x0}}{h_0} & -\beta^* q_{x0} & 0 & 0 \\ 0 & 0 & -\frac{q_{x0}}{h_0^2 L_1} & \frac{q_{x0}}{h_0} & 0 & 0 \\ \frac{-q_{x0}}{h_0} \frac{\partial q_{bx}}{\partial q_x} \Big|_0 & \frac{\partial q_{bx}}{\partial q_x} \Big|_0 & 0 & 0 & 0 & \left[\frac{\partial q_{bx}}{\partial M_{al}} \Big|_0 \right] \\ \left[\frac{-q_{x0}}{h_0} \frac{\partial q_{bk}}{\partial q_x} \Big|_0 + f_{k0}^I \frac{q_{x0}}{h_0} \frac{\partial q_b}{\partial q_x} \Big|_0 \right] & \left[\frac{\partial q_{bxk}}{\partial q_x} \Big|_0 - f_{k0}^I \frac{\partial q_{bx}}{\partial q_x} \Big|_0 \right] & 0 & 0 & 0 & \left[\frac{\partial q_{bxk}}{\partial M_{al}} \Big|_0 - f_{k0}^I \frac{\partial q_{bx}}{\partial M_{al}} \Big|_0 \right] \end{bmatrix}. \quad (3.28)$$

The advective matrix in y direction is:

$$\mathbf{A}_{y0} = \begin{bmatrix} 0 & 0 & 1 & 0 & 0 & 0 \\ 0 & 0 & \frac{q_{x0}}{h_0} & -\beta^* q_{x0} & 0 & 0 \\ g h_0 & 0 & 0 & 0 & g h_0 & 0 \\ 0 & 0 & 0 & 0 & 0 & 0 \\ 0 & 0 & \frac{\partial q_{by}}{\partial q_y} \Big|_0 & \frac{\partial q_{by}}{\partial T} \Big|_0 & 0 & 0 \\ 0 & 0 & \left[\frac{\partial q_{byk}}{\partial q_y} \Big|_0 - f_{k0}^I \frac{\partial q_{by}}{\partial q_y} \Big|_0 \right] & \left[\frac{\partial q_{byk}}{\partial T} \Big|_0 - f_{k0}^I \frac{\partial q_{by}}{\partial T} \Big|_0 \right] & 0 & 0 \end{bmatrix}. \quad (3.29)$$

The matrix of linear terms is:

$$\mathbf{B}_0 = \begin{bmatrix} 0 & 0 & 0 & 0 & 0 & 0 \\ \frac{-3C_f q_{x0}^2}{h_0^3} & \frac{2C_f q_{x0}}{h_0^2} & 0 & 0 & 0 & 0 \\ 0 & 0 & \frac{C_f q_{x0}}{h_0^2} & 0 & 0 & 0 \\ 0 & 0 & 0 & \frac{q_{x0}}{h_0^2 L_1} & 0 & 0 \\ 0 & 0 & 0 & 0 & 0 & 0 \\ 0 & 0 & 0 & 0 & 0 & 0 \end{bmatrix}. \quad (3.30)$$

We assume that the perturbations can be represented as a Fourier series, which implies that they are piecewise smooth and bounded for $x = \pm\infty$. Using this assumption the solution of the perturbed system is expressed in the form of normal modes:

$$\mathbf{Q}' = \text{Re} \left(\mathbf{V} e^{i(k_{wx} + k_{wy} - \omega t)} \right), \quad (3.31)$$

where i is the imaginary unit, k_{wx} [rad/m] and k_{wy} [rad/m] are the real wave numbers in x and y direction, respectively, $\omega = \omega_r + i\omega_i$ [rad/s] is the complex angular frequency, \mathbf{V} is the complex amplitude vector, and Re denotes the real part of the solution (which we will omit in the subsequent steps). The variable ω_r is the angular frequency and ω_i the attenuation coefficient. A value of $\omega_i > 0$ implies growth of perturbations and $\omega_i < 0$ decay. Substitution of Equation (3.31) in Equation (3.24) yields:

$$[\mathbf{M}_0 - \omega \mathbf{1}] \mathbf{V} = 0, \quad (3.32)$$

where:

$$\mathbf{M}_0 = \mathbf{D}_{x0} k_{wx}^2 \mathbf{i} + \mathbf{D}_{y0} k_{wy}^2 \mathbf{i} + \mathbf{A}_{x0} k_{wx} + \mathbf{A}_{y0} k_{wy} - \mathbf{B}_0 \mathbf{i}, \quad (3.33)$$

and $\mathbf{1}$ denotes the unit matrix. Equation (3.32) is an eigenvalue problem in which the eigenvalues of \mathbf{M}_0 (as a function of the wave number) are the values of ω satisfying Equation (3.32).

The solution of the linear model provides information regarding the development of small amplitude oscillations only, but for an arbitrary wave number. For this reason the linear model is convenient for studying the well-posedness of the model, which we will assess in the following section.

3.3. Instability, Hyperbolicity, and Ill-Posedness

Ill-posedness has been related to the system of governing equations losing its hyperbolic character. Stability analysis investigates growth and decay of perturbations of a base state. The two mathematical problems may seem unrelated but in fact they are strongly linked. In this section we clarify the terms unstable, hyperbolic, and ill-posed, and present the mathematical framework that we use to study the well-posedness of the system of equations.

A system is stable if perturbations to an equilibrium state decay and the solution returns to its original state. This is equivalent to saying that all possible combinations of wave numbers in the x and y directions yield a negative growth rate (ω , Equation (3.31)). An example of a stable system in hydrodynamics is the inviscid Shallow Water Equations (iSWE) for a Froude number smaller than 2 (Jeffreys, 1925; Balmforth and Mandre, 2004; Colombini and Stocchino, 2005). In Figure 3.1a we show the maximum growth rate of perturbations to a reference solution (Case I1, tables 3.1 and 3.2) of the iSWE on an inclined plane (i.e., the first 3 equations of the complete system, Equation (3.24), with neither secondary flow nor diffusion). The growth rate is obtained numerically by computing the eigenvalues of the reduced matrix \mathbf{M}_0 (the first 3 rows and columns in Equation (3.33)) for wave numbers between 0 and 250 rad/m, which is equivalent to wavelengths ($l_{wx} = 2\pi/k_{wx}$ and equivalently for y) down to 1 cm. Figure 3.1b presents the same information as Figure 3.1a in terms of wavelength rather than wave number to better illustrate the behaviour for large wavelengths. The growth rate is negative for all wave numbers, which confirms that the iSWE for $Fr < 2$ yield a stable solution.

u [m/s]	v [m/s]	h [m]	C_f [—]
1	0	1	0.007

Table 3.1: Reference state.

A system is unstable when perturbations to an equilibrium state grow and the solution diverges from the initial equilibrium state. The growth of river bars is an example of an unstable system in river morphodynamics. A straight alluvial channel is stable if the width-to-depth ratio is sufficiently small and, above a certain threshold value, the channel

Case	model	Fr	stability	mathematical character
I1	iSWE	0.32	stable	well-posed
B1	iSWE + Exner	0.32	unstable	well-posed
I2	iSWE	2.01	unstable	ill-posed

Table 3.2: Cases of a stable well-posed model (I1), an unstable well-posed model (B1), and an ill-posed model (I2). Case I2 has the same parameter values as Case I1 but for the mean flow velocity which is equal to 6.30 m/s.

becomes unstable and free alternate bars grow (Engelund and Skovgaard, 1973; Fredsøe, 1978; Colombini et al., 1987; Schielen et al., 1993). Mathematically, an unstable system has a region, a domain in the wave number space, in which the growth rate of perturbations is positive. In Figure 3.1c-d we present the growth rate of perturbations to a reference solution consisting of uniform flow (table 3.1) on an alluvial bed composed of unisize sediment with a characteristic grain size equal to 0.001 m (Case B1, table 3.2). The sediment transport rate is computed using the relation by Engelund and Hansen (1967) (Equation (B.6)) and the effect of the bed slope on the sediment transport direction is accounted for using the simplest formulation, $g_s = 1$. Figure 3.1d confirms the classical result of linear bar theory: there exists a critical transverse wavelength (l_{wyc}) below which all perturbations decay. In our particular case $l_{wyc} = 40.2$ m. Impermeable boundary conditions at the river banks limit the possible wavelengths to fractions of the channel width B [m] such that $l_{wy} = 2B/m$ for $m = 1, 2, \dots$ (Callander, 1969). As the most unstable mode is the first one (i.e., $m = 1$, alternate bars) (Colombini et al., 1987; Schielen et al., 1993), the minimum channel width above which perturbations grow is $B_c = l_{wyc}/2 = 20.1$ m, which confirms the results of Schielen et al. (1993). Figure 3.1c highlights, as for case I1, the decay of short waves.

A particular case of instability is that in which the domain of positive growth rate extends to infinitely large wave numbers (i.e., short waves). Under this condition there is no cutoff wave number above which we can neglect the contribution of ever shorter waves with non-zero growth rates. For any unstable perturbation a shorter one can be found which is even more unstable. This implies that the growth rate of an infinitesimal perturbation (i.e., noise) tends to infinity. Such a system cannot represent a physical phenomenon, as the growth rate of any physical process in nature is bounded. A system in which the growth rate of infinitesimal perturbations tends to infinity does not have a unique solution depending continuously on the initial and boundary conditions, which implies that the system is ill-posed (Hadamard, 1923; Joseph and Saut, 1990). An example of an ill-posed hydrodynamic model is the iSWE for flow with a Froude number larger than 2. In Figure 3.1e-f we show the growth rate of perturbations to the reference solution of a case in which the Froude number is slightly larger than 2 (Case I2, table 3.2). The growth rate extends to infinitely large wave numbers, which confirms that this case is ill-posed. A model being ill-posed is an indication that there is a relevant physical mechanism that has been neglected in the model derivation (Fowler, 1997). Viscous forces regularise the iSWE (i.e., make the model well-posed) and rather than ill-posed, the viscous Shallow Water Equations become simply unstable for a Froude number larger than 2, predict-

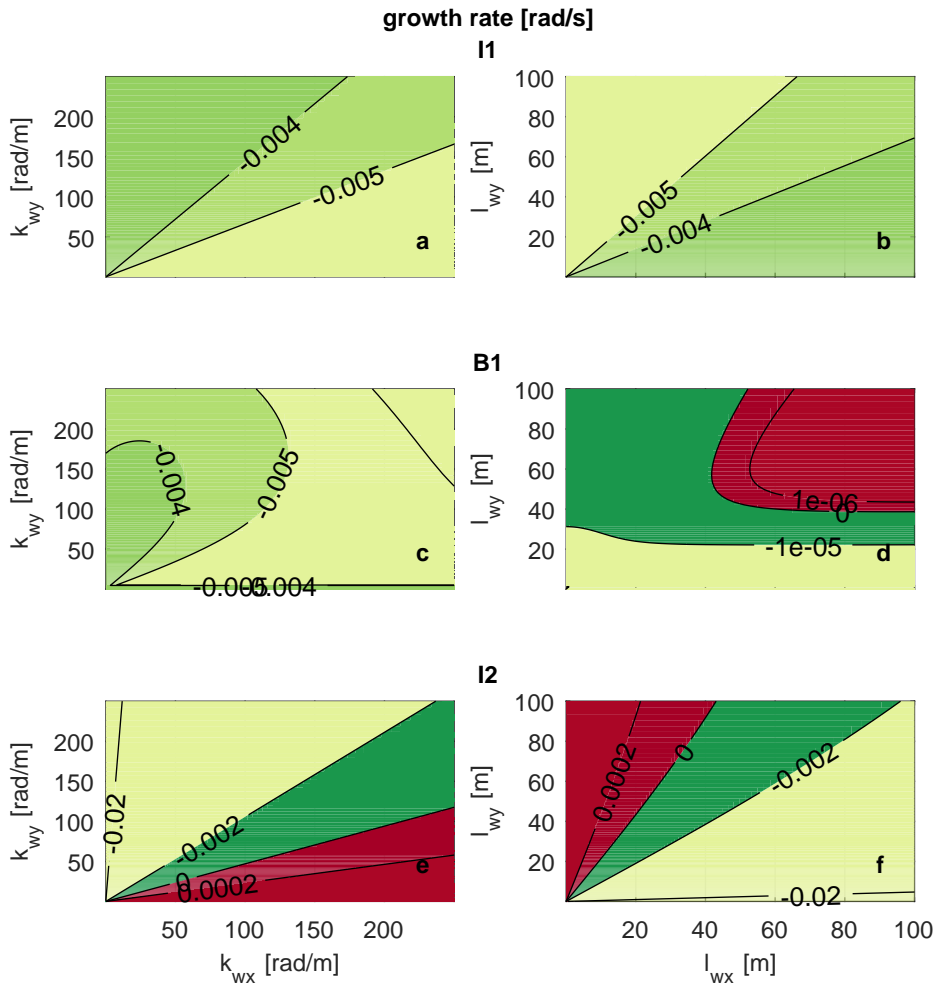


Figure 3.1: Growth rate of perturbations added to the reference case (tables 3.1 and 3.2) as a function of the wave number and the wavelength: (a)-(b) iSWE, $Fr < 2$ (Case I1, well-posed), (c)-(d) iSHE + Exner (Case B1, well-posed), and (e)-(f) iSWE, $Fr > 2$ (Case I2, ill-posed). The subplots in the two columns show the same information but highlight the behaviour for large wave numbers (left column) and for large wavelengths (right column). Red and green indicates growth and decay of perturbations, respectively.

ing the formation of roll-waves (Balmforth and Mandre, 2004; Balmforth and Vakil, 2012; Rodrigues and Zumbrun, 2016; Barker et al., 2017a,b).

Chaotic models, just as ill-posed models, are sensitive to the initial and boundary conditions and lose their predictive capabilities in a deterministic sense (Lorenz, 1963). Yet, there are two essential differences. First, chaotic systems lose their predictive capabilities after a certain time (Devaney, 1989; Banks et al., 1992), yet there exists a finite time in which the dynamics are predictable. In ill-posed models infinitesimal perturbations to

the initial condition cause a finite divergence in the solution in an arbitrarily (but fixed) short time. Second, while the dynamics of a chaotic model are not predictable in deterministic terms after a certain time, these continue to be predictable in statistical terms. For this reason, although being sensitive to the initial and boundary conditions, a model presenting chaotic properties can be used, for instance, to capture the essential dynamics and spatio-temporal features of river braiding (*Murray and Paola, 1994, 1997*). On the contrary, the dynamics of an ill-posed model cannot be analysed in statistical terms.

The numerical solution of an ill-posed problem continues to change as the grid is refined because a smaller grid size resolves larger wave numbers with faster growth rates (*Joseph and Saut, 1990; Kabanikhin, 2008; Barker et al., 2015; Woodhouse et al., 2012*). In other words, the numerical solution of an ill-posed problem does not converge when the grid cell size is reduced. This property emphasizes the unrealistic nature of ill-posed problems and shows that ill-posed models cannot be applied in practice.

We present an example of grid dependence specifically related to river morphodynamics under conditions with mixed-size sediment. We consider a case of degradation into a substrate finer than the active layer, as this is a situation in which the active layer model is prone to be ill-posed (Section 3.1). The reference state is the same as in Case B₁, yet the sediment is a mixture of two sizes equal to 0.001 m and 0.010 m. The bed surface is composed of 10 % of fine sediment. The active layer thickness is equal to 0.05 m, which in this case is representative of small dunes covering the bed (e.g. *Deigaard and Fredsøe, 1978; Armanini and Di Silvio, 1988; Blom, 2008*). Depending on the substrate composition, this situation yields an ill-posed model (*Chavarrías et al., 2018a*). When the substrate is composed of 50 % of fine sediment (Case H₁, table 3.3), the problem is well-posed and it is ill-posed when the substrate is composed of 90 % of fine sediment (Case H₂, table 3.3).

We use the software package Delft3D (*Lesser et al., 2004*) to solve the system of equations. We stress that the problem of ill-posedness is inherent to the system of equations and independent from the numerical solver. We have implemented a subroutine that assesses the well-posedness of the system of equations at each node and time step. The domain is 100 m long and 10 m wide. The downstream water level is lowered at a rate of 0.01 m/h to induce degradational conditions. The upstream sediment load is constant and equal to the equilibrium value of the reference state (*Blom et al., 2017b*). The cells are square and we consider three different sizes (table 3.3). The time step varies between simulations to maintain a constant value of the CFL number.

Case	f_1^1 [—]	Δx [m]	mathematical character
H1a	0.5	0.50	well-posed
H1b	0.5	0.25	well-posed
H1c	0.5	0.10	well-posed
H2a	0.9	0.50	ill-posed
H2b	0.9	0.25	ill-posed
H2c	0.9	0.10	ill-posed

Table 3.3: Cases showing the effect of grid cell size on the numerical solution of well-posed and ill-posed models.

Figure 3.2 presents the bed elevation after 10 h. The result of the well-posed case (H₁, left column) is grid independent. The result of the ill-posed case (H₂, right column) changes as the grid is refined and presents an oscillatory pattern characteristic of ill-posed simulations (Joseph and Saut, 1990; Woodhouse et al., 2012; Barker et al., 2015; Chavarrías et al., 2018a). The bed seems to be flat in the ill-posed simulation with a coarser grid (Figure 3.2b). This is because oscillations grow slowly on a coarse grid and require more time to be perceptible. The waviness of the bed is seen in the result of the check routine, as it predicts ill-posedness only at those locations where the bed degrades (the stoss face of the oscillations). The fact that the model is well-posed in almost the entire domain in the ill-posed case solved using a cell sizes equal to 0.25 m (H₂b, Figure 3.2d) and 0.10 m (H₂c, Figure 3.2f) does not mean that the results are realistic. Non-physical oscillations have grown and vertically mixed the sediment such that the situation is well-posed after 10 h (Chavarrías et al., 2018a). We provide a movie of Figure 3.2 in the online supplementary material.

In the above idealised situations it is evident that the oscillations are non-physical and it is straightforward to do a converge test to clarify that the solution is grid dependent. In complex domains in which several processes play a role, it is more difficult to associate oscillations to ill-posedness. Moreover, in long term applications the growth rate of perturbations may be fast compared to the frequency at which model results are assessed, which may hide the consequences of ill-posedness. If one studies a process that covers months or years (and consequently analyses the results on a monthly basis) but perturbations due to ill-posedness grow on an hourly scale, it may be difficult to identify that the problem is ill-posed. Using poor numerical techniques to solve the system of equations also contributes to hiding the consequences of ill-posedness as numerical diffusion dampens perturbations. These factors may explain why the problem of ill-posedness in mixed-sediment river morphodynamics is not widely acknowledged.

In the river morphodynamics community, the term ellipticity has been used to refer to ill-posedness of the system of equations in contrast to hyperbolicity, which is associated to well-posedness (Ribberink, 1987; Mosselman, 2005; Stecca et al., 2014; Siviglia et al., 2017; Chavarrías et al., 2018a). In general the terms are equivalent, but not always. We consider a unit vector \hat{n} in the direction (x, y) , $\hat{n} = (\hat{n}_x, \hat{n}_y)$. The system of equations (3.24) is hyperbolic if matrix $\mathbf{A} = \mathbf{A}_{x0}\hat{n}_x + \mathbf{A}_{y0}\hat{n}_y$ diagonalises with real eigenvalues $\forall \hat{n}$ (e.g. LeVeque, 2004; Castro et al., 2009). Neglecting friction and diffusive processes (i.e., $\mathbf{B}_0 = \mathbf{D}_{x0} = \mathbf{D}_{y0} = 0$), hyperbolicity implies that the eigenvalues of \mathbf{M}_0 (Equation (3.33)) are real. In this case, as the growth rate of perturbations (i.e., the imaginary part of the eigenvalues of \mathbf{M}_0) is equal to 0 regardless of the wave number, the system of equations is well-posed. As the coefficients of \mathbf{A} are real, complex eigenvalues appear in conjugate pairs. This means that if \mathbf{A} has a complex eigenvalue (i.e., the problem is not hyperbolic), at least one wave will have a positive growth rate. Neglecting friction and diffusive processes, non-hyperbolicity implies that infinitely large wave numbers have a positive growth rate. We conclude that, in the absence of diffusion and friction, lack of hyperbolicity implies ill-posedness. Note that ellipticity (i.e., the eigenvalues of \mathbf{A} are all complex) is not required for the problem to be ill-posed, as it suffices that the problem is not hyperbolic. When considering diffusion and friction even when \mathbf{A} has complex eigenvalues, the imaginary part of the eigenvalues of \mathbf{M}_0 may all be negative and the problem well-posed.

Finally, well-posedness and hyperbolicity are similar terms when dealing with problems arising from conservation laws and changes with time, as hyperbolicity guarantees the existence of wave solutions (*Lax*, 1980; *Courant and Hilbert*, 1989; *Strikwerda*, 2004; *Toro*, 2009; *Dafermos*, 2010; *Bressan*, 2011; *Dafermos*, 2016). In communities such as materials science, it is the term hyperbolicity that is associated to ill-posedness, as a smooth solution of, for instance the stress, requires that the system is elliptic (*Knowles and Sternberg*, 1975, 1976; *Veprek et al.*, 2007).

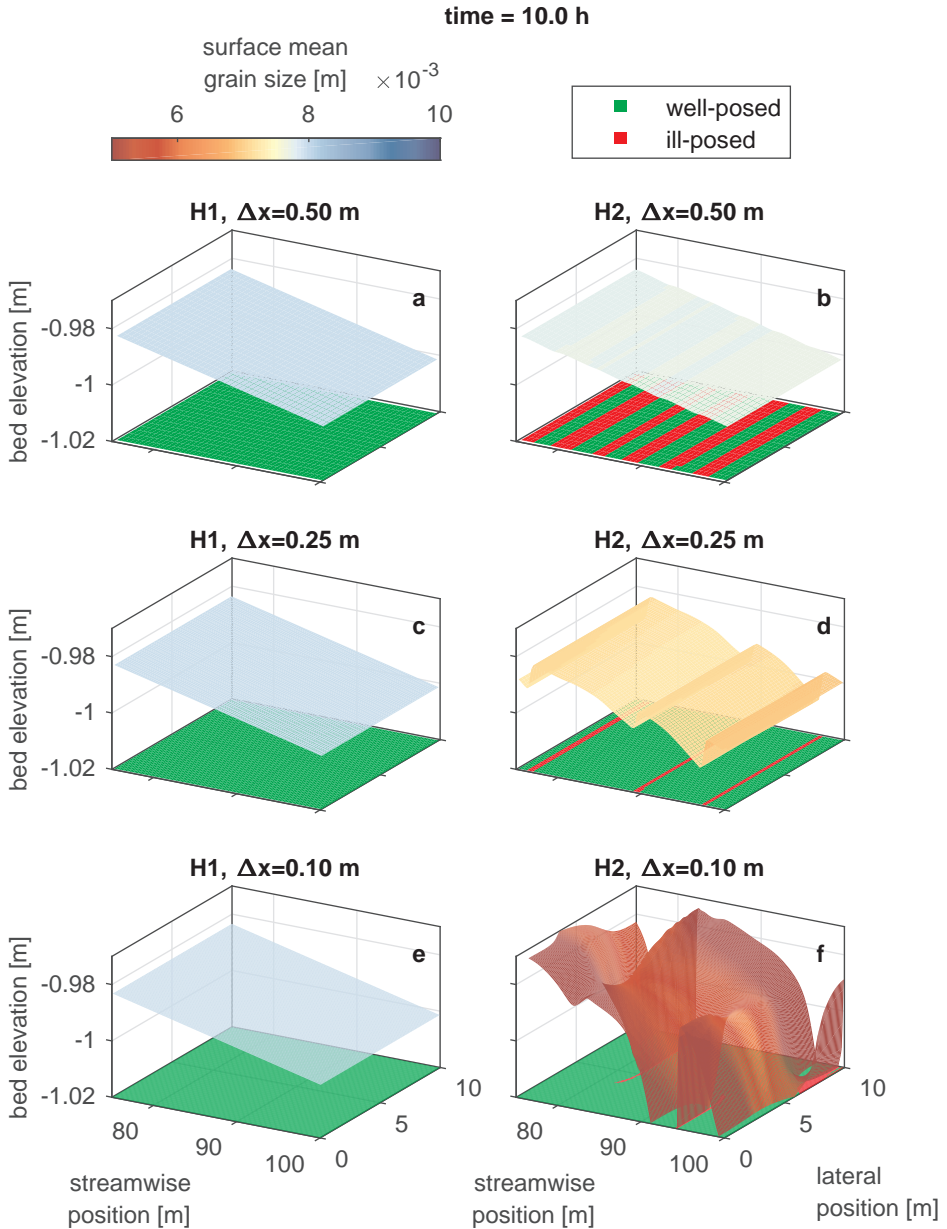


Figure 3.2: Simulated bed elevation (surface) and mean grain size at the bed surface (colour) of a well-posed case (left column, H1, table 3.3) and an ill-posed case (right column, H2, table 3.3). In each row we present the results for varying cell size. The colour of the $x - y$ plane shows the result of the routine that checks whether the conditions at each node yield a well-posed (green) or an ill-posed (red) model.

3.4. Stability Analysis

In this section we study the applicability of the system of equations to model two-dimensional river morphodynamics by means of a stability analysis of perturbations. We study the effects of the secondary flow model (Sections 3.4.1) and the bed slope (Section 3.4.2) on model ill-posedness.

3.4.1. Ill-Posedness Due to Secondary Flow

In this section we study how the stability of the system of equations is affected by the secondary flow model. To gain insight we compare three cases. In the first case we omit secondary flow. In the second and third cases we include the secondary flow model with and without considering diffusion (table 3.4).

Case	secondary flow	ν	stability	mathematical character
S1	no	ν_E	stable	well-posed
S2	yes	ν_E	unstable	well-posed
S3	yes	0	unstable	ill-posed

Table 3.4: Variations to the reference state (table 3.1) and results of the linear analysis with respect to secondary flow.

The first case is equivalent to I1 (table 3.2), yet the eddy viscosity is equal to the value derived by *Elder* (Equation (3.4)), $\nu = \nu_E = 0.0057 \text{ m}^2/\text{s}$. In Figure 3.3a-b we plot the maximum growth rate of perturbations as a function of the wave number and the wavelength, respectively. Diffusion appears to significantly dampen perturbations (compare Figure 3.1a in which diffusion is neglected to Figure 3.3a).

In the second case we repeat the analysis including the equation for advection and diffusion of the secondary flow intensity (i.e., the first 4 rows and columns of matrix \mathbf{M}_0 in Equation (3.33), Case S2, table 3.4). We observe that accounting for secondary flow introduces an instability mechanism (Figure 3.3d). For the specific conditions of the case, a growth domain appears for wavelengths between 0.7 m and 39 m long and between 0.4 m and 19 m wide. The maximum growth corresponds to a wavelength in the x and y direction equal to 1.29 m and 0.74 m, respectively. This situation is well-posed, as for large wave numbers perturbations decay (Figure 3.3c). Yet, the model is unsuitable for reproducing such instability, as it predicts growth of perturbations with a length scale of the order of the flow depth and shorter, for which the SWE model is not suited. Given the fact that we consider a depth-averaged formulation of the primary flow, processes that scale with the flow depth are not resolved by the model and consequently perturbations at that scale must decay to yield physically realistic results. Otherwise, scales of the order of the flow depth become relevant, which contradicts the assumptions of the depth-averaged formulation. To model processes that scale with the flow depth such as dune growth, it is necessary to account for non-depth-averaged flow formulations that consider, for instance, rotational flow (*Colombini and Stocchino, 2011, 2012*), or non-hydrostatic pressure (*Giri and Shimizu, 2006; Shimizu et al., 2009*).

In the third case we test the secondary flow model without accounting for diffusion

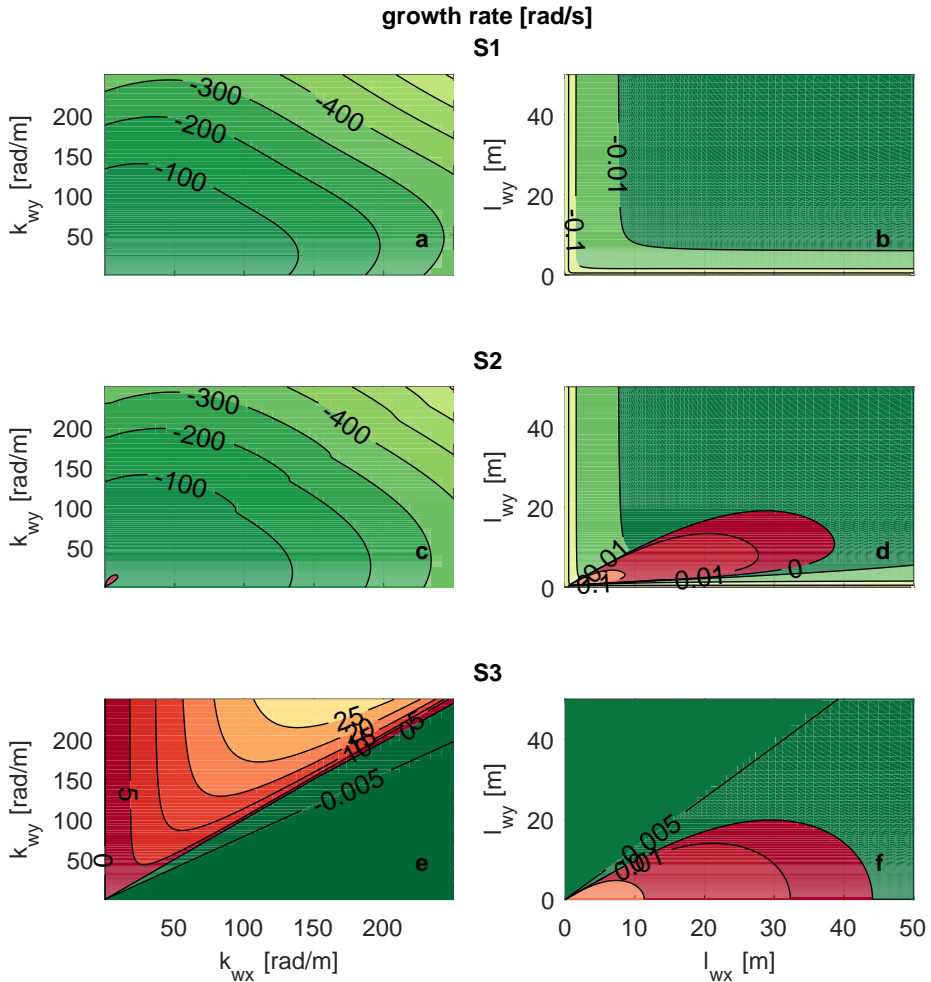


Figure 3.3: Growth rate of perturbations added to the reference case (tables 3.1 and 3.4) as a function of the wave number and the wavelength: (a)-(b) without secondary flow (Case S1, well-posed), (c)-(d) accounting for secondary flow with diffusion (Case S2, well-posed), and (e)-(f) accounting for secondary flow without diffusion (Case S3, ill-posed). The subplots in the two columns show the same information but highlight the behaviour for large wave numbers (left column) and for large wavelengths (right column). Red and green indicates growth and decay of perturbations, respectively.

in the system of equations ($\nu = 0$, Case S3, table 3.4). We observe that the instability domain extends to infinitely large wave numbers (Figure 3.3e), which implies that this model is ill-posed (Section 3.3). We now aim to prove that the Shallow Water Equations in combination with the secondary flow model without diffusion always yields an ill-posed model. To this end we obtain the characteristic polynomial of matrix \mathbf{M}_0 (Equation (3.33)). We compute the discriminant of the fourth order characteristic polynomial and

we find that for $k_{wx} < k_{wy}$ the growth rate of perturbations is positive (Appendix B.3). The model is ill-posed, as there always exists a domain of growth extending to infinitely large wave numbers in the transverse direction.

We assess how the length scale of the instability related to the secondary flow model depends on the flow parameters. For this purpose we compute the shortest wave with positive growth for a varying diffusion coefficient and flow conditions (Figure 3.4). We observe that, independently from the flow conditions, the theoretical value of the diffusion coefficient derived by *Elder (1959)* (Equation (3.4)) is insufficient for dampening oscillations scaling with the flow depth. We conclude that if the diffusion coefficient is realistic, the treatment of the secondary flow yields an unrealistic model. It is necessary to use an unrealistically large value of the diffusion coefficient to obtain a realistic depth-averaged model in which perturbations scaling with the flow depth decay.

3.4.2. Ill-Posedness Due to Bed Slope Effect

In this section we study the influence of considering the effect of the bed slope on model well-posedness. To gain insight we compare 5 cases in which we consider unisize and mixed-size sediment, various sediment transport relations, and various bed slope functions (table 3.5). We neglect secondary flow and diffusion to reduce the complexity of the problem (*Parker, 1976; Fredsøe, 1978; Colombini et al., 1987; Schielen et al., 1993*).

Our reference case is B1 (Section 3.3) which considers unisize sediment conditions, and the effect of the bed slope on the sediment transport direction is accounted for using the simplest formulation, $g_s = 1$. We have shown that this case is well-posed. Neglecting the effect of the bed slope on the sediment transport direction (Case B2, table 3.5) makes the problem ill-posed (Figure 3.5a). This illustrates that accounting for the effect of the bed slope is required for obtaining not only physically realistic but also mathematically well-posed results. We prove that the Shallow Water Equations in combination with the *Exner (1920)* equation without considering the effect of the bed slope always yields an ill-posed model by studying the growth rate of perturbations in the limit for the wave number k_{wy} tending to infinity (Appendix B.4).

Case	sediment	d_2 [m]	sed. trans.	bed slope	mathematical character
B1	unisize	-	EH	$g_s = 1$	well-posed
B2	unisize	-	EH	No	ill-posed
B3	mixed-size	0.004	AM	$g_{sk} = 1$	well-posed
B4	mixed-size	0.004	AM	$g_{sk} = 1.7\theta_k^{0.5}$	ill-posed
B5	mixed-size	0.012	AM	$g_{sk} = 1$	ill-posed

Table 3.5: Variations to the reference state (table 3.1) and results of the linear analysis with respect to the effect of the bed slope on the sediment transport direction. EH and AM refer to the sediment transport relations by *Engelund and Hansen (1967)* and *Ashida and Michiue (1971)*, respectively.

The fact that the bed slope effect dampens perturbations under unisize conditions is expected from the fact that the only diffusive term in the system of equations is $\partial q_{by}/\partial s_y$ (Equation (3.27)), where $s_y = \partial \eta / \partial y$. This term is negative and approximately equal

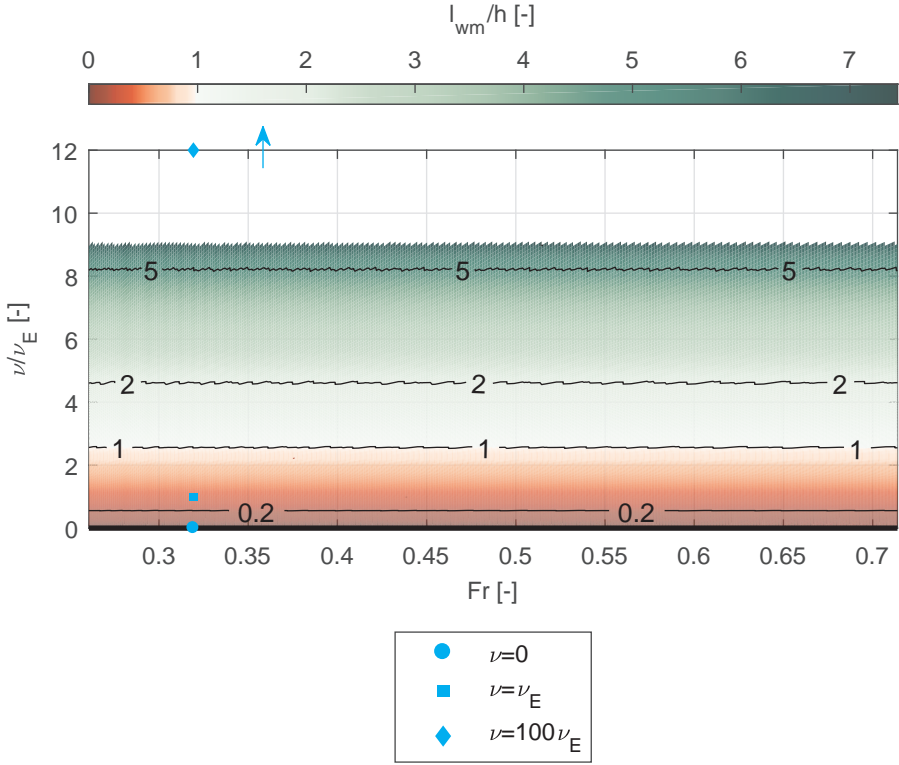


Figure 3.4: Wavelength of the shortest perturbation with positive growth rate (l_{wm}) relative to the flow depth (h) as a function of the Froude number (Fr) and the diffusion coefficient (ν) relative to the diffusion coefficient according to *Elder (1959)* (ν_E). Different flow conditions are studied varying the flow depth between 0.2 m and 1.5 m from the reference case (table 3.1). The cyan markers indicate the conditions of three numerical simulations with different values of the diffusion coefficient (Section 3.5.1). The arrow next to the diamond marker indicates that the value lies outside the figure. Red (green) colours indicate that the shortest wave length with positive growth rate are smaller (larger) than the flow depth.

to $-q_b/g_s$ for a small streamwise slope. When we consider more than one grain size, diffusive terms appear in each active layer equation. We find that these diffusive terms may be positive, which hints at the possibility of an antidiffusive behaviour, which may lead to ill-posedness. To study this possibility we compute the growth rate of perturbations of a simplified case consisting of two sediment size fractions. In the limit for the wave numbers tending to infinity, the maximum growth rate is:

$$\omega_i^{\text{lim}} = \alpha_1 (r_{y1} - d_{x1,1})^2 + \alpha_2 (r_{y1} - d_{x1,1}) + \alpha_3, \tag{3.34}$$

where α_i for $i = 1, 2, 3$ are parameters relating the flow and the sediment transport rate (Appendix B.5). The parameter r_{y1} explains how the sediment transport rate of the fine

fraction is affected by changes in the transverse bed slope:

$$r_{y1} = \frac{\partial q_{by1} / \partial s_y}{\partial q_{by} / \partial s_y}, \quad (3.35)$$

and the parameter $d_{x1,1}$ relates changes in the sediment transport rate to changes in the volume of sediment in the active layer:

$$d_{x1,1} = \frac{\partial q_{bx1} / \partial M_{a1}}{\partial q_{bx} / \partial M_{a1}}. \quad (3.36)$$

As $\alpha_1 > 0$ (Appendix B.5), there exist an interval $(r_{y1} - d_{x1,1})^- < (r_{y1} - d_{x1,1}) < (r_{y1} - d_{x1,1})^+$ in which $\omega_i^{\text{lim}} < 0$ and the model is well-posed. Outside the interval, $\omega_i^{\text{lim}} > 0$ and the problem is ill-posed.

The physical interpretation of the limit values for obtaining a well-posed model is as follows. The effect of the transverse bed slope (r_{y1}) needs to be balanced with respect to the effect of changes in surface texture ($d_{x1,1}$) to obtain a well-posed model. For a given $d_{x1,1}$, if parameter r_{y1} is too small (i.e., the bed slope effect is not sufficiently strong) perturbations in the transverse direction are not dampened and the model is ill-posed. On the other hand, for a given r_{y1} , if parameter $d_{x1,1}$ is too small (e.g. due to relatively strong hiding or in conditions close to incipient motion) perturbations in the streamwise direction do not decay and the model is also ill-posed. The critical values r_{y1}^\pm that allow for a well-posed model are shown in Appendix B.5.

In Cases B3-B5 we illustrate the possibility of ill-posedness due to the bed slope closure relation (table 3.5). In Case B3 the sediment mixture consists of two grain size fractions with characteristic grain sizes equal to 0.001 m and 0.004 m. The volume fraction content of the fine sediment in the active layer and at the interface between the active layer and the substrate is equal to 0.5. The sediment transport rate is computed using the relation developed by *Ashida and Michiue* (1971). The other parameters are equal to the reference case (table 3.1). The system is well-posed when the effect of the bed slope does not depend on the bed shear stress (Figure 3.5c). The situation is ill-posed if the effect of the bed slope depends on the bed shear stress (Case B4, table 3.5, Figure 3.5e). The cause of ill-posedness is not found in the closure relation for the bed slope effect only but in the combination of the closure relation with the flow and bed surface conditions. A case equal to B3 except for the fact that the coarse grain size is equal to 0.012 m is ill-posed (Case B5, table 3.5, Figure 3.5g).

We assess how the domain of ill-posedness due to the bed slope effect depends on the model parameters. For given sediment sizes, flow, and bed surface texture, parameter B_s (Equation (3.23)) controls the effect of the bed slope by modifying r_{y1} only. The parameter A_s (Equation (3.23)) cancels in r_{y1} and does not play a role. For this reason we study how $g_{s1}/A_s [-]$ affects the domain of ill-posedness for varying sediment properties, flow, and bed surface grain size distribution (Figure 3.6). We consider Case B3 and we vary B_s between 0 and 0.5 to vary the bed slope effect. The sediment size of the coarse fraction varies between d_1 and 0.020 m. The mean flow velocity varies between 1 m/s and 2.8 m/s. The volume fraction content of fine sediment at the bed surface varies between

0 and 1. We aim to isolate the problem of ill-posedness due to bed slope effect from the problem of ill-posedness due to a different grain size distribution at the bed surface and at the interface between the bed surface and the substrate (*Chavarrías et al.*, 2018a). For this reason, in this analysis the volume fraction content of fine sediment at the interface is equal to the one at the bed surface. Under this condition the problem can be ill-posed due to the effect of the bed slope only.

As we have shown analytically, under unisize conditions (i.e., $d_1/d_2 = 1$ or $F_{a1} = 1$ or $F_{a1} = 0$) the model is well-posed (Figure 3.6a and 3.6c). For sufficiently different grain sizes ($d_1/d_2 \lesssim 0.15$) the model is well-posed regardless of the bed slope effect but for a small range of values ($0.08 \lesssim d_1/d_2 \lesssim 0.1$). This small range of ill-posed values is associated with r_{y1} increasing for decreasing values of d_1/d_2 and acquiring a value larger than r_{y1}^+ such that the model becomes ill-posed for all values of the bed slope effect. A further decrease in d_1/d_2 increases the limit value r_{y1}^+ faster than r_{y1} such that the model becomes well-posed for all values of the bed slope effect.

An increase in the Froude number decreases the domain of well-posedness, which is explained from the fact that an increase in Froude number decreases r_{y1} while it does not modify r_{y1}^- . We have assumed steady flow in deriving ω_1^{lim} to reduce the complexity of the model such that we can find an analytical solution (Appendix B.5). This causes a physically unrealistic resonance phenomenon for $\text{Fr} \rightarrow 1$ (*Colombini and Stocchino*, 2005). In reality we do not expect that for $\text{Fr} = 1$ the model is always ill-posed regardless of the bed slope effect. Apart from the limit values in which the problem becomes unisize, the surface volume fraction content does not significantly affect the domain of ill-posedness (Figure 3.6c) as it rescales in more or less a similar way r_{y1}^\pm and r_{y1} .

While Case B₄ is ill-posed because the effect of the bed slope (r_{y1}) is small, Case B₅ is ill-posed because parameter $d_{x1,1}$ is small. The different origin of ill-posedness does not cause a significant difference in the growth rate of perturbations as a function of the wave number (Figure 3.5e-g). However, we will find out that the pattern resulting from the perturbations depends on the origin of ill-posedness.

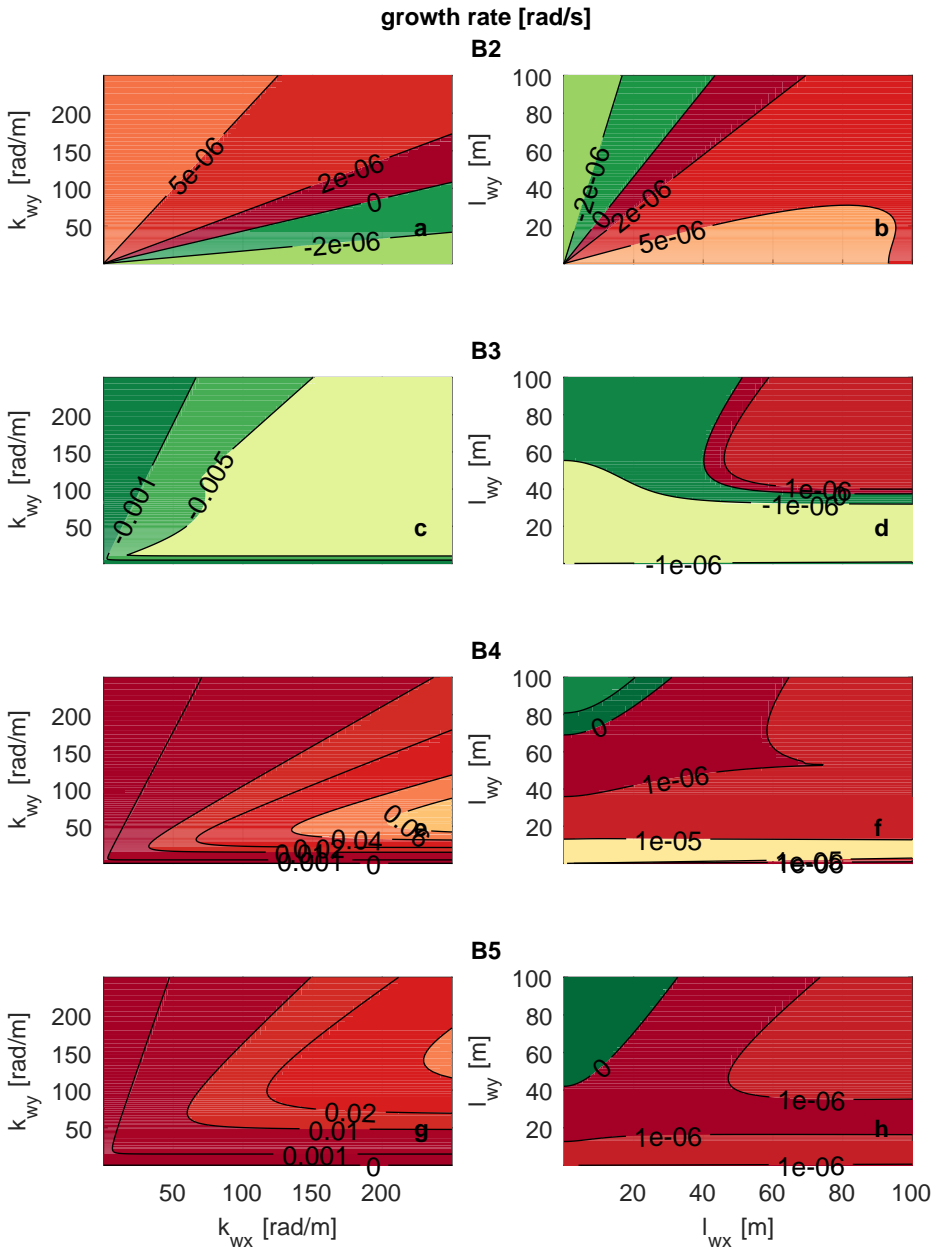


Figure 3.5: Growth rate of perturbations added to the reference case (tables 3.1 and 3.5) as a function of the wave number and the wavelength: (a)-(b) Case B2 (ill-posed), (c)-(d) Case B3 (well-posed), (e)-(f) Case B4 (ill-posed), and (g)-(h) Case B5 (ill-posed). The subplots in the two columns show the same information but highlight the behaviour for large wave numbers (left column) and for large wavelengths (right column). Red and green indicates growth and decay of perturbations, respectively.

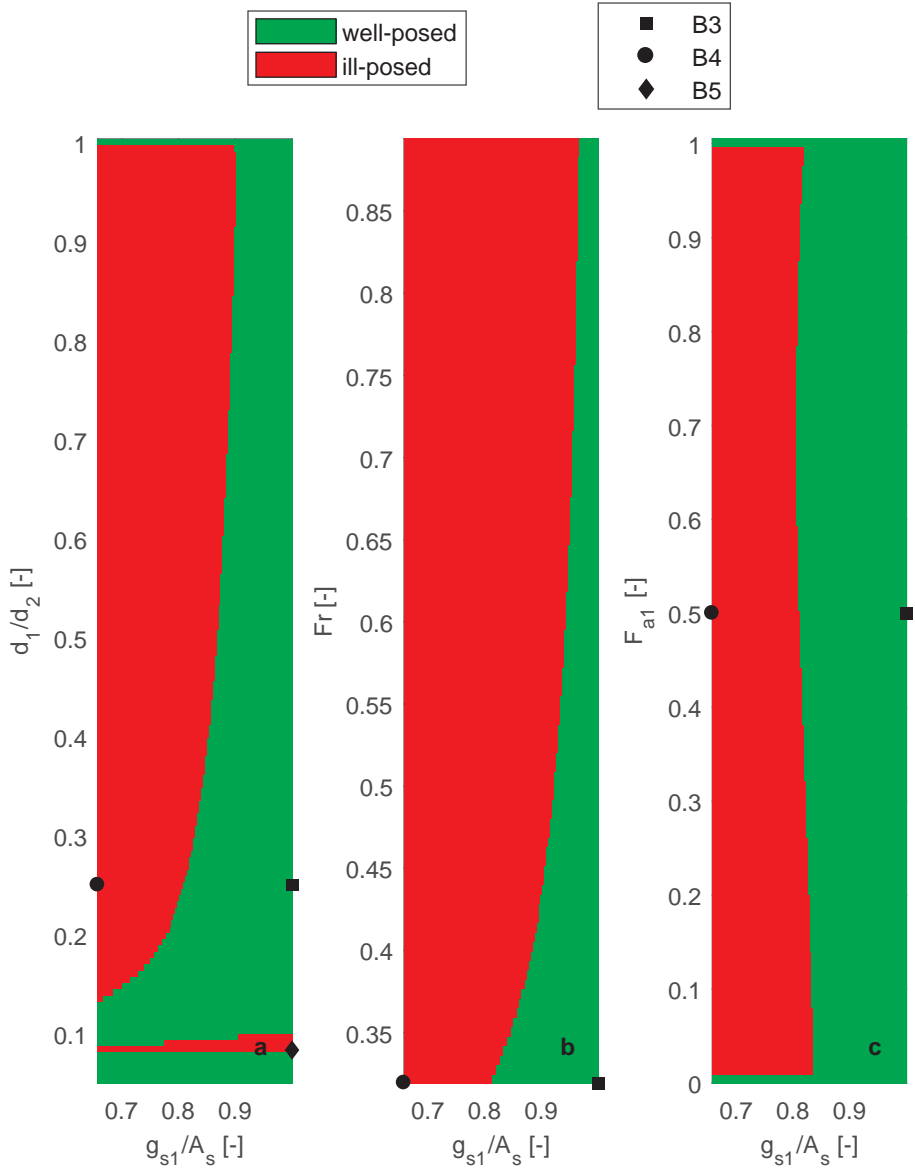


Figure 3.6: Domain of ill-posedness due to the bed slope effect under mixed-size sediment conditions: as a function of the ratio between fine and coarse sediment (a), the Froude number (b), and the volume fraction content of fine sediment in the active layer (c). The bed slope effect is measured by g_{s1}/A_s and the range of parameters is obtained by varying B_s (Equation (3.23)). The range of values of d_1/d_2 is obtained by varying d_2 . The range of values of the Froude number is obtained by varying u . The volume fraction content of fine sediment at the interface between the active layer and the substrate is kept equal to the volume fraction content of fine sediment in the active layer. The conditions represent unize sediment when $d_1/d_2 = 1$, $F_{a1} = 0$, or $F_{a1} = 1$.

3.5. Application

The results of the linear stability analysis (Section 3.4) neglect second order terms and non-linear interactions. In this section we study the effects of the terms neglected in the linear analysis and the development of perturbations by means of numerical simulations. We use the software package Delft3D (*Lesser et al.*, 2004). This exercise provides information on the consequences of ill-posedness in numerical simulations and clarifies the limitations of the current modelling approach. We study the effect of secondary flow (Section 3.5.1) and the bed slope effect (Section 3.5.2).

3.5.1. Secondary Flow

We run 5 numerical simulations with a fixed bed (i.e., only the flow is computed) to study the role of the secondary flow model and the diffusion coefficient on the ill-posedness of the system of equations. The first 3 simulations reproduce the conditions of Cases S1, S2, and S3 (table 3.4). The domain is rectangular, 100 m long and 10 m wide. We use square cells with size equal to 0.1 m. The time step is equal to 0.01 s and we simulate 10 minutes of flow. We set a constant water discharge and the downstream water level remains constant with time. The initial condition represents normal flow for the values in table 3.1 (i.e., equilibrium conditions).

The simulation not accounting for secondary flow does not present growth of perturbations as predicted by the linear analysis and remains stable with time (Figure 3.7a). We observe growth of perturbations when we account for secondary flow with the diffusion coefficient derived by *Elder* (1959) (Figure 3.7b). The results are physically unrealistic as the flow depth presents variations of up to 7 % of the normal flow depth and the length scale of perturbations is smaller than the flow depth. We have not introduced any perturbation in the initial or boundary conditions which implies that perturbations grow from numerical truncation errors. This supports the fact that the simulation is physically unrealistic. The case with a diffusion coefficient equal to 0 is ill-posed and the solution presents unreasonably large oscillations (Figure 3.7c). These numerical results confirm the results of the linear stability analysis.

In the fourth simulation we set a diffusion coefficient 100 times larger than the one derived by *Elder* (1959) (Figure 3.7d). Under this condition the linear analysis predicts all short waves to decay (diamond in Figure 3.4). These numerical results confirm the linear theory. The last simulation is equal to Case S2 except for the fact that we use a coarser grid ($\Delta x = \Delta y = 1$ m). In this case the numerical grid is not sufficiently detailed for resolving the perturbations due to secondary flow and the simulation is stable (Figure 3.7e). This last case highlights an important limitation of a physically unrealistic model. Although Case S2 is mathematically well-posed, the solution presents similarities with ill-posed cases in the sense that a refinement of the grid causes non-physical oscillations to appear.

3.5.2. Bed Slope Effect

In this section we focus on the consequences of accounting for the bed slope effect on the mathematical character of the model. To this end we run 5 more numerical simulations without accounting for secondary flow and updating the bed (i.e., accounting for mor-

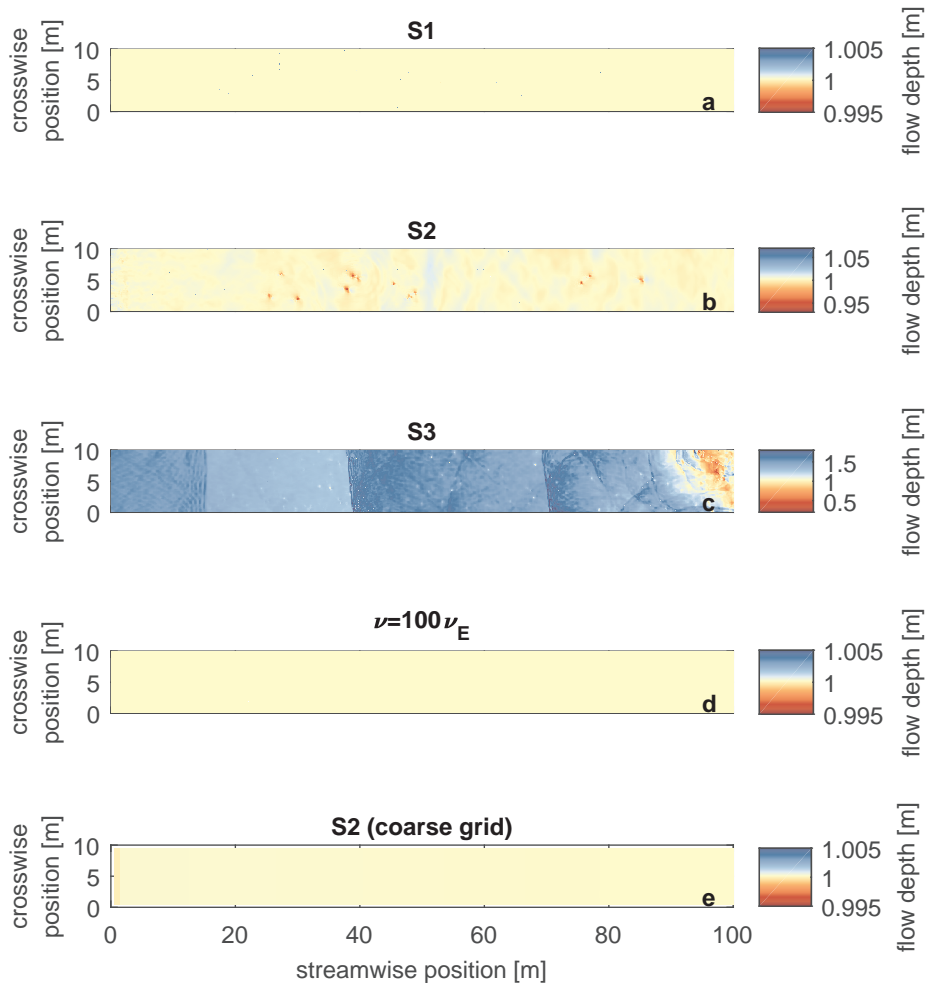


Figure 3.7: Flow depth at the end of the simulations: (a) without accounting for secondary flow (Case S1), (b) setting $\nu = \nu_E$ (Case S2), (c) setting $\nu = 0$ (Case S3), (d) setting $\nu = 100\nu_E$, and (e) setting $\nu = \nu_E$ using a coarser numerical grid (Case S2). The colour map is adjusted for each case and centred around the initial and equilibrium value ($h = 1$ m).

phodynamic change). The simulations reproduce Cases B1-B5 (table 3.5). We simulate 8 h using a time step $\Delta t = 0.1$ s.

We have proved that accounting for the effect of the bed slope makes a unisize simulation well-posed (Section 3.4.2 and Figure 3.1c). The numerical solution of this case (B1, table 3.2) is stable and perturbations do not grow (Figure 3.8a). Moreover, no alternate bars appear as the channel width is below the critical value (Section 3.3). Perturbations grow when the effect of the bed slope is not taken into account (Case B2, Figure 3.8b),

which confirms that this case is ill-posed.

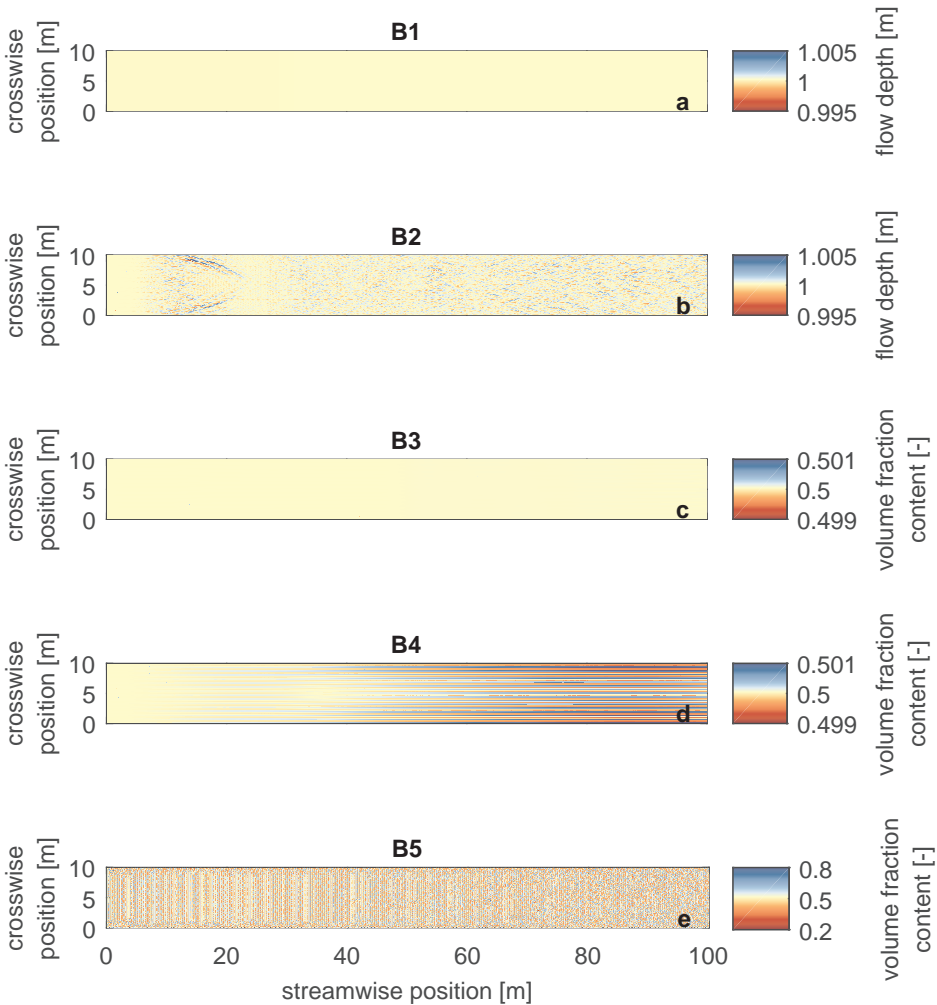


Figure 3.8: Flow depth at the end of the simulations of: (a) Case B1, (b) Case B2; and volume fraction content of fine sediment in the active layer: (c) Case B3, (d) Case B4, (e) Case B5. The colour map is adjusted for each case and centred around the initial and equilibrium value.

The mixed-size sediment conditions of Case B3 yield a well-posed model (Figure 3.5e) and the simulation is stable (Figure 3.8c). On the other hand, the ill-posed cases B4 and B5 present growth of unrealistic and non-physical perturbations (Figure 3.8d-e). While the growth of perturbations in Case B5 seems random, in Case B4 we observe a clear pattern. Moreover, oscillations have grown significantly faster in Case B5 than in Case B4. While after 8 h the changes in volume fraction content at the bed surface are of the order of 10^{-3}

in Case B₄, these are of order 1 in Case B₅.

The fact that oscillations grow faster in Case B₅ than in Case B₄ is related to the different origin of ill-posedness. While Case B₄ is ill-posed because the effect of the bed slope is not sufficiently strong (i.e., $r_{y1} < r_{y1}^-$), Case B₅ is ill-posed because changes in the sediment transport rate due to changes in the volume of fine sediment in the active layer are too small (i.e., $r_{y1} > r_{y1}^+$). The first case is closely linked to the lateral direction, in which sediment transport is initially zero. The fact that initially the lateral sediment transport rate is zero limits the rate at which lateral changes occur. In the second case perturbations are linked to the streamwise direction, in which the sediment transport rate initially is non-zero, which enhances the rate at which changes develop.

3.6. Discussion

The origin of the instability due to secondary flow is found in the source term (S_s in Equation (3.11)). As the source term depends on the flow curvature, the source term is 0 in a straight flow. A small perturbation in the flow causes the flow to curve. The flow curvature causes a source of secondary flow intensity, which further increases the flow curvature, causing a positive feedback. The flow curvature is largest for the smallest perturbations, which explains why the model is ill-posed if a dampening mechanism (i.e., diffusion) is not taken into account. This destabilizing mechanism may seem plausible to explain secondary flow circulation observed in straight channels (*Nikuradse, 1930; Brundrett and Baines, 1964; Nezu and Nakagawa, 1984; Gavrilakis, 1992*). However, secondary flow in a straight channel can only be caused by anisotropy of turbulence (*Einstein and Li, 1958; Gessner and Jones, 1965; Bradshaw, 1987; Colombini, 1993*), which is not included in the model for secondary flow. For this reason, the secondary flow model must predict decay of secondary flow intensity in case of straight flow. Diffusion of secondary flow intensity causes decay of perturbations, but the theoretical diffusion coefficient derived by *Elder (1959)* appears to be insufficient to dampen perturbations.

The advection equation of the secondary flow intensity was initially derived for steady decaying secondary flow on a straight reach after a bend neglecting the effect of diffusion (*De Vriend, 1981*). It is assumed that the same advective behaviour is valid for a varying curvature (*De Vriend, 1981; Olesen, 1982*) and in an unsteady situation (*Booij and Pennekamp, 1984*). These assumptions have, to our knowledge, not been tested. Moreover, secondary flow affects the vertical profile of the primary flow. This feedback mechanism, which limits the development of secondary flow (*Blanckaert and De Vriend, 2004; Blanckaert, 2009*), is not included in the model. *Blanckaert and de Vriend (2003), Blanckaert and Graf (2004)* and *Ottevanger et al. (2013)* propose non-linear models that take into consideration this mechanism. We expect that accounting for the feedback mechanism yields a well-posed model.

The feedback mechanism between the secondary and the primary flow may be seen as an increase of diffusivity, as it causes an enhanced momentum redistribution. For a situation in which the non-linear model for the secondary flow appears to be excessively expensive in computational terms, a diffusion coefficient depending on the secondary flow intensity would (partially) account for the enhanced momentum redistribution and provide a well-posed and realistic model.

We have assumed that the diffusion coefficient is constant and equal in all directions, which is a crude approximation, as in the streamwise direction diffusion is larger than in the transverse direction (Appendix B.1). It would be interesting to study the effect of anisotropic diffusion, however, we do not expect that this will significantly alter our results. This is because a larger diffusion coefficient in the streamwise direction will not alter the most unstable wavelength in the lateral direction. For this reason the shortest unstable waves remain to be of the order of the flow depth.

The non-linear relation between the flow and the sediment transport rate causes the growth of perturbations in bed elevation. Worded differently, a deep flow attracts the flow and vice versa, which enhances the growth of perturbations. This mechanism is counteracted by the bed slope effect, which causes deep parts to fill in. In this sense, it seems logical that it is necessary to account for bed slope effects to obtain a well-posed model. This may be confirmed by the facts that *Parker (1976)*, by not considering the bed slope effect, found that all streams tend to form bars and, similarly, *Olesen (1982)* concluded that “the stream will develop an infinite number of submerged bars”. From our point of view the fact that all streams seem to be unstable and develop an infinite number of submerged bars is a consequence of the model being ill-posed. Our analysis shows that the bed slope effect is a crucial physical process in analysing two-dimensional morphodynamic processes.

Nevertheless, the numerical simulations by *Qian et al. (2016)* of bar development without accounting for the bed slope effect do not show unrealistic oscillatory behaviour as is characteristic of ill-posedness. Yet, there is an essential difference between their model and the one we analyse here. We do not model the interaction between the sediment in the bed and the sediment in transport as we assume that the sediment transport rate adapts instantaneously to changes in the flow (i.e., the sediment transport rate depends on the flow variables only). Essentially, sediment in transport is not conserved and bed elevation and surface texture changes depend on the divergence of the sediment transport rate at capacity conditions. *Qian et al. (2016)* account for the conservation of mass of the sediment in transport and use an entrainment-deposition formulation for modelling bed elevation and surface texture changes (*Parker et al., 2000*). In this formulation changes depend on the difference between the rate at which sediment is entrained from the bed and at which it is deposited on the bed. The fact that their model does not show symptoms of ill-posedness, while the effect of the bed slope is not taken into consideration, raises the question whether the entrainment-deposition formulation in combination with mass conservation of the sediment in transport is responsible, like the bed slope effect, for a mechanism that counteracts growth of perturbations in bed elevation. If the model used by *Qian et al. (2016)* is indeed well-posed, the effect of the bed slope may be a crucial process only when mass conservation of the sediment in transport is not considered.

Lanzoni and Tubino (1999) investigated the development of alternate bars under mixed-size sediment conditions using a model similar to the one we apply here. They assumed secondary flow to be negligible and considered a different set of closure relations for friction, the sediment transport rate, and the effect of the bed slope. Under the conditions they studied, they found that, similarly to the unisize case, growth of perturbations occurs if the width-to-depth ratio is above a critical value. This implies that they found that their model is well-posed, as short wave length perturbations decay. Given that the essence of

the closure relations they considered is the same as the ones considered here and there is no fundamental difference, we suppose that their model may become ill-posed if different conditions are studied (i.e., different flow or sediment parameters). This is because well-posedness is not related to the model equations only, but also to the conditions in which the model is applied.

The bed slope effect (represented by the parameter r_{y1}) needs to be balanced with respect to the effect of changes in the bed surface grain size distribution (represented by $d_{x1,1}$) to yield a well-posed model. The balance depends on the flow and bed conditions. For this reason, a particular closure relation may yield an ill-posed model in some subdomain of a simulation and a well-posed model in some other subdomain. It is necessary to further study the development of the transverse bed slope under mixed-size sediment conditions (e.g. *Baar et al.*, 2018) to obtain a universally applicable closure relation.

Overall, there are three causes of ill-posedness of the model: (1) the secondary flow parametrisation, (2) the closure relation for the bed slope effect, and (3) the representation of the vertical mixing processes when using the active layer model (*Ribberink*, 1987; *Chavarrías et al.*, 2018a). We summarise all the conditions in which the model may become ill-posed in Figure 3.9.

Only in idealised simulations it is straightforward to relate instability of the system of equations to ill-posedness. We advocate for an *a priori* test of whether the system of equations is well-posed or ill-posed, especially when dealing with mixed-size sediment cases. If at some time a location in the model becomes ill-posed, the model results should be carefully evaluated. The fact that some domain area has always been well-posed does not guarantee a unique solution, as oscillations caused by upstream or downstream ill-posed areas propagate through the domain. Similarly, the fact that the entire domain is well-posed at some time is no guarantee of a unique solution, as past oscillations due to ill-posedness affect the present solution.

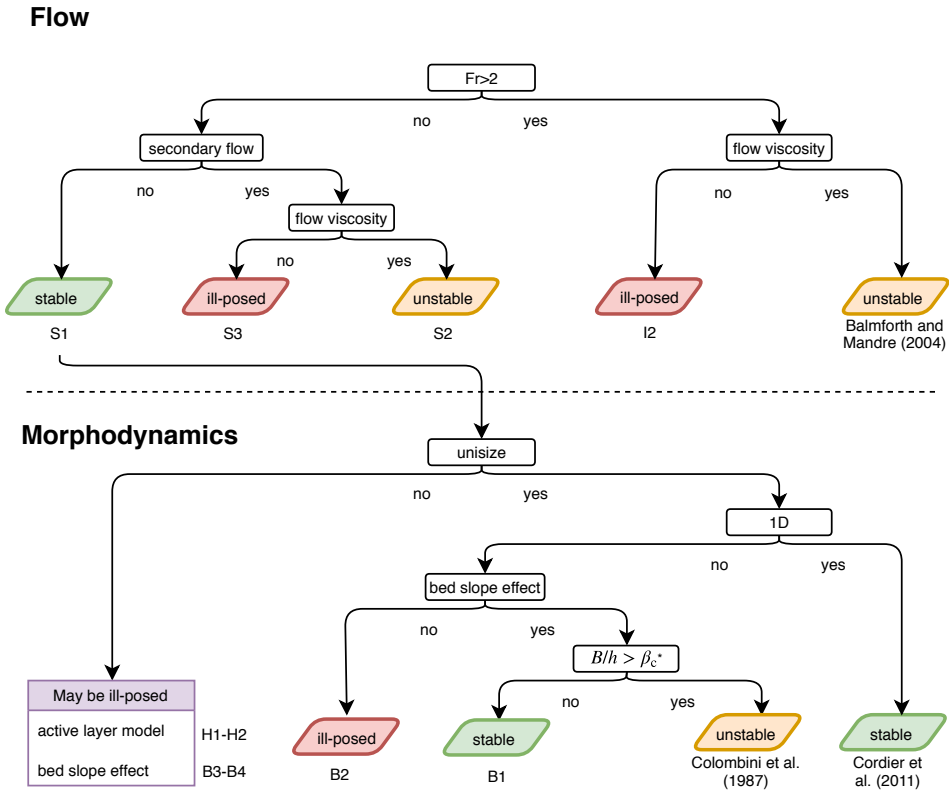


Figure 3.9: Conditions in which the flow model (top) and the morphodynamic model (bottom) is stable, unstable, or ill-posed. The code below the model type (e.g., S1) indicates an example case of such a situation. See tables 3.2, 3.3, 3.4, and 3.5 for an explanation of the cases S1-3, B1-4, H1-2, and I2. * Parameter β_c denotes the critical width-to-depth ratio (Engelund and Skovgaard, 1973; Colombini et al., 1987; Schielen et al., 1993).

3.7. Conclusions

We have studied a two-dimensional system of equations used to model mixed-size river morphodynamics as regards to its well-posedness. The model is based on the depth-averaged Shallow Water Equations in combination with the *Exner* (1920) and active layer (Hirano, 1971) equations to model bed elevation and surface texture changes, respectively. In particular we have focused on modelling of the secondary flow induced by flow curvature and the effect of the bed slope on the sediment transport direction, which causes particles to deviate from the direction of the bed shear stress.

By means of a linear stability analysis of the system of equations we find that:

- The parametrisation accounting for secondary flow yields an ill-posed model if diffusion is not accounted for.
- The theoretical amount of diffusion due to depth-averaging the vertical profile of

the primary flow (*Elder, 1959*) yields a well-posed model but it predicts growth of perturbations that are incompatible with the shallow water assumption.

- The effect of the bed slope on the direction of the sediment transport is a necessary mechanism for the model being well-posed. Yet, a different modelling strategy accounting for conservation of the sediment in transport and an entrainment-deposition formulation may yield a well-posed model without accounting for the effect of the bed slope.
- Not all closure relations accounting for the bed slope effect are valid under mixed-size sediment conditions. There needs to be a balance between the effect of the bed slope and the effect of the streamwise variation of grain size distribution on the sediment transport rate.

Numerical simulations of idealised cases confirm the above results of the linear stability analysis.

4

A Regularization Strategy for Modelling Mixed-Sediment River Morphodynamics

*It is important to rethink the notion
that the best ideas reliably rise to the top.*

Poole (2016)

*Si (como afirma el griego en el Cratilo)
El nombre es arquetipo de la cosa,
En las letras de rosa está la rosa
Y todo el Nilo en la palabra Nilo.*

Borges (1964)

A notable drawback in mixed-size sediment morphodynamic modeling is the fact that the most commonly used mathematical model in this field (i.e., the active layer model (Hirano, 1971)) can be ill-posed under certain circumstances. Under these conditions the model loses its predictive capabilities, as negligible perturbations in the initial or boundary conditions produce significant differences in the solution. In this chapter we propose a preconditioning method that regularizes the model to recover well-posedness by altering the time scale of the sediment mixing processes. We compare results of the regularized model to data from four new laboratory experiments conducted under conditions in which the active layer model is ill-posed. The

This chapter has been published in *Advances in Water Resources* 127, (2019) 291–309.

regularized active layer model captures the change of bed elevation and surface texture averaged over the passage of several bedforms. Neither the active layer model nor the regularized one account for small scale changes due to individual bedforms.

4.1. Introduction

The presence of mixed-size sediment is a key feature of rivers. Sediment sorting patterns develop in the streamwise direction (e.g., the characteristic downstream fining profile (Sternberg, 1875)), in the transverse direction (e.g., bend sorting (Allen, 1970)), and in the vertical direction (e.g., bed armoring (Parker and Klingeman, 1982) and dune sorting (Blom *et al.*, 2003)). Modeling applications in which the mixed-size character of river morphodynamics is not negligible mandate the use of a suitable continuity model accounting for mass conservation of each of the considered sediment size fractions. Hirano (1971) was the first to develop a mixed-sediment continuity model. He assumed that the river bed can be vertically divided into an active top part (the active layer), which interacts with the flow, and an inactive substrate. In the model, sediment transport and friction depend on the texture of the active layer, whereas the sediment in the substrate only plays a role if net aggradation creates new substrate sediment or net degradation leads to the entrainment of substrate sediment into the active layer.

Although it has been fruitfully used to represent physical phenomena related to mixed-sediment for nearly half a century (see Chavarrías *et al.* (2018a)), the active layer model suffers from a drawback. Under certain conditions it becomes ill-posed (Ribberink, 1987; Stecca *et al.*, 2014; Chavarrías *et al.*, 2018a). A model is ill-posed if a unique solution does not exist, or if the solution does not depend continuously on the initial and boundary conditions (Hadamard, 1923). If a model is ill-posed, infinitesimal variations in the initial or boundary conditions yield a significant deviation of the solution within an infinitesimal time (Hadamard, 1923). When solving the mathematical model by numerical approximations, perturbations in the initial and boundary conditions simply arise by truncation errors. This makes an ill-posed model unsuitable in practice.

The problem of ill-posedness arises from an inaccurate representation of the physical processes (Joseph and Saut, 1990). For instance, a two-fluid model for incompressible and inviscid flow in two layers with a velocity discontinuity is ill-posed (Kelvin, 1871; Von Helmholtz, 1868). It is regularized (i.e., becomes well-posed) if viscous effects are taken into account (Joseph and Saut, 1990). From this perspective, the preferred approach to regularize the active layer model would be the development of a new model that includes those physical mechanisms that are not accounted for by the active layer model.

There exist alternatives to the active layer that typically aim to improve the physical description of sediment mixing process. Ribberink (1987) introduced a second layer to account for the mixing due to dunes exceptionally larger than the average dune height. Besides producing a vertical sorting profile that better reproduces the results of a laboratory experiment (Blom, 2008), Ribberink's two-layer model makes the occurrence of ill-posedness less likely, although it does not completely avoid it (Sieben, 1994). Luu *et al.* (2004, 2006) proposed a model in which the active layer is replaced by the sediment transport layer representing the sediment in transport rather than the sediment at the bed surface. The thickness of the sediment transport layer is estimated with a closure relation such as the one developed by Egashira and Ashida (1992). Although conceptually different, the model by Luu *et al.* (2004, 2006) is mathematically equivalent to the active layer model, which implies that it can also be ill-posed.

Blom and Parker (2004) and Blom *et al.* (2006, 2008) developed a model in which both bed elevation and bed grain size distribution are treated using a vertically continuous for-

mulation (*Parker et al.*, 2000). This implies that there is no distinction between the active and inactive part of the bed. The model by Blom and coauthors satisfactorily describes the vertical stratigraphy due to dunes at laboratory scale, but it requires a time step too small to be applicable at large scale. Moreover, its well-posedness has not been studied. Simplifying the continuous framework proposed by *Parker et al.* (2000), the vertically continuous model by *Viparelli et al.* (2017) overcomes the need for a small time step. Although applicable at large spatial and temporal scales, their model does not solve the problem of ill-posedness (*Chavarrías et al.*, 2018a).

Given the facts that: (a) there is not yet a practically feasible alternative to the active layer model, (b) the active layer model remains well-posed over a large range of applications (*Chavarrías et al.*, 2018a), and (c) it is a computationally cheap model implemented in several software packages, here our objective is to develop a strategy to avoid ill-posedness while maintaining the conceptual framework of the active layer model. To this end, we develop a regularization strategy that recovers well-posedness of the active layer model and we conduct 4 laboratory experiments under conditions in which the active layer model is ill-posed to obtain data to which we compare the results of our regularized model.

The chapter is organized as follows. In Section 4.2 we review strategies for regularizing ill-posed models. In Section 4.3 we present the regularization strategy. Section 4.4 presents the laboratory experiments and Section 4.5 focuses on the numerical runs to reproduce the experimental results. In Section 4.6 we discuss the limitations of the regularization strategy, as well as other possible modeling strategies.

4.2. Overview of Regularization Techniques

In this section we review techniques used to regularize ill-posed problems. Propagation problems are most completely mathematically represented by a set of partial differential equations constituting an initial value problem. In these problems an initial state changes with time subject to conditions at the boundaries of the domain. The matrix-vector formulation provides a compact expression of the set of equations (e.g., *Lyn and Goodwin*, 1987; *Courant and Hilbert*, 1989; *Toro*, 2001):

$$\frac{\partial \mathbf{Q}}{\partial t} + \mathbf{A} \frac{\partial \mathbf{Q}}{\partial x} = \mathbf{S}, \quad (4.1)$$

where \mathbf{Q} is the vector of dependent variables, \mathbf{A} is the system matrix, and \mathbf{S} is the vector of source terms. The velocity at which small waves propagate throughout the domain (i.e., the eigenvalues of matrix \mathbf{A}) must be real for the problem to be well-posed (e.g., *Hadamard*, 1923; *Lax*, 1957, 1958; *Mizohata*, 1961; *Ivrii and Petkov*, 1974; *Lax*, 1980; *Kabanikhin*, 2008). When the eigenvalues are real, the problem is hyperbolic. If the eigenvalues have an imaginary component (the problem being elliptic or of mixed-type), an initial value problem is ill-posed.

The two-fluid shallow flow model (i.e., a model of the flow of two layers of superimposed fluids at different velocities) is known to be ill-posed when the difference in flow velocity between the upper and lower layers exceeds a certain threshold (*Long*, 1956; *Ardron*, 1980; *Armi*, 1986; *Lawrence*, 1990; *Pelanti et al.*, 2008). In general terms ill-posedness arises in multiphase models (e.g., bubbles in a fluid) (*Murray*, 1965; *Harlow and Amsden*, 1975;

Stewart, 1979; Stewart and Wendroff, 1984; Kumbaro and Ndjinga, 2011). Multiphase models are regularized by accounting for the forces at the interface between the two fluids (Travis et al., 1976; Lyczkowski et al., 1978; Stuhmiller, 1977; Stewart, 1979; Ramshaw and Trapp, 1978; Drew et al., 1979; Liska et al., 1995; Tiselj and Petelin, 1997; Abgrall and Karni, 2009). Although the physics of multiphase problems is better represented when including the effects of the interface forces, this approach does not completely eliminate the possibility of the problem being ill-posed.

Fernández Nieto (2003), Castro Díaz et al. (2011), and Sarno et al. (2017) introduce an additional term in the momentum equations to account for friction between the fluid layers. Their regularization strategy yields a well-posed model and has a physical origin. However, the additional physical term depends on the time step of the numerical solution, which implies that it cannot be considered a fully physically-based solution.

The numerical solution of a mathematically ill-posed model can be well-posed (Savary and Zech, 2007; Chen and Peng, 2006; Chen et al., 2007; Spinewine et al., 2011) if the numerical solution neglects information in the physical equations (Greco et al., 2008). Worded differently, in such a case the physical equations are ill-posed, but the numerical equations that we actually solve are well-posed. In particular, when using the HLL solver (a common approximate Riemann solver proposed by Harten, Lax, and Van Leer (Harten et al., 1983; Toro, 2009)), one only uses the fastest and slowest eigenvalues of the system, which implies that the dynamics due to the intermediate celerities are not resolved. This hides the problem of ill-posedness rather than solves it.

In determining the steady (equilibrium) state of a fluid dynamics problem, a commonly adopted strategy to achieve fast convergence is to modify the celerities at which information propagates (i.e., the system eigenvalues) (Chorin, 1967; Plows, 1968; Grabowski and Berger, 1976; Soh and Berger, 1984). For instance, in aerodynamics, the speed of sound may differ significantly from the air velocity, which causes a slow convergence to steady state (Feng and Merkle, 1990; Van Leer et al., 1991; Godfrey et al., 1993; Choi and Merkle, 1993). Preconditioning methods (Turkel, 1987, 1993, 1999) aim at bringing the eigenvalues of the system closer to each other such that a larger time step is allowed.

Analogously, the “bed celerity” (i.e., the speed of the wave related to changes in bed elevation (De Vries, 1965; Morris and Williams, 1996; Lyn and Altinakar, 2002; Stecca et al., 2014)) is generally slow compared to the celerities associated with perturbations of the flow. This fact has encouraged the use of a “morphodynamic acceleration factor” in morphodynamic modeling to reduce the computational time (Latteux, 1995; Lesser et al., 2004; Roelvink, 2006; Ranasinghe et al., 2011). Mathematically, as we will show later, the use of a morphodynamic acceleration factor is equivalent to the application of a particular preconditioning method.

By altering the celerity at which information propagates, the transient state of the preconditioned problem is altered with respect to the original problem, but both problems converge to the same steady state solution if the boundary conditions are steady. A drawback of preconditioning is the fact that, when the problem is subject to unsteady boundary conditions, preconditioning methods modify the steady state, as they indirectly modify the timing of the boundary conditions (Turkel, 1999). For this reason, the boundary conditions of a preconditioned model need to be adjusted if these vary with time.

The fact that a preconditioning method alters the transient state was used by Zanotti

et al. (2007) to regularize the two-fluid model. They modified the system of equations by introducing two parameters. One parameter modifies the continuity equation, which affects the imaginary part of the eigenvalues. Depending on the relations between velocities and densities of the two fluids, a specific value of this parameter makes the imaginary part equal to zero. Apart from modifying the imaginary component, the parameter also modifies the real part of the eigenvalues. They introduce a second parameter that affects all equations to recover the original real part of the eigenvalues. They compare the solution of the regularized model to analytical solutions and they show that the regularized two-fluid model is stable. In the next section we will follow a similar approach to derive a regularization strategy for the active layer model.

4.3. Regularization Strategy for the Active Layer Model

In this section we propose a strategy for recovering the well-posed character of the system of equations for modeling mixed-sediment river morphodynamics. The modified set of equations is presented in Section 4.3.1. In Section 4.3.2 we derive the parameters used to recover the well-posed character of the model considering a simplified case with two sediment size fractions and steady flow, which allows us to obtain analytical expressions. We then extend the validity to unsteady flow conditions (Section 4.3.3) and to conditions with more than 2 sediment size fractions (Section 4.3.4). In Section 4.3.5 we discuss the implementation of the strategy.

4.3.1. Modified System of Equations

We consider one-dimensional hydrostatic flow over a bed composed of N non-cohesive size fractions. The flow is described by the *Saint-Venant* (1871) equations. We assume a Chézy-type friction in which the nondimensional friction coefficient is independent of the flow and bed parameters. The sediment transport rate is considered to adapt instantaneously to changes in the bed shear stress (*Bell and Sutherland*, 1983). The mass conservation of the bed sediment is described by the *Exner* (1920) equation, and the $N - 1$ active layer equations (*Hirano*, 1971) account for the conservation of the mass of each grain size fraction within a discrete top layer of the bed surface (i.e., the active layer). Given the flow, friction, and sediment transport assumptions, the model cannot represent small-scale processes (i.e., processes at the scale of bed elevation fluctuations due the stochastic nature of sediment transport, ripples, dunes, or bed load sheets). In other words, the variables represent parameters averaged over a period larger than the characteristic time of small-scale bed elevation fluctuations (*Ribberink*, 1987; *Armanini and Di Silvio*, 1988; *Parker et al.*, 2000; *Blom et al.*, 2008; *Wong and Parker*, 2006b). We refer to Appendix C.1 for the model equations and the matrix-vector formulation of the system.

Analogous to *Zanotti et al.* (2007) (Section 4.2), the system of equations in Equation (4.1) is modified multiplying the time derivative term by a diagonal matrix \mathbf{M} to regularize the problem:

$$\mathbf{M} \frac{\partial \mathbf{Q}}{\partial t} + \mathbf{A} \frac{\partial \mathbf{Q}}{\partial x} = \mathbf{S}. \quad (4.2)$$

Matrix \mathbf{M} modifies the transient state only. The preconditioning technique does not affect the solution of the steady state (i.e., $\partial/\partial t = 0$).

The morphodynamic model under unisize conditions was analyzed by *Cordier et al.* (2011). They found that the Saint-Venant-Exner model is always well-posed assuming a Chézy-type friction. This confirms that the ill-posed character of the mixed-size sediment model results from the inappropriate representation of the mixing processes by the active layer model (*Chavarrías et al.*, 2018a). For this reason, we propose a regularization strategy that recovers the well-posed character modifying the celerities at which mixed sediment processes occur. This is done by means of a set of parameters α_k [—] for $1 \leq k \leq N - 1$ that multiply the time derivative of each active layer equation. Similarly to *Zanotti et al.* (2007), we consider a parameter β [—] that can be used to rescale the celerities after being modified by α_k . We stipulate that this parameter β affects only the sediment processes (including the *Exner* (1920) equation) but not the flow.

The modified system of equations must be mass conservative with respect to the sediment. This implies that α_k cannot be grain size dependent (i.e., $\alpha_k = \alpha \forall k$) and that the preconditioning technique is only applicable when the active layer thickness is constant (Appendix C.2).

4.3.2. Derivation of the Regularization Coefficients

In this section we derive the values of the coefficients α and β that enable regularization of the active layer model. We consider a simplified case with two sediment size fractions under steady flow conditions, as this allows us to obtain analytical expressions of the regularization parameters.

In this case, the dependent variables of the system are the bed elevation η [m] and the volume of fine sediment in the active layer per unit of bed area, M_{a1} [—] (*Chavarrías et al.* (2018a) and Appendix C.1):

$$\mathbf{Q}_{s2} = [\eta, M_{a1}]^T. \quad (4.3)$$

The system matrix is:

$$\mathbf{A}_{s2} = u \begin{bmatrix} \lambda_b & \lambda_{s1} \\ \lambda_b \gamma_1 & \mu_{1,1} \lambda_{s1} \end{bmatrix}, \quad (4.4)$$

where the parameters λ_b [—] and λ_{s1} [—] are the nondimensional approximated bed and sorting celerities, which (approximately) represent the celerities at which infinitesimal perturbations in bed level and grain size distribution of the bed surface propagate through the domain (*De Vries* (1965); *Stecca et al.* (2014); *Chavarrías et al.* (2018a) and Appendix 2.2.5), and u [m/s] is the mean flow velocity. The parameters γ_1 [—] and $\mu_{1,1}$ [—] relate the changes in the sediment transport rate to the properties of the bed (Appendix 2.2.5). Subscript s indicates that the model is steady and subscript 2 highlights that it accounts for two sediment size fractions only.

The preconditioning matrix is:

$$\mathbf{M}_{s2} = \beta \begin{bmatrix} 1 & 0 \\ 0 & \alpha \end{bmatrix}. \quad (4.5)$$

Note that β does not affect the mathematical character of the system, as it modifies all equations equally. Worded differently, the parameter β changes the magnitude of the eigenvalues but not the type (real or complex). We compute the eigenvalues (λ_k for $k =$

1,2) of the modified system of equations as the roots of the characteristic polynomial $\det(\mathbf{M}_{s2}\lambda - \mathbf{A}_{s2}) = 0$:

$$\lambda_k = \frac{u}{2\beta} \left(\lambda_b + \frac{\lambda_{s1}}{\alpha} \pm \frac{\sqrt{\Delta}}{\alpha} \right) \quad \text{for } k = 1, 2, \quad (4.6)$$

where the discriminant Δ is a second degree polynomial on α equal to:

$$\Delta = \lambda_b^2 \alpha^2 + 2\lambda_b \lambda_{s1} \left(\frac{2\gamma_1}{\mu_{1,1}} - 1 \right) \alpha + \lambda_{s1}^2. \quad (4.7)$$

We consider a situation which is ill-posed if the regularization strategy is not applied. This implies that when $\alpha = 1$ (the regularization strategy is not applied), $\Delta < 0$ (the eigenvalues are complex). We aim to modify the system of equations as little as possible in regularizing it. Worded differently, we aim at changing α as little as possible from 1. The minimum modification is obtained when the discriminant is equal to 0 (i.e., the eigenvalues are in the limit for having an imaginary part different than 0). The threshold values α_c that modify the system of equations as little as possible are found by equating (4.7) to zero:

$$\alpha_c = \frac{\lambda_{s1}}{\lambda_b} \left(1 - 2 \frac{\gamma_1}{\mu_{1,1}} \pm 2 \sqrt{\frac{\gamma_1}{\mu_{1,1}} \left(\frac{\gamma_1}{\mu_{1,1}} - 1 \right)} \right). \quad (4.8)$$

There are two possible values of α_c that yield real eigenvalues. The discriminant (Equation (4.7)) as a function of α is a concave parabola as $\lambda_b^2 > 0$. Moreover, when $\alpha = 0$, $\Delta = \lambda_{s1}^2 > 0$ and when $\alpha = 1$, $\Delta < 0$. This shows that one critical value of parameter α is between 0 and 1, and the second value is larger than 1 (i.e., $0 < \alpha_{c1} < 1 < \alpha_{c2}$).

We compute the value of parameter β that, assuming $\alpha = \alpha_c$, recovers the real part that the eigenvalues would have if they had not been modified using the parameter α :

$$\beta = \frac{\lambda_b + \lambda_{s1}/\alpha_c}{\lambda_b + \lambda_{s1}}. \quad (4.9)$$

In this case, irrespective of the value of α , the eigenvalues of the regularized system are equal to:

$$\lambda_k = \frac{u}{2} (\lambda_b + \lambda_{s1}) \quad \text{for } k = 1, 2. \quad (4.10)$$

If we do not use β to recover the original real part of the eigenvalues (i.e., if $\beta = 1$), the eigenvalues of the regularized system are equal to

$$\lambda_k = \frac{u}{2} \left(\lambda_b + \frac{\lambda_{s1}}{\alpha} \right) \quad \text{for } k = 1, 2. \quad (4.11)$$

Parameter α can be selected to be larger or smaller than 1 and if we choose to use β (i.e., if $\beta \neq 1$) the eigenvalues are independent of α . Summarizing, we find three possible regularization strategies:

1. $\alpha \neq 1$ and $\beta \neq 1$
2. $\alpha < 1$ and $\beta = 1$
3. $\alpha > 1$ and $\beta = 1$

In general terms, the approximated sorting celerities are positive, and under subcritical flow conditions (i.e., $Fr < 1$) the approximated bed celerity is also positive. However, due to hiding in the sediment transport relation, under conditions in which ill-posedness likely occurs, λ_{s1} may be negative regardless of the Froude number (*Chavarrías et al.*, 2018a). In this case, Strategies 1 and 2 do not guarantee that the eigenvalues $\lambda_k > 0$. We consider that it is physically unrealistic that morphodynamic information travels in the upstream direction under subcritical flow conditions. A negative eigenvalue would imply that the boundary condition for morphology needs to be imposed at the downstream end to yield a well-posed model, and this is contradictory to the fact that the morphodynamic state under subcritical flow conditions depends on the load coming from upstream (*Blom et al.*, 2016, 2017b). On the other hand, Strategy 3 guarantees that $\lambda_k > 0$ (Appendix C.4). Thus, we consider that the only possible regularization strategy is the one in which $\alpha > 1$ and $\beta = 1$.

We need to guarantee that the celerities of the system of equations modified by the regularization strategy are not physically unrealistic. In particular, under a sufficiently small Froude number, the modified bed and sorting celerities must be significantly smaller than the celerities of the flow. The regularization technique does not modify the approximated celerity associated with bed elevation changes (i.e., $\beta = 1$) and decreases the celerity associated with mixing processes (i.e., $\alpha > 1$, we will discuss this point in Section 4.6.1). For this reason, the regularization technique does not cause the celerities to be physically unrealistic.

The regularization strategy is not limited to a particular range of parameter settings. Yet, when using the value of α derived in this section, the Froude number cannot be in the transcritical region, as in this case the quasi-steady approximation is not valid (*Lyn*, 1987; *Sieben*, 1999; *Lyn and Altinakar*, 2002; *Cao and Carling*, 2002b; *Cao et al.*, 2002; *Colombini and Stocchino*, 2005). In the following section we consider unsteady flow, which extends the regularization technique to the transcritical region.

4.3.3. Validity under Unsteady Flow Conditions

In this section we extend the validity of the regularization parameter α found for steady flow cases (Section 4.3.2) to unsteady flow conditions.

When considering unsteady flow conditions, we cannot obtain an analytical expression of α_c for regularizing the system of equations. Nevertheless we can numerically find the smallest value of $\alpha > 1$ for which the roots of the characteristic polynomial of $\det(\mathbf{M}_u \lambda - \mathbf{A}_u) = 0$ are real values (i.e., the eigenvalues are real), where subscript *u* indicates that the model is unsteady. Matrices \mathbf{M}_u and \mathbf{A}_u are listed in Appendix 2.2.5. This procedure is nonetheless expensive computationally in comparison with an algebraic calculation. Figure 4.1 shows the maximum imaginary part of all eigenvalues of a reference ill-posed case (Table 4.1) considering unsteady flow for varying α . The sediment transport rate is computed using a fractional version of the *Engelund and Hansen* (1967) sediment

transport relation (Blom *et al.*, 2017b). A value $\alpha > 16.1$ yields a well-posed model (i.e., all eigenvalues are real).

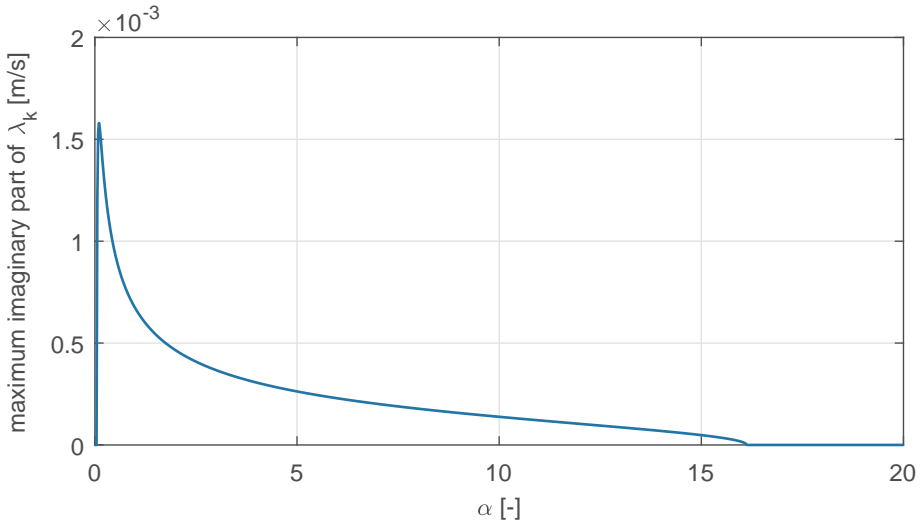


Figure 4.1: Maximum imaginary part of all the eigenvalues of the reference case (Table 4.1) as a function of α . In this case $\alpha_c = 16.1$ is the smallest value of $\alpha > 1$ that yields a well-posed model (i.e., all eigenvalues are real).

u [m/s]	h [m]	C_f [-]	L_a [m]	F_{a1} [-]	f_1^I [-]	d_1 [m]	d_2 [m]
1	1	0.01	0.20	0	1	0.001	0.005

Table 4.1: Reference values in the comparison of the value of α_c computed analytically and numerically.

To test the validity of the algebraic value of α_c obtained assuming steady flow we consider the same reference case (Table 4.1) and we vary the flow velocity to obtain a range of conditions. In Figure 4.2a we present the value of α_c necessary to obtain a well-posed model computed assuming steady flow (Equation (4.8)) and numerically considering unsteady flow. We conclude that for a Froude number below approximately 0.6, there is no significant difference between the values for steady and unsteady flow. This implies that, for $Fr < 0.6$, the value of α_c obtained analytically assuming steady flow is a good approximation of the actual value.

4.3.4. Validity under Multiple Size Fractions Conditions

In a model with more than 2 size fractions, we cannot analytically obtain the value of α_c that regularizes the active layer model. Similar to the unsteady case, it is possible to numerically obtain the smallest value of $\alpha > 1$ that yields real eigenvalues computed as the roots of the characteristic polynomial $\det(\mathbf{M}_s \lambda - \mathbf{A}_s) = 0$ (matrices \mathbf{M}_s and \mathbf{A}_s are presented in Appendix 2.2.5). Again, this process is relatively expensive in computational

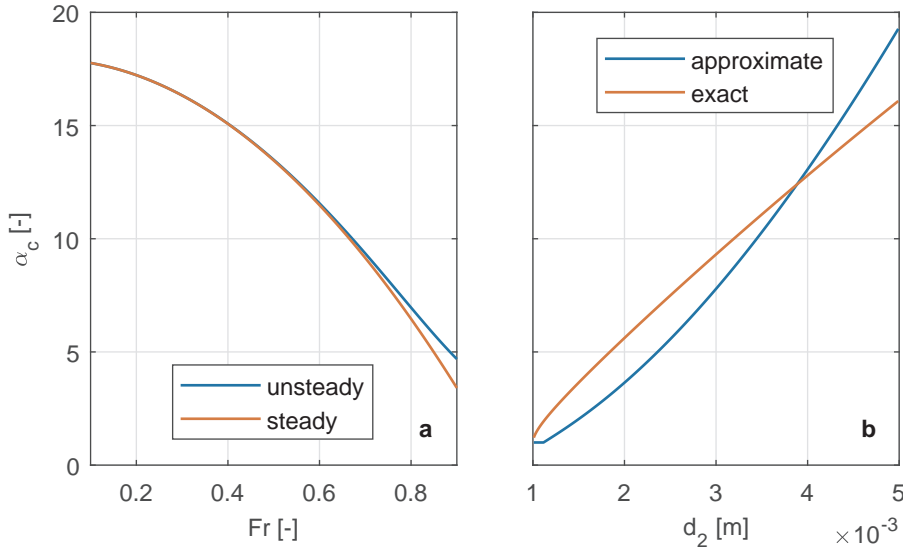


Figure 4.2: Comparison between (a) the steady and unsteady values of the regularization parameter α_c , and (b) the exact and approximate values for a 3 size fractions case.

terms. In this section we propose a method to obtain an approximate value of α_c for such cases and compare it to the exact value obtained numerically.

Assuming steady flow, a system that models N sediment size fractions has N equations (Appendix C.1). We reduce the system of N equations to an approximate system of 2 equations following the approach of *Ribberink* (1987). We sum the N active layer equations to obtain one equation that models the changes of the mean grain size of the bed surface sediment (Appendix C.1.3). Subsequently, we apply the same technique as the one we have used in the case of 2 size fractions to obtain a critical value of α that guarantees that the approximate model is well-posed:

$$\alpha_{cm} = \frac{\lambda_m}{\lambda_b} \left(1 - 2 \frac{\gamma_m}{\mu_m} \pm 2 \sqrt{\frac{\gamma_m}{\mu_m} \left(\frac{\gamma_m}{\mu_m} - 1 \right)} \right), \quad (4.12)$$

where the symbols are the equivalent of the case for two size fractions in the approximate model (Appendix 2.2.5).

We consider a case with 3 sediment size fractions, where the fine and coarse fractions have characteristic sizes equal to $d_1 = 0.001$ m and $d_3 = 0.005$ m, respectively. The volume fraction contents of the 3 size fractions in the active layer are $F_{a1} = 0$, $F_{a2} = 0.9$, and $F_{a3} = 0.1$. The substrate is fully composed of fine sediment. We vary the medium grain size (d_2) to obtain a range of conditions. The remaining parameters are the same as the ones presented in Table 4.1. In Figure 4.2b we compare the exact value of α_c (computed numerically) to the approximated one (computed using Equation (4.12)). The approximated value of α_c follows the same trend as the exact one. However, the approximated

value is both larger and smaller than the exact one depending on the sediment conditions. This implies that the current approximate approach may be insufficient to regularize the active layer model in the case of more than 2 sediment size fractions.

The approximate system of equations can be ill-posed under degradational conditions into a fine substrate only (*Ribberink, 1987; Chavarrías et al., 2018a*). However, a 3 size fractions case can be ill-posed under degradational conditions into a coarse substrate (*Chavarrías et al., 2018a*), which further limits the applicability of the approximate solution for the threshold value of α .

4.3.5. Implementation

In this section we describe our approach for numerically solving the system of equations and apply the regularization strategy.

We have developed the numerical research code Elv to model mixed-size sediment river morphodynamics (*Blom et al., 2017b,a*) which solves the equations for flow, bed elevation, and the bed surface grain size distribution in a decoupled manner (i.e., in series and not as a coupled system of equations). Thus, our code is not appropriate for solving transcritical situations (*Lyn, 1987; Lyn and Altinakar, 2002; Sieben, 1999*) or cases with a high sediment concentration (*Morris and Williams, 1996; Cao and Carling, 2002a*).

The one-dimensional spatial domain is discretized using an equispaced grid. All variables are computed at the cell centers and are considered constant in each time step. Here we assume steady flow, which is represented by the backwater equation (Eq. (C.3)). This ordinary differential equation is integrated using the standard fourth-order finite difference Runge-Kutta method (RK4). The *Exner* (1920) equation (Eq. (A.4)) and active layer equation (Eq. (C.6)) are solved in conservative form using a first order upwind scheme in combination with forward Euler to integrate in time. We discretize the vertical domain in a finite number of cells having a certain thickness to account for stratigraphic changes in the substrate. Our scheme is balanced for the vertical fluxes between the active layer and the substrate (*Stecca et al., 2016*). This means that mass conservation is guaranteed independent of the substrate discretization. The time step varies with time and is computed such that the CFL number (*Courant et al., 1928*) is constant and equal to 0.9 (*Wu, 2007; Toro, 2009*). The details of the numerical implementation are described in Appendix C.5.

When the regularization strategy is applied, we first determine the mathematical character of the model (i.e., well-posed or ill-posed) at each node using the approach proposed by *Chavarrías et al. (2018a)*. For the case of 2 size fractions, this is done evaluating an algebraic equation, and for more than 2 size fractions we numerically compute the eigenvalues of the system matrix. At continuation, for each node we compute the threshold value α_c that guarantees that the model is well-posed. Again, this is done evaluating an algebraic expression (Equation (4.8)) for 2 size fractions and it is done numerically for more than 2 size fractions (Section 4.3.4).

The regularization strategy yields equal eigenvalues (i.e., in a two size fractions case $\lambda_1 = \lambda_2$, Equation (4.11)). This implies that the problem is hyperbolic but not strictly hyperbolic (*Lax, 1980; Toro, 2009; Cordier et al., 2011*). In a non-strictly hyperbolic problem, the solution may not be unique and resonance may occur, which gives rise to strong non-linear interactions (*Liu, 1987; Isaacson and Temple, 1992*). In avoiding a non-strictly hyperbolic, problem we modify the value of α_c using a small parameter $\epsilon > 0$ [–] such

that $\alpha^* = \alpha_c(1 + \epsilon)$, where $\alpha^* [-]$ is the value used for updating the bed surface grain size distribution. For the cases we have studied a value of $\epsilon = 0.005$ is sufficient to avoid the problems associated with non-strict hyperbolicity.

Ill-posedness causes short-wave instability (Joseph and Saut (1990); Chavarrías et al. (2018a) and Section 4.5.1) meaning that perturbations will grow unstable at rates depending on the inverse of their length. Diffusion counteracts these effects by dampening perturbations (Gray and Ancey, 2011). Regularization of the problem can be provided by numerical diffusion if a first-order (diffusive) method is used. However, if the underlying problem is ill-posed, cell refinement will be able to reveal its ill-posed character even if a first-order method is used in its solution, as we do in this chapter. This is because, with decreasing cell size, the numerical diffusion coefficient of a first-order method will generally decrease, while at the same time shorter (more unstable) perturbations will be solved. Therefore, an ill-posed problem will show no convergence due to its inherent instability when the mesh is progressively refined, regardless of the low-order method in use.

We observe such a behavior in Section 4.5.1 where we show that our low-order numerical scheme suffices to capture the consequences of ill-posedness by revealing instability and non-converging character in simulations conducted within the ill-posed range. It is likely that, with a higher-order (non-diffusive) method, these features would have become apparent even at lower mesh resolution due to absence of spurious diffusion dampening perturbations. However, it must be considered that our upwind scheme is characterized by small numerical diffusion coefficient, and that Stecca et al. (2016) and Siviglia et al. (2017) have shown that a first-order upwind scheme with a fine grid resolution is sufficient to capture the main features of mixed-size sediment morphodynamic simulations such as the ones we conduct.

4.4. Laboratory Experiments

In this section we describe the laboratory experiments conducted under conditions in which the active layer model (Hirano, 1971) is ill-posed in order to obtain a data set to which we can compare the results of the proposed regularization strategy. We describe the experimental plan, materials, and measurements in Section 4.4.1. In Section 4.4.2 we present the experimental results.

4.4.1. Experimental Plan and Measurements

We conducted 4 laboratory experiments (I1, I2, I3, and I4). The experiments reproduced degradational conditions into a fine substrate, which are conditions prone to be ill-posed (Ribberink, 1987; Stecca et al., 2014; Chavarrías et al., 2018a). The experiments were conducted in a 14 m long, 0.40 m wide, and 0.45 m high tilting flume in the Water Laboratory of the Faculty of Civil Engineering and Geosciences of Delft University of Technology. At the upstream end, a turbulence dissipation device was installed (item (a) in Figure 4.3). An inclined plane was placed downstream from the turbulence dissipation device (item (b) in Figure 4.3) to allow for an alluvial bed (item (c) in Figure 4.3). The structure was covered with glued sediment such that friction was similar to the one of the alluvial bed. Its elevation could be adjusted.

We consider a reference system with coordinate origin at the bottom of the flume at

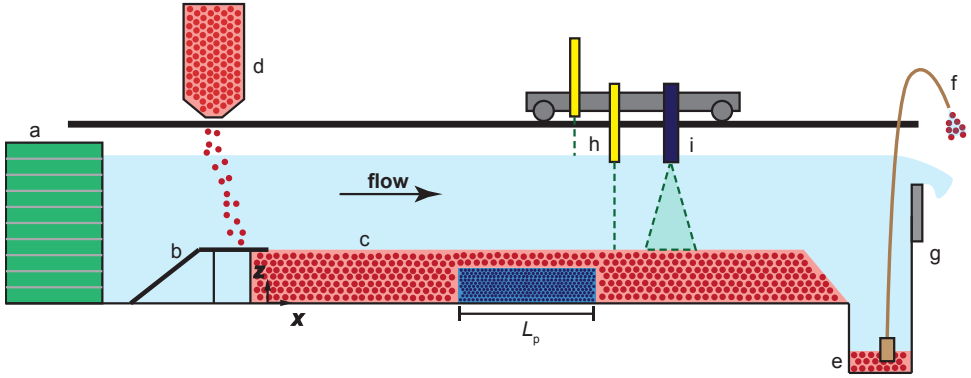


Figure 4.3: Sketch of the flume set-up: (a) turbulence dissipator, (b) metal plate with glued sediment, (c) alluvial bed, (d) feeder, (e) sand trap, (f) sediment pump, (g) weir, (h) laser sensors for water and bed surface elevation, and (i) camera for measuring the bed surface grain size distribution.

Experiment	L_p [m]	x_{p0} [m]	x_{pf} [m]
I ₁	0.50	4.70	5.20
I ₂	1.00	4.49	5.49
I ₃	2.00	4.47	6.47
I ₄	4.00	4.47	8.47

Table 4.2: Length (L_p) and position (initial x_{p0} and final x_{pf} coordinates) of the patch of fine sediment below the coarse bed surface.

the downstream end of the metal structure. The z -axis is parallel to gravity and pointing up. The x -axis follows the streamwise direction of the flume, being positive in the direction of the flow. The y -axis is perpendicular to the other two axes forming a right handed orthonormal basis.

We used two sediment size fractions (fine and coarse) with characteristic grain sizes (computed as the arithmetic mean in ϕ scale) equal to 2.1 mm and 5.5 mm. The standard deviation of the two size fractions is 1.1 mm and 1.2 mm, respectively. The bed surface was initially flat, with a constant slope, and composed of coarse sediment only. Below a 0.03 m thick layer of coarse sediment, we installed a patch of fine sediment of varying length L_p [m] (Figure 4.3 and Table 4.2). We imposed a constant water discharge and a constant sediment feed rate of the coarse fraction only, which was in equilibrium with the initial condition (Table 4.3 and Appendix C.6). The sediment was introduced using a feeder placed on top of the flume (item (d) in Figure 4.3). The downstream water level was lowered at a rate of 0.01 m/h during 8 h by adjusting a sharp-crested weir at $x = 12.60$ m (item (g) in Figure 4.3). The lowering of the water level led to bed degradation and entrainment of the fine sediment in the patch. We have tested that in these conditions the active layer model is ill-posed regardless of the active layer thickness and sediment transport relation.

q [m ² /s]	s_0 [—]	q_{b0} [m ² /s]	h [m]	u [m/s]	Fr [—]
0.150	3.50×10^{-3}	7.86×10^{-6}	0.187	0.799	0.59

Table 4.3: Experimental conditions, where q denotes water discharge per unit width, s_0 initial bed slope, q_{b0} sediment feed rate per unit width, h flow depth, u mean flow velocity, and Fr is the Froude number.

Sediment was collected in a sand trap (item (e) in Figure 4.3) at the downstream end of the flume ($x = 12.10$ m). The sediment was pumped from the sand trap (item (f) in Figure 4.3) into a tank positioned on a weight balance next to the flume. This system allowed us to continuously measure the sediment transport rate. The water inflow was measured using an ultrasonic flow meter and the downstream water level using a position sensor. We obtained profiles of the water and bed elevation using laser sensors that were fixed to a carriage (item (h) in Figure 4.3). A camera was mounted on the carriage to measure the grain size distribution of the bed surface using the technique developed by Orrú *et al.* (2016a,b) (item (i) in Figure 4.3). To this end, the coarse sediment was painted red and the fine sediment blue. Our experimental set-up allowed us to measure either a profile of bed and water surface elevation or the bed surface grain size distribution at a certain location with time.

For the modeling of the laboratory experiments (Section 4.5), it is important to obtain turbulent flow conditions of a relatively deep flow (i.e., flow cannot be affected by individual grains), where sediment is predominantly transported as bed load. The concentration of sediment needs to be so small that we can assume clear water. These conditions were satisfied (Appendix C.6).

4.4.2. Results

All experiments were governed by the same conditions before the fine sediment in the patch was entrained. We observed the superposition of bedforms of two different length scales (Figure 4.4). Secondary bedforms approximately 0.5 m long and 0.01 m high were superimposed on primary longer bedforms of the order of 3 m and twice as high. The primary bedforms are interpreted as incipient gravel dunes (Carling, 1999; Carling *et al.*, 2005). The characteristics of these features remained steady as the bed degraded. The steadiness of the features' characteristics is confirmed in a preparatory experimental run without a patch of fine sediment (Appendix C.6).

After approximately 2 h the bed had degraded up to a point at which the trough of a long bedform was lower than the top part of the patch (Figure 4.5a). At that moment fine sediment was exposed, entrained, and transported. The larger mobility of the fine sediment created a downstream moving degradational wave (Figure 4.5b). As erosion proceeded, the shear stress was reduced (due to the increased flow depth), which reduced the degradation rate. Meanwhile, the subsequent bedform advanced and started to fill the degradational pit with coarse sediment (Figure 4.5c). Overall, the passage of bedforms induced entrainment of fine sediment and subsequent coarsening of the top part of the substrate. Since the degradational wave increased in depth in downstream direction, also the thickness of the coarse top layer increased in downstream direction (Figure 4.5d).

The substrate coarsening mechanism created an irregular interface between coarse

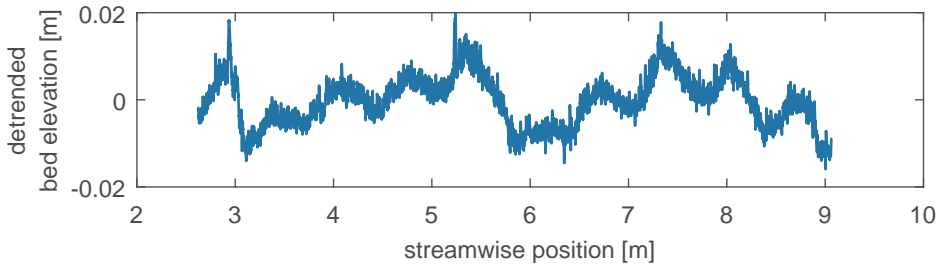


Figure 4.4: Measured bed elevation before fine sediment of the patches is entrained showing the superposition of bedforms of two different length scales (Experiment I₄ at 1:51 h).

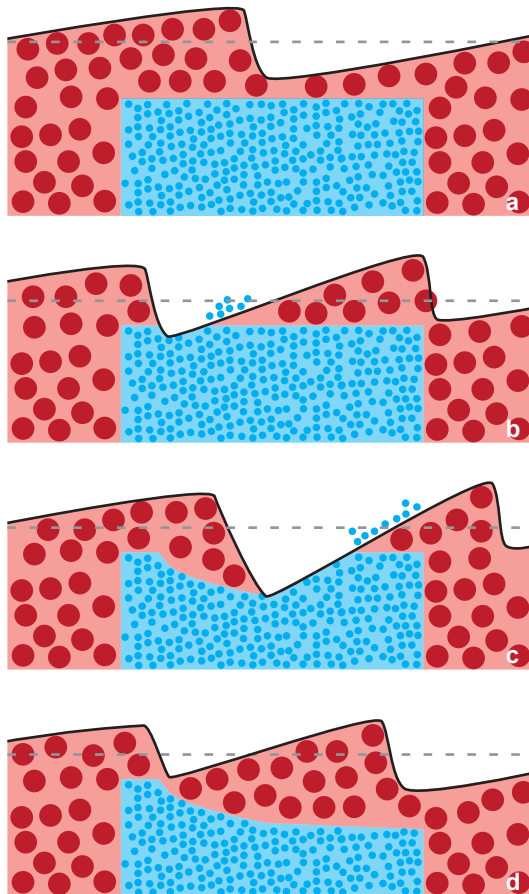


Figure 4.5: Sketch of the cyclic entrainment of substrate sediment: (a) bedforms formed out of coarse sediments only, (b) fine sediment from the patch is entrained in the trough of a bedform, (c) a degradational wave forms and travels downstream, (d) coarse sediment from upstream fills the pit left by the degradational wave.

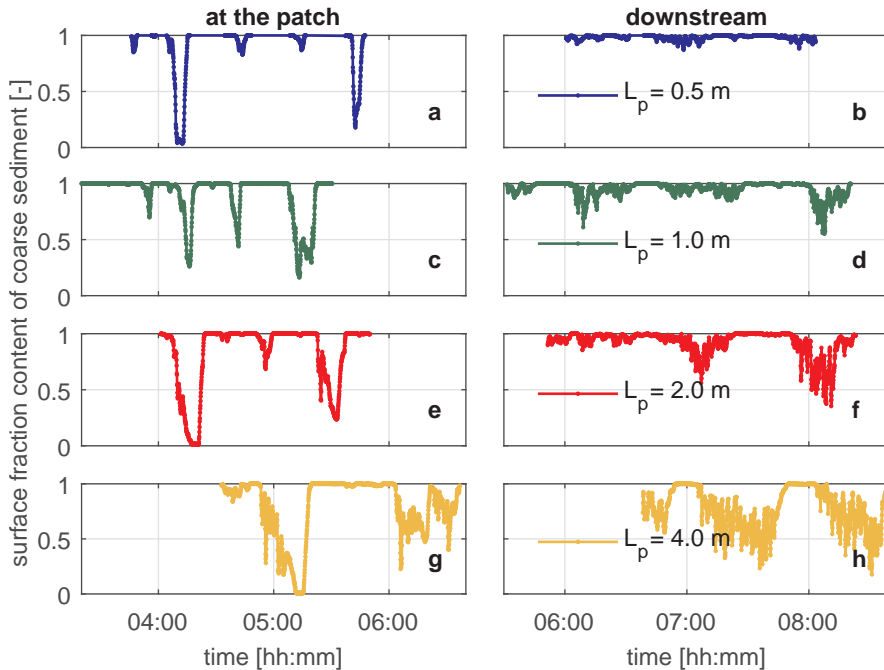


Figure 4.6: Measured surface fraction content of coarse sediment as a function of time for various lengths of the patch L_p : at the center of the patch (a,c,e,g), and at the downstream end (b,d,f,h). Note that the streamwise location of the center of the patch varies for each experiment while the downstream position is the same for all cases ($x = 9.15$ m).

and fine sediment compared to the initial situation where the interface was parallel to the bed surface. As a consequence, the entrainment of fine sediment became a pseudo-random process in space and time. Degradational waves formed at those locations where fine sediment was closest to the bed surface. Yet, most of the waves grew for only a limited length, as, due to the irregular interface, at some point the sediment present at the trough was coarse rather than fine. Sometimes the interface was sufficiently parallel to the bed surface and a large degradational wave formed. This is seen in the content of coarse sediment at the bed surface of the patch (Figure 4.6a,c,e,g) and in the bed elevation (Figure 4.7). One or two small degradational waves formed after the passage of a large degradational wave, characterized by the fact that the bed surface is composed of mainly fine sediment and the trough of a bedform reaches elevations significantly lower than average.

A longer patch allowed for the development of longer (in space and time) and deeper erosional waves (Figures 4.6 and 4.7). Yet, the decrease in degradation rate as the wave advanced acted as a saturation mechanism limiting the height of the wave. Thus, the probability of lower bed elevation at the patch zone was not significantly larger for an increasing patch length (Figure 4.8). After the patch, where the substrate was composed of coarse sediment only, wave height decreased and the bed elevation profile tended to the

one upstream of the patch (Figure 4.7). Yet, the presence of fine sediment downstream of the patch slightly increased the height of the bedforms with respect to the bedforms upstream of the patch (Figure 4.8a,c). Bedforms downstream of the patch were characterized by a coarse front and fine tail, and were approximately 2 grain sizes of the coarse sediment high. These characteristics may indicate the presence of bedload sheets (*Whiting et al.*, 1988; *Dietrich et al.*, 1989; *Recking et al.*, 2009) or bedforms in a transitional phase to small dunes. The domain downstream from the patch was not long enough to precisely conclude on the type of bedforms. The changes in volume fraction content of coarse sediment at the bed surface were less pronounced downstream of the patch compared to at the patch (Figure 4.6b,d,f,h). This is because fine sediment entrained at the patch dispersed in the downstream direction.

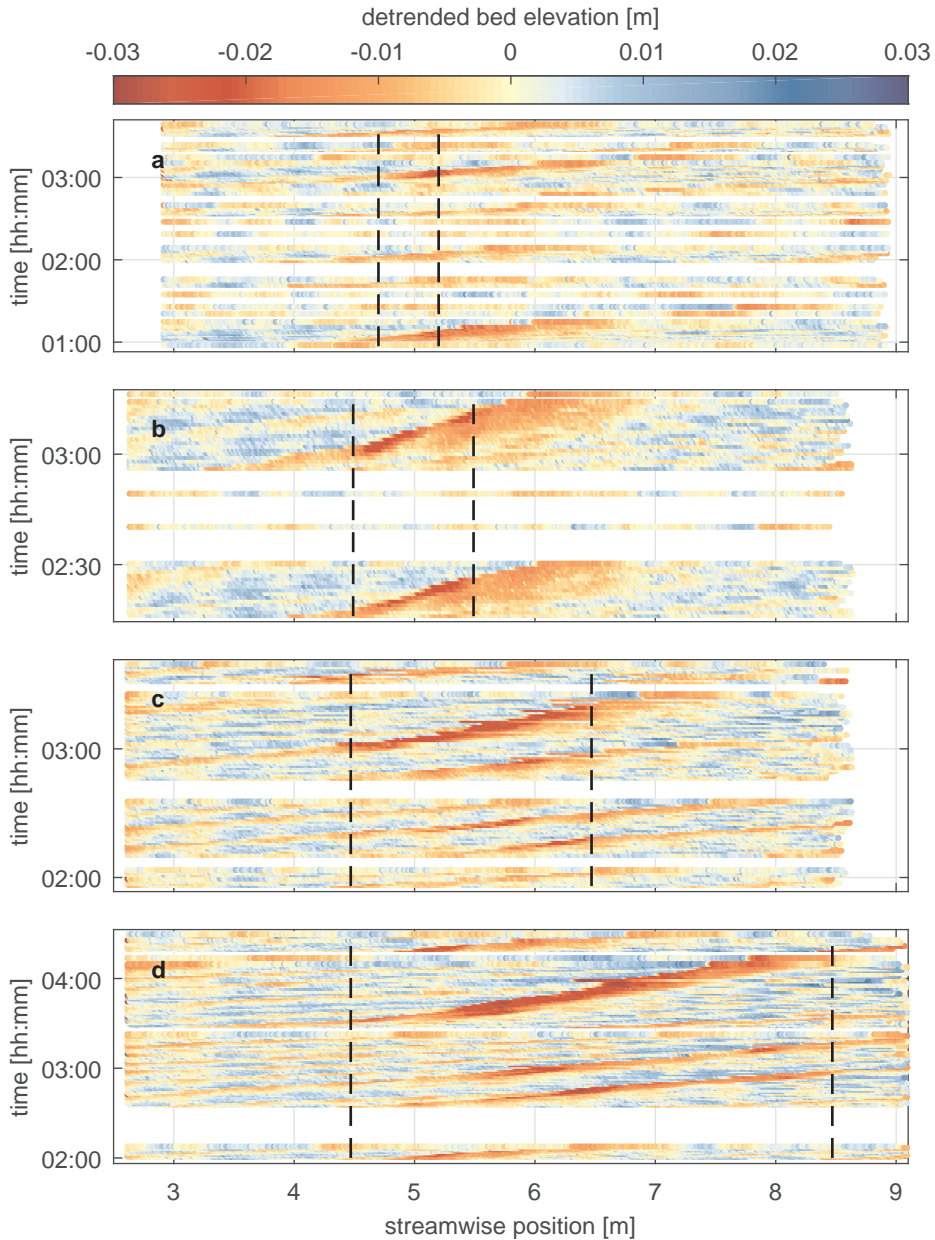


Figure 4.7: Detrended bed elevation as a function of time in Experiment (a) I₁, (b) I₂, (c) I₃, and (d) I₄. The dashed black lines indicate the boundaries of the patch. The bed elevation is detrended subtracting the bed slope of each profile individually, obtained fitting a first degree polynomial.

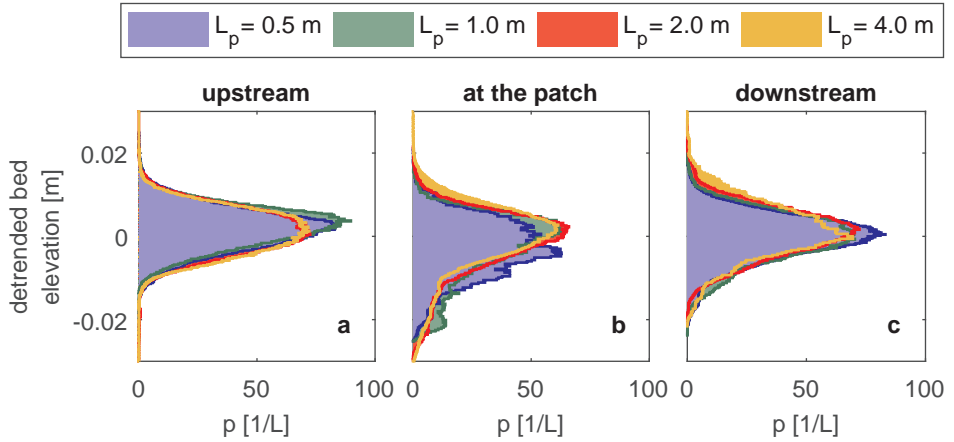


Figure 4.8: Probability density of detrended bed elevation: (a) upstream of the patch, (b) at the patch, (c) and downstream of the patch.

4.5. Numerical Modeling

In this section we apply the regularization strategy in modeling the laboratory experiments conducted under conditions in which the active layer model is ill-posed (Section 4.5.1). In Section 4.5.2 we compare the results of the regularized active layer model to the results of the two-layer model developed by *Ribberink* (1987) by applying them to a thought experiment under conditions in which the active layer model is ill-posed.

4.5.1. Modeling of our Laboratory Experiments

In Section 4.5.1 we calibrate the numerical model. In Section 4.5.1 we conduct a convergence test to show the consequences of ill-posedness and the benefits of the regularization strategy. In Section 4.5.1 we apply the numerical model to the laboratory experiments described in the previous section. In Section 4.5.1 we test the regularization strategy assuming three sediment size fractions.

Calibration

Modeling the laboratory experiments requires values for the active layer thickness and the friction coefficient, and the choice of a sediment transport relation. To this end we use the results of a set of preparatory experiments (Appendix C.6). To choose a sediment transport relation, we run two experiments conducted under equilibrium conditions, while feeding the fine and the coarse sediment size fractions. The sediment transport relation by *Ashida and Michine* (1971) reproduces our results reasonably well (Appendix C.7). To obtain the skin friction coefficient (C_{fb}) for computing the sediment transport rate (Appendix C.1.4) we correct the total measured friction coefficient C_f for side wall friction with the method developed by *Johnson* (1942) (see *Guo* (2015)). We obtain the values $C_f = 0.0104$ and $C_{fb} = 0.0084$. Bedform drag was negligible during the initial phase as bedforms were low. When fine sediment was entrained, bedforms grew and bedform drag may have played a role. It is not reasonable to model this additional friction using standard relations (e.g.

Engelund and Hansen, 1967; Haque and Mahmood, 1983; Wright and Parker, 2004), as these relations provide a bedform-averaged friction coefficient, while in our case large bedforms were isolated in space and time. We decide to use a constant friction coefficient and we think that the most sensible approach is to neglect bedform drag.

A reasonable value for the active layer thickness is 0.01 m, which corresponds to the distance below the mean bed elevation with a probability of entrainment below approximately 5% (*Ribberink, 1987; Blom, 2008*). This value is also in accordance with 1–3 times D_{90} as proposed by, for instance, *Hirano (1971), Hoey and Ferguson (1994), and Seminara et al. (1996)*.

In one preparatory experiment under equilibrium conditions, we fed coarse sediment only and, from some point, we started feeding tracer sediment (i.e., sediment of a different color). Modeling the propagation of the front of tracer sediment, we confirm that 0.01 m is a reasonable value for the active layer thickness (Appendix C.7).

Convergence Test

First we aim to show the consequences of ill-posedness. To this end, we simulate conditions similar to the ones of the experiments using the active layer model. In the experiments, degradation into a coarse substrate (i.e., under well-posed conditions) occurred for approximately 2 h, as the patch of fine sediment was placed 3 cm below the initial bed surface. In order to obtain ill-posed conditions at the start of the simulations, the patch of fine sediment is placed right below the active layer. In this manner, 300 s simulations suffice for our purpose. Moreover, the patch extends over a distance of 8 m (from $x = 1$ m to $x = 9$ m) to maximize the domain over which the model is ill-posed.

We conduct 13 simulations using cell sizes ranging from 0.1 m down to 2.44×10^{-5} m. The results do not converge and continue to change as the grid is refined (Figure 4.9a). We compute the error as a function of the cell size to quantify the (lack of) convergence. As there is no analytical solution to which we can compare the results of the numerical runs, we compute the error between the results of two successive simulations s and $s + 1$ (*Roy, 2005; Love and Rider, 2013*). To this end, first we interpolate the bed elevation results of all simulations using the smallest cell size. The interpolation, rather than linear, takes into consideration that each value is constant inside a cell. Second, we compute the error as the norm 1 of the difference between bed elevations of two successive simulations at a certain time t :

$$\text{error}_s^t = \frac{1}{LN_x} \sum_{r=1}^{N_x} \left| \eta_{r_s}^t - \eta_{r_{s+1}}^t \right|, \quad (4.13)$$

where N_x denotes the number of cells of the simulation with the smallest cell size, and L [m] the domain length. Figure 4.9c shows the error as a function of the cell size for several times. If the cell size is large (for instance, larger than 0.01 m), for short simulation times (for instance, shorter than 10 s), the results seem to converge. Yet, using the same cell size, the results do not converge if one considers a longer simulation time. Similarly, considering a simulation time equal to 10 s, the results do not converge when the cell size is smaller than 0.002 m. This behavior is characteristic of ill-posed simulations. The growth rate of perturbations increases with decreasing cell size. For this reason, the consequences of ill-posedness arise earlier for smaller cell sizes. Given a certain cell size,

if the simulation is short enough, perturbations do not have time to grow and the solution seems to converge. For a fixed time, simulations seem to converge after the error grows (for instance, for $t = 120$ s, simulations seem to converge for cell sizes between 0.001 m and 0.01 m). This is due to the fact that, at the given time, perturbations have already grown significantly and have coarsened the bed material causing the simulation to be well-posed. A further decrease of the cell size or an analysis at a different time shows that the active layer model does not converge.

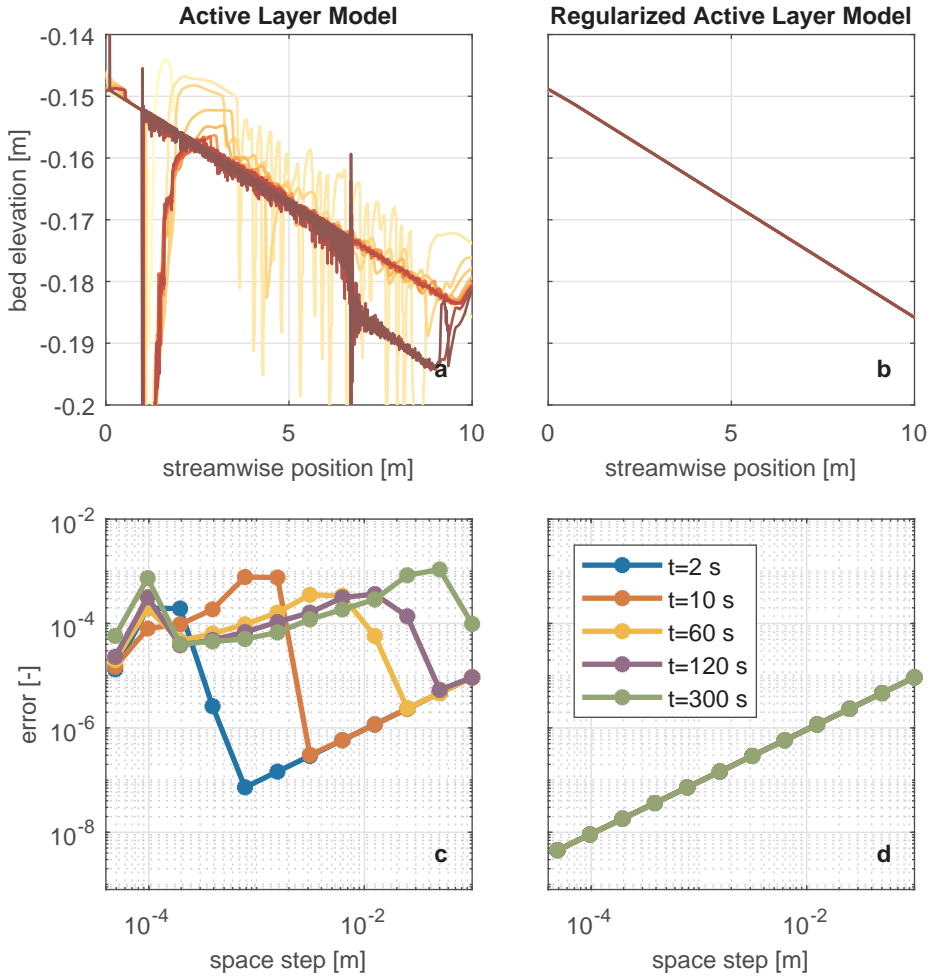


Figure 4.9: Bed elevation at $t = 300$ s predicted using the (a) active layer model (Hirano, 1971) and (b) regularized active layer model. Each of the 13 lines presents the results computed using a different cell size (ranging from 0.1 m down to 2.44×10^{-5} m, where darker colors represent smaller cell sizes). Panels (c) and (d) present the error at a certain time using a particular cell size (see Equation (4.13)) when using the active layer model and the regularized active layer model, respectively. In panels (b) and (d) only one line is visible, as it overlaps all other lines.

We repeat the same simulations applying the regularization strategy. The initial value of the parameter that recovers the well-posed character of the system is $\alpha_c = 11.6$. In this case the solution does not show oscillations (Figure 4.9b). Moreover, the solution converges for a decreasing cell size independently from the time at which convergence is tested (Figure 4.9d). This supports the fact that the regularized model is well-posed, contrary to the active layer model. The rate at which the solution converges confirms that the numerical scheme is first-order accurate (Section 4.3.5).

Two sediment size fractions

We reproduce all laboratory experiments using a cell size equal to 0.05 m. The regularized model shows spatial or temporal oscillations in none of the cases (Figure 4.10). For all cases the bed elevation decreases smoothly in the streamwise direction (Figure 4.10b,f,j,n). This contrasts with the measured temporal change of bed elevation, which presents bedforms and the formation of degradational waves at the upstream end of the patch (Figure 4.10a,e,i,m). The measured increase in wave height at the patch (Figure 4.10a,e,i,m and Section 4.4.2) is not captured. The effect of the patch is observed in the model results in the fact that degradation occurs faster for a long patch (Figure 4.10n) than for a short one (Figure 4.10b).

The continuous and smooth predicted entrainment of substrate sediment yields an almost steady volume fraction content of sediment in the active layer both at the patch (Figure 4.10c,g,k,o) and at the downstream end (Figure 4.10d,h,l,p). The measured data shows, on the other hand, a variable volume fraction content at the bed surface. The model correctly captures the mean value and nicely reproduces that a longer patch causes an increase in the amount of fine sediment at the bed surface. The fact that the model does not capture bedforms is not surprising, as the mechanisms necessary for bedform formation are not present in the model. For instance, the fact that the flow model is based on the hydrostatic pressure assumption prevents modelling processes such as flow separation. The possibility of capturing the formation of the degradational waves at the patch is also discarded, as from the analysis of well-posedness we see that the regularized model does not show any instability mechanism that could induce wave growth. For this reason, the model results represent values averaged over the passage of several bedforms and degradational waves. We choose not to filter the measured bed elevation data, as given the characteristics of the bedforms, it would introduce a large amount of spurious information (e.g., the degradational wave would start at the wrong location) and we would lose a significant amount of data at the beginning and end of the domain.

Overall the regularized model yields a reasonable approximation of the mean temporal change of the measured data. The degradational trend is captured and the surface grain size distribution approximates the average measured values. The substrate is not unrealistically altered as there are no oscillations in the solution.

Three sediment size fractions

To test the regularization strategy for multiple grain sizes, we model Experiment I4 (Table 4.2) using 3 different grain sizes by applying the exact solution to obtain the regularization parameter. The fine size fraction remains the same and the previous coarse size fraction is represented in this case by two characteristic grain sizes equal to 4.895 mm and 5.895 mm. For an initial volume fraction content at the bed surface of the medium size sediment

equal to 0.375, the initial bed slope is the same as when using two characteristic sizes and the sum of the sediment transport rate of the medium and coarse fractions when using three sizes is equal to the sediment transport rate of the coarse fraction when using two sizes. In this manner the simulation accounting for three sediment fractions is comparable to the one accounting for two size fractions.

In Figure 4.11 we compare the bed elevation and mean grain size of the bed surface sediment predicted by the regularized model using 2 and 3 sediment size fractions. The evolution of the bed elevation shows only a weak dependence on the number of size fractions used to discretize the sediment mixture. The model with 3 size fractions presents a mild coarsening (0.2% increase in mean grain size) with time before sediment from the patch is entrained (after 2 h). This coarsening is not visible when using 2 size fractions, because in this case, during the initial state, the bed surface sediment consists of one single grain size only. We conclude that the regularization technique is applicable for a general case with more than 2 size fractions.

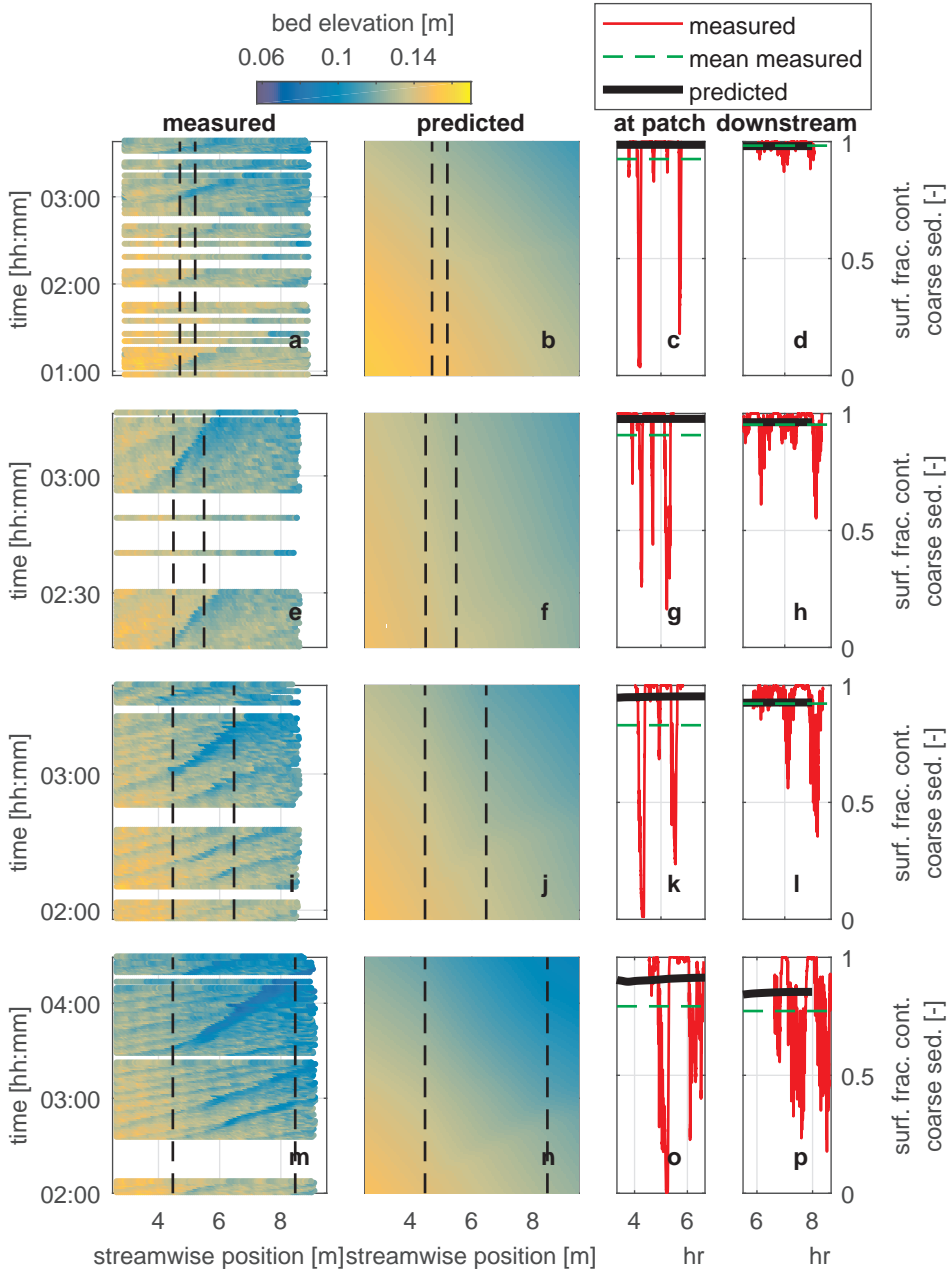


Figure 4.10: Comparison between measured data and regularized model results: Experiment I1 (a-d), Experiment I2 (e-h), Experiment I3 (i-l), and Experiment I4 (m-p). The first and second columns show the measured and predicted bed elevation with time, respectively. The vertical dashed lines indicate the position of the patch of fine sediment. The third and fourth columns present the surface fraction content of coarse sediment at the center of the patch of fine sediment and at the downstream end of the flume, respectively.

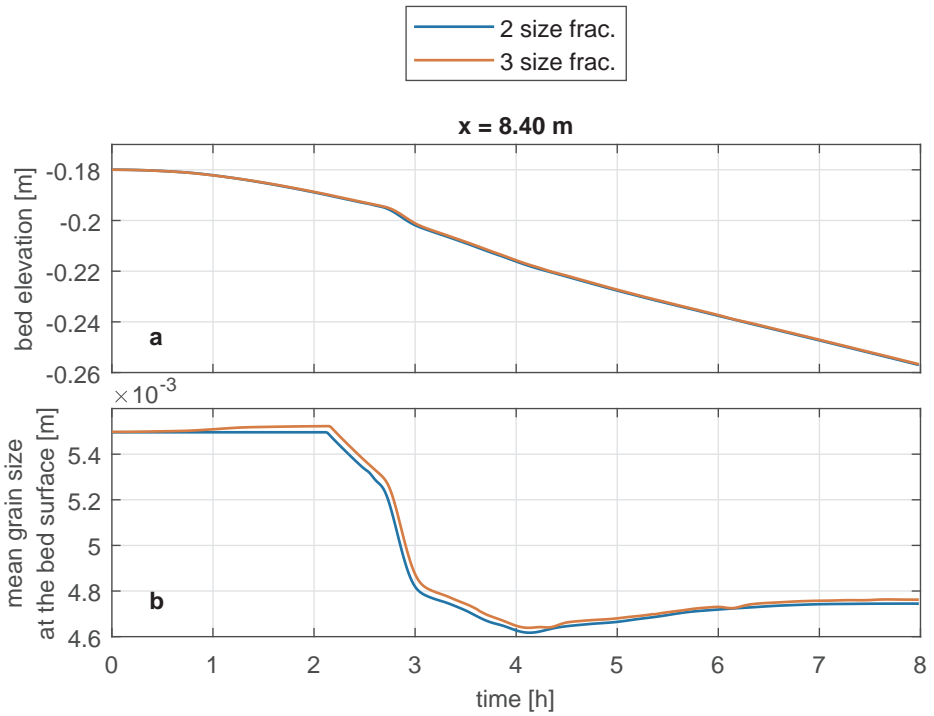


Figure 4.11: Bed elevation (a) and mean grain size at the bed surface (b) as a function of time predicted in Experiment I4 using the regularized active layer model using 2 and 3 sediment sizes.

4.5.2. Comparison between Ribberink's (1987) Two-Layer Model and the Regularized Model

To our knowledge there is no other laboratory data set apart from the one presented in Section 4.4 to which we can apply the regularized active layer model to test its performance. This is because either the conditions that other researchers have studied yield a well-posed active layer model (e.g. *Ashida and Michiue, 1971*) or the active layer model is ill-posed but the active layer thickness varies with time due to dune growth (*Blom et al., 2003*). The latter case is a situation that the regularization strategy cannot deal with (Section 4.3.1). However, *Ribberink (1987)* applies his two-layer model to a thought experiment under conditions in which the active layer model is ill-posed. In this section we apply the regularized active layer model to his thought experiment and compare it to the two-layer model.

Ribberink (1987) conducted a laboratory experiment with mixed-size sediment, which was dominated by aggradation after a period of degradation (Experiment E8-E9). The initial bed was characterized by a uniform slope, composed of a bimodal mixture (a coarse and fine fraction), and well mixed both in the streamwise and vertical direction. The sediment supply was initially in equilibrium. A temporal increase of the proportion of the coarse fraction in the sediment supply perturbed the equilibrium condition and induced the downstream propagation of a coarsening wave. The downstream migration of the coarsening front caused a preceding and temporary bed degradation as a result of the difference in sediment mobility between the coarse sediment forming the wedge and the fine sediment downstream of the front of the wedge. Eventually, the bed aggraded and was characterized by a larger slope than the initial one, so as to allow for the transport of the coarser fed sediment under equilibrium conditions.

During the short degradational part of the experiment, the bed surface was coarser than the substrate (i.e., conditions in which the active layer model is prone to be ill-posed (*Ribberink, 1987; Stecca et al., 2014; Chavarrías et al., 2018a*)). However, while reproducing the experiment numerically, *Ribberink (1987)* found that the active layer model was well-posed. Subsequently, *Ribberink (1987)* applied his two-layer model to a thought experiment that was equal to E8-E9 except for the fact that the substrate sediment was finer than in the flume experiment such that the active layer model is ill-posed. A numerical simulation of the thought experiment using the active layer model showed oscillations that eventually made the code crash (*Ribberink, 1987*). The thought experiment was reproduced well by a numerical code implementing *Ribberink's (1987)* two-layer model.

Here we run a numerical simulation of the thought experiment using our regularized active layer model and compare it to the results of *Ribberink's (1987)* two-layer model reported in Figure 7.9 of *Ribberink (1987)*. Simulation details can be found in Appendix C.3.

Figure 4.12 presents the time series of bed elevation and mean grain size of the bed surface sediment at a location 20 m downstream from the inlet. During the first 20 h the effects of the coarsening of the fed sediment are not felt 20 m downstream from the inlet. While the regularized active layer model predicts a constant bed elevation and grain size distribution of the bed surface sediment during this period of time, the two-layer model predicts a fining of the bed surface (Figure 4.12b). This is due to the fact that the initial grain size distribution of the exchange layer is not in equilibrium with the one at the

active layer and causes a vertical flux of sediment. However, the bed elevation remains constant as predicted by both models (Figure 4.12a).

The aggradational phase is preceded by a degradational wave, which is much more pronounced in the regularized active layer model than in the two-layer model. This is because in the regularized active layer model degradation causes entrainment of the fine substrate sediment, whereas in the two-layer model the exchange layer acts as a buffer that slows down the process. The coarsening of the bed surface between approximately 25 h and 40 h as predicted by both models is very similar. While after 40 h the regularized active layer model predicts a constant grain size distribution of the bed surface sediment, the two-layer model predicts an asymptotic adaptation toward equilibrium conditions. This effect is again caused by the exchange layer that coarsens slowly compared to the active layer on top of it, as it accounts for the effects of occasionally large bedforms. The equilibrium state differs between the two models. We believe that this is due to the fact that we do not know exactly what values were used by *Ribberink* (1987) for the constants in the sediment transport relation (Appendix C.3).

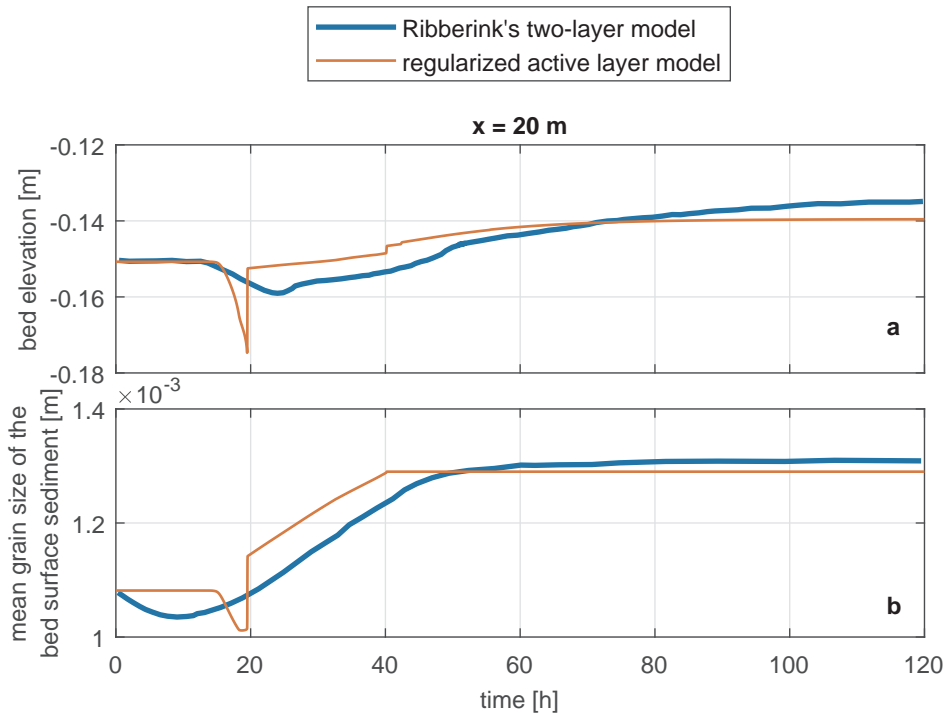


Figure 4.12: Bed elevation (a) and mean grain size of the bed surface sediment (b) with time predicted for the thought experiment based on Experiment E8-E9 conducted by *Ribberink* (1987) using Ribberink's two-layer model and the regularized active layer model. The results of the two-layer model are extracted from Figure 7.9 of *Ribberink* (1987).

The regularized active layer model captures the dynamics predicted by the two-layer

model of *Ribberink* (1987). The advantage of the two-layer model is that it accounts for a source of vertical mixing that the regularized active layer model does not take into consideration (i.e., the mixing due to occasionally large bedforms). On the other hand, the two-layer model may become ill-posed (*Sieben*, 1994) while the regularized active layer model is always well-posed.

4.6. Discussion

In this section we discuss the physical interpretation of the regularization strategy (Section 4.6.1), as well as possible extensions and further development (Section 4.6.2).

4.6.1. Physical Interpretation of the Regularization Strategy

The ill-posed solution predicted by the active layer model is characterized by oscillations that temporarily fine the bed surface and coarsen the substrate. This behavior is also observed in our laboratory experiments (Figures 4.6 and 4.7). One may be tempted to conclude that the active layer model, although being mathematically ill-posed, provides reasonable results. This argument is wrong for two reasons. The first reason is that the numerical solution does not converge for a decreasing mesh size. The solution keeps changing and oscillations become larger when the cell size is reduced (*Joseph and Saut*, 1990; *Chavarrías et al.*, 2018a). Such a solution cannot be representative of physical phenomena. Second, the physical processes responsible for the small scale variability in bed elevation (i.e., ripples, bedload sheets) are not accounted for by the active layer model (Section 4.3.1). Any resemblance of the model results with bed elevation fluctuations due to small scale bedforms is therefore coincidence.

The frequently used morphodynamic factor (Φ_η) (*Latteux*, 1995; *Roelvink*, 2006; *Ranasinghe et al.*, 2011) is a particular case of a preconditioning matrix with parameters $\beta = 1/\Phi_\eta$ and $\alpha_k = 1 \forall k$. The proposed regularization strategy can be considered as the use of a morphodynamic factor not only for the changes in bed elevation (η) but also for the changes in grain size distribution of the bed surface (M_{sk}). The “sorting morphodynamic factor” (Φ_{sk}) is then defined as $\Phi_{sk} = 1/(\alpha_k \beta)$. We have seen that the only applicable regularization strategy is that in which $\alpha_k = \alpha > 1 \forall k$ and $\beta = 1$, which is equivalent to saying that the regularization strategy is based on a “sorting morphodynamic factor” $0 < \Phi_s < 1$. This implies that the mixing or sorting processes associated with changes in grain size distribution of the bed surface sediment are slowed down with respect to the celerity predicted by the active layer model.

The effect of applying the regularization strategy is a slowdown of the sediment mixing processes in the model computations. This effect is similar to the effect of a (temporary) increase of the active layer thickness. From a physical perspective this slowdown of mixing processes may be associated with a (temporary) increase of the range of elevations covered by the bed level fluctuations (*Blom et al.*, 2008). The slowdown of mixing processes resulting from applying the regularization strategy implies that the regularized active layer model can be applied to a wider range of physical problems (i.e., also those characterized by a fairly small time scale of mixing) than the active layer model.

4.6.2. Alternatives to the Regularization Strategy

Our regularization strategy is applied locally and temporally. Worded differently, only when and where the model is ill-posed, we update the grain size distribution of the bed surface sediment using the parameter α_c . Moreover, α_c depends only on the conditions at the location under consideration (note that the preconditioning matrix is diagonal). This is the simplest strategy but one could decide to avoid discontinuities in the value of α_c throughout the domain by coupling neighboring nodes.

Carraro et al. (2018) propose a technique to decrease the computational cost of morphodynamic simulations. As in our case, their strategy can be seen as a preconditioning technique. They consider unisize sediment conditions and modify not only the *Exner* (1920) equation but also the continuity equation. Here we modify the active layer equation but not the flow equations or the *Exner* (1920) equation. A combination of both strategies could yield a technique that both decreases the cost of numerical simulations and guarantees that the model is well-posed.

We have focused on restoring the hyperbolic character of the system of equations and to this end we based our study on the linear solution (i.e., short waves). This focus suffices here, as short waves are most sensitive to ill-posedness (*Joseph and Saut*, 1990). However, the regularization strategy modifies the celerity and growth rate not only of short waves but also of long ones. For this reason, we suggest to further study how long waves are affected and whether the results of the regularization strategy are physically realistic based on a similar analysis to that of *Lanzoni et al.* (2006).

We have assumed a constant active layer thickness to avoid the added complexity due to a cumbersome closure relation linking the preconditioning parameters to the change in time of the active layer thickness. It may be possible to extend our regularization strategy to situations in which the active layer thickness changes with time (e.g., due to dune growth) by providing such a closure relation. On the other hand, it is reasonable that the regularization strategy requires a constant active layer thickness given the fact that mathematically the strategy has the same effect as an increase in the active layer thickness (i.e., a decrease in the celerity of the mixing processes).

We have concluded that the regularization strategy needs to slowdown the mixing processes (i.e., $\alpha_c > 1$) to guarantee that the eigenvalues are always positive regardless of the value of the sorting celerity λ_{s1} . However, if the sorting celerity is guaranteed to be positive (e.g., because hiding is negligible), the acceleration of the mixing processes also yields positive eigenvalues and a well-posed model. There may be cases in which the latter strategy yields more realistic results. Moreover, we have chosen to guarantee that the regularized eigenvalues are positive reasoning that morphodynamic information travels in the downstream direction under subcritical conditions (*Suzuki*, 1976; *Lyn and Altinakar*, 2002; *Lanzoni et al.*, 2006; *Stecca et al.*, 2014). This statement is partially contradictory to recent studies that consider sediment transport as a stochastic process (*Furbish et al.*, 2012a; *Ancey and Heyman*, 2014). The stochastic nature of sediment transport yields an advection-diffusion equation that models the amount of moving particles per unit of bed area. The diffusive character implies that information also travels in the upstream direction. For this reason, a regularization strategy in which information travels in the upstream direction may be physically realistic under certain circumstances.

For a case with more than two sediment size fractions (Section 4.3.4), the approxi-

mate value of the parameter α_c is not (completely) satisfactory as well-posedness is not guaranteed. We have observed in our tests that ill-posedness occurs when (at least) two eigenvalues of the bed and sorting eigenvalues are similar with respect to the other bed and sorting eigenvalues. For a case considering two sediment size fractions this is referred in literature as the “crossing of eigenvalues” (Sieben, 1997; Stecca *et al.*, 2014). Worded differently, the difference between two eigenvalues must be large enough for the model to be well-posed. A regularization strategy based on guaranteeing a minimum distance between eigenvalues could yield an inexpensive solution for the case with more than two sediment size fractions.

4.7. Conclusions

We have developed a preconditioning method for regularizing the active layer model (Hirano, 1971) used in modeling mixed-sediment river morphodynamics. Our method recovers the well-posed character of the system of equations by means of one parameter that modifies the celerity of the mixing processes. Physically this means that the mixing processes are slowed down or the time scale of the mixing processes is increased.

We conduct 4 laboratory experiments under conditions in which the active layer model is ill-posed and we compare the observations to the predictions of the regularized active layer model. The regularized active layer model captures the mean behavior observed in the experiments associated with changes averaged over the passage of several bedforms.

5

A Well-posed Alternative to the Hirano Active Layer Model for Mixed-Size Sediment Rivers

All models are wrong, but some are useful.

Box (1976)

*Mirar el río hecho de tiempo y agua
Y recordar que el tiempo es otro río,
Saber que nos perdemos como el río
Y que los rostros pasan como el agua.*

Borges (1977)

The active layer model (Hirano, 1971) is most frequently used for modelling mixed-size sediment river morphodynamic processes. It assumes that all the dynamics of the bed surface are captured by a top homogeneous layer that interacts with the flow. Although successful in reproducing a wide range of phenomena, it has two problems: (1) it may become mathematically ill-posed, which causes the model to lose its predictive capabilities, and (2) it does not capture dispersion of tracer sediment. We extend the active layer model by accounting for conservation of the sediment in transport and obtain a new model that overcomes the two problems. We analytically assess the model properties and discover an instability mechanism associated with the formation of waves under conditions in which the active layer model is ill-posed. Numerical simulations of tracer dispersion show that the model reproduces reasonably well a

This chapter has been accepted for publication in the *Journal of Geophysical Research: Earth Surface*

laboratory experiment under conditions in which the effect of temporary burial of sediment due to bedforms is negligible. Simulations of a field experiment show that the model does not capture the effect of temporary burial of sediment by bedforms. We are capable of reproducing two laboratory experiments conducted under conditions in which the active layer model is ill-posed. The new model captures the formation of waves and mixing due to an increase in active layer thickness.

5.1. Introduction

A common approach in modelling river morphodynamic changes in space and time consists of solving a set of differential equations that account for the flow and bed changes. As the hydrostatic pressure assumption is typically valid in fluvial problems, the flow is often modelled using the Shallow Water Equations (e.g. *Tan, 1992; Vreugdenhil, 1994*) in two-dimensional systems, which reduce to the *Saint-Venant (1871)* equations under one-dimensional conditions. Bed elevation changes are accounted for using the *Exner (1920)* equation and changes in the bed surface texture using the active layer model (*Hirano, 1971*). Changes in bed elevation and surface texture depend on the gradient of the sediment transport rate. This modelling framework has been applied for decades (e.g. *Bennett and Nordin, 1977; Ferguson et al., 2015*), it is implemented in major software packages (e.g. *Vetsch et al., 2006; Mosselman and Sloff, 2007; Sloff and Mosselman, 2012; Villaret et al., 2013*), and has proven to be a powerful tool able to model processes from the lab to the field scale (e.g. *Cui et al., 2003; Williams et al., 2016; Orrú et al., 2016a*).

Yet, the above modelling approach has two drawbacks. First, the solution may be invalid as the system of equations may become mathematically ill-posed (*Ribberink, 1987; Stecca et al., 2014; Chavarrías et al., 2018a*). In ill-posed problems, the growth rate of perturbations tends to infinite as the wavelength decreases (*Hadamard, 1923; Joseph and Saut, 1990; Kabanikhin, 2008*). This is physically unrealistic, as physical processes are subject to short-wavelength perturbations (e.g., noise) that do not grow unbounded. Numerical solutions of ill-posed problems continue to change as the grid is refined (i.e., do not converge with the grid) (*Joseph and Saut, 1990*). Ill-posedness is a symptom of a model not capturing key physical elements (*Joseph and Saut, 1990; Fowler, 1997*).

Chavarrías et al. (2018a) show an example of the consequences of ill-posedness in river morphodynamic simulations. As the model becomes ill-posed, perturbations due to numerical truncation error grow up to the scale of the flow depth and alter the stratigraphy in an unrealistic manner.

The second limitation of the active layer model is related to sediment dispersion. The active layer model predicts tracer sediment to be advected downstream without dispersing (*Iwasaki et al., 2017; Chavarrías et al., 2019a*). Yet, both in the field (e.g. *Sayre and Hubbell, 1965; Rathbun et al., 1971; Drake et al., 1988; Hassan et al., 1991; Nikora et al., 2002; Bradley and Tucker, 2012; Bradley, 2017*), and in the laboratory (e.g. *Hill et al., 2010; Roseberry et al., 2012; Martin et al., 2012*), traced sediment particles are observed to disperse as they move downstream. In general, particles may disperse in a superdiffusive, subdiffusive, or normal (Fickian) manner (*Havlin and Ben-Avraham, 1987; Metzler and Klafter, 2000*). Normal diffusion means that the variance of the particle position scales linearly with time. This behavior arises from collisions between a large amount of particles (*Einstein, 1905*) and is ubiquitous in nature. If variance does not scale linearly with time, particle diffusion is called anomalous. Anomalous diffusion is superdiffusive or subdiffusive depending on whether the relation between the variance and the time is larger or smaller than linear, respectively (*Havlin and Ben-Avraham, 1987; Metzler and Klafter, 2000*). As the variance characterizes the celerity at which particles spread, anomalous diffusion implies that dispersion is scale-dependent (i.e., it depends on the time scale (*Bouchaud and Georges, 1990*)).

In order to solve for the first limitation and recover well-posedness of the active layer

model, *Chavarrías et al.* (2019a) have proposed a regularization strategy. The strategy is based on identifying the locations at which the active layer model is ill-posed and locally modifying the celerity at which mixing processes occur. In essence, the strategy alters the celerity of the mixing processes predicted by the active layer model, such that the regularized model is well-posed. *Chavarrías et al.* (2019a) conducted a set of laboratory experiments under conditions in which the active layer model is ill-posed to test the regularization strategy. In particular, the experiments were characterized by degradation of a coarse bed surface into a substrate consisting of fine sediment. The situation appeared to be unstable: bedforms composed of coarse sediment grew due to entrainment of fine sediment in the troughs, and decayed when coarse sediment coming from upstream covered the bed. The oscillations due to the instability mechanism were superimposed on the overall degradational trend. The regularized model captured the overall degradational trend but did not reproduce the oscillations due to the instability mechanism (*Chavarrías et al.*, 2019a). Another drawback of the regularization strategy is the fact that it can only be applied if the active layer thickness remains constant with time.

As regards to the second limitation of the active layer model, dispersion of tracer sediment is captured when sediment transport is treated in a stochastic manner, which was first shown by *Einstein* (1936). He described sediment transport as particles traveling in a series of jumps of varying length and frequency. This allowed for deriving the probability that a tracer particle is at a certain location as a function of time, although the model was not linked to flow and bed elevation changes. *Einstein* (1936)'s theory was applied by *Sayre and Hubbell* (1965) and *Habersack* (2001), among others, to explain tracer dispersion in field cases in the United States and New Zealand, respectively. Recent refinements of *Einstein* (1936)'s theory include, for instance, the work by *Fan et al.* (2016, 2017), who considered the effect of the travel time in simulating tracer motion. Yet, just as in *Einstein* (1936), their approach to sediment transport is not combined with flow and morphodynamic change.

A different approach for modelling tracer dispersion consists of accounting for the number of static and moving particles in the bed. In this way, *Lajeunesse et al.* (2013, 2017, 2018) model dispersion of a plume of unisize tracer sediment. In their idealized conditions, sediment disperses in a Fickian manner. *Ancey et al.* (2006, 2008) considered the statistics of unisize sediment transport and showed that this can be well captured using a discrete statistic theory (i.e., birth-death discrete Markov processes). A continuum version of the theory was derived by *Ancey* (2010) and *Ancey and Heyman* (2014), who accounted for the variability in particle velocity. This led to an advection-diffusion equation modeling the ensemble average of the volume of sediment in transport per unit of bed area. The diffusive behavior of the equation explains tracer dispersion. *Boborquez and Ancey* (2015) coupled the model developed by *Ancey and Heyman* (2014) to the *Saint-Venant* (1871) flow equations to model the formation of antidunes. Interestingly, an advection-diffusion equation for modelling the volume of sediment in transport was obtained also by *Furbish et al.* (2012a) starting from a continuous probabilistic formulation. These recent advances improve our understanding of sediment transport, but remain focused on unisize sediment conditions.

Our objective is to develop a model that accounts for mixed-size sediment river morphodynamic changes and overcomes the two limitations mentioned above. In particular,

we aim at a well-posed model that captures tracer dispersion and the instability mechanism due to the entrainment of fine substrate sediment. To this end, we combine the active layer model with the model by *Bohorquez and Ancey* (2015), after we extend the latter to mixed-size sediment conditions.

In Section 5.2 we present the mathematical model. In Section 5.3 we linearize the system of equations and study the growth rate of perturbations to explain the instability associated with the entrainment of fine substrate sediment. We follow this approach, as it has been useful to explain the formation of other patterns such as ripples (*Sumer and Bakioglu*, 1984; *Colombini and Stocchino*, 2011), dunes (*Kennedy*, 1963; *Colombini and Stocchino*, 2008), bars (*Callander*, 1969; *Schielen et al.*, 1993), and meanders (*Ikeda et al.*, 1981; *Seminara*, 2006). We also use the linear model to corroborate the well-posedness of the system of equations and to study the manner in which tracer sediment disperses. In Section 5.4 we reproduce two cases of tracer propagation under laboratory and field conditions, and two laboratory cases conducted under conditions in which the active layer model is ill-posed. In Section 5.5 we discuss the results.

5.2. The SILKE model

In this section we present the SILKE model (Sediment Layers with source-sinK Exchange) for mixed-size sediment river morphodynamics. In Section 5.2.1 we present the model equations. The closure relations are shown in Section 5.2.2. In Section 5.2.3 we explain the numerical technique that allows for solving the system of equations.

5.2.1. Conservation Equations

We consider one-dimensional flow over a bed composed of an arbitrary number of non-cohesive sediment fractions. The sediment fractions are characterized by a grain size d_k [m], where the subscript k identifies each fraction in increasing size (i.e., $d_1 < d_2 < \dots < d_N$) and N is the total number of size fractions.

We assume that the concentration of solid to liquid discharge is below 6×10^{-3} , so that the effect of the concentration of sediment on the flow is negligible (*Garegnani et al.*, 2011, 2013). Under these conditions, unsteady depth-averaged flow is modelled by the *Saint-Venant* (1871) equations. Here, for simplicity, we assume steady flow to obtain the backwater equation (e.g. *Chow*, 1959).

Similarly to *Hirano* (1971), we assume that sediment can be in 3 states: (1) in motion, predominantly in the streamwise direction, (2) at the bed surface, where it can be entrained into motion and deposited, or (3) in the substrate, where sediment is immobile and cannot be entrained. Subsequently, we will provide equations describing the conservation of mass of the sediment in each of the three states. *Hirano* (1971) did not consider conservation of the sediment in transport in deriving the active layer model. This was done by *Armanini and Di Silvio* (1988), who extended the active layer model with two more layers to account for suspended load and bed load. In applying their model, they simplified it by assuming that the sediment transport rate is at capacity and that the temporal change of the volume of sediment in the bed load layer is negligible compared to the divergence of the sediment transport rate and the flux of sediment to the bed load layer. These two assumptions essentially remove the dynamics of the bed load layer, which is

the key focus of our analysis.

Bohorquez and Ancey (2015) describe the motion of unisize sediment based on a stochastic interpretation of sediment transport. We extend their framework to mixed-size sediment conditions by considering all variables to be grain size dependent. Conservation of the mass of sediment in transport is described by:

$$\frac{\partial \Gamma_k}{\partial t} + \frac{\partial v_{pk} \Gamma_k}{\partial x} - \frac{\partial^2 \chi_k \Gamma_k}{\partial x^2} = E_k - D_k, \quad (5.1)$$

where t [s] denotes the time coordinate, x [m] is the streamwise coordinate, E_k [m/s] and D_k [m/s] are entrainment and deposition rates of each size fraction k , and v_{pk} [m/s] is the ensemble average of the instantaneous velocity of the moving particles of size fraction k . Parameter χ_k [m²/s] is the diffusivity of size fraction k due to the variability in particle velocity from an Eulerian perspective (*Roseberry et al.*, 2012; *Furbish et al.*, 2012b, 2017). This is essentially different from the Lagrangian diffusivity obtained from tracer dispersion experiments. Parameter Γ_k [m] is the ensemble average of the volume of sediment in transport of size fraction k per unit of bed area. Following *Furbish et al.* (2012a) we will term Γ_k the particle activity.

The particle activity can be interpreted as a fictitious layer with thickness Γ_k . Yet, it is important to note that here no thickness of the bed load layer is specified as opposed to, for instance, *Van Rijn* (1984), *Luu et al.* (2004), *Wu* (2004), *Colombini* (2004), and *Colombini and Stocchino* (2005). Contrary to *Armanini and Di Silvio* (1988), we do not make a distinction between suspended and bed load sediment. In our extension to mixed-size sediment conditions, we implicitly neglect the covariance terms that appear in Equation (5.1) due to the correlation between particle size, velocity, and diffusivity (*Furbish et al.*, 2012a). The possible implications of this assumption are assessed in Section 5.5.2.

The sediment transport rate of size fraction k (q_{bk} [m²/s]) does not depend on the flow properties only and is equal to:

$$q_{bk} = v_{pk} \Gamma_k - \frac{\partial \chi_k \Gamma_k}{\partial x}. \quad (5.2)$$

This expression is a mixed-size sediment version of the expression derived by *Furbish et al.* (2012a), where we have assumed that all variables are grain size dependent.

Following *Einstein* (1950), we assume that the changes in bed elevation are due to the difference between entrainment and deposition rates. Mass conservation of the bed surface sediment (considering all sediment size fractions) yields the entrainment form of the *Exner* (1920) equation (*Nakagawa and Tsujimoto*, 1980a; *Borah et al.*, 1982; *Parker et al.*, 2000; *Furbish et al.*, 2012a):

$$(1-p) \frac{\partial \eta}{\partial t} = D - E, \quad (5.3)$$

where p [—] denotes the bed porosity, η [m] the bed elevation, and E [m/s] and D [m/s] are the total entrainment and deposition rates. For simplicity, mechanisms such as subsidence and uplift, compaction and dilation of sediment are neglected in the above equation (*Paola and Voller*, 2005).

Following *Hirano* (1971), we assume that only the top part of the bed, characterized by a certain thickness (i.e., the active layer thickness), interacts with the flow. Sediment in

the active layer is homogeneously mixed such that the layer has no vertical stratigraphy. Sediment is entrained from and deposited in the active layer, and a vertical flux of sediment between the active layer and the substrate occurs if the elevation of the interface between the active layer and the substrate changes.

Using this formulation, one implicitly assumes that the probability of entrainment is constant within the active layer and equal to 0 in the substrate (*Parker et al.*, 2000). This is an approximation, as in reality there is no discrete distinction between the active and inactive part of the bed. In reality, the probability of a particle of being entrained depends on its probability of being exposed to the flow (*Galvin*, 1965; *Ribberink*, 1987; *Hassan and Church*, 1994; *Parker et al.*, 2000; *Blom and Parker*, 2004). Bed elevation fluctuations due to ripples, dunes, bars, or any other sort of bedforms, cause the probability of exposure to vary with vertical position. Particles deposited at lower elevations have a smaller probability of being re-entrained. For this reason, using a single discrete active layer it is not possible to capture the effect of temporary burial of sediment due to bedforms reworking sediment at an elevation significantly lower than the lower limit of the active layer (*Ribberink*, 1987; *Blom*, 2008).

The entrainment formulation of the active layer model reads (*Parker et al.*, 2000):

$$(1-p) \frac{\partial M_{ak}}{\partial t} + (1-p) f_k^I \frac{\partial (\eta - L_a)}{\partial t} = D_k - E_k, \quad (5.4)$$

where $M_{ak} = F_{ak} L_a$ [m] is the volume of sediment of size fraction k in the active layer per unit of bed area, L_a [m] is the active layer thickness, and $F_{ak} \in [0, 1]$ [-] and $f_k^I \in [0, 1]$ [-] are the volume fraction content of size fraction k in the active layer and at the interface between the active layer and the substrate, respectively. Conservation of sediment in the substrate for each size fraction yields (*Stecca et al.*, 2014):

$$(1-p) \frac{\partial M_{sk}}{\partial t} - (1-p) f_k^I \frac{\partial (\eta - L_a)}{\partial t} = 0, \quad (5.5)$$

where M_{sk} [m] represents the volume of sediment in the substrate per unit of bed area. By definition, the sum of the volume fraction content over all size fractions equals 1:

$$\sum_{k=1}^N f_k^I = 1, \quad \sum_{k=1}^N F_{ak} = 1, \quad (5.6)$$

and the total entrainment and deposition rates are the sum of the rates per size fraction:

$$E = \sum_{k=1}^N E_k, \quad D = \sum_{k=1}^N D_k. \quad (5.7)$$

The main variables of the SILKE model are shown in Figure 5.1, together with the active layer model for comparison.

The model requires closure relations for the entrainment and deposition rates, the particle velocity, diffusivity, as well as friction. In the following section we will discuss these closure relations.

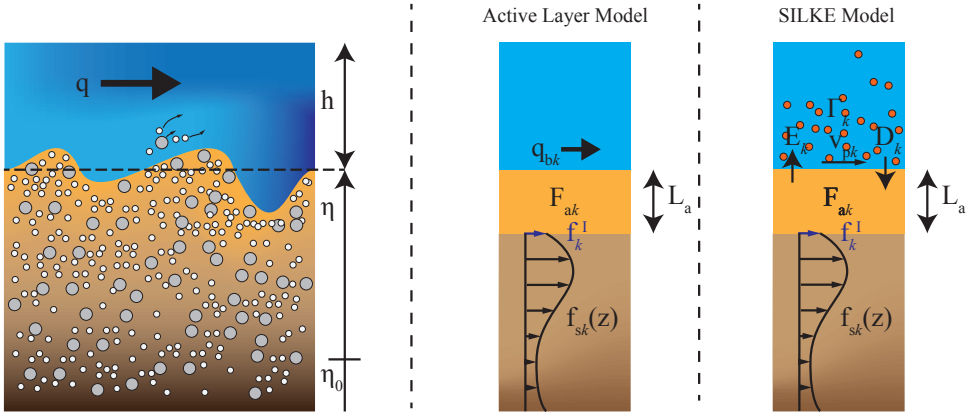


Figure 5.1: Sketch representing the main variables of the active layer model (Hirano, 1971) and the SILKE model. The figure is adapted from Figure 2 in Chavarrías et al. (2018a).

5.2.2. Closure Relations

In this section we introduce the closure relations of the model. We assume a Chézy-type friction such that $S_f = C_f Fr^2$, where $S_f [-]$ denotes the friction slope, $C_f [-]$ is a nondimensional friction coefficient that we assume to be independent of the flow and bed parameters, and $Fr = u / \sqrt{g h} [-]$ is the Froude number. Parameter u [m/s] denotes the mean flow velocity, h [m] the mean flow depth, and g [m/s²] is the acceleration due to gravity.

We assume that, for a given bed shear stress, the rate at which particles of size fraction k are set into motion per unit of bed area, E_k , depends on the volume fraction content of sediment of size fraction k in the active layer F_{ak} (e.g. Parker, 2008). The rate at which particles of size fraction k settle per unit of bed area, D_k , depends, for a given bed shear stress, on the volume of sediment of size fraction k in transport per unit of bed area, Γ_k (e.g. Seminara et al., 2002). The particle activity, Γ_k , is nondimensionalized using the grain size and the entrainment and deposition rates are nondimensionalized using the parameter $\sqrt{R g d_k}$ (Kalinske, 1947; Einstein, 1950; Fernandez-Luque and Van Beek, 1976; Seminara et al., 2002), where $R = (\rho_s - \rho_w) / \rho_w [-]$ is the submerged specific gravity, ρ_s [kg/m³] is the sediment density, and ρ_w [kg/m³] the water density. We assume $\rho_s = 2650$ kg/m³ and $\rho_w = 1000$ kg/m³. It is convenient to define a capacity of entrainment and deposition (\hat{E}_k [1/s] and \hat{D}_k [1/s], respectively), which depend on the variables of the model M_{ak} and Γ_k , for the later mathematical analysis of the model:

$$E_k = M_{ak} \hat{E}_k, \quad D_k = \Gamma_k \hat{D}_k. \quad (5.8)$$

Parameters \hat{E}_k and \hat{D}_k expressed in terms of the nondimensional entrainment and deposition rates E_k^* and D_k^* are:

$$\hat{E}_k = \frac{\sqrt{R g d_k}}{L_a} E_k^*, \quad \hat{D}_k = \frac{\sqrt{R g d_k}}{d_k} D_k^*. \quad (5.9)$$

The entrainment rate does not depend on the amount of particles being transported, which implies we neglect the entrainment due to collisions of particles in transport with the bed (i.e., collective entrainment (*Ancey and Heyman, 2014*)).

The nondimensional particle velocity v_{pk}^* [–] is defined as (*Fernandez-Luque and Van Beek, 1976; Seminara et al., 2002*):

$$v_{pk}^* = \frac{v_{pk}}{\sqrt{Rgd_k}}. \quad (5.10)$$

We need to specify closure relations for the dimensionless particle entrainment E_k^* , deposition D_k^* , and velocity v_{pk}^* . Yet, the sediment transport rate under equilibrium conditions, $q_{bk_{eq}}$ [m²/s], is the variable traditionally related to the flow properties (e.g. *Meyer-Peter and Müller, 1948; Engelund and Hansen, 1967; Ashida and Michiue, 1971; Wilcock and Crowe, 2003*). Under equilibrium conditions, we find the following relation between entrainment, deposition, velocity, and transport:

$$q_{bk_{eq}}^* = \frac{E_k^* v_{pk}^*}{D_k^*}, \quad (5.11)$$

where $q_{bk_{eq}}^* = q_{bk_{eq}} / \sqrt{Rgd_k^3}$ [–] is the nondimensional equilibrium sediment transport rate. One can decide which three variables are specified using closure relations. We choose for E_k^* , v_{pk}^* , and $q_{bk_{eq}}^*$. In principle any combination of closure relations can be used. However, attention needs to be paid when using closure relations which account for a critical *Shields* (1936) stress in conditions close to incipient motion, as this may create discontinuities in, for instance, $q_{bk_{eq}}^*$ if D_k^* is zero but not the product $E_k^* v_{pk}^*$.

Fernandez-Luque and Van Beek (1976) developed closure relations for unisize sediment conditions. We generalize their expressions to mixed-size sediment conditions. To this end, we consider the bed shear stress for each size fraction and account for hiding effects. These hiding effects represent the facts that: (a) fine fractions in a sediment mixture hide behind large grains and experience a larger critical bed shear stress than under unisize conditions and (b) coarse particles are more exposed to the flow than under unisize sediment conditions (and so experience a smaller critical bed shear stress) (*Einstein, 1950*). The relations by *Fernandez-Luque and Van Beek* (1976) extended to mixed-size sediment conditions read:

$$E_k^* = 0.0199(\theta_k - \xi_k \theta_c)^{3/2}, \quad (5.12)$$

$$v_{pk}^* = 11.5 \left(\sqrt{\theta_k} - 0.7 \sqrt{\xi_k \theta_c} \right), \quad (5.13)$$

$$q_{bk_{eq}}^* = 5.7(\theta_k - \xi_k \theta_c)^{3/2}, \quad (5.14)$$

where $\theta_k = C_{fb} u^2 / g R d_k$ [–] is the *Shields* (1936) stress, θ_c [–] is the critical *Shields* (1936) stress, and ξ_k [–] is the hiding function. The parameter C_{fb} [–] is the skin friction coefficient.

We also apply the sediment transport relation developed by *Ashida and Michiue* (1971):

$$q_{bk_{eq}}^* = 17(\theta_k - \xi_k \theta_c) \left(\sqrt{\theta_k} - \sqrt{\xi_k \theta_c} \right), \quad (5.15)$$

where:

$$\xi_k = \begin{cases} 0.843 \left(\frac{d_k}{D_m} \right)^{-1} & \text{for } \frac{d_k}{D_m} \leq 0.4 \\ \left(\frac{\log_{10}(19)}{\log_{10}(19 \frac{d_k}{D_m})} \right)^2 & \text{for } \frac{d_k}{D_m} > 0.4 \end{cases}, \quad (5.16)$$

where D_m [m] denotes the geometric mean grain size of the bed surface sediment and $\theta_c = 0.05$. To avoid discontinuities under conditions close to incipient motion, we derive an entrainment function that prevents discontinuities in the deposition rate. The discontinuity is avoided using an entrainment function that depends on the excess bed shear stress in a similar manner as the sediment transport rate. As a result, the deposition rate is a constant multiplying the relation for the particle velocity function (see Equation 5.11). The entrainment function reads:

$$E_k^* = 0.0591(\theta_k - \xi_k \theta_c) \left(\sqrt{\theta_k} - \sqrt{\xi_k \theta_c} \right), \quad (5.17)$$

where the value of the constant is chosen such that the deposition rate is equal to the one found by *Fernandez-Luque and Van Beek* (1976), as we lack data to derive a relation ourselves. This decision is arbitrary but fine for our purpose.

The diffusivity in the sediment transport α_k is equal to the product of the variance of the particle velocity and the Lagrangian integral time scale of the particle velocity, which is a measure of the time over which the particle velocity is significantly autocorrelated (e.g. *Niewstadt et al.*, 2016). Assuming an exponential distribution of particle velocities (*Lajeunesse et al.*, 2010; *Roseberry et al.*, 2012; *Furbish et al.*, 2012c; *Furbish and Schmeckle*, 2013; *Fathel et al.*, 2015), the variance of the particle velocity is equal to the square of the average particle velocity. As particle travel time is of the same order of magnitude as the integral time scale (*Roseberry et al.*, 2012), particle diffusivity is proportional and of the same order of magnitude as the product of the average particle velocity and the step length (*Furbish et al.*, 2012b).

Various relations for the mean step length have been proposed. *Nakagawa and Tsujimoto* (1980b) found that, under mixed-size sediment conditions, the step length is 10–30 times the grain size and it slightly increases with the bed shear stress. *Sekine and Kikkawa* (1992) derived a relation depending on the bed shear stress and the sediment fall velocity and *Niño et al.* (1994) found that the step length varies between 4.5–8 times the grain size. Similar results were obtained by *Hu and Hui* (1996a,b), who included the effect of sediment density. In our analysis only the order of magnitude of the diffusivity matters. For this reason, we choose the simple relation by *Fernandez-Luque and Van Beek* (1976) in which the mean step length is 16 times the grain size. Then, the particle diffusivity is:

$$\alpha_k = 16v_{pk}d_k. \quad (5.18)$$

We can analytically derive some model properties that help us understand its behavior and mathematical character (Section 5.3). Yet, in a general case we need to solve the

problem numerically. In the next section we explain the technique to numerically solve the system of equations.

5.2.3. Numerical Solution

To numerically solve the system of equations of the active layer model, we use the numerical research code Elv as explained in *Chavarrías et al.* (2019a). In brief, we solve the backwater equation in combination with the flux form of the *Exner* (1920) and active layer equations in a decoupled manner. This implies that the equations are assumed to weakly interact with each other, which is acceptable if the Froude number is below approximately 0.7 (*Lyn*, 1987; *Lyn and Altinakar*, 2002; *Sieben*, 1999). The backwater equation is solved using the standard fourth order Runge-Kutta method, and the *Exner* (1920) and active layer equations are solved using a first order upwind scheme (i.e., FTBS (*Sonke et al.*, 2003; *Long et al.*, 2008; *Zima et al.*, 2015)) using a variable time step to guarantee a CFL number equal to 0.9. The substrate is discretized using Eulerian cells such that only the cell below the active layer has a variable thickness. Cells are created when a specified thickness of this cell is reached under aggradational conditions. The implementation is mass conservative independent of the number of cells created or consumed in one time step (*Stecca et al.*, 2016).

We have extended Elv to solve the system of equations of the SILKE model. Equation (5.3) for the bed elevation and Equation (5.4) for the volume of sediment of each size fraction in the active layer are solved using a first order forward Euler scheme. When the diffusion coefficient of Equation (5.1) for the particle activity is set to 0, the equation is solved using an FTBS scheme. When considering diffusion, the difference in the order of magnitude between the advective and diffusive components limits the application of a second order centered scheme. In order to reduce the computational time, we solve the advective term using an upwind scheme and the diffusive term using centered differences. The time integration is performed using the scheme proposed by *Crank and Nicolson* (1947). The source term complicates the implementation of an automatic time stepping method. For this reason, the time step is fixed and the largest possible value that guarantees a monotone solution is found by trial and error.

Boundary conditions are necessary for the backwater and particle activity equations only. Regarding the backwater equation, we impose the downstream water surface elevation, which agrees with the fact that the flow is subcritical. Regarding the particle activity, we consider two possibilities: a recirculating and a feed flume-like simulation (*Parker and Wilcock*, 1993). In the case of recirculating flume-like simulation, we impose cyclic boundary conditions on the particle activity by copying the downstream value of the particle activity at the upstream end (i.e., a Dirichlet boundary conditions).

In the case of a feed flume-like simulation, we make a distinction between the cases accounting for diffusion and the cases neglecting it. When diffusion is neglected ($\chi_k = 0 \forall k$), information in the particle activity equation travels in the downstream direction only. In this case, only an upstream boundary condition is required to solve the particle activity equation. The variable that is usually set is the sediment transport rate, which in this case is equivalent to a condition on the particle activity (i.e., a Dirichlet boundary condition, see Equation (5.2)). Diffusion requires both upstream and downstream boundary conditions to solve the equation. Imposing the sediment transport rate at the

upstream end involves a condition on the particle activity and its derivative (i.e., a Robin boundary condition, see Equation (5.2)). It is difficult to impose a boundary condition at the downstream end, as there is no physical constraint regarding the sediment transport rate or the particle activity. As in our simulations the downstream end of the domain is initially under equilibrium conditions, we impose equilibrium sediment transport rate at the downstream end (i.e., a Robin boundary condition) and ensure that the domain is long enough such that this downstream boundary condition does not affect the solution within the domain of interest.

5.3. Instability, Well-Posedness, and Dispersion

Before applying the model to laboratory and field cases, this section aims to gain insight on its properties and characteristics. To be able to conduct the study in analytical terms, we simplify the equations and work with a linearized version of the model (Section 5.3.1). We focus on the 3 characteristics that the model is expected to capture (Section 5.1). We study the stability of the model (Section 5.3.2), its well-posedness (Section 5.3.3), and the dispersion of tracer sediment (Section 5.3.4).

5

5.3.1. Linear Model

In this section we linearize the SILKE model. The dependent variables of the system are $\eta, \Gamma_k \forall k, M_{ak} \forall k \in \{1, N-1\}$. Note that the N -th volume of sediment in the active layer is not a variable of the system due to the constraint on the volume fraction content in Equation (5.6). As the substrate equation is a linear combination of Equations (5.3) and (5.4), the substrate equations does not play a role in the dynamics of the system and can be treated in a decoupled form (Stecca *et al.*, 2014; Chavarrías *et al.*, 2018a).

To linearize the system of equations we consider a reference state of dependent variables $\eta_0, \Gamma_{k0} \forall k, M_{ak0} \forall k \in \{1, N-1\}$, which is a solution of the system of equations. The subscript 0 indicates that these are constant values at the reference state, which represents steady uniform straight flow over a flat sloping bed composed of an arbitrary but uniform grain size distribution. A small perturbation $\eta', \Gamma'_k \forall k, M'_{ak} \forall k \in \{1, N-1\}$ is added to the reference state, such that $\eta = \eta_0 + \eta', \Gamma_k = \Gamma_{k0} + \Gamma'_k \forall k, M_{ak} = M_{ak0} + M'_{ak} \forall k \in \{1, N-1\}$. We substitute the perturbed variables in the system of equations, and we neglect all non-linear terms. By substituting the reference solution, we obtain a system of equations of the perturbed variables that we arrange in matrix form:

$$\frac{\partial \mathbf{Q}'}{\partial t} + \mathbf{K}_0 \frac{\partial^2 \mathbf{Q}'}{\partial x^2} + \mathbf{A}_0 \frac{\partial \mathbf{Q}'}{\partial x} + \mathbf{B}_0 \mathbf{Q}' = \mathbf{0}. \quad (5.19)$$

where \mathbf{Q}' is the vector of dependent variables:

$$\mathbf{Q}' = \left[\eta', \underbrace{[\Gamma'_k]}_{N-1}, \Gamma'_N, \underbrace{[M'_{ak}]}_{N-1} \right]^T. \quad (5.20)$$

Matrices \mathbf{K}_0 , \mathbf{A}_0 , and \mathbf{B}_0 contain the diffusive, advective, and linear terms, respectively (Appendix D.1).

We assume that the perturbations can be represented by means of a Fourier series, which implies that the functions representing the variables are piecewise smooth and

bounded for $x = \pm\infty$. In this case, the solution of the system of equations can be expressed in the form of normal modes:

$$\mathbf{Q}' = \text{Re}\left(\mathbf{V}e^{i(k_w x - \omega t)}\right), \quad (5.21)$$

where k_w [rad/m] is the real wave number and \mathbf{V} is the complex amplitude vector. Re denotes the real part of the solution and i is the imaginary unit. The variable $\omega = \omega_r + i\omega_i$ [rad/s] is the complex angular frequency, where ω_r is the angular frequency and ω_i the attenuation coefficient. Perturbations grow if $\omega_i > 0$ and decay if $\omega_i < 0$. Substitution of Equation (5.21) in Equation (5.19) yields:

$$[\mathbf{M}_0 - \omega \mathbb{1}] \mathbf{V} = 0, \quad (5.22)$$

where $\mathbb{1}$ is the unit matrix and:

$$\mathbf{M}_0 = \mathbf{K}_0 k_w^2 \mathbf{i} + \mathbf{A}_0 k_w - \mathbf{B}_0 \mathbf{i}. \quad (5.23)$$

Equation (5.22) is an eigenvalue problem. The eigenvalues of \mathbf{M}_0 are the values of ω that satisfy the equation. In the following sections we solve this eigenvalue problem to gain insight on the model behavior.

5.3.2. Instability Mechanism

In this section we analyze the stability of the model. To this end and following the framework set by *Callander* (1969) (Section 5.1), we study the growth rate of perturbations using the linear model (Section 5.3.1) as a function of the wave number.

Considering a two sediment size fractions case, we reduce the variables of the linear model to 4 (η , Γ_1 , Γ_2 , and M_{a1}). Furthermore, we neglect the variability in particle velocity, which implies that particle diffusion is zero (i.e., $x_k = 0 \forall k$). The model is still too complex to be solved analytically. We observe that the particle activity equation has an advective character (second term on the left hand side in Equation (5.1)) which is not present neither in the equation for the bed elevation (Equation (5.3)) nor in the one for the bed surface texture (Equation (5.4)). Moreover, in the source term of all equations (i.e., the right hand side of Equations (5.1), (5.3), and (5.4)) the term multiplying the particle activity (i.e., \hat{D}_k) is larger than the term multiplying the volume of sediment in the active layer (i.e., \hat{E}_k). These differences hint at the possibility of two different time scales, one associated with changes in particle activity and one with changes in bed elevation and the bed surface texture. Appendix D.2 indeed confirms that there exist two different time scales and that the time scale of changes associated with particle activity is shorter (changes are faster) than the time scale associated with changes in bed elevation and bed surface texture. We use this property to decouple the model and obtain an approximate solution of the fast variables (ω_1^f , ω_2^f) and the slow variables (ω_1^s and ω_2^s).

The complex angular frequencies of the fast variables are:

$$\omega_1^f = v_{p1} k_w - \hat{D}_1 \mathbf{i}, \quad (5.24)$$

$$\omega_2^f = v_{p2} k_w - \hat{D}_2 \mathbf{i}. \quad (5.25)$$

Independently of the wave number, the growth rate is negative, which means that the fast variables are stable.

The complex angular frequencies of the slow variables are the solution to the second order polynomial equation:

$$b_2\omega^s + b_1\omega^s + c_0 = 0, \quad (5.26)$$

where parameters b_1 , b_2 , and c_0 are complex numbers depending on the wave number (Appendix D.2). Depending on the value of these parameters, the imaginary part of ω^s can be positive, which means that perturbations grow.

We identify 3 main parameters controlling the growth or decay of perturbations. The first parameter is Ψ [–] (Appendix D.2):

$$\Psi = F_{a1}[(1 - f_1^I)\phi V + (f_1^I - 2)] + (1 - F_{a1})\left[f_1^I \frac{1}{\phi} - V(1 + f_1^I)\right], \quad (5.27)$$

where $\phi = \hat{E}_1 \hat{D}_2 / \hat{E}_2 \hat{D}_1$ is a parameter relating the entrainment and deposition rates of the two size fractions and $V = v_{p1} / v_{p2}$ relates the particle velocities. Parameter Ψ is a measure of the grain size distribution of the active layer sediment relative to the grain size distribution at the interface between the active layer and the substrate. Parameter Ψ decreases when the active layer is coarse compared to the interface between the active layer and the substrate. Perturbations are stable if $\Psi > 0$, and perturbations may grow if $\Psi < 0$ (Appendix D.2). Parameter Ψ is small under the conditions in which the active layer model is prone to be ill-posed (i.e., degradation into a fine substrate (Ribberink, 1987; Stecca et al., 2014; Chavarrías et al., 2018a)). Hence, under the conditions in which the active layer model is ill-posed, the SILKE model may be unstable.

The second parameter is the ratio between the grain size of the fine sediment and the active layer thickness, d_1/L_a . This parameter relates the particle activity to the volume of sediment in the active layer, as the first scales with the grain size and the second with the active layer thickness.

The third parameter is the ratio between grain sizes, d_1/d_2 . A ratio close to one indicates conditions close to unisize sediment.

In Figure 5.2 we present the separatrix between growth (G) and decay (D) of perturbations as a function of the wave number based on the reference case of Table 5.1. The results are presented as a function of the three dimensionless parameters. Considering the reference case, we vary the volume fraction content of fine sediment at the interface between the active layer and the substrate between 0.5 and 1. In Figure 5.2a the active layer thickness varies between 3 times the coarse grain size (representative of plane bed conditions (Petts et al., 1989; Rahuel et al., 1989; Parker and Sutherland, 1990)) and 0.2 times the water depth (representative of a dune dominated case (Deigaard and Fredsøe, 1978; Lee and Odgaard, 1986)). In Figure 5.2b the characteristic size of the fine sediment varies between 0.0005 m and 0.003 m.

A fining of the sediment at the interface (i.e., an increase in f_1^I , which causes a decrease in Ψ) increases the instability domain (i.e., there is a larger range of unstable wave numbers (Figure 5.2)). When the fine sediment at the interface is below a minimum threshold, the model is stable and perturbations do not grow. For instance, for $d_1/L_a < 0.01$, all

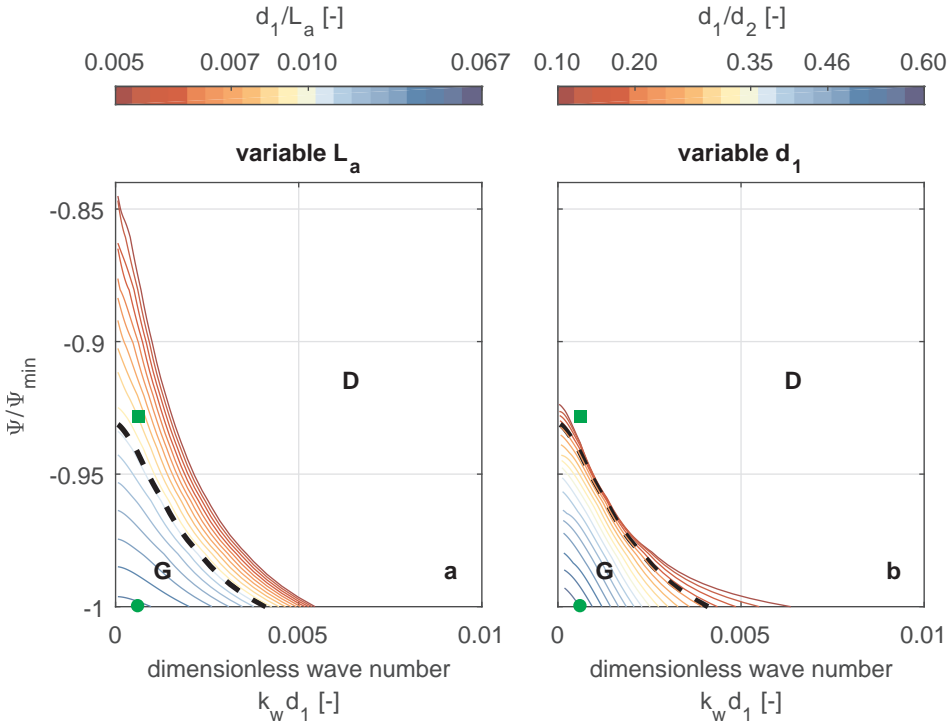


Figure 5.2: Separatrix between the growth domain (G) and decay domain (D) as a function of the wave number (k_w) and Ψ (Equation (5.27)). The wave number is nondimensionalized using the fine grain size. Parameter Ψ is relative to its minimum value $\Psi_{\min} = 1/\phi - 2V$. Each line represents a separatrix as a function of the ratio between: (a) the grain size of the fine fraction and the active layer thickness, and (b) the grain sizes. In (a) the active layer thickness is varied to obtain different conditions while in (b) we vary the grain size of the fine size fraction. The green markers represent the conditions of two numerical simulation under growth (circle) and decay (square) conditions. In the numerical simulations $d_1/L_a = 0.01$ and $d_1/d_2 = 0.2$, and the separatrix is highlighted using a dashed black line.

h [m]	u [m/s]	Fr [-]	C_f [-]	C_{fb} [-]	L_a [m]	d_1 [m]	d_2 [m]
1	1	0.32	0.008	0.008	0.10	0.001	0.005

Table 5.1: Reference parameters for studying the domain in which perturbations grow or decay.

perturbations decay if $\Psi/\Psi_{\min} > -0.93$, which is equivalent to $f_1^1 < 0.8$. This shows that the mechanism underlying growth of perturbations is associated with the origin of ill-posedness in the active layer model. The active layer thickness significantly affects the domain in which perturbations grow (Figure 5.2a). This corresponds to the active layer model, where the active layer thickness plays a significant role in defining the region in which the model is ill-posed (Chavarrías *et al.*, 2018a). A decrease in active layer thickness (i.e., an increase in d_1/L_a) decreases the unstable domain, which is consistent with the

fact that the active layer model is well-posed if the active layer thickness is sufficiently thin (Chavarrías *et al.*, 2018a). The active layer model is well-posed if the active layer thickness is sufficiently thick too. Yet, we do not see an eventual decrease in the growth domain for increasing values of the active layer thickness (i.e., decreasing values of parameter d_1/L_a), as, in our reference case, this effect occurs for unrealistically large values of the active layer thickness. The domain of instability decreases when the ratio of the two grain sizes tends to 1 (Figure 5.2b). This shows that the model is stable under unisize conditions, which supports the fact that the mixed-sediment character is a condition that allows for instability.

When using the backwater equation, we implicitly assume that the relevant processes occur on a length scale longer than the flow depth (e.g. Battjes and Labeyrie, 2017), as for waves shorter than the flow depth hydrostatic flow cannot be assumed. For this reason, the model would be physically unrealistic if perturbations shorter than the flow depth would grow. In this reference case, perturbations with a wave length below approximately 5 m do not grow. Thus, the length scale of growing perturbations is at least 5 times the flow depth ($h = 1$ m, see Table 5.1). We conclude that the minimum length scale of growing perturbations is consistent with the assumption of hydrostatic flow in the derivation of the backwater equation. The minimum length scale also indicates that instabilities are strongly linked to the process of adaptation of the particle activity to changing conditions, as this process occurs over lengths characterized by v_{pk}/\hat{D}_k (Bohorquez and Ancey, 2016), which is of order 1.

We run two idealized numerical simulations with the parameters of the reference case (Table 5.1) to test the results of the linear analysis and to verify that under the conditions in which we predict growth, the solution of the system of equations including non-linear terms shows growth of perturbations. The domain is 200 m long and is discretized using 0.25 m long cells. The initial bed elevation is formed by a sinusoidal perturbation with an amplitude equal to 0.001 m and wave length equal 10 m superimposed to a constant slope equal to 8.2×10^{-4} , which is the equilibrium bed slope (Blom *et al.*, 2016, 2017a,b). The small value of the amplitude of the perturbation guarantees that the linear solution is initially valid. The active layer is initially composed of coarse sediment only. We use periodic boundary conditions. The two simulations differ only regarding the initial composition of the substrate sediment. In one case the substrate is composed of fine sediment only, and the linear analysis predicts growth (circle in Figure 5.2), while in the second case the substrate is composed of 80% fine sediment and the linear analysis predicts decay of the perturbation (square in Figure 5.2). Figure 5.3 shows the bed elevation relative to the mean longitudinal bed profile as a function of time. A fine substrate causes oscillations to grow (Figure 5.3a), whereas a slightly coarser substrate yields decay of perturbations (Figure 5.3b).

The numerical results confirm that the model presents an instability mechanism strongly linked to the mixed-size character of the sediment. An active layer coarser than the interface between the active layer and the substrate triggers the formation of waves, as was observed by Chavarrías *et al.* (2019a) in laboratory experiments. The numerical results also confirm the validity of the analytical predictor for instability conditions.

We note that we are not the first authors reporting a one-dimensional instability mechanism linked to the mixed-size character of sediment. Tsujimoto and Motohashi (1989) and

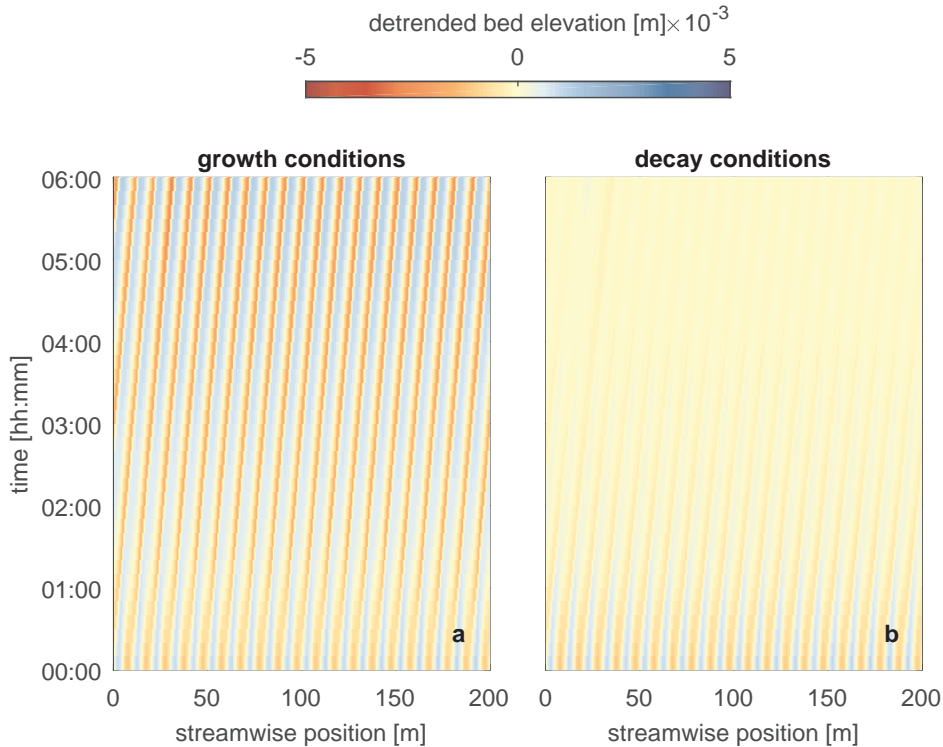


Figure 5.3: Detrended bed elevation (i.e., bed elevation subtracting the initial bed elevation) as a function of space and time for two numerical simulations run under conditions in which the linear model predicts: (a) growth of perturbations, and (b) decay of perturbations.

Tsujimoto (1989a,b, 1990, 1989c) also found an instability mechanism. In their case the instability was driven by a spatial lag between the sediment transport rate and the bed surface grain size distribution. The phase difference originates from considering the sediment transport rate as the convolution integral of the product of the entrainment rate and probability of step length. This instability mechanism explains the formation of alternating fine and coarse stripes in the streamwise direction, as well as in the transversal direction (*Ikeda and Iseya, 1986; Iseya and Ikeda, 1987; Kuhnle and Southard, 1988*). In both the SILKE model and the model by *Tsujimoto* and coauthors, the instability mechanism is intrinsically related to mixed-size sediment, it is one-dimensional, and predicts the formation of alternate fine and coarse stripes. Yet, the models represent different processes, as only in the SILKE model the substrate sediment plays a role. In the SILKE model, a homogeneous mixed-size sediment bed is stable and waves do not grow, contrary to the model by *Tsujimoto* and coauthors. The instability mechanism due to entrainment of fine substrate sediment is only captured by the SILKE model.

The fact that for an increasing wave number the domain in which perturbations decay increases (Figure 5.2) indicates that the SILKE model may be well-posed. In the following section we prove that this is true.

5.3.3. Well-Posedness

In this section we show that the SILKE model considering two sediment size fractions is well-posed. To this end we study the growth rate of infinitely short perturbations (e.g. *Barker and Gray, 2017*).

We first consider negligible diffusion in the sediment transport rate. The growth rates of the two fast variables are always negative regardless of the wave number (Equations (5.24) and (5.25)). This implies that they are stable. For a wave number tending to infinity, the angular frequencies of the slow variables are:

$$\omega_{1\text{lim}}^s = -i \frac{1}{2(1-p)} H_1, \quad (5.28)$$

$$\omega_{2\text{lim}}^s = -i \frac{1}{2(1-p)} H_2, \quad (5.29)$$

where H_1 and H_2 are complex numbers with positive real part (Appendix D.2). For this reason, the angular frequency is a negative pure imaginary number. As a consequence, the growth rate of perturbations for both fast and slow variables is negative for a wave number tending to infinity. Thus, the model is well-posed.

To account for the effect of particle diffusivity, we assume the same value of diffusion for both grain sizes. We find that for a wave number tending to infinity the angular frequency of the slow variables are:

$$\omega_{1\text{lim}}^{\text{sK}} = 0, \quad (5.30)$$

$$\omega_{2\text{lim}}^{\text{sK}} = -\frac{1}{1-p} e_3 i, \quad (5.31)$$

where the superscript K indicates that these values are the ones accounting for particle diffusion. As the growth rate (i.e., the imaginary part of the angular frequencies) is negative, the model is well-posed. We conclude that, independently from diffusion in the sediment transport, the model is well-posed.

Interestingly, for intermediate wave numbers diffusion increases the instability domain, although in the limit for a wave number tending to infinity diffusion dampens oscillations. Perturbations that decay when diffusion in the sediment transport is not accounted for appear to grow when diffusion is considered. This result is consistent with the results of *Bohorquez and Ancey (2015)*. Using their unisize sediment model, they found that diffusion increases the instability domain.

5.3.4. Tracer Sediment Dispersion

In this section we analytically study the propagation of tracer sediment predicted by the SILKE model. While the active layer model predicts no dispersion of tracer sediment (Section 5.1), we expect that in the SILKE model the interaction between the sediment at the bed surface and the sediment in transport captures sediment dispersion.

We consider a simplified case of tracer dispersion under unisize and normal flow conditions. We assume the active layer thickness to be constant. Under these conditions and neglecting the effect of diffusion in sediment transport, the SILKE model is similar to

the one developed by *Lajeunesse et al.* (2013, 2017, 2018) based on the sediment balance model developed by *Charru et al.* (2004), *Charru and Hinch* (2006), *Charru* (2006), and *Lajeunesse et al.* (2010). The difference is that here we include particle diffusion and we maintain the active layer concept, whereas *Lajeunesse et al.* (2013, 2017, 2018) model the number of static and moving particles.

Under the above conditions the equation modelling change in the volume fraction content of tracer sediment is:

$$\frac{\partial F_{a1}}{\partial t} = -\frac{1}{1-p} \frac{\Gamma_T}{L_a} \hat{D} (F_{a1} - F_{\Gamma1}), \quad (5.32)$$

and changes in particle activity are modelled by:

$$\frac{\partial F_{\Gamma1}}{\partial t} + v_p \frac{\partial F_{\Gamma1}}{\partial x} - \chi \frac{\partial^2 F_{\Gamma1}}{\partial x^2} = \hat{D} (F_{a1} - F_{\Gamma1}), \quad (5.33)$$

where $\Gamma_T = \Gamma_1 + \Gamma_2$ [m] is the total volume of active particles per unit of bed area and $F_{\Gamma1} = \Gamma_1 / \Gamma_T$ [-] is the fraction of active tracer particles. Appendix D.3 details the derivation of Equations (5.32) and (5.33). As the measurements of tracer sediment in experiments and field cases usually provide the total amount of tracer sediment without distinguishing between the sediment at the bed surface and the sediment in transport (*Lajeunesse et al.*, 2018), we introduce the variable c [-] that accounts for the total concentration of tracer sediment:

$$c = \frac{M_{a1} + \Gamma_1}{L_a + \Gamma_T} = \frac{F_{a1} L_a + F_{\Gamma1} \Gamma_T}{L_a + \Gamma_T}. \quad (5.34)$$

It is convenient to define the variable $\delta = F_{a1} - F_{\Gamma1}$ [-], which represents the difference between the fraction of tracer sediment at the bed surface and the fraction of tracer sediment in transport. This variable drives the transient state of the system, as it is the sink term of Equation (5.32) and the source term of Equation (5.33). We conduct a change of variables and replace $F_{\Gamma1}$ and F_{a1} by c and δ . The change of variables yields two advection-diffusion equations modelling changes of c and δ (Appendix D.3). In the steady state (i.e., $\partial/\partial t = 0$), $\delta = 0$ while $c \neq 0$. This means that, after a long time, $\delta \ll c$. We use this property to obtain an analytical solution of c at first order:

$$\frac{\partial c_0}{\partial t} + v_c \frac{\partial c_0}{\partial x} - \chi_c \frac{\partial^2 c_0}{\partial x^2} = 0, \quad (5.35)$$

where the subscript 0 indicates the approximate value of the solution at first order. This is an advection-diffusion equation in which the advective velocity is:

$$v_c = v_p \frac{\Gamma_T}{(1-p)L_a + \Gamma_T}, \quad (5.36)$$

and the diffusivity is

$$\chi_c = \frac{\Gamma_T}{L_a + \Gamma_T} \left[\chi + \frac{v_p^2}{\hat{D}} \left(\frac{L_a}{L_a + \Gamma_T} \right) \left(\frac{(1-p)L_a}{(1-p)L_a + \Gamma_T} \right) \right]. \quad (5.37)$$

When $\alpha = 0$, the diffusivity is not equal to 0. This result shows that the model predicts dispersion of tracer sediment as a result of the interaction between the active layer and the particle activity equations. In particular, tracer sediment diffuses in a normal (Fickian) manner as it propagates in the downstream direction. Long particle travel distances, characterized either by a large particle velocity or a small deposition flux, increase particle diffusion. The propagation velocity of tracer sediment is smaller than the particle velocity, and it depends on the inverse of the active layer thickness. The dependence on the active layer thickness is consistent with the fact that a thick active layer represents conditions in which vertical mixing occurs over a significant range of elevations, which slows down the streamwise propagation of tracer sediment.

An advection-diffusion equation for the propagation of tracer sediment in the long term was also obtained by *Lajeunesse et al.* (2018) using their sediment balance model. In the following, we compare their results to the ones of the SILKE model. The advective velocity in both models is mathematically equivalent if we consider that the number of static and moving particles in their model is represented by the active layer thickness and the particle activity, respectively, in our model. The diffusivity of the model by *Lajeunesse et al.* (2018) depends on the square of the particle step length and inversely on the particle travel time. Our results are mathematically equivalent to theirs if we relate the deposition rate to the inverse of the particle travel time. Although mathematically equivalent, the variables represent different properties, such that each model is most suited for reproducing certain physical processes. For instance, the active layer thickness is representative of the range of elevations at which the sediment interacts with the flow and that are responsible for significant vertical mixing, and this property is not physically equivalent to the number of static particles. Moreover, while in the model by *Lajeunesse et al.* (2018) the number of static particles is a variable of the model under unsteady conditions, in our case the active layer thickness is *a priori* assigned (or related to flow and bed properties).

An advantage of the SILKE model is that it explicitly accounts for the effect of porosity. If bed particles are loosely packed and the porosity is large, there are less particles per unit of bed area and tracer sediment propagates faster, as there is less interaction with the bed surface. Moreover, the SILKE model shows the effect of the variability in particle velocity: it increases the diffusive behavior caused by the interaction between particles at the bed surface and in transport.

In summary, we have shown that our model is well-posed and predicts tracer dispersion and an instability mechanism linked to mixed-size sediment which causes perturbations to grow under the conditions in which the active layer model is ill-posed. We need to analyze whether the results of the model are physically realistic. In the next section we compare the results of the model to laboratory and field data to answer this question.

5.4. Model Application

In this section we run numerical simulations of laboratory and field cases to test the performance of the SILKE model against measured data and to compare the results to those of the active layer model. In Section 5.4.1 we study a case of tracer propagation in which the effect of temporary burial due to bedforms is negligible. In Section 5.4.2 we model tracer propagation under conditions in which temporary burial due to bedforms plays a significant role. In Sections 5.4.3 and 5.4.4 we model two experiments conducted

under conditions in which the active layer model is ill-posed. In the first case it is reasonable to assume a constant active layer thickness, while in the second one the active layer thickness varies with time.

5.4.1. Tracer Propagation Without Temporary Burial

In this section we model a laboratory experiment conducted by *Chavarrías et al.* (2019a) to study whether the model captures tracer propagation under conditions in which the effect of temporary burial of sediment due to bedforms is negligible (Section 5.1). We also investigate the role played by diffusion in sediment transport. The experiment consisted of feeding painted (i.e., tracer) unisize sediment under equilibrium conditions. A regular pattern of small bedforms approximately 2 cm high covered the bed surface. Measurements of bed elevation fluctuations confirm that the active part of the bed was restricted to a narrow range of elevations. Worded differently, the probability of entrainment and deposition decreases fast at lower elevations, such that temporary burial due to bedforms is negligible. The content of tracer sediment at the bed surface at the downstream end of the flume was measured using a submerged camera. Appendix D.4 explains further details of the experiment.

In modeling the experiment we use the same closure relations and parameters as the ones used by *Chavarrías et al.* (2019a). The sediment transport rate at capacity is computed using the relation by *Ashida and Michiue* (1971). The domain of interest is 10 m long. We add an additional 40 m at the downstream end to guarantee that the downstream boundary condition for the particle activity does not affect the domain of interest (Section 5.2.3). The domain is discretized using 0.01 m long cells.

In Figure 5.4 we compare the measured content of tracer sediment to the results predicted using the active layer model and the SILKE model. The active layer model predicts that tracer propagates as a front and does not capture the slow increase in tracer content at the bed surface. The deviation of the solution from a step function is due to numerical diffusion. The overall rate of adaptation of the bed surface fraction content is captured by the SILKE model. In particular, when considering an active layer thickness equal to 0.01 m, which is reasonable based on measurements of the bed elevation fluctuations, the agreement is satisfactory. Although the general trend due to the exchange of particles between the bed surface (i.e., in the active layer) and the particles in motion (i.e., the particle activity) is captured by the SILKE model, the fluctuations in tracer content due to bed elevation fluctuations is not captured. This is because the dynamics due to individual bedforms are resolved neither by the active layer model nor the SILKE model. Yet, deep burial of sediment at elevations significantly lower than the lower limit of the active layer was negligible, such that temporary trapping of sediment can be neglected and the active layer captures the dynamics of the system.

Diffusion in sediment transport does not play a significant role in the dispersion of tracer sediment (Figure 5.4). This is explained from the fact that there exist three time scales in which different physical processes play a role in dispersing tracer sediment (*Nikora et al.*, 2002). The shortest (local) scale considers the movement of particles between impacts with the bed surface. Processes at this scale are not included in the model. The intermediate scale considers processes related to a single entrainment and deposition cycle. The variability in particle velocity is a relevant process in this scale. For this reason,

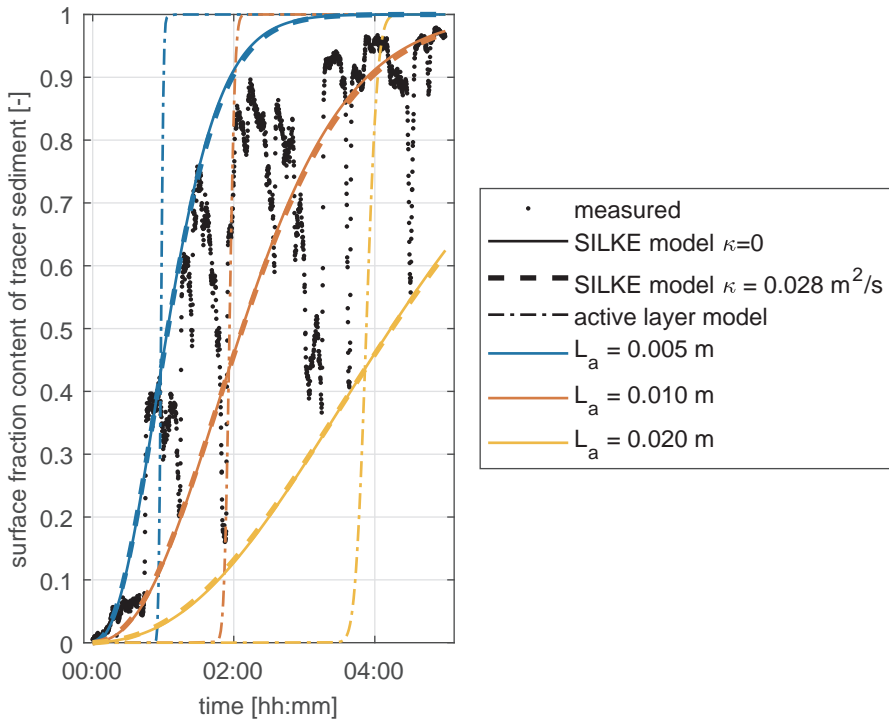


Figure 5.4: Bed surface fraction content of tracer sediment 9.17 m downstream from the feeding location. The black dots are measured data (Chavarrías et al., 2019a) and the lines are the results of numerical simulations. The dash-dotted, dashed, and continuous lines present the results using the active layer model (Hirano, 1971), and the SILKE model with and without diffusion, respectively. The different colors represent a different active layer thickness.

diffusion plays a role in this scale. In the global scale, sediment dispersion is governed by the rest time of sediment particles and the interaction between the bed surface and the sediment in transport (Martin et al., 2012, 2014; Voepel et al., 2013; Pelosi et al., 2014; Furbish et al., 2017). This scale is captured by the interaction between the active layer and the particle activity equations regardless of the diffusion in sediment transport.

Nikora et al. (2002) sets the limit time between the intermediate and global scales in $t = 15d_k/u^*$ (which is of the order of 1 s for the specifications of the present experiment). This supports the fact that diffusion is not relevant to explain dispersion of sediment on a time scale of 5 h.

5.4.2. Tracer Propagation With Temporary Burial

In this section we study tracer propagation under conditions in which the effect of temporary burial of sediment due to bedforms may not be negligible. To this end, we consider the study conducted by Sayre and Hubbell (1965). They tracked the propagation of tracer sediment along a 550 m long stretch of the North Loup River (Nebraska, US) during

approximately 12 days. The minimum and maximum sizes of the bed sediment were equal to 0.088 mm and 9.424 mm, respectively, with a geometric mean grain size equal to 0.315 mm. The bed was covered with dunes between 0.30 m and 0.46 m height, and based on core samples the average maximum depth at which tracer was found was 0.44 m below the bed surface. The flow conditions did not significantly vary during the measurement campaign and a reasonably constant flow depth was measured. Figure 5.5 presents the measured concentration of tracer sediment at the end of the experiment. Details about the conditions of the experiment are presented in Appendix D.5.

The active layer model predicts no dispersion of tracer sediment under unisize conditions (Sections 5.1 and 5.4.1). Under mixed-size sediment conditions, the active layer model does predict sediment dispersion, as the sediment transport rate varies per size fraction. Contrary to the active layer model, the SILKE model predicts sediment dispersion even without considering diffusion in the sediment transport rate (Sections 5.3.4 and 5.4.1). Here our objective is twofold. First, we study whether the mixed-size sediment character is enough to capture tracer dispersion using the active layer model. Second, we study whether the SILKE model is capable of reproducing the propagation of tracer dispersion under conditions in which the effect of temporary burial of sediment may play a significant role.

We select appropriate closure relations and a reasonable value for the skin friction coefficient and active layer thickness to model the field case. We find that the sediment transport relation by *Ashida and Michiue* (1971) in combination with the skin friction predictor by *Engelund and Hansen* (1967) performs best with an error of only 3 % (Appendix D.5). For simplicity, we assume that normal flow prevailed in the study area. We assume that the active layer thickness is equal to the average maximum depth below the bed surface at which tracer was found. We discretize the domain using 0.5 m long cells.

We run two numerical simulations using the active layer model to test whether the mixed-size sediment character is enough to capture tracer sediment dispersion. In the first simulation, we consider unisize sediment with a characteristic size equal to the geometric mean grain size of the bed surface sediment. In the second one, we approximate the grain size distribution of the bulk mixture using 11 grain size fractions (which is the number of sieves reported by *Sayre and Hubbell* (1965)). The tracer sediment had a narrower grain size distribution than the parent material and is represented by 3 grain size fractions (Appendix D.5).

In Figure 5.5a we present the total (i.e., considering the mass in both the active layer and in transport) tracer concentration at the final time assuming unisize sediment. The small dispersion in Figure 5.5a is entirely due to numerical diffusion. In Figure 5.5b we observe that accounting for mixed-size sediment causes dispersion. We see three peaks corresponding to the three fractions which, in total, cover a longer river stretch than under unisize conditions. We run two simulations under the same conditions as the ones with the active layer model but using the SILKE model (Figure 5.5c-d). Dispersion as predicted by the SILKE model is larger than when using the active layer model. Yet, for all cases the amount of dispersion is an order of magnitude smaller than the measured one. Moreover, the model predicts that tracer sediment disperses in the form of normal (i.e., Fickian) diffusion (Section 5.3.4), whereas the field data suggest that the downstream tail spreads faster than normal (i.e., it decreases linearly in logarithmic scale).

We consider three possible explanations for the discrepancy between the measured and the predicted results in Figure 5.5. First is that *Sayre and Hubbell* (1965) explain that the measurements of the right-hand side after approximately 120 h could be affected by the late re-entrainment of tracer sediment placed on the left-hand side. It appears to be that sediment placed on the left-hand side was initially trapped at the location where it was dumped and only later re-entrained, reaching the right-hand side. This two-dimensional effect cannot be captured using our one-dimensional model. The second explanation is that the imposed diffusivity in sediment transport is too small. This may be due to the assumption of an exponential distribution of particle velocities (Section 5.2.2). It is possible that particle velocities are better approximated by a different probability distribution that causes a larger diffusivity. The third explanation is that the dominant mechanism responsible for sediment mixing is not captured by the combination of the active layer and the particle activity equations. In particular, this mechanism may be temporary burial due to bedforms (Section 5.2.1).

To study whether the first possibility (i.e., the late re-entrainment of trapped sediment) is responsible for the disagreement between the data and the modelling results, we compare the measured concentrations along the last longitudinal traverse that was unaffected by the re-entrainment to the results of the model (Figure 5.6). The predicted peak concentration is six times larger than the measured concentration and the amount of predicted dispersion is significantly smaller than the measured dispersion. We conclude that the late re-entrainment of sediment is not responsible for the disagreement between the measured and predicted results.

We test the second possibility (i.e., an underestimation of the diffusion in sediment transport) (Figure 5.6). The peak concentration would be captured if the diffusion coefficient is 1000 times larger than our original value. Apart from the fact that this amount of diffusion is not physically realistic, the downstream tail is not captured independently of the diffusion coefficient. We conclude that the SILKE model is not capable of reproducing the measured data of tracer propagation, as it lacks an important mechanism responsible for sediment mixing that is relevant under the conditions of the experiment.

The main conclusion here is the fact that the assumption that the part of the bed that interacts with the flow is well represented by an active layer becomes questionable when large rest times occur due to temporary tracer burial by bedforms (*Ribberink, 1987; Blom, 2008*).

This exercise highlights the limitations of active layer based models. Yet, the main strength of the model is that it is mathematically well-posed. In the following two sections we study this property in detail.

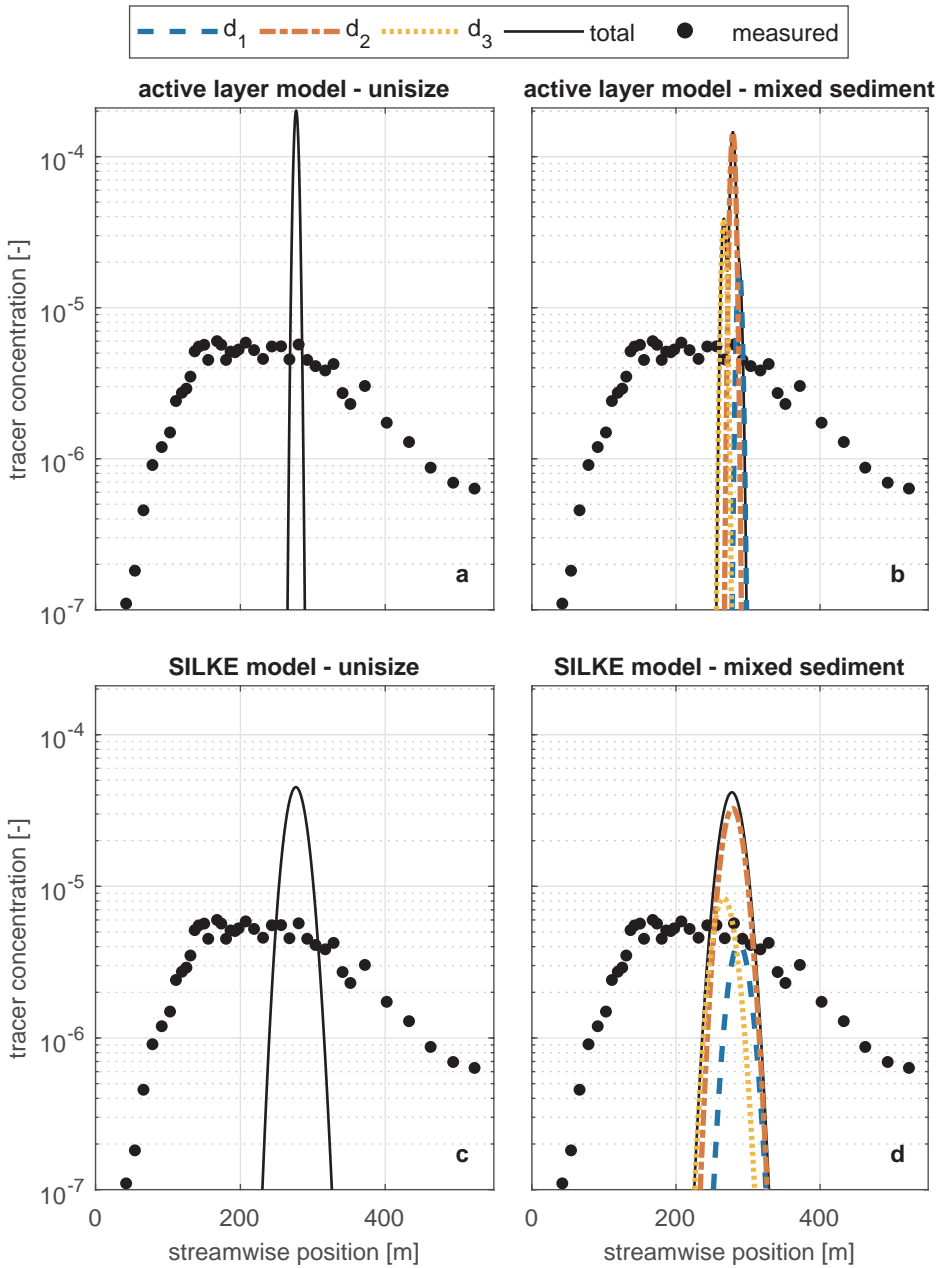


Figure 5.5: Tracer concentration (accounting for the sediment in the active layer and in transport) along a reach of the North Loup River (Nebraska, US) 287.4 h after placing the tracer sediment. Results are computed using: (a) the active layer model under unisize conditions, (b) the active layer model under mixed-size conditions, (c) the SILKE model under unisize conditions, and (d) the SILKE model under mixed-size conditions. The dots represent the measured data by *Sayre and Hubbell (1965)* (profile 12R). The black lines indicate the total tracer concentration which is the sum over all tracer size fractions (i.e., d_1 , d_2 , and d_3) in the mixed-size sediment simulations.

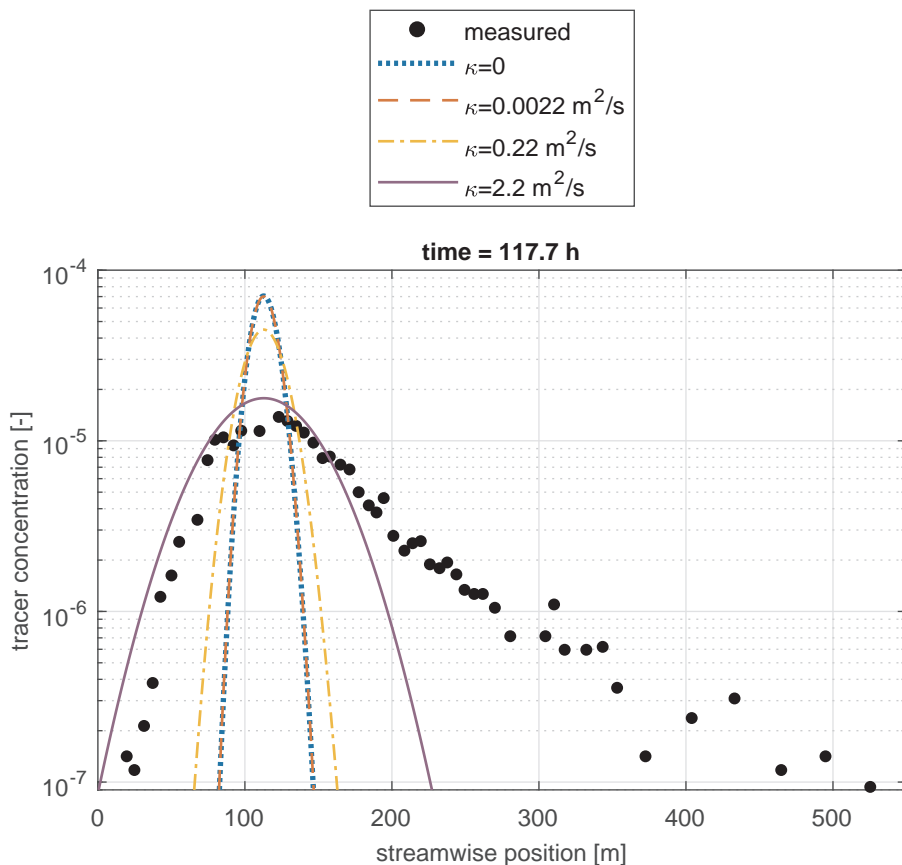


Figure 5.6: Tracer concentration (accounting for the sediment in the active layer and in transport) along a reach of the North Loup River (Nebraska, US) 117.7 h after placing the tracer sediment. Results are computed considering: no diffusion (dotted blue line), a realistic amount of diffusion ($0.0022 \text{ m}^2/\text{s}$) (dashed red line), 100 times the realistic amount of diffusion (dash-dotted yellow line), and 1000 times the realistic amount of diffusion (continuous purple line). The dots represent the measured data by *Sayre and Hubbell* (1965) (profile 6R).

5.4.3. Ill-posed Conditions Assuming Constant Active Layer Thickness

The fact that the SILKE model is always well-posed is particularly important when reproducing a situation of degradation into a substrate finer than the bed surface, as under these conditions the active layer model is prone to be ill-posed (Ribberink, 1987; Stecca et al., 2014; Chavarrías et al., 2018a). In this section we model Experiment I4 conducted by Chavarrías et al. (2019a) and compare the results to predictions using the active layer model, the regularized model (Chavarrías et al., 2019a), and the SILKE model.

Experiment I4 consisted of a 4 m long patch of fine sediment ($d_1 = 2.1$ mm) placed below a 3 cm layer of coarse sediment ($d_2 = 5.5$ mm). Degradational conditions were imposed by lowering the downstream water level 8 cm during 8 h. All other parameters were the same as in the experiment considered in Section 5.4.1.

Figure 5.7a shows the bed elevation data. Before fine sediment from the patch was entrained, the bed was covered by bedforms. As degradation proceeded, fine sediment from the substrate started to be entrained at the troughs of bedforms. The entrainment of fine sediment caused the bedforms to grow. Coarse sediment was deposited in the troughs, which prevented subsequent entrainment of fine sediment. Fine sediment was again available for entrainment as degradation continued, which caused the periodic formation of large bedforms superimposed to the original ones.

The active layer model is ill-posed when reproducing this experiment and the consequences are clearly seen in the predicted bed elevation (Figure 5.7b). An unrealistically large oscillation develops as soon as the interface between the active layer and the substrate is composed of fine sediment. Moreover, the solution is grid dependent and a simulation using a smaller grid size causes ever larger oscillations (Chavarrías et al., 2018a). The regularized model provides more satisfactory results (Figure 5.7c). The solution is well-posed and captures the changes in mean bed elevation, but it does not capture the oscillatory behavior when large bedforms entrain fine substrate sediment (Chavarrías et al., 2019a). On the contrary, the SILKE model shows oscillatory behavior that starts right where the patch starts (Figure 5.7d). Fine sediment from the substrate is transferred to the active layer and entrained. The particle activity adapts in the streamwise direction, which causes an imbalance between erosion and deposition and induces oscillations superimposed to the overall degradational trend.

The oscillatory behavior is also observed in the volume fraction content of coarse sediment at the bed surface (Figure 5.8). The bed is composed of coarse sediment only and the growth of large bedforms that lead to the entrainment of fine sediment is associated with a fining of the bed surface (Figure 5.8a). The entrainment cycles are less clear downstream from the patch, as fine sediment entrained at the patch mixes with coarse sediment while traveling downstream.

The result of the active layer model is meaningless. It predicts that the bed surface is composed of coarse sediment only. This is because, after the large nonphysical oscillation, coarse sediment from upstream fills the space and forms a new coarse substrate. Hence, further degradation does not entrain fine sediment. The regularized model predicts a constant bed surface grain size distribution as a function of time at each location after a short period of adjustment at the beginning of the run (not visible in Figure 5.8). The bed surface becomes finer with increasing streamwise position, as fine sediment is entrained from the patch. The instability mechanism of the SILKE model induces oscil-

latory behavior in the bed surface grain size distribution. Yet, the variation in bed surface volume fraction content is smaller than the measured one. Similarly to the field tracer case (Section 5.4.2), this indicates that our model lacks some mechanisms responsible for the fast fining and coarsening that we will discuss in Section 5.5.2.

The SILKE model shows a clear advantage with respect to the regularized model, as it contains an instability mechanism responsible for mixing which is not captured by the regularized model. Even though the SILKE model explains more physical processes than the regularized model, both models are well-posed and reproduce the overall degradational trend. For this reason, the regularized model may yield a satisfactory solution if only the general trend is to be captured. However, as the regularized model requires that the active layer thickness is constant with time (*Chavarrías et al.*, 2019a), there are cases that cannot be modelled using the regularized model. In the following section we study a case that only the SILKE model can reproduce.

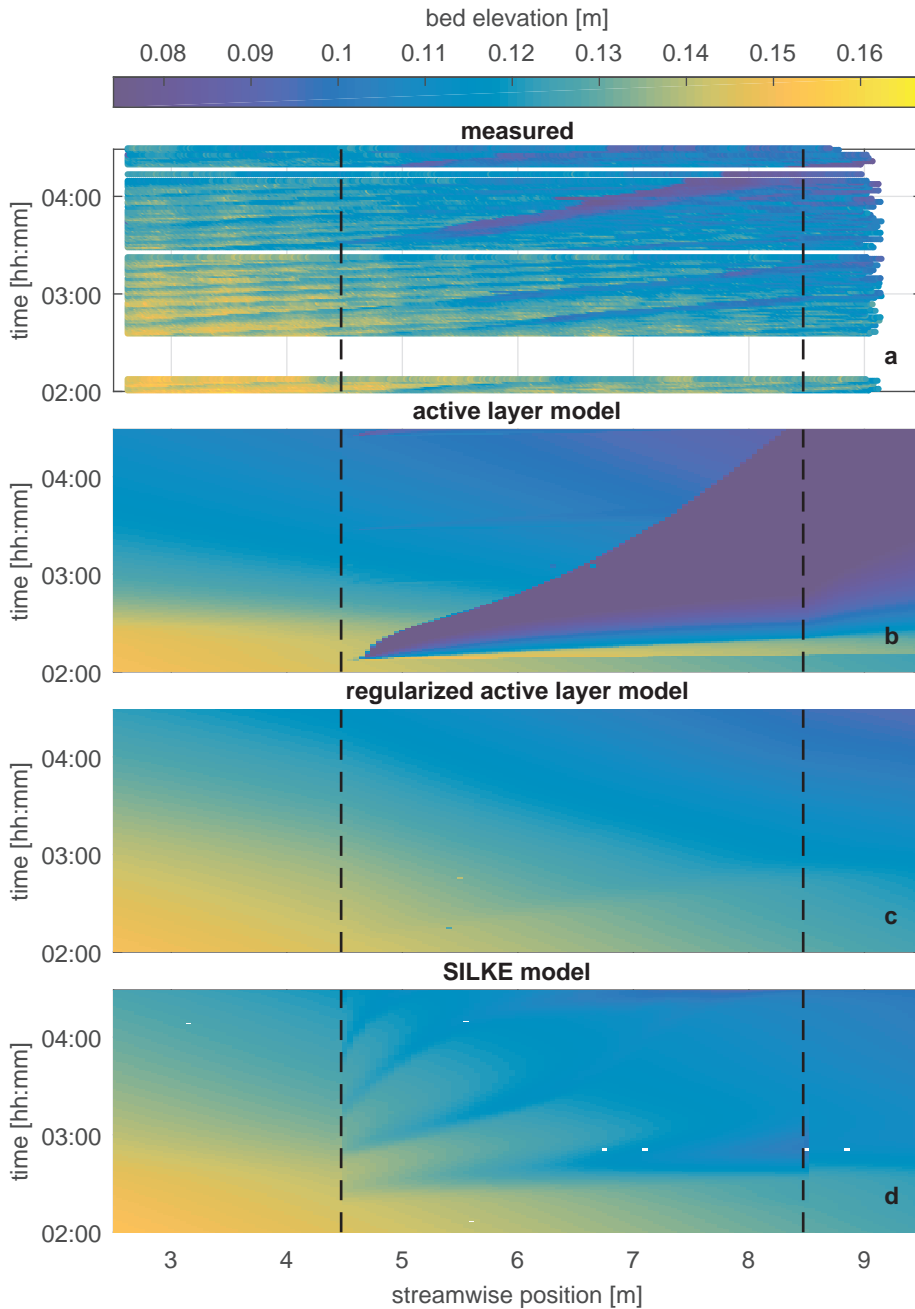


Figure 5.7: Bed elevation as a function of time in Experiment I4 conducted by *Chavarrías et al. (2019a)*: (a) measured, (b) predicted using the active layer model (*Hirano, 1971*), (c) predicted using the regularized active layer model (*Chavarrías et al., 2019a*), and (d) predicted using the SILKE model. Dashed lines indicate the position of the patch of fine sediment.

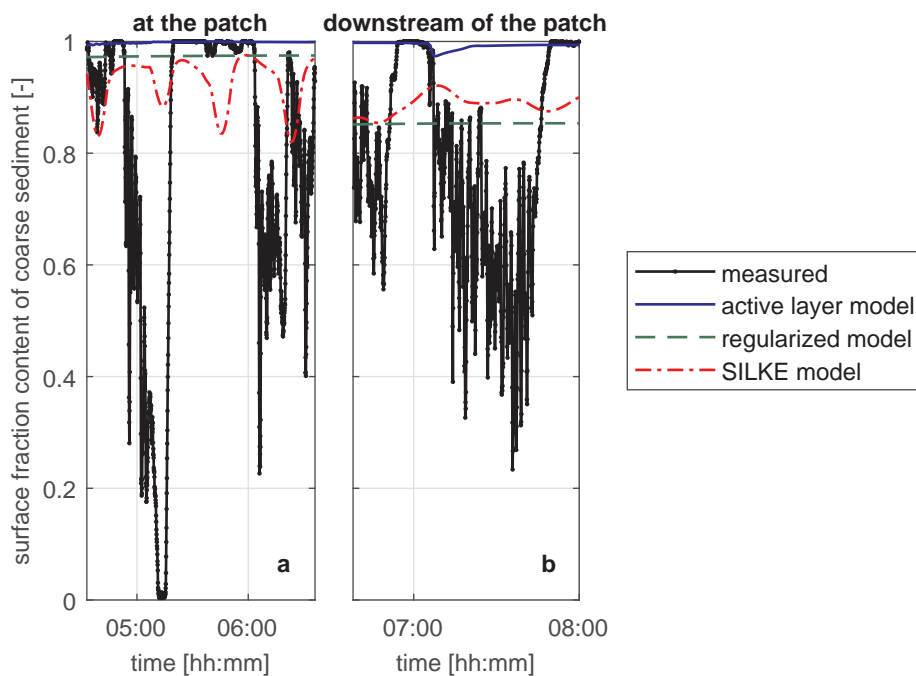


Figure 5.8: Surface volume fraction content of coarse sediment as a function of time in Experiment I₄ conducted by *Chavarrías et al. (2019a)*. Measured data is shown using black dots, results using the active layer model are shown using a blue line, the regularized model using a green dashed line, and the SILKE model using a dashed-dotted red line.

5.4.4. Ill-posed Conditions Assuming Variable Active Layer Thickness

In this section we reproduce a laboratory experiment that cannot be reproduced using neither the active layer model (*Hirano, 1971*) nor the regularized active layer model (*Chavarrías et al., 2019a*). We consider Experiment B2 conducted by *Blom et al. (2003)*.

Blom et al. (2003) studied vertical mixing of sediment due to dune growth using a trimodal sediment mixture. Barchan dunes migrating over a coarse sediment layer characterized the starting conditions of the experiment. Below the coarse layer, a fine substrate was present, which was not exposed to the flow. The water discharge was increased, which mobilized the coarse layer, led to the entrainment of fine substrate sediment, and caused dunes to grow adapting to a new equilibrium situation. Sediment was recirculated and normal flow conditions were maintained during the entire experiment. The details of the experiment are described in Appendix D.6.

As normal flow conditions were maintained, the mean bed elevation (averaged over the passage of several bedforms) remained constant with time. For this reason, in modelling the experiment using the active layer model, the only source of mixing in the active layer is the flux of sediment from the substrate due to a lowering of the interface between the active layer and the substrate. The lowering of the interface occurs due to an increase of the active layer thickness that represents the increase in dune height.

We have tested the mathematical character of the active layer model using the approach by *Chavarrías et al. (2018a)* and we find that when fine substrate sediment is entrained, the active layer model is ill-posed. We run a numerical simulation of the 50 m long flume discretized using 0.02 m long cells to study the consequences of modelling this experiment using the active layer model. The substrate is discretized using 0.005 m thick cells and the measured initial grain size distribution is used as initial condition of the substrate. We impose a linear increase of the active layer thickness with time between half the initial and final values of the mean dune height during the first 4 h of the 25 h experiment, as this is the approximate period of time over which dunes adapted to the new equilibrium value (*Blom et al., 2003*). Based on the initial and final values of the sediment transport rate, flow conditions, and volume fraction content in the active layer, we select a sediment transport relation which reasonably approximates the initial and final conditions. We find that the relation by *Meyer-Peter and Müller (1948)* using the hiding correction by *Parker et al. (1982)* with a power parameter equal to 0.9 yields a reasonable approximation.

In Figure 5.9 we present the volume fraction content in the sediment transport rate as a function of time at the downstream end of the flume. The coarsening of the load over the first hour is due to the entrainment of the coarse layer underneath the migrating barchan dunes. This is captured by the active layer model. Subsequently, the sediment at the interface between the active layer and the substrate becomes fine and the active layer model becomes ill-posed. The oscillations due to ill-posedness are not instantly felt at the downstream end. A large wave develops that makes the bed surface to consist of fine sediment only. The wave is felt at the downstream end after approximately 5 h. The solution breaks down after 10 h, as the flow solver is incapable of dealing with such abrupt changes in bed elevation. A decrease of the grid size causes the large wave to arrive downstream at a different time and the simulation to break down earlier.

We simulate the same conditions using the SILKE model without accounting for the effect of diffusion in sediment transport and we find a stable solution (Figure 5.9). Initially,

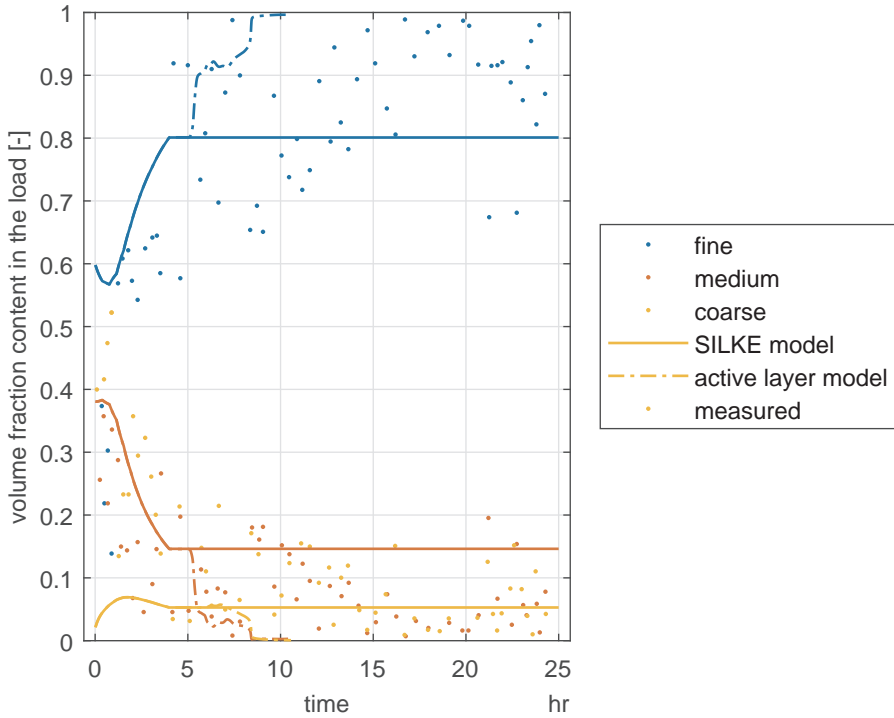


Figure 5.9: Volume fraction content of fine, medium, and coarse grain size fractions in the transported sediment as a function of time in Experiment B2 conducted by *Blom et al.* (2003).

the solution is very similar to the one predicted using the active layer model. This is reasonable, as variations in particle activity are much faster than changes in the active layer thickness. For this reason, over the 4 h increase in active layer thickness, we can assume that the particle activity is at capacity conditions. Yet, although the effect seems negligible initially, the consequences of accounting for the dynamics of the particle activity become striking after 4 h. The simulation does not lose its well-posed character and after the active layer thickness becomes constant with time, there no longer is a flux of sediment between the substrate and the active layer and the grain size distribution of the active layer becomes constant with time too.

In conclusion, it is crucial to account for the interaction between the bed surface and the sediment in transport occurring at “short” time scales to obtain a well-posed model that captures the dynamics of the “long” time scale. Although the effect of accounting for particle activity may seem negligible at first instance, as changes in the volume fraction content of sediment in the active layer are slow, we have to consider the small short time scale to obtain a physically realistic model at long time scales.

5.5. Discussion

In this section we discuss the reasons for the SILKE model to be well-posed (Section 5.5.1). Subsequently, we discuss the limitations of the model (Section 5.5.2), and of the model's instability mechanism (Section 5.5.3). We provide remarks on the modelling of the experiment by *Blom et al.* (2003) in Section 5.5.4.

5.5.1. Physical Reasoning of the Well-Posedness of the Model

In Section 5.3.3 we have shown that the SILKE model is well-posed, a property shared with the regularized model (*Chavarrías et al.*, 2019a). Here we clarify why, although being totally different approaches, both the SILKE model and the regularized model yield well-posed problems.

We consider a situation in which the active layer model is ill-posed such as the laboratory experiment in Section 5.4.3. The active layer model becomes ill-posed because it is incapable of reproducing the “short” time scale phenomena related to the entrainment of fine substrate sediment. In the active layer model, the sediment transport is assumed to be at capacity conditions and this results in a too crude approximation of the cycles of fine sediment entrainment.

The regularization strategy slows down the mixing processes (*Chavarrías et al.*, 2019a), which is mathematically equivalent to considering a thicker active layer. The active layer represents the part of the bed material that can be entrained into transport and where sediment is deposited and mixed. Worded differently, it represents the part of the bed that interacts with the flow. This means that the active layer thickness actually is a stochastic parameter depending on the time scale under consideration (see recent discussions by *Church and Haschenburger* (2017) and *Ashmore et al.* (2018)). A thick active layer represents changes over a “long” time scale that encompasses the effect of large and less frequent bed elevation fluctuations. A slowdown of the mixing processes by the regularization strategy yields a well-posed model, as “short” term processes of entrainment and deposition are filtered out and not resolved.

The SILKE model resolves the “short” time scale by accounting for conservation of the sediment in transport. Sediment transport is not assumed to be at capacity, and this allows for the formation of oscillations that enhance vertical mixing of sediment. Solving for this physical process yields a well-posed model.

In summary, in both cases the regularized model and the SILKE model yield a well-posed model by considering the processes occurring at a “short” time scale. The regularized model filters the processes while the SILKE model resolves them.

5.5.2. Limitations of the SILKE Model

In developing the SILKE model, we combine and extend previous modelling strategies. We maintain the active layer concept of *Hirano* (1971) to capture mixed-size sediment processes at the bed surface. In dealing with the sediment in transport, we consider the variability in particle velocity (*Furbish et al.*, 2012a; *Ancey and Heyman*, 2014; *Bohorquez and Ancey*, 2015). Nevertheless, in our generalization to mixed-size sediment conditions, we neglect the correlation terms that appear in the particle activity equation (*Furbish et al.*, 2012a). Worded differently, we consider sediment of different sizes travelling at different

speeds, yet each size fraction is treated independently from the other fractions. There is a need to derive a particle activity equation which considers the effect of the correlation terms. This, presumably, would affect both the advective and diffusive components of the particle activity. As we have seen, if one is interested in the “long” time scale, the diffusive component does not significantly affect the solution. For this reason, we do not expect that sediment dispersion at a “long” time scale differs considerably when taking into consideration the correlation terms if these only affect the diffusive component. Yet, the advective component may also be affected by the correlation terms and this could have a significant influence.

In the field, large rest times are measured due to sediment being trapped in bars, pools, and floodplains (*Hassan et al.*, 1991; *Schmidt and Ergenzinger*, 1992; *Ferguson et al.*, 2002; *Pyrce and Ashmore*, 2003; *Malmon et al.*, 2003). *Nakagawa and Tsujimoto* (1979) argue that under plane bed conditions the rest period and step length follow an exponential distribution and ripples and dunes cause them to be non-exponential, as the rest period depends on the elevation at which particles are deposited. The lowest elevation at which tracer sediment is found increases with time, as the probability of a large bedform that deposits sediment lower in the substrate increases (*Crickmore and Lean*, 1962a,b). This process also decreases the lowest elevation at which tracer sediment is found in the streamwise direction (*Galvin*, 1965; *Hassan et al.*, 1999). These effects are not included in the model, as all sediment in the active layer has the same probability of being entrained and there is no sediment flux to the substrate under normal flow conditions.

The fact that the model does not capture large resting times due to the temporary burial of sediment by bedforms, causes it to not properly reproduce tracer dispersion under conditions in which the active layer does not properly represent the probability of bed elevation fluctuations (Section 5.4.2). The existence of large rest times is related to the manner in which sediment disperses. Laboratory and field data suggest that tracer sediment diffuses anomalously (*Nikora et al.*, 2002; *Ferguson et al.*, 2002; *Haschenburger*, 2011, 2013; *Bradley et al.*, 2010; *Bradley*, 2017; *Fan et al.*, 2017), whereas the model predicts normal (i.e., Fickian) diffusion. The propagation of tracer sediment is best represented by means of a fractional advection-diffusion equation (*Schumer and Jerolmack*, 2009; *Ancey*, 2010; *Martin et al.*, 2012), which originates, for instance, from heavy-tail resting times under unisize sediment conditions (*Fan et al.*, 2016), as well as from a relation between the travel distance and grain size under mixed-size sediment conditions (*Ganti et al.*, 2010; *Hill et al.*, 2010).

To model the increased complexity and the possibility of large rest times, it may be necessary to abandon the active layer model embedded in the SILKE model in favor of a continuous formulation of the bed sediment such as that by *Pelosi et al.* (2016). The latter predicts anomalous diffusion in the propagation of tracer sediment (i.e., scale dependence) even considering thin-tailed sediment statistics, as it models the trapping of sediment deep in the substrate. The challenge is to combine this formulation with mixed-size sediment, bed elevation change, and mass conservation of the sediment in transport. Recently, *Wu et al.* (2019) captured anomalous diffusion using an adapted version of the active layer model that accounts for permanent burial of tracer sediment by means of an extra sink term in the active layer equation. This line of research may allow for the possibility of preserving the essence of the active layer model in improving our understanding of mor-

phodynamic processes. A following step may be to consider the effect of a variable active layer thickness due to, for instance, changes in bedform geometry, on tracer dispersion. An analysis similar to the one conducted in Section 5.3.4 including this effect may yield anomalous diffusion as observed in the field.

5.5.3. Limitations of the Interpretation of the Model Instability

In Section 5.3.2 we found that the SILKE model presents an instability mechanism and in Section 5.4.3 we related the mechanisms to the formation of waves in the experiments conducted by *Chavarrías et al.* (2019a). In this section we discuss limitations in the interpretation of the mathematical instability.

One limiting factor in physically interpreting the mathematical instability is the linearization of the model. The solution is only valid for small perturbations and short times such that non-linearities do not play a significant role. In this sense, as in all other linear studies, the main outcome of the analysis is the fact that it predicts the initial formation of waves but not their evolution. A second limitation specific to our mathematical analysis is the fact that we assume that the grain size distribution of the sediment at the interface between the active layer and the substrate is constant and equal to the one of the substrate. This is valid under degradational conditions or when the active layer grows. However, as soon as a wave is formed, there exist aggradational (i.e., the lee face) and degradational (i.e., the stoss face) zones. In the aggradational zone, the grain size distribution at the interface between the active layer and the substrate is a combination of the grain size distribution of the sediment in the active layer and in transport (*Hoey and Ferguson, 1994; Toro-Escobar et al., 1996*). For this reason, the formation of a wave coarsens the substrate sediment. This substrate coarsening mechanism reduces the time over which our linear solution is valid. Nevertheless, numerical simulations confirm the persistence of the instability mechanism at the non-linear level.

We have assumed steady flow in the analysis. This assumption is reasonable for long waves (i.e., wavelength of several times the flow depth), but it may be interesting to study whether the result is significantly different when considering unsteady flow. Assuming unsteady flow would not only yield a more accurate result for the cases we have considered, but also increase the applicability range to supercritical conditions. This would allow for studying, for instance, the effect of mixed-size sediment in antidune formation.

The modelling of the experiment conducted under conditions in which the active layer model is ill-posed and the active layer thickness can be assumed to be constant (Section 5.4.3) predicts the formation of waves that we relate to the oscillatory behavior measured in the laboratory experiment. Yet, there are several differences. In the laboratory experiment the formation of waves was strongly linked to bedforms. Bedforms developed upstream of the patch of fine sediment (i.e., under unisize conditions) grew when fine sediment was entrained at the troughs. The SILKE model does not predict the formation of bedforms, which implies that the physical mechanism of entrainment of fine sediment at the troughs may be similar but not completely equivalent to the instability causing wave formation in the model.

Moreover, there is also a difference between the waves predicted in the numerical simulation of the experiment and the ones predicted by the linear analysis. In the numerical simulation of the laboratory experiment, waves form at a discontinuity in the grain size

distribution of the substrate sediment in the streamwise direction because of the presence of a patch of fine sediment. This mechanism of wave formation is related but not equivalent to the one predicted in the linear analysis, in which the substrate is uniform. As the predicted wave length is of the order of several meters, we would need laboratory experiments in a longer flume to capture these waves. Such laboratory experiments would shed light on the evolution of oscillations for long time scales and the validity of the instability domain.

5.5.4. Modelling of the Experiment by Blom et al. (2003)

One of the reasons to develop the SILKE model is that there are conditions, such as the ones in the experiment conducted by *Blom et al.* (2003), that cannot be reproduced using neither the active layer model (*Hirano*, 1971) nor the regularized model (*Chavarrías et al.*, 2019a). Yet, *Blom* (2008) modelled this experiment using the active layer model and compared it to the results of the model developed by *Blom and Parker* (2004) and *Blom et al.* (2006, 2008), in which the bed is treated in a continuous fashion and specifically accounts for mixing due to dunes. This was possible because, by considering normal flow conditions, *Blom* (2008) neglected all spatial derivatives. As there is no dependence on the spatial coordinate, the active layer equation is no longer a partial differential equation and it does not suffer from ill-posedness.

The continuous model by *Blom and Parker* (2004) and *Blom et al.* (2006, 2008) satisfactorily reproduced the experimental data, yet spatial changes are not accounted for and an instability mechanism cannot be captured. It would be interesting to model spatial changes using the continuous formulation under conditions in which we predict growth of perturbations. Maybe the model by *Blom and Parker* (2004) and *Blom et al.* (2006, 2008) also predicts an instability mechanism and captures the formation of waves that contribute to the vertical mixing caused by dunes. If this mechanism is not present, the continuous formulation could be extended relating the dune size to the grain size distribution of the bed surface. This would increase the vertical mixing when dunes migrate over a fine substrate.

5.6. Conclusions

We derive the SILKE model that accounts for mixed-size sediment morphodynamic processes. The model combines the active layer concept (*Hirano*, 1971) for mass conservation of sediment in the top part of the bed and the particle activity concept (*Furbish et al.*, 2012a; *Ancey and Heyman*, 2014) for mass conservation of transported sediment. The model is unconditionally well-posed. This is contrary to the active layer model, which can be ill-posed primarily under degradational conditions into a fine substrate (*Ribberink*, 1987; *Stecca et al.*, 2014; *Chavarrías et al.*, 2018a).

Chavarrías et al. (2019a) derived a regularized active layer model that can deal with situations in which the active layer model is ill-posed. Yet, the regularized active layer model cannot deal with situations in which the active layer thickness changes with time, for instance, when representing the vertical mixing due to changes in dune height. This limitation is overcome by the newly proposed model.

Analytically we find that (1) the SILKE model presents an instability mechanism caus-

ing growth of perturbations, and (2) unisize tracer sediment advects and diffuses in a normal (i.e., Fickian) manner for long time scales. The instability mechanism is triggered by substrate sediment that is fine compared to the bed surface. We compare model results to data from laboratory experiments conducted by *Chavarrías et al.* (2019a) under conditions in which the active layer model is ill-posed. The instability mechanism is related to the formation of waves observed in the experiments. As the new model allows for an increase in active layer thickness with time, we are able to model the laboratory experiment by *Blom et al.* (2003) accounting for spatial changes.

The model is compared to laboratory and field data of tracer propagation. When conditions are such that the effect of large rest times caused by temporary burial due to bedforms is negligible, the model well predicts tracer propagation. When the effect of temporary burial of sediment becomes the dominant mechanism, the model yields an underprediction of sediment dispersion. Moreover, dispersion may be anomalous (non-Fickian) while our model predicts normal diffusion.

6

Discussion

*I am not so enamoured of my own opinions
that I disregard what others may think of them.*

Copernicus (1543)

*There exists, in the depth of the oceans,
in the rivers and in the evolution of turbulent vortices,
the phenomena complexity of which gives you vertigo.*

Alexander Preissmann (see Cunge and Hager (2015)).

In this section we discuss a few overarching topics from the individual chapters. We connect the research we have conducted to gain perspective and to be able to have an outlook on the general implications and the future of river morphodynamic modelling. We first focus on the general problem of ill-posedness in morphodynamic modelling (Section 6.1). Subsequently, we comment on the proposed solutions to avoid ill-posedness due to accounting for mixed-size sediment (Section 6.2). In Section 6.4 we reflect on how to select one of the proposed solutions. Section 6.5 deals with how to approach the problem of ill-posedness due to accounting for the secondary flow and the bed slope effect. Section 6.6 discusses the possibility of ill-posedness in other topics relevant for river morphodynamic modelling.

6.1. The Problem of Ill-Posedness

The complete picture of the evolution of rivers is too complex to be tackled holistically. For this reason, the current tendency to improve our predicting capabilities and the accuracy of our predictions consists of identifying and studying processes individually (i.e., methodological reductionism). The complete picture is made a mosaic in which each tessera represents a particular physical process. Each process is studied ignoring or simplifying all other processes such that we comprehend the physical principles behind it. These principles are translated into mathematical terms in a model representing the process in question. Eventually, through the combination of separate models representing different processes we obtain a view of the complete picture. For instance, on the basis that for the cases we consider, changes in bed elevation and grain size distribution depend most predominantly on bed load transport (*Carling et al.*, 2000; *Ten Brinke*, 2005; *Jerolmack and Mohrig*, 2005; *Naqshband et al.*, 2014), we have neglected in this study the influence of suspended load, although it represents at least 75 % of the sediment transported by the Rhine as it enters the Netherlands (*Frings et al.*, 2015). Similarly, we have not considered the effect of vegetation, which has a direct impact on the morphology of rivers contributing not only to friction but also to preventing bank migration and shape river bars (*Vargas-Luna et al.*, 2014; *Corenblit et al.*, 2015; *Vargas-Luna*, 2016). Likewise, in modelling vegetation processes the effects of mixed-size sediment are neglected to reduce the complexity of the problem (*Caponi and Siviglia*, 2018).

Approaching the big picture through small pieces certainly works for increasing our understanding but the fact that the color of a tessera is beautiful does not imply that the mosaic is beautiful. The combination of sound submodels may yield an overall ill-posed model that is unable to represent the combination of physical processes. For instance, *Talmon et al.* (1995) derived a model to account for the effect of the bed slope on the direction of the sediment transport based on experiments conducted under unisize conditions. Their model is reasonable and well-posed when applied to conditions similar to the ones of their experiments, but, when combined with fractional sediment transport, the model may become ill-posed (Chapter 3).

The tendency to increase the number of processes combined in a model increases the likelihood that the model is ill-posed, as the different parts of it may interact in unexpected manners. In avoiding this problem it is crucial to conduct a mathematical analysis that confirms that the addition of independently realistic models is realistic. Furthermore, in deriving models, empirical fit to data should be avoided in favor of theoretical construc-

tions, as the ultimate goal is not to accurately fit particular data relevant for each individual process (i.e., each tessera), but to reflect the structures underlying physical processes (i.e., the mosaic). Elementary particle physics provides an inspiring example. The existence of the Higgs field, which in simple terms gives mass to the universe, was predicted in 1964 (Higgs, 1964; Englert and Brout, 1964; Guralnik et al., 1964), while it was shown to exist experimentally nearly half a century later (Cho, 2012). On the contrary, an essential concept in river morphodynamics such as the critical bed shear stress remains based on empirical fit to data (Shields, 1936; Dey, 1999). Experimentation should preferably be used to gain insight into physical phenomena and to strengthen a theory rather than to derive it.

The problem of ill-posedness of the system of equations stems from an incorrect mathematical representation of the physical processes, which originates from excessive extrapolation of results based on empirical knowledge. A deeper theoretical understanding of the physical processes, responsible for river morphodynamics and the interaction between processes aids in decreasing the likelihood that a model is ill-posed.

6.2. Extending the Regularization Strategy

A solution to the problem of ill-posedness of the active layer model (Hirano, 1971) accounting for mixed-size sediment processes has been provided purely based on a mathematical analysis of the system of equations (i.e., the regularization strategy, Chapter 4). Although the strategy guarantees that the model is well-posed, it does not guarantee that the results are realistic. The regularization strategy captures the mean (i.e., averaged over the passage of several bedforms) changes in bed elevation and surface texture measured in laboratory experiments specifically conducted for the purpose of testing the regularization strategy. The fact that there is no other data set to which we can apply the strategy clearly limits the proven range of applicability. It is necessary to test the strategy against a large data set of experiments conducted under conditions in which the active layer model is ill-posed to analyze the limits of the strategy in representing reality. Once its applicability is broadly tested under isolated conditions, it is necessary to test the strategy in more complex field cases in which several processes play a role.

As we have derived the regularization strategy under one-dimensional conditions, the following step in order to increase the applicability of the strategy is to extend it to account for morphodynamic processes in two dimensions. The extension is straightforward. Under two-dimensional conditions, one has to consider that not only the gradient of the sediment transport rate in the streamwise direction, but also in the lateral direction, is affected by the preconditioning factor. Interestingly, preliminary results show that the modification of the time scale of the mixing processes does not regularize the two-dimensional active layer model. This may be explained from the fact that, while under two-dimensional conditions the bed slope effect plays a role in model well-posedness (Chapter 3), this effect is neglected in deriving the regularization strategy. It seems that the regularization strategy solves for the problem associated to the incorrect representation of the mixing processes in the streamwise direction only and it has no effect regarding the problem associated to an incorrect description of the effect of the bed slope.

These preliminary results encourage us to explore other strategies to regularize the two-dimensional active layer model. In obtaining a solution applicable under two-dimensional

conditions, we aim at a modification of the active layer model that has similar implications as the regularization strategy has on the one-dimensional model. Worded differently, we aim at filtering out the small time scale processes in capturing the mean value averaged over the passage of several bedforms. We find an analogy in turbulence. The effect of the instantaneous flow velocity on the mean value can be accounted for by means of diffusion. Worded differently, the small time scale processes are accounted for by means of a diffusive component in the equations for the mean motion. We consider that diffusion in the active layer equation (i.e., diffusion in the volume of sediment of a certain grain size fraction in the active layer per unit of bed area) may be a reasonable mechanism accounting for the small time scale mixing processes. Preliminary results show that, indeed, accounting for a diffusive mechanism regularizes the two-dimensional active layer model.

The regularization strategy derived in Chapter 4 may become redundant if the addition of a diffusive mechanism guarantees model well-posedness. Yet, similarly to the fact that the regularization strategy guarantees well-posedness of the one-dimensional model but not of the two-dimensional model, the diffusive mechanism may guarantee well-posedness of the two-dimensional model but not of the one-dimensional model. Interestingly, preliminary results confirm this point. If this result is verified, we find that we need two different strategies to guarantee well-posedness of the active layer model depending on whether we account for one or for two dimensions. However, both strategies implicitly account for the same physical process: mixing of sediment occurring on a small scale.

6.3. Extending the SILKE model

Our second solution to the problem of ill-posedness arises from considering the interaction between the sediment at the bed surface and the sediment in transport (Chapter 5). Apart from being well-posed, the most striking feature of the new model is the fact that it is unstable under the conditions in which the active layer model is ill-posed. It predicts growth of perturbations under conditions in which the active layer model fails. The oscillations observed in the experiments conducted to test the regularization strategy seem to support the idea that the instability mechanism responsible for growth of perturbations indeed occurs in nature. However, the length scale of the feature as predicted by the model is too large to be clearly captured in those experiments. For this reason, there is a need to conduct similar laboratory experiments on a larger scale, such that the predicted instability can be clearly captured.

Another feature of the new model is that, contrary to the active layer and the regularization strategy, it predicts dispersion of tracer sediment and the rate of dispersion is realistic when compared to our laboratory data. Yet, when applied to the experiment conducted by *Sayre and Hubbell* (1965) the agreement is less satisfactory. We speculate that this is due to the fact that temporary burial of tracer sediment due to bedforms is a mechanism not included in the SILKE model. This mechanism is not relevant in our laboratory experiments, but becomes important under the conditions studied by *Sayre and Hubbell* (1965). Essentially, when the probability density distribution of bed elevation is well approximated by a constant value along a limited height, we expect that the SILKE model will yield reasonable results. This is because, in these cases, the active layer well approximates the actual probability distribution of bed elevation. As temporary burial of

sediment becomes relevant, the probability that sediment is deposited at a lower elevation increases and the lower tail of the probability density distribution becomes non-negligible. Laboratory experiments at a larger scale than the ones we conducted, such that temporary burial due to bedforms becomes relevant, may provide insight into this matter.

An added complexity in modelling such experiments is that, as the model does not explicitly resolve the dynamics of dunes, the particle velocity, activity, and diffusivity, are values representative of the conditions averaged throughout the passage of several bedforms. Using the latest measuring techniques that we have developed, the experiments can also be used to study the variability of particle motions due to bedforms under mixed-size sediment conditions.

Well-posedness of the new model comes at the expense of resolving the short time scale related to entrainment and deposition of sediment and the interaction between sediment at the bed surface and sediment load. If one is interested in long term processes (i.e., years or decades), solving the short time scale processes results in an unnecessary computational burden. A different modelling strategy may yield a well-posed model without resolving the small scale dynamics. The active layer model can be seen as a multiphase model (one phase being the sediment in the active layer and the other the sediment in the substrate) with a sharp interface between the phases. Ill-posedness is ubiquitous in mathematical models accounting for different phases (e.g. *Ardron, 1980; Toro et al., 2018*). This suggests that the solution may come from abandoning the idea of discretizing in multiple phases by treating the medium in a continuous form. In river morphodynamics this would mean abandoning the active layer concept by treating the bed in a vertically continuous form (*Parker et al., 2000; Blom et al., 2006, 2008; Pelosi et al., 2016; Viparelli et al., 2017*). We have seen that the continuous formulation by *Viparelli et al. (2017)* may yield an ill-posed model too (Chapter 2), but a more refined continuous formulation may lead to a well-posed model applicable at large time and spatial scales.

6.4. Selecting a Solution to Account for Mixed-Size Sediment

We have presented two solutions for the problem of ill-posedness in morphodynamic simulations accounting for mixed-size sediment. The question that arises is: Which one should we use? In fact, there are three possibilities, the first being to do nothing (i.e., to use the active layer model (*Hirano, 1971*)). To continue using the active layer model should not be disregarded immediately. The active layer model is well-posed in most cases, and, under certain conditions, we are certain that it is well-posed (Chapter 2). The active layer model is computationally cheap, easy to implement, and it is already implemented in a large amount of software packages. Moreover, the growth rate of perturbations is limited by the numerical grid (Chapter 2). For this reason, even when the problem becomes ill-posed, the consequences of ill-posedness may be limited if the simulation is short enough (relative to the growth rate of perturbations), such that perturbations do not grow significantly during the simulation time.

From our point of view, doing nothing is a valid solution if one checks for ill-posedness and sets a strategy to deal with ill-posed cases. The check can better be done in the code with a routine such as the one implemented in the research code Elv (Chapter 4) or in

Delft3D (*Chavarrías et al.*, 2018b, 2019b). If for some reason this is not possible, one can manually test whether the conditions of the simulation are prone to be ill-posed by checking the eigenvalues of a representative condition. For evaluating the likelihood of ill-posedness in an approximate manner, one can reduce the sediment mixture to two grain sizes and test whether the situation is prone to be ill-posed by means of an analytical expression (Equation 2.26). This approach can only identify ill-posedness due to a substrate finer than the active layer. Despite this, this effort is a useful one, as a fine substrate relative to the active layer remains the most likely cause of ill-posedness (Chapter 2).

If one finds that the conditions are (prone to be) ill-posed the simplest approach to avoid ill-posedness is to consider a different value of the active layer thickness. This “simple” approach hides a difficult problem. A change in the active layer thickness essentially changes the physical interpretation of the problem, as it modifies the time scale associated with sediment mixing and sorting processes. When increasing the active layer thickness in a particular case, one considers mixing due to less frequent bed elevation fluctuations that are able to entrain and remix sediment from deeper in the substrate. For this reason, an increase in active layer thickness implies that the results represent values averaged over a longer time and vice versa. Summarizing, changing the active layer thickness is a valid strategy if one first changes the interpretation of the model results. Worded differently, an increase in active layer thickness is a valid strategy if one considers that the results of the model represent values averaged over the time necessary for infrequent bed elevation fluctuations to play a significant role in mixing sediment.

If one faces an unavoidable ill-posed case, the approach should be to set a threshold for the maximum amplitude of spurious perturbations accepted in the solution. By computing the fastest growth rate of perturbations, one can set a limit time below which a simulation is acceptable. The fastest growth rate is associated to the shortest wave length, which is associated to the smallest cell size. Given the usual values of maximum growth rate, we expect that this approach yields, in general, a limit time below the time of interest. One can increase the limit time at the expenses of the model resolution (i.e., by increasing the cell size).

When considering the above points, using the active layer model is a valid approach. Yet, we do not advocate for continuing using the active layer model for two reasons. First, a change in the active layer thickness implies a change in the physical interpretation of the situation that is modelled, which may not be wanted. Moreover, a change in the active layer thickness to guarantee that a location is well-posed may cause the model to become ill-posed at a different location or at a different time. Second, limiting the extent of the validity of a numerical run based on the fact that the numerical grid limits the growth of physically unrealistic perturbations is dangerous, as the basic requirement of grid convergence of a numerical simulation is lost.

Nevertheless, the major reason to be against continuing using the active layer model is that the implementation of the regularization strategy is simple and the essence of the active layer model is left untouched. Moreover, if one tests for ill-posedness in the code, the first step of the regularization strategy is already done. The implementation of the new model is not particularly more complex, as it is an extension of the active layer model. The main consideration to choose between the two solutions regards the different phys-

ical processes accounted for by each model. If one is interested in an overall trend, the regularization strategy may be the preferred solution. The new model may be preferred if one wants to resolve the small scale morphodynamic processes related to entrainment, deposition, and non-local sediment transport. The main difference between the two models lies on the fact that the new model captures an instability which is averaged out by the regularization strategy. Although it may seem that the regularization strategy yields simpler results, from our point of view is opposite, as the results require the interpretation of the effects of the regularization parameter. The vertical mixing of sediment due to the instabilities that is evident in the new model has to be inferred when using the regularization strategy from the value of the regularization parameter.

A second consideration to choose between the two solutions is based on the idea that physical processes associated with non-capacity sediment transport are usually regarded to be relevant at laboratory scale or when dealing with suspended load only. This may favor the use of the regularization strategy for field applications in which bed load is the dominant process leading to aggradation, degradation, and changes in bed surface grain size distribution (*Carling et al., 2000; Ten Brinke, 2005; Jerolmack and Mohrig, 2005; Naqshband et al., 2014*). However, there is a reason to abandon the concept of sediment transport at capacity for all cases. The boundary condition at the upstream end of the domain in both field and laboratory cases is usually the sediment transport rate. This is *per se* inconsistent with assuming the sediment transport rate to be at capacity. If it is at capacity, it is determined by the flow conditions and it cannot be imposed. This yields a grid-dependency problem in numerical simulations. The bed elevation change at the upstream end depends on the difference between the sediment transport rate set as boundary condition and the sediment transport rate (at capacity) computed at the first node, divided by the grid size. As the difference between the sediment transport rates is finite regardless of the grid size, in the limit for the grid size tending to 0 (i.e., in the continuous limit), the rate of change of the bed elevation at the upstream end becomes infinite. The numerical discretization hides this problem but does not solve it.

Other possibilities for the upstream boundary condition such as imposing the bed elevation or the sediment load under normal flow conditions yield the same problem. For all these cases the boundary condition is inconsistent with the equations. For this reason we advocate for abandoning the concept of sediment transport rate at capacity for all cases in favor of the new model. The new model not only solves for the problem of ill-posedness but also for the problem associated with the upstream boundary condition.

With regard to the computational time, the new model requires a smaller time step than the regularized active layer model, which may seem a burden. Yet, the strategy involves solving several eigenvalue problems in which the size of the matrix increases quadratically with the number of grain sizes. Which solution requires more computational time depends on the number of size fractions and the number of cells in which the domain is discretized, among other factors. There is no clear guideline on which solution yields a faster numerical model and the speed will largely depend on implementation details such as the eigenvalue problem solver.

6.5. Solution to Ill-posedness due to Accounting for Secondary Flow and Bed Slope Effect

We have provided solutions to the problem of ill-posedness associated with the active layer model, but not for the problem of ill-posedness associated with the secondary flow and the bed slope effect. In this section we discuss possible solutions to this origin of ill-posedness and paths to explore.

Similarly to how we have approached the problem of the active layer model, we consider two types of solutions: a simple strategy that retains the basic principles and a more sophisticated solution that includes the relevant physical processes necessary to yield a well-posed model. As regards to the bed slope effect, we have seen that, under mixed-size sediment conditions, the model may become ill-posed depending on the closure relation for the direction of the sediment transport rate. A simple strategy could be to compute the parameters of the closure relation to guarantee that the problem is well-posed. We foresee the difficulty that there is no unique set of parameters which guarantee model well-posedness, which implies that there is a need to decide which would be the most representative of reality. We suggest to conduct experiments under the conditions in which the model is ill-posed to gain insight into the physical reasons that cause the model to be ill-posed. This is not as simple as it may seem. While in the experiments that we conducted, ill-posedness was governed by the size of the sediment initially placed in the substrate, in the experiments we suggest here, ill-posedness is governed by the closure relation used to model the bed slope effect. One can easily set the size of the substrate sediment, but one cannot easily set up an experiment in which the sediment transport rate has the direction predicted by a certain closure relation. It is plausible that it is impossible to conduct an experiment under such conditions. Even more, we suspect that this could be the case, as the fact that the model becomes ill-posed indicates that, under the studied conditions, the closure relation to account for the effect of the bed slope yields unrealistic results which do not occur in nature.

In obtaining a well-posed model we suggest to “start from the physics”. Rather than to conduct experiments varying the grain size, the sediment mixture, the flow parameters, and curve-fitting the results, we suggest to derive a model based on physical principles that is guaranteed to be always well-posed and then test whether the predictions of the model agree with experiments. Well-posedness (i.e., the mosaic) is much more important than accurately reproducing a limited set of experiments (i.e., the tessera). Furthermore, we suggest to study whether an entrainment-deposition formulation of the equations to account for bed elevation and surface grain size distribution contributes to the well-posedness of the system of equations when considering the effect of the bed slope, as the entrainment-deposition formulation has proven to be key in solving for the problem of ill-posedness due to the modelling of mixed-size sediment.

As regards to modelling of secondary flow in depth-averaged simulations, a simple strategy to guarantee that the length scale of the oscillations predicted by the model is compatible with the shallow water assumption could be to consider that the diffusion coefficient of the secondary flow equation depends on the secondary flow intensity. This mechanism would account for the fact that when the secondary flow increases, the vertical profile of the primary flow changes and the momentum redistribution increases. In

testing how physically realistic are the results of such strategy, it is simpler to compare the results to the ones of three-dimensional simulations than to the ones of laboratory experiments. A sophisticated solution to guarantee a reasonable length scale of the oscillations predicted by the model could consider the effect of non-linearities in secondary flow when the secondary flow increases significantly (Chapter 3). Non-linearities limit the development of secondary flow, and we suspect that including this effect would yield a more realistic model.

6.6. Ill-posedness in Other Topics and Remaining Challenges

A striking outcome of our research is that all the models that we have studied (i.e., the active layer model, the secondary flow model, and the bed slope effect model) have a domain in which they are ill-posed. Ill-posedness appears to be ubiquitous. For this reason, it is likely that there are other models that have a yet unknown domain of ill-posedness. In this section we focus on two processes which may yield an ill-posed model: interaction with mud and with vegetation.

One candidate is the model to account for the interaction between mud and sand (Van Ledden, 2003; Van Ledden *et al.*, 2004a,b; Van Kessel *et al.*, 2011a,b). Two-dimensional model results show a pattern of mud concentration that resembles a chessboard (*M. Kleinhans*, personal communication). Worded differently, areas of high and low mud concentration alternate at the scale of the numerical grid. It is possible that the length scale of a particular process related to mud is smaller than the cell size used in the numerical runs. In this case, the numerical results will converge if the grid is refined. Once the cell size is sufficiently small such that it captures the particular length scale, the alternate pattern will disappear.

Another possibility is that the model is ill-posed. The fact that the smallest waves resolved by the model (i.e., waves with wavelength equal to two times the cell size) are the fastest growing waves, explains the chessboard pattern (see, for instance, Figure 3.8b). In this case, similarly to the cases we have shown here, the results will not converge with decreasing cell size and the chessboard pattern will replicate at smaller scales. The reason for us to consider that a domain in which the model is ill-posed is likely to exist is that, similarly to the active layer model, the mud model combines discrete layers with empirical closure relations. An analysis as the one we have conducted in Chapter 3 would be useful to test whether the mud model has a domain in which it is ill-posed. If it proves to be well-posed, the analysis would yield the length scale of all processes described in the model. This result would be useful to determine the minimum cell size in numerical simulations.

A second remaining challenge is modelling of vegetation. Vegetation plays an important role in shaping rivers (e.g. *Corenblit et al.*, 2015) by, for instance, increasing flow resistance (*Västilä and Järvelä*, 2014) and reducing the bed shear stress (*Vargas-Luna et al.*, 2014). In modelling the effect of vegetation, empirical closure relations are used to, for instance, compute the flow resistance exerted by vegetation (*Västilä and Järvelä*, 2014). The applicability of the relation derived by *Västilä and Järvelä* (2014) is limited to conditions in which the flow velocity is sufficiently large due to the asymptotic nature of the expression as the velocity tends to 0. We find similarities with the closure relation to account for granular viscosity in the model describing the dynamics of granular flow (*Jop et al.* (2005, 2006), Section 3.1). The closure relation by *Jop et al.* (2005, 2006) is derived

for condition in which the dimensionless shear rate is above a certain threshold value and yields an ill-posed model otherwise (*Barker et al.*, 2015). It is likely that a similar problem occurs when accounting for vegetation in morphodynamic modeling. One way to prevent ill-posedness (in case it occurs) is to improve the closure relation accounting for the dynamics of vegetation under low flow velocity conditions. This is equivalent to the strategy followed by *Barker and Gray* (2017) in extending the well-posed domain of the model describing granular flow.

7

Conclusions and Recommendations

*Everything is changing,
nothing has endurance,
and nothing is completely satisfying.*

Three marks of existence in Buddhism (see e.g. *Walsh* (1995))

*All our life passes in this way:
we seek rest by struggling against certain obstacles,
and once they are overcome,
rest proves intolerable because of the boredom it produces.*

Blaise Pascal, Pensées, 136.

In this chapter we summarize the main conclusions by answering the research questions we initially posed (Section 7.1) and we outline the topics that need further research (Section 7.2).

7.1. Conclusions

Our objectives were to assess the problem of ill-posedness in river morphodynamic modelling and to provide solutions to it. In Section 1.4 we formulated the following research questions:

1. Under which conditions are current models accounting for mixed-size sediment mechanisms ill-posed?
2. What is the role of two-dimensional effects with respect to model well-posedness?
3. How can we prevent the active layer model from being ill-posed?
4. How can we obtain a new model describing mixed-size sediment river morphodynamics that avoids ill-posedness?

These questions will be answered in the following sections.

7.1.1. Ill-Posedness due to Accounting for Mixed-Size Sediment

In this section we answer the first research question:

Under which conditions are current models accounting for mixed-size sediment mechanisms ill-posed?

1. How can we determine whether the active layer model is ill-posed?
2. What is the role of the active layer thickness as well as other model parameters in the domain of ill-posedness of the active layer model?
3. How do we recognize ill-posed numerical simulations?
4. Under which conditions does a vertically continuous representation of the bed yield an ill-posed model?

Through mathematical analysis of the active layer model (*Hirano, 1971*) in one-dimensional problems, we find an expression to discretize between ill-posed and well-posed cases. The expression applies to simplified conditions assuming steady flow and two sediment size fractions. Using this expression we prove that the active layer thickness plays a major role in the well-posedness of the system of equations. The problem is always well-posed for a sufficiently thin and sufficiently thick active layer. However, the values of the active layer thickness to obtain a well-posed model may be physically unrealistic. We find that, when accounting for hiding in the sediment transport relation, the likelihood that the model is ill-posedness increases. Strong hiding can cause the active layer model to be ill-posed even under aggradational conditions. This is a new finding as earlier the only case possibly leading to ill-posedness was degradation into a substrate finer than the active layer. Furthermore, ill-posedness under aggradational conditions can also arise if the

sediment transferred to the substrate consists not only of active layer sediment but also of transported sediment.

For more complex cases (e.g. with more than two sediment size fractions or unsteady flow), it is not possible to obtain a simple expression for discretizing between ill-posed and well-posed cases, but we provide a method to determine whether a case is ill-posed. Using this method we find another new case in which the active layer model may be ill-posed. Under degradational conditions into a substrate coarser than the active layer, the model may become ill-posed without accounting for hiding if one considers more than two sediment size fractions.

We conduct a similar analysis to the system of equations of the vertically continuous model derived by *Viparelli et al.* (2017) and we find that this model can also be ill-posed. A large vertical gradient in the volume fraction content of the bed sediment increases the likelihood that the model is ill-posed.

These analyses provide means to predict the occurrence of ill-posedness but do not predict the consequences. By means of numerical simulations, we studied the effect of non-linear interactions in the development of ill-posed simulations and in general the consequences of ill-posedness in numerical simulations. Ill-posedness causes growth of infinitesimal perturbations. Numerical truncation errors are sufficient to trigger the formation of physically unrealistic waves in numerical simulations. Waves grow until the situation becomes well-posed. The formation of waves acts as a regularization mechanism as the waves enhance unrealistic vertical mixing of sediment that yields conditions in which the model is well-posed.

7.1.2. Ill-Posedness due to Two-Dimensional Effects

In this section we answer the second research question:

What is the role of two-dimensional effects with respect to model well-posedness?

1. How does the formulation accounting for the secondary flow affect model well-posedness?
2. How does the formulation accounting for the transverse bed slope affect model well-posedness?

We extend the analysis of the system of equations to two-dimensional conditions. In particular, we focus on the effect of the secondary flow that originates from the flow curvature, as well as the effect of the bed slope on the direction of the sediment transport. We find that modelling of the secondary flow yields an ill-posed model if the diffusion coefficient of the equation accounting for the transport of the secondary flow intensity is equal to 0. This situation is physically unrealistic though. When considering a physically realistic value of the diffusion coefficient, the system of equations is well-posed. Nevertheless, it predicts growth of perturbations that are not compatible with the shallow water assumption used in deriving the two-dimensional flow equations. Only, an unrealistically large amount of diffusion dampens the oscillations.

The effect of the bed slope on the direction of the sediment transport is crucial to obtain a well-posed model. Under mixed-size sediment conditions, it is not only important to account for the bed slope effect, but also to carefully select the closure relation for

this purpose. We derive an expression to test whether, in a simple case considering two sediment size fractions, a certain closure relation yields an ill-posed model.

7.1.3. Regularization of the Active Layer Model

In this section we answer the third research question:

How can we prevent the active layer model from being ill-posed?

1. Which possible strategies can we follow to avoid ill-posedness of the active layer model?
2. How physically realistic are the results applying the strategy to avoid ill-posedness?

We derive a regularization strategy to recover well-posedness of the active layer model (Hirano, 1971). The regularization strategy modifies the active layer model when and where this is ill-posed only. The strategy is based on the use of preconditioning techniques to modify the time scales of the physical processes. We consider a diagonal preconditioning matrix and we choose not to modify the time scales associated with flow processes. Under these conditions, we find that the only possibility to regularize the active layer model is by slowing down the time scale related to the mixing processes while not modifying the time scale associated to bed elevation change. A limitation of the proposed regularization strategy is the fact that it can be applied when the active layer thickness is constant only. Otherwise, mass is not conserved.

There is a close mathematical similarity between the regularization strategy and the morphodynamic acceleration factor used to decrease the computational time of numerical simulations (Latteux, 1995; Lesser *et al.*, 2004; Roelvink, 2006; Ranasinghe *et al.*, 2011). In physical terms the morphodynamic acceleration factor speeds up the bed elevation changes with respect to the flow and sediment mixing processes. The regularization strategy slows down the sediment mixing processes with respect to the flow and bed elevation changes.

We derive an analytical expression of the parameter controlling the time scale of the mixing processes that regularizes the active layer model. The expression is only applicable to mixtures of sediment composed of two sediment size fractions. For a general case with more than two sediment size fractions, the method to find the value of the regularizing parameter involves minimization of an eigenvalue problem (i.e., solving several eigenvalue problems). For this reason, the general case is at this moment relatively expensive in computational terms.

The results of the regularization strategy cannot be compared to those of the active layer model, as when the regularization strategy affects the solution the active layer model is ill-posed and not applicable. In testing the ability of the regularization strategy to reproduce physical phenomena, we need to compare its results to data from physical experiments. We find no data set obtained under conditions in which the active layer model is ill-posed and the active layer thickness can be assumed to be constant with time. For this reason we conduct a set of laboratory experiments to which we can apply the regularization technique. The experiments consist of imposing degradational conditions on a situation that is initially under equilibrium conditions. Fine sediment is placed below a top

layer composed of coarse sediment. The entrainment of fine sediment from the substrate results to be a cyclic process. Initially the bed surface is covered by bedforms composed of coarse sediment only. Degradation causes fine sediment to be entrained at the trough of coarse bedforms. The difference in mobility between the coarse and fine sediment triggers the formation of a degradational wave traveling downstream. The erosional pit left by the degradational wave is filled by coarse sediment. Degradation continues over the newly formed coarse deposit until fine sediment from the substrate is exposed again.

The regularization strategy does not explicitly capture the formation of the degradational waves. However, it reproduces the enhanced vertical mixing of sediment due to the formation of degradational waves.

7.1.4. Development of a New Model to Account for Mixed-Size Sediment Morphodynamics

In this section we answer the fourth research question:

How can we obtain a new model describing mixed-size sediment river morphodynamics that avoids ill-posedness?

1. Which physical mechanisms need to be considered in the new model to guarantee its well-posedness?
2. How physically realistic are the results of the new model?

In obtaining a well-posed model, it appears to be crucial to account for the short term processes associated with the entrainment and deposition of sediment. Accounting for these processes relaxes the hypothesis that the sediment transport rate is at capacity conditions. We propose a new model that results from combining the active layer concept (*Hirano, 1971*) with a model conserving the mass of the sediment in transport. The model for mass conservation of the sediment in transport originates from a stochastic treatment of sediment transport (*Furbish et al., 2012a; Ancey and Heyman, 2014*). We prove that the new model is always well-posed. The new model presents an instability mechanism under conditions in which the active layer model is ill-posed. The new model captures the oscillatory behavior measured in our experiments conducted under conditions in which the active layer model is ill-posed.

The interaction between the bed surface and the sediment in transport leads to dispersion of tracer sediment, which the active layer model cannot reproduce. While the active layer model predicts tracer sediment to propagate downstream in a purely advective form, the new model predicts tracer sediment to diffuse as it is advected downstream. We compare predictions of the new model to data regarding tracer sediment dispersion. The new model captures dispersion as measured in our laboratory experiments. However, it does not well reproduce the dispersion measured in the field experiment conducted by *Sayre and Hubbell (1965)*. This is explained from the fact that temporary burial of sediment due to bedforms is not included in the model. This mechanism is not relevant for the conditions of our experiments but it is relevant for the conditions of the experiment by *Sayre and Hubbell (1965)*.

Contrary to the regularization strategy, the new model can account for a temporal change in the active layer thickness. The new model satisfactorily reproduces a laboratory experiment conducted by *Blom et al.* (2003). This laboratory experiment was conducted under conditions in which the active layer model is ill-posed and in which vertical mixing in the active layer model can only be induced by a temporal change in the active layer thickness accounting for an increase in dune height.

7.2. Recommendations

In this section we recapitulate our main recommendations in terms of suggestions to be considered in the short, mid, and long term with a focus to the practical relevance of our research.

In the short term, it is important to test the validity of the regularization strategy against a large variety of cases and, in particular, against field cases. The ability of the strategy to regularize two-dimensional conditions needs to be further explored. If it is confirmed that the strategy does not regularize two-dimensional cases, the alternative consisting in adding a diffusive mechanism to the active layer equation needs to be further explored. A strategy that regularizes the two-dimensional model needs to be implemented in software used to predict the consequences of river interventions. We think that it would be interesting for practitioners to re-run engineering cases such as the DVR simulations (*Ottevaenger et al.*, 2015) using the regularization strategy to test whether ill-posedness has significantly affected the results of the simulations.

In the mid term, we recommend to test the validity of the SILKE model conducting a set of laboratory experiments. In particular, the laboratory experiments should be aimed at capturing the instability mechanism predicted by the SILKE model. Furthermore, it is important to study tracer dispersion at a laboratory scale larger than the one we studied such that temporary burial due to bedforms becomes a relevant mechanism. This exercise may provide insight into the reasons why the SILKE model does not capture dispersion for the conditions of the experiment by *Sayre and Hubbell* (1965). The simple strategy to avoid ill-posedness due to the bed slope effect (i.e., the strategy consisting in modifying the parameters of the closure relation) should be implemented and its validity should be tested. Similarly, the possibility of a diffusion coefficient depending on the secondary flow intensity should be considered in avoiding physically unrealistic oscillations.

In the long term, we advocate for rejecting the capacity-based sediment transport approximation. Accounting for conservation of the sediment in transport not only recovers well-posedness of the system of equations but also prevents inconsistent boundary conditions in morphodynamic modelling. We suggest to study the possibility of modifying the SILKE model by replacing the active layer with a continuous formulation of the bed (*Parker et al.*, 2000) that allows modelling of spatial changes (e.g. *Pelosi et al.*, 2016). This modified model may be able to capture anomalous (i.e., non-Fickian) diffusion of sediment and account for changes in bed elevation and surface texture. As regards to secondary flow, its parameterization in two-dimensional cases should be further studied. Accounting for the effect of the secondary flow in the vertical profile of the primary flow could yield a model that, considering a physically realistic amount of diffusion, it does not predict growth of perturbations at a scale incompatible with the shallow water assumption.

Overall, we recommend a methodological reductionist approach in improving the prediction of morphodynamic change in rivers. First, the small scale processes need to be well understood and modelled. Models need to be based on theoretical analysis and principles. Detailed laboratory experiments and field data should be used to gain insight and inspiration and to test the models, but not to derive them. Integrating and filtering the short time scale processes, one derives the effects and implications at the large scale. The approach we recommend is opposed to a holistic approach in which predictions at the large scale are derived from observation at the large scale including all the complexity without detailed understanding of the small scale processes.

A reductionist approach cannot outperform predictions obtained by means of holistic methods in the range of conditions in which a holistic method has been based. However, a reductionist approach is expected to yield reasonable results for all conditions, apart from the most important outcome: deep understanding of nature.

References

- Abgrall, R., and S. Karni (2009), Two-layer shallow water system: A relaxation approach, *SIAM J. Sci. Comput.*, 31(3), 1603–1627, doi:10.1137/06067167X.
- Allen, J. R. L. (1968a), *Current Ripples. Their relation to patterns of water and sediment motion.*, 433 pp., North Holland Publishing Company, Amsterdam, the Netherlands.
- Allen, J. R. L. (1968b), The nature and origin of bed-form hierarchies, *Sedimentology*, 10(3), 161–182, doi:10.1111/j.1365-3091.1968.tb01110.x.
- Allen, J. R. L. (1970), A quantitative model of grain size and sedimentary structures in lateral deposits, *Geol. J.*, 7(1), 129–146, doi:10.1002/gj.3350070108.
- Allen, J. R. L. (1985), *Principles of Physical Sedimentology*, 272 pp., Springer Netherlands, Dordrecht, the Netherlands, doi:10.1007/978-94-010-9683-6.
- Ancey, C. (2010), Stochastic modeling in sediment dynamics: Exner equation for planar bed incipient bed load transport conditions, *J. Geophys. Res., Earth Surface*, 115(F2), F00A11, doi:10.1029/2009JF001260.
- Ancey, C., and J. Heyman (2014), A microstructural approach to bed load transport: Mean behaviour and fluctuations of particle transport rates, *J. Fluid Mech.*, 744, 129–168, doi:10.1017/jfm.2014.74.
- Ancey, C., T. Böhm, M. Jodeau, and P. Frey (2006), Statistical description of sediment transport experiments, *Phys. Rev. E*, 74, 011302, doi:10.1103/PhysRevE.74.011302.
- Ancey, C., A. C. Davison, T. Böhm, M. Jodeau, and P. Frey (2008), Entrainment and motion of coarse particles in a shallow water stream down a steep slope, *J. Fluid Mech.*, 595, 83–114, doi:10.1017/S0022112007008774.
- Anderson, H. L. (1986), Metropolis, Monte Carlo, and the MANIAC, *Los Alamos Science*, pp. 96–107.
- Ardron, K. (1980), One-dimensional two-fluid equations for horizontal stratified two-phase flow, *Int. J. Multiphase Flow*, 6(4), 295–304, doi:10.1016/0301-9322(80)90022-1.
- Armanini, A. (1995), Non-uniform sediment transport: Dynamics of the active layer, *J. Hydraul. Res.*, 33(5), 611–622, doi:10.1080/00221689509498560.
- Armanini, A., and G. di Silvio (1988), A one-dimensional model for the transport of a sediment mixture in non-equilibrium conditions, *J. Hydraul. Res.*, 26(3), 275–292, doi:10.1080/00221688809499212.

- Armi, L. (1986), The hydraulics of two flowing layers with different densities, *J. Fluid Mech.*, 163, 27–58, doi:10.1017/S0022112086002197.
- Ashida, K., and M. Michiue (1971), An investigation of river bed degradation downstream of a dam, in *Proc. of the 14th IAHR World Congress, 29 August–3 Septemeber, Paris, France*, vol. 3, pp. 247–255.
- Ashida, K., and M. Michiue (1972), Study on hydraulic resistance and bed-load transport rate in alluvial streams, *Proc. Jpn. Soc. Civ. Eng.*, 206, 59–69, doi:10.2208/jscej1969.1972.206_59.
- Ashmore, P., S. Peirce, and P. Leduc (2018), Expanding the “active layer”: Discussion of Church and Haschenburger (2017) What is the “active layer”? *Water Resources Research* 53(1), 5–10, *Water Resour. Res.*, 54(3), 1425–1427, doi:10.1002/2017WR022438.
- Baar, A. W., J. de Smit, W. S. J. Uijttewaal, and M. G. Kleinhans (2018), Sediment transport of fine sand to fine gravel on transverse bed slopes in rotating annular flume experiments, *Water Resour. Res.*, 54(1), 19–45, doi:10.1002/2017WR020604.
- Balmforth, N. J., and S. Mandre (2004), Dynamics of roll waves, *J. Fluid Mech.*, 514, 1–33, doi:10.1017/S0022112004009930.
- Balmforth, N. J., and A. Vakil (2012), Cyclic steps and roll waves in shallow water flow over an erodible bed, *J. Fluid Mech.*, 695, 35–62, doi:10.1017/jfm.2011.555.
- Banks, J., J. Brooks, G. Cairns, G. Davis, and P. Stacey (1992), On Devaney’s definition of chaos, *The American Mathematical Monthly*, 99(4), 332–334, doi:10.2307/2324899.
- Barker, B., M. A. Johnson, P. Noble, L. M. Rodrigues, and K. Zumbrun (2017a), Note on the stability of viscous roll waves, *C. R. Mec.*, 345(2), 125–129, doi:10.1016/j.crme.2016.11.001.
- Barker, B., M. A. Johnson, P. Noble, L. M. Rodrigues, and K. Zumbrun (2017b), Stability of viscous St. Venant roll waves: From onset to infinite Froude number limit, *J. Nonlinear Sci.*, 27(1), 285–342, doi:10.1007/s00332-016-9333-6.
- Barker, T., and J. M. N. T. Gray (2017), Partial regularisation of the incompressible μ -rheology for granular flow, *J. Fluid Mech.*, 828, 5–32, doi:10.1017/jfm.2017.428.
- Barker, T., D. G. Schaeffer, P. Bohorquez, and J. M. N. T. Gray (2015), Well-posed and ill-posed behaviour of the μ -rheology for granular flow, *J. Fluid Mech.*, 779, 794–818, doi:10.1017/jfm.2015.412.
- Battjes, J., and R. J. Labeur (2017), *Unsteady flow in open channels*, 288 pp., Cambridge University Press, Cambridge, United Kingdom.
- Beeler, M., R. W. Gosper, and R. C. Schroeppel (1972), HAKMEM, *MIT AI Memo 239*, Artificial Intelligence Laboratory, Massachusetts Institute of Technology, Cambridge, MA, United States, 107 pp.

- Begnudelli, L., A. Valiani, and B. F. Sanders (2010), A balanced treatment of secondary currents, turbulence and dispersion in a depth-integrated hydrodynamic and bed deformation model for channel bends, *Adv. Water Resour.*, 33(1), 17–33, doi:10.1016/j.advwatres.2009.10.004.
- Bell, R. G., and A. J. Sutherland (1983), Nonequilibrium bedload transport by steady flows, *J. Hydraul. Eng.*, 109(3), 351–367, doi:10.1061/(ASCE)0733-9429(1983)109:3(351).
- van Bendegom, L. (1947), Eenige beschouwingen over riviermorphofogie en rivierverbetering, *De Ingenieur*, 59(4), 1–11, (in Dutch).
- Bennett, J. P., and C. F. Nordin (1977), Simulation of sediment transport and armouring, *Hydrol. Sci. Bull.*, 22(4), 555–569, doi:10.1080/02626667709491760.
- Best, J. (2005), The fluid dynamics of river dunes: A review and some future research directions, *J. Geophys. Res., Earth Surface*, 110(F4), F04S02, doi:10.1029/2004JF000218.
- Bettess, R., and A. Frangipane (2003), A one-layer model to predict the time development of static armour, *J. Hydraul. Res.*, 41(2), 179–194, doi:10.1080/00221680309499960.
- Biondini, G., and T. Trogdon (2017), Gibbs phenomenon for dispersive PDEs on the line, *SIAM J. Appl. Math.*, 77(3), 813–837, doi:10.1137/16M1090892.
- Blancaert, K. (2009), Saturation of curvature-induced secondary flow, energy losses, and turbulence in sharp open-channel bends: Laboratory experiments, analysis, and modeling, *J. Geophys. Res., Earth Surface*, 114(F3), F03015, doi:10.1029/2008JF001137.
- Blancaert, K., and H. J. de Vriend (2003), Nonlinear modeling of mean flow redistribution in curved open channels, *Water Resour. Res.*, 39(12), 1375, doi:10.1029/2003WR002068.
- Blancaert, K., and W. H. Graf (2004), Momentum transport in sharp open-channel bends, *J. Hydraul. Eng.*, 130(3), 186–198, doi:10.1061/(ASCE)0733-9429(2004)130:3(186).
- Blancaert, K., and H. J. de Vriend (2004), Secondary flow in sharp open-channel bends, *J. Fluid Mech.*, 498, 353–380, doi:10.1017/S0022112003006979.
- Blom, A. (2008), Different approaches to handling vertical and streamwise sorting in modeling river morphodynamics, *Water Resour. Res.*, 44(3), W03415, doi:10.1029/2006WR005474.
- Blom, A., and G. Parker (2004), Vertical sorting and the morphodynamics of bed-form dominated rivers: A modeling framework, *J. Geophys. Res., Earth Surface*, 109(F2), F02007, doi:10.1029/2003JF000069.
- Blom, A., J. S. Ribberink, and H. J. de Vriend (2003), Vertical sorting in bed forms: Flume experiments with a natural and a trimodal sediment mixture, *Water Resour. Res.*, 39(2), 1025, doi:10.1029/2001WR001088.

- Blom, A., G. Parker, J. S. Ribberink, and H. J. de Vriend (2006), Vertical sorting and the morphodynamics of bed-form-dominated rivers: An equilibrium sorting model, *J. Geophys. Res., Earth Surface*, 111(F1), F01006, doi:10.1029/2004JF000175.
- Blom, A., J. S. Ribberink, and G. Parker (2008), Vertical sorting and the morphodynamics of bed form-dominated rivers: A sorting evolution model, *J. Geophys. Res., Earth Surface*, 113(F1), F01019, doi:10.1029/2006JF000618.
- Blom, A., E. Viparelli, and V. Chavarrías (2016), The graded alluvial river: Profile concavity and downstream fining, *Geophys. Res. Lett.*, 43(12), 6285–6293, doi:10.1002/2016GL068898.
- Blom, A., V. Chavarrías, R. I. Ferguson, and E. Viparelli (2017a), Advance, retreat, and halt of abrupt gravel-sand transitions in alluvial rivers, *Geophys. Res. Lett.*, 44(19), 9751–9760, doi:10.1002/2017GL074231.
- Blom, A., L. Arkesteijn, V. Chavarrías, and E. Viparelli (2017b), The equilibrium alluvial river under variable flow and its channel-forming discharge, *J. Geophys. Res., Earth Surface*, 122(10), 1924–1948, doi:10.1002/2017JF004213.
- Bohorquez, P., and C. Ancey (2015), Stochastic-deterministic modeling of bed load transport in shallow water flow over erodible slope: Linear stability analysis and numerical simulation, *Adv. Water Resour.*, 83, 36–54, doi:10.1016/j.advwatres.2015.05.016.
- Bohorquez, P., and C. Ancey (2016), Particle diffusion in non-equilibrium bedload transport simulations, *Appl. Math. Modell.*, 40(17), 7474 – 7492, doi:10.1016/j.apm.2016.03.044.
- Booij, R., and J. G. S. Pennekamp (1983), Simulation of main flow and secondary flow in a curved open channel, *Tech. Rep. 10-83*, Laboratory of Fluid Mechanics, Faculty of Civil Engineering and Geosciences, Delft University of Technology, Delft, the Netherlands, 62 pp.
- Booij, R., and J. G. S. Pennekamp (1984), Measurements of the rate of adjustment of the secondary flow in a curved open channel with varying discharge, *Tech. Rep. 15-84*, Laboratory of Fluid Mechanics, Faculty of Civil Engineering and Geosciences, Delft University of Technology, Delft, the Netherlands, 44 pp.
- Booß-Bavnbeek, B., and J. Høyrup (Eds.) (2003), *Mathematics and War*, 463 pp., Birkhäuser, Basel, Switzerland.
- Borah, D., C. V. Alonso, and S. N. Prasad (1982), Routing graded sediments in streams: Formulations, *J. Hydraulics Div.*, 108(HY12), 1486–1503.
- Borges, J. L. (1964), El golem, in *El otro, el mismo*, Emecé, Buenos Aires, Argentina, (in Spanish).
- Borges, J. L. (1977), Arte poética, in *Obra poética (1923–1976)*, Emecé, Buenos Aires, Argentina, (in Spanish).

- Bosch, T. (2014), Dutch water management in an era of revolution, restoration and the advance of Liberalism, 1795–1850, in *Two Centuries of Experience in Water Resources Management. A Dutch-U.S. Retrospective*, edited by J. Lonnguest, B. Toussaint, J. Joe Manous, and M. Ertsen, chap. 2, pp. 11–49, Institute for Water Resources, US Army Corps of Engineers and Rijkswaterstaat, Ministry of Infrastructure and the Environment.
- Bouchaud, J.-P., and A. Georges (1990), Anomalous diffusion in disordered media: Statistical mechanisms, models and physical applications, *Phys. Rep.*, 195(4), 127–293, doi:10.1016/0370-1573(90)90099-N.
- Box, G. E. P. (1976), Science and statistics, *J. Am. Stat. Assoc.*, 71(356), 791–799.
- Bradley, D. N. (2017), Direct observation of heavy-tailed storage times of bed load tracer particles causing anomalous superdiffusion, *Geophys. Res. Lett.*, 44(24), 12227–12235, doi:10.1002/2017GL075045.
- Bradley, D. N., and G. E. Tucker (2012), Measuring gravel transport and dispersion in a mountain river using passive radio tracers, *Earth Surf. Process. Landf.*, 37(10), 1034–1045, doi:10.1002/esp.3223.
- Bradley, D. N., G. E. Tucker, and D. A. Benson (2010), Fractional dispersion in a sand bed river, *J. Geophys. Res., Earth Surface*, 115(F1), F00A09, doi:10.1029/2009JF001268.
- Bradshaw, P. (1987), Turbulent secondary flows, *Annu. Rev. Fluid Mech.*, 19(1), 53–74, doi:10.1146/annurev.fl.19.010187.000413.
- Bressan, A. (2011), Hyperbolic conservation laws, in *Mathematics of Complexity and Dynamical Systems*, edited by R. A. Meyers, chap. 44, pp. 729–739, Springer, New York, NY, United States, doi:10.1007/978-1-4614-1806-1_44.
- ten Brinke, W. B. M. (2005), *The Dutch Rhine: A restrained river*, 229 pp., Veen Magazines, Amsterdam, the Netherlands.
- de Bruijn, H. E. (1911), Invloed van de afsluiting van de Zuiderzee op de vloedhoogte buiten den afsluitdijk, *De Ingenieur*, 26(1), 28–30, (in Dutch).
- Brundrett, E., and W. D. Baines (1964), The production and diffusion of vorticity in duct flow, *J. Fluid Mech.*, 19(3), 375–394, doi:10.1017/S0022112064000799.
- Buffington, J. M., and D. R. Montgomery (1997), A systematic analysis of eight decades of incipient motion studies, with special reference to gravel-bedded rivers, *Water Resour. Res.*, 33(8), 1993–2029, doi:10.1029/96WR03190.
- Butcher, J. C. (1996), A history of Runge-Kutta methods, *Appl. Numer. Math.*, 20(3), 247–260, doi:10.1016/0168-9274(95)00108-5.
- Butcher, J. C., and G. Wanner (1996), Runge-Kutta methods: Some historical notes, *Appl. Numer. Math.*, 22(1), 113–151, doi:10.1016/S0168-9274(96)00048-7.

- Callander, R. A. (1969), Instability and river channels, *J. Fluid Mech.*, 36, 465–480, doi:10.1017/S0022112069001765.
- Cao, Z., and P. A. Carling (2002a), Mathematical modelling of alluvial rivers: Reality and myth. Part 1: General review, *Proceedings of the Institution of Civil Engineers Water & Maritime Engineering*, 154(3), 207–219.
- Cao, Z., and P. A. Carling (2002b), Mathematical modelling of alluvial rivers: Reality and myth. Part 2: Special issues, *Proceedings of the Institution of Civil Engineers Water & Maritime Engineering*, 154(4), 297–307.
- Cao, Z., R. Day, and S. Egashira (2002), Coupled and decoupled numerical modeling of flow and morphological evolution in alluvial rivers, *J. Hydraul. Eng.*, 128(3), 306–321, doi:10.1061/(ASCE)0733-9429(2002)128:3(306).
- Caponi, F., and A. Siviglia (2018), Numerical modeling of plant root controls on gravel bed river morphodynamics, *Geophys. Res. Lett.*, 45(17), 9013–9023, doi:10.1029/2018GL078696.
- Carling, Williams, Göz, and Kelsey (2000), The morphodynamics of fluvial sand dunes in the River Rhine, near Mainz, Germany. II. Hydrodynamics and sediment transport, *Sedimentology*, 47(1), 253–278, doi:10.1046/j.1365-3091.2000.00291.x.
- Carling, P. A. (1999), Subaqueous gravel dunes, *J. Sediment. Res.*, 69(3), 534–545, doi:10.2110/jsr.69.534.
- Carling, P. A., K. Richardson, and H. Ikeda (2005), A flume experiment on the development of subaqueous fine-gravel dunes from a lower-stage plane bed, *J. Geophys. Res., Earth Surface*, 110(F4), F04S05, doi:10.1029/2004JF000205.
- Carniello, L., A. Defina, and L. D'Alpaos (2012), Modeling sand-mud transport induced by tidal currents and wind waves in shallow microtidal basins: Application to the Venice Lagoon (Italy), *Estuarine Coastal Shelf Sci.*, 102, 105–115, doi:10.1016/j.ecss.2012.03.016.
- Carraro, F., D. Vanzo, V. Caleffi, A. Valiani, and A. Siviglia (2018), Mathematical study of linear morphodynamic acceleration and derivation of the MASSPEED approach, *Adv. Water Resour.*, 117, 40–52, doi:10.1016/j.advwatres.2018.05.002.
- Carson, R. (1951), *The Sea Around Us*, 250 pp., Oxford University Press, Cambridge, United Kingdom.
- Carver, M. B., and H. W. Hinds (1978), The method of lines and the advective equation, *Simulation*, 31(2), 59–69, doi:10.1177/003754977803100205.
- Castro, M. J., E. D. Fernández-Nieto, A. M. Ferreiro, J. A. García-Rodríguez, and C. Parés (2009), High order extensions of Roe schemes for two-dimensional nonconservative hyperbolic systems, *J. Sci. Comput.*, 39(1), 67–114, doi:10.1007/s10915-008-9250-4.

- Castro Díaz, M. J., E. D. Fernández Nieto, J. M. González Vida, and C. Parés Madroñal (2011), Numerical treatment of the loss of hyperbolicity of the two-layer shallow-water system, *J. Sci. Comput.*, 48(1-3), 16–40, doi:10.1007/s10915-010-9427-5.
- Charru, F. (2006), Selection of the ripple length on a granular bed sheared by a liquid flow, *Phys. Fluids*, 18, 121508, doi:10.1063/1.2397005.
- Charru, F., and E. J. Hinch (2006), Ripple formation on a particle bed sheared by a viscous liquid. Part 1. Steady flow, *J. Fluid Mech.*, 550, 111–121, doi:10.1017/S002211200500786X.
- Charru, F., H. Mouilleron, and O. Eiff (2004), Erosion and deposition of particles on a bed sheared by a viscous flow, *J. Fluid Mech.*, 519, 55–80, doi:10.1017/S0022112004001028.
- Chavarrías, V., G. Stecca, and A. Blom (2018a), Ill-posedness in modelling mixed-sediment river morphodynamics, *Adv. Water Resour.*, 114, 219–235, doi:10.1016/j.advwatres.2018.02.011.
- Chavarrías, V., W. Ottevanger, R. Schielen, and A. Blom (2018b), Ill-posedness in 2D mixed sediment river morphodynamics, *Tech. Rep. RWS 4500268550, TUD 17363*, Delft University of Technology, Delft, the Netherlands.
- Chavarrías, V., G. Stecca, A. Siviglia, and A. Blom (2019a), A regularization strategy for modeling mixed-sediment river morphodynamics, *Adv. Water Resour.*, 127, 291–309, doi:10.1016/j.advwatres.2019.04.001.
- Chavarrías, V., R. Schielen, W. Ottevanger, and A. Blom (2019b), Ill posedness in modelling two-dimensional morphodynamic problems: Effects of bed slope and secondary flow, *J. Fluid Mech.*, 868, 461–500, doi:10.1017/jfm.2019.166.
- Chen, S.-C., and S.-H. Peng (2006), Two-dimensional numerical model of two-layer shallow water equations for confluence simulation, *Adv. Water Resour.*, 29(11), 1608–1617, doi:10.1016/j.advwatres.2005.12.001.
- Chen, S.-C., S.-H. Peng, and H. Capart (2007), Two-layer shallow water computation of mud flow intrusions into quiescent water, *J. Hydraul. Res.*, 45(1), 13–25, doi:10.1080/00221686.2007.9521739.
- Chen, S.-H. (2015), *Hydraulic Structures*, 1029 pp., Springer-Verlag Berlin-Heidelberg, Heidelberg, Germany, doi:10.1007/978-3-662-47331-3.
- Cho, A. (2012), Higgs boson makes its debut after decades-long search, *Science*, 337(6091), 141–143, doi:10.1126/science.337.6091.141.
- Choi, Y.-H., and C. Merkle (1993), The application of preconditioning in viscous flows, *J. Comput. Phys.*, 105(2), 207–223, doi:10.1006/jcph.1993.1069.
- Chorin, A. J. (1967), A numerical method for solving incompressible viscous flow problems, *J. Comput. Phys.*, 2(1), 12–26, doi:10.1016/0021-9991(67)90037-X.

- Chow, V. T. (1959), *Open-Channel Hydraulics*, 680 pp., McGraw-Hill, New York, NY, United States.
- Church, M. (2013), Steep headwater channels, in *Treatise on Geomorphology, Fluvial Geomorphology*, vol. 9, edited by J. Shroder and E. Wohl, pp. 528–549, Academic Press, San Diego, CA, United States.
- Church, M. (2015), Channel stability: Morphodynamics and the morphology of rivers, in *Rivers - physical, fluvial and environmental processes*, edited by A. Radecki-Pawlik and P. Rowiński, chap. 12, pp. 281–321, Springer, Switzerland, doi:10.1007/978-3-319-17719-9_12.
- Church, M., and J. K. Haschenburger (2017), What is the “active layer”?, *Water Resour. Res.*, 53(1), 5–10, doi:10.1002/2016WR019675.
- Colombini, M. (1993), Turbulence-driven secondary flows and formation of sand ridges, *J. Fluid Mech.*, 254, 701–719, doi:10.1017/S0022112093002319.
- Colombini, M. (2004), Revisiting the linear theory of sand dune formation, *J. Fluid Mech.*, 502, 1–16, doi:10.1017/S0022112003007201.
- Colombini, M., and A. Stocchino (2005), Coupling or decoupling bed and flow dynamics: Fast and slow sediment waves at high froude numbers, *Phys. Fluids*, 17(3), 036602, doi:10.1063/1.1848731.
- Colombini, M., and A. Stocchino (2008), Finite-amplitude river dunes, *J. Fluid Mech.*, 611, 283–306, doi:10.1017/S0022112008002814.
- Colombini, M., and A. Stocchino (2011), Ripple and dune formation in rivers, *J. Fluid Mech.*, 673, 121–131, doi:10.1017/S0022112011000048.
- Colombini, M., and A. Stocchino (2012), Three-dimensional river bed forms, *J. Fluid Mech.*, 695, 63–80, doi:10.1017/jfm.2011.556.
- Colombini, M., G. Seminara, and M. Tubino (1987), Finite-amplitude alternate bars, *J. Fluid Mech.*, 181, 213–232, doi:10.1017/S0022112087002064.
- Copernicus, N. (1543), *De revolutionibus orbium coelestium*, 405 pp., Johannes Petreius, Nuremberg, Holy Roman Empire, (in Latin).
- Cordier, S., M. Le, and T. M. de Luna (2011), Bedload transport in shallow water models: Why splitting (may) fail, how hyperbolicity (can) help, *Adv. Water Resour.*, 34(8), 980–989, doi:10.1016/j.advwatres.2011.05.002.
- Corenblit, D., A. Baas, T. Balke, T. Bouma, F. Fromard, V. Garófano-Gómez, E. González, A. M. Gurnell, B. Hortobágyi, F. Julien, D. Kim, L. Lambs, J. A. Stallins, J. Steiger, E. Tabacchi, and R. Walcker (2015), Engineer pioneer plants respond to and affect geomorphic constraints similarly along water-terrestrial interfaces world-wide, *Global Ecol. Biogeogr.*, 24(12), 1363–1376, doi:10.1111/geb.12373.

- Correia, L. R. P., B. G. Krishnappan, and W. H. Graf (1992), Fully coupled unsteady mobile boundary flow model, *J. Hydraul. Eng.*, 118(3), 476–494, doi:10.1061/(ASCE)0733-9429(1992)118:3(476).
- Courant, R., and D. Hilbert (1989), *Methods of Mathematical Physics, Volume 2: Differential Equations*, 852 pp., John Wiley & Sons, New York, NY, United States.
- Courant, R., K. Friedrichs, and H. Lewy (1928), Über die partiellen Differenzgleichungen der mathematischen Physik, *Mathematische Annalen*, 100, 32–74, (in German).
- Crank, J., and P. Nicolson (1947), A practical method for numerical evaluation of solutions of partial differential equations of the heat-conduction type, *Proc. Camb. Phil. Soc.*, 43, 50–67.
- Crickmore, M. J., and G. H. Lean (1962a), The measurement of sand transport by means of radioactive tracers, *Proc. Roy. Soc. London Serie A*, 266(1326), 402–421, doi:10.1098/rspa.1962.0069.
- Crickmore, M. J., and G. H. Lean (1962b), The measurement of sand transport by the time-integration method with radioactive tracers, *Proc. Roy. Soc. London Serie A*, 270(1340), 27–47.
- Cui, Y., G. Parker, J. Pizzuto, and T. E. Lisle (2003), Sediment pulses in mountain rivers: 2. Comparison between experiments and numerical predictions, *Water Resour. Res.*, 39(9), 1240, doi:10.1029/2002WR001805.
- Cunge, J. A., and W. H. Hager (2015), Alexandre Preissmann: His scheme and his career, *J. Hydraul. Res.*, 53(4), 413–422, doi:10.1080/00221686.2015.1076894.
- Dade, W. B., and P. F. Friend (1998), Grain-size, sediment-transport regime, and channel slope in alluvial rivers, *J. Geol.*, 106(6), 661–676, doi:10.1086/516052.
- Dafermos, C. M. (2010), *Hyperbolic Conservation Laws in Continuum Physics*, no. 325 in *Grundlehren der mathematischen Wissenschaften*, 3 ed., 708 pp., Springer-Verlag Berlin-Heidelberg, Heidelberg, Germany.
- Dafermos, C. M. (2016), Introduction to the theory of hyperbolic conservation laws, in *Handbook of Numerical Methods for Hyperbolic Problems, Handbook of Numerical Analysis*, vol. 17, edited by R. Abgrall and C.-W. Shu, chap. 1, pp. 1–18, Elsevier, Amsterdam, the Netherlands, doi:10.1016/bs.hna.2016.08.003.
- Deigaard, R., and J. Fredsøe (1978), Longitudinal grain sorting by current in alluvial streams, *Nord. Hydrol.*, 9(1), 7–16, doi:10.2166/nh.1978.002.
- Devaney, R. L. (1989), *An Introduction to Chaotic Dynamical Systems*, 336 pp., Addison-Wesley, Boston, MA, United States.
- Dey, S. (1999), Sediment threshold, *Appl. Math. Modell.*, 23(5), 399–417, doi:10.1016/S0307-904X(98)10081-1.

- Dhamotharan, S., A. Wood, G. Parker, and H. Stefan (1980), Bedload transport in a model gravel stream, *Tech. Rep. 190*, St. Anthony Falls Hydraulic Laboratory, University of Minnesota, Minneapolis, MN, United States, 71 pp.
- Dietrich, W. E., and J. D. Smith (1984), Bed load transport in a river meander, *Water Resour. Res.*, 20(10), 1355–1380, doi:10.1029/WR020i010p01355.
- Dietrich, W. E., J. W. Kirchner, H. Ikeda, and F. Iseya (1989), Sediment supply and the development of the coarse surface layer in gravel-bedded rivers, *Nature*, 340, 215–217, doi:10.1038/340215a0.
- Disco, C., and J. van den Ende (2003), “Strong, invincible arguments”? Tidal models as management instruments in twentieth-century Dutch coastal engineering, *Technology and Culture*, 44(3), 502–535, doi:10.1353/tech.2003.0108.
- Disco, N., and B. Toussaint (2014), From projects to systems: the emergence of a national hydraulic technocracy, 1900–1970, in *Two Centuries of Experience in Water Resources Management. A Dutch-U.S. Retrospective*, edited by J. Lonnquest, B. Toussaint, J. Joe Manous, and M. Ertsen, chap. 6, pp. 155–204, Institute for Water Resources, U.S. Army Corps of Engineers and Rijkswaterstaat, Ministry of Infrastructure and the Environment.
- Drake, T. G., R. L. Shreve, W. E. Dietrich, P. J. Whiting, and L. B. Leopold (1988), Bedload transport of fine gravel observed by motion-picture photography, *J. Fluid Mech.*, 192, 193–217, doi:10.1017/S0022112088001831.
- Drew, D., L. Cheng, and R. Lahey (1979), The analysis of virtual mass effects in two-phase flow, *Int. J. Multiphase Flow*, 5(4), 233–242, doi:10.1016/0301-9322(79)90023-5.
- Egashira, S., and K. Ashida (1992), Unified view of the mechanics of debris flow and bed-load, in *Advances in Micromechanics of Granular Materials, Studies in Applied Mechanics*, vol. 31, edited by H. H. Shen, M. Satake, M. Mehrabadi, C. S. Chang, and C. S. Campbell, pp. 391–400, Elsevier, Amsterdam, the Netherlands, doi:10.1016/B978-0-444-89213-3.50046-8.
- Egiazaroff, I. V. (1965), Calculation of nonuniform sediment concentrations, *J. Hydraulics Div.*, 91(4), 225–247.
- Einstein, A. (1905), Über die von der molekularkinetischen Theorie der Wärme geforderte Bewegung von in ruhenden Flüssigkeiten suspendierten Teilchen, *Ann. Phys.*, 322(8), 549–560, doi:10.1002/andp.19053220806, (in German).
- Einstein, H. A. (1936), Der Geschiebetrieb als Wahrscheinlichkeitsproblem, Ph.D. thesis, Eidgenössische Technische Hochschule Zürich, Zürich, Switzerland, doi:10.3929/ethz-a-000092036, (in German).
- Einstein, H. A. (1950), The bed-load function for sediment transportation in open channel flows, *Tech. Bull. 1026*, US Department of Agriculture, Soil Conservation Service, Washington, DC, United States, 70 pp.

- Einstein, H. A., and H. Li (1958), Secondary currents in straight channels, *EOS, Trans. Am. Geophys. Union*, 39(6), 1085–1088, doi:10.1029/TR039i06p01085.
- Elder, J. W. (1959), The dispersion of marked fluid in turbulent shear flow, *J. Fluid Mech.*, 5(4), 544–560, doi:10.1017/S0022112059000374.
- van den Ende, J. (1992), Tidal calculations in the Netherlands, *IEEE Annals Hist. Comput.*, 14(3), 23–33.
- Engelund, F. (1974), Flow and bed topography in channel bends, *J. Hydraulics Div.*, 100(11), 1631–1648.
- Engelund, F. (1975), Instability of flow in a curved alluvial channel, *J. Fluid Mech.*, 72(1), 145–160, doi:10.1017/S002211207500300X.
- Engelund, F., and E. Hansen (1967), Monograph on sediment transport in alluvial streams, *Tech. Rep.*, Hydraulics Laboratory, Technical University of Denmark, Copenhagen, Denmark, 63 pp.
- Engelund, F., and O. Skovgaard (1973), On the origin of meandering and braiding in alluvial streams, *J. Fluid Mech.*, 57(2), 289–302, doi:10.1017/S0022112073001163.
- Englert, F., and R. Brout (1964), Broken symmetry and the mass of gauge vector mesons, *Phys. Rev. Lett.*, 13, 321–323, doi:10.1103/PhysRevLett.13.321.
- Erdogan, M. E., and P. C. Chatwin (1967), The effects of curvature and buoyancy on the laminar dispersion of solute in a horizontal tube, *J. Fluid Mech.*, 29(3), 465–484, doi:10.1017/S0022112067000977.
- Esfahanian, V., H. M. Darian, and S. M. I. Gohari (2013), Assessment of WENO schemes for numerical simulation of some hyperbolic equations using GPU, *Comput. Fluids*, 80, 260–268, doi:10.1016/j.compfluid.2012.02.031.
- Exner, F. M. (1920), Zur Physik der Dünen, *Akad. Wiss. Wien Math. Naturwiss.*, 129(2a), 929–952, (in German).
- Falconer, R. A. (1980), Modelling of planform influence on circulation in harbours, in *Proc. 17th Int. Conference on Coastal Eng., 23-28 March, Sydney, Australia*, pp. 2726–2744, doi:10.1061/9780872622647.164.
- Fan, N., A. Singh, M. Guala, E. Foufoula-Georgiou, and B. Wu (2016), Exploring a semimechanistic episodic Langevin model for bed load transport: Emergence of normal and anomalous advection and diffusion regimes, *Water Resour. Res.*, 52(4), 2789–2801, doi:10.1002/2015WR018023.
- Fan, N., Y. Xie, and R. Nie (2017), Bed load transport for a mixture of particle sizes: Downstream sorting rather than anomalous diffusion, *J. Hydrol.*, 553, 26–34, doi:10.1016/j.jhydrol.2017.07.012.
- Fargue, L. (1894), Expériences relatives à l'action de l'eau courante sur un fond de sable, *Annales des Pont et Chaussées*, 64, 427–466, (in French).

- Fathel, S. L., D. J. Furbish, and M. W. Schmeeckle (2015), Experimental evidence of statistical ensemble behavior in bed load sediment transport, *J. Geophys. Res., Earth Surface*, 120(11), 2298–2317, doi:10.1002/2015JF003552.
- Feng, J., and C. Merkle (1990), Evaluation of preconditioning methods for time-marching systems, *Tech. Rep. 90-0016*, AIAA, Washington, DC, United States, 10 pp., doi:10.2514/6.1990-16.
- Ferguson, R. (2007), Flow resistance equations for gravel- and boulder-bed streams, *Water Resources Research*, 43(5), W05427, doi:10.1029/2006WR005422.
- Ferguson, R. I., D. J. Bloomer, T. B. Hoey, and A. Werritty (2002), Mobility of river tracer pebbles over different timescales, *Water Resour. Res.*, 38(5), 1045, doi:10.1029/2001WR000254.
- Ferguson, R. I., M. Church, C. D. Rennie, and J. G. Venditti (2015), Reconstructing a sediment pulse: Modeling the effect of placer mining on Fraser River, Canada, *J. Geophys. Res., Earth Surface*, 120(7), 1436–1454, doi:10.1002/2015JF003491.
- Fernandez-Luque, R., and R. van Beek (1976), Erosion and transport of bed-load sediment, *J. Hydraul. Res.*, 14(2), 127–144, doi:10.1080/00221687609499677.
- Fernández Nieto, E. D. (2003), Aproximación numérica de leyes de conservación hiperbólicas no homogéneas. Aplicación a las ecuaciones de aguas someras., Ph.D. thesis, University of Sevilla, Sevilla, Spain, (in Spanish).
- Fischer, H. B. (1967), The mechanics of dispersion in natural streams, *J. Hydraulics Div.*, 96(6), 187–216.
- Fischer, H. B. (1969), The effect of bends on dispersion in streams, *Water Resour. Res.*, 5(2), 496–506, doi:10.1029/WR005i002p00496.
- Fischer, H. B. (1973), Longitudinal dispersion and turbulent mixing in open-channel flow, *Annu. Rev. Fluid Mech.*, 5(1), 59–78, doi:10.1146/annurev.fl.05.010173.000423.
- Flokstra, C. (1977), The closure problem for depth-averaged 2-D flow, in *Proc. 18th IAHR World Congress, 15–19 August, Baden-Baden, Germany*, p. 580.
- Fowler, A. C. (1997), *Mathematical Models in the Applied Sciences*, Cambridge Texts in Applied Mathematics, 424 pp., Cambridge University Press, Cambridge, United Kingdom.
- Francalanci, S., and L. Solari (2007), Gravitational effects on bed load transport at low Shields stress: Experimental observations, *Water Resour. Res.*, 43(3), W03424, doi:10.1029/2005WR004715.
- Francalanci, S., and L. Solari (2008), Bed-load transport equation on arbitrarily sloping beds, *J. Hydraul. Eng.*, 134(1), 110–115, doi:10.1061/(ASCE)0733-9429(2008)134:1(110).
- Fredsøe, J. (1978), Meandering and braiding of rivers, *J. Fluid Mech.*, 84(4), 609–624, doi:10.1017/S0022112078000373.

- Frings, R., K. Banhold, and I. Evers (2015), Sedimentbilanz des Oberen Rheindeltas für den Zeitraum 1991-2010, *Tech. Rep. 2015.019*, Institut für Wasserbau und Wasserwirtschaft, RWTH Aachen, Aachen, Deutschland, (in German).
- Furbish, D. J., and M. W. Schmeeckle (2013), A probabilistic derivation of the exponential-like distribution of bed load particle velocities, *Water Resour. Res.*, *49*(3), 1537–1551, doi:10.1002/wrcr.20074.
- Furbish, D. J., P. K. Haff, J. C. Roseberry, and M. W. Schmeeckle (2012a), A probabilistic description of the bed load sediment flux: 1. Theory, *J. Geophys. Res., Earth Surface*, *117*(F3), F03031, doi:10.1029/2012JF002352.
- Furbish, D. J., A. E. Ball, and M. W. Schmeeckle (2012b), A probabilistic description of the bed load sediment flux: 4. Fickian diffusion at low transport rates, *J. Geophys. Res., Earth Surface*, *117*(F3), F03034, doi:10.1029/2012JF002356.
- Furbish, D. J., J. C. Roseberry, and M. W. Schmeeckle (2012c), A probabilistic description of the bed load sediment flux: 3. The particle velocity distribution and the diffusive flux, *J. Geophys. Res., Earth Surface*, *117*(F3), F03033, doi:10.1029/2012JF002355.
- Furbish, D. J., S. L. Fathel, M. W. Schmeeckle, D. J. Jerolmack, and R. Schumer (2017), The elements and richness of particle diffusion during sediment transport at small timescales, *Earth Surf. Process. Landf.*, *42*(1), 214–237, doi:10.1002/esp.4084.
- Gad, A. (2008), Water culture in Egypt, in *Water culture and water conflict in the Mediterranean area*, edited by M. El Moujabber, M. Shatanawi, G. Trisorio-Liuzzi, M. Ouessar, P. Laureano, and R. Rodríguez, no. A 83 in *Options Méditerranéennes*, pp. 85–96, CIHEAM.
- Galvin, C. J. (1965), Discussion: Sand transport studies with radioactive tracers, by D. W. Hubbell and W. W. Sayre, *J. Hydraulics Div.*, *91*, 173–178.
- Ganti, V., M. M. Meerschaert, E. Foufoula-Georgiou, E. Viparelli, and G. Parker (2010), Normal and anomalous diffusion of gravel tracer particles in rivers, *J. Geophys. Res., Earth Surface*, *115*(F2), F00A12, doi:10.1029/2008JF001222.
- Garegnani, G., G. Rosatti, and L. Bonaventura (2011), Free surface flows over mobile bed: Mathematical analysis and numerical modeling of coupled and decoupled approaches, *Commun. Appl. Ind. Math.*, *2*(1), e371, doi:10.1685/journal.caim.371.
- Garegnani, G., G. Rosatti, and L. Bonaventura (2013), On the range of validity of the Exner-based models for mobile-bed river flow simulations, *J. Hydraul. Res.*, *51*(4), 380–391, doi:10.1080/00221686.2013.791647.
- Gavrilakis, S. (1992), Numerical simulation of low-Reynolds-number turbulent flow through a straight square duct, *J. Fluid Mech.*, *244*, 101–129, doi:10.1017/S0022112092002982.
- Gessner, F. B., and J. B. Jones (1965), On some aspects of fully-developed turbulent flow in rectangular channels, *J. Fluid Mech.*, *23*(4), 689–713, doi:10.1017/S0022112065001635.

- Gibbs, J. W. (1898), Fourier's series, *Nature*, 59(1522), 200, doi:10.1038/059200bo.
- Gibbs, J. W. (1899), Fourier's series, *Nature*, 59(1539), 606, doi:10.1038/059606ao.
- Gill, M. A. (1971), Height of sand dunes in open channel flows, *J. Hydraulics Div.*, 97(12), 2067–2074.
- Giri, S., and Y. Shimizu (2006), Numerical computation of sand dune migration with free surface flow, *Water Resour. Res.*, 42(10), W10422, doi:10.1029/2005WR004588.
- Godfrey, A. G., R. W. Walters, and B. van Leer (1993), Preconditioning for the Navier-Stokes equations with finite-rate chemistry, *Tech. Rep. 1993-535*, AIAA, Washington, DC, United States, 23 pp.
- Godunov, S. K. (1959), A difference method for numerical calculation of discontinuous solutions of the equations of hydrodynamics, *Mat. Sb.*, 47(89), 271–306, (in Russian).
- Godunov, S. K. (1999), Reminiscences about difference schemes, *J. Comput. Phys.*, 153, 6–25.
- Grabowski, W. J., and S. A. Berger (1976), Solutions of the Navier-Stokes equations for vortex breakdown, *J. Fluid Mech.*, 75(3), 525–544, doi:10.1017/S0022112076000360.
- Gray, J. M. N. T., and C. Ancey (2011), Multi-component particle-size segregation in shallow granular avalanches, *J. Fluid Mech.*, 678, 535–588, doi:10.1017/jfm.2011.138.
- Greco, M., M. Iervolino, and A. Vacca (2008), Boundary conditions in a two-layer geomorphological model: Application to a hydraulic jump over a mobile bed, *J. Hydraul. Res.*, 46(6), 856–860, doi:10.1080/00221686.2008.9521933.
- Greco, M., M. Iervolino, A. Leopardi, and A. Vacca (2012), A two-phase model for fast geomorphic shallow flows, *Int. J. Sediment Res.*, 27(4), 409–425, doi:10.1016/S1001-6279(13)60001-3.
- Guo, J. (2015), Sidewall and non-uniformity corrections for flume experiments, *J. Hydraul. Res.*, 53(2), 218–229, doi:10.1080/00221686.2014.971449.
- Guralnik, G. S., C. R. Hagen, and T. W. B. Kibble (1964), Global conservation laws and massless particles, *Phys. Rev. Lett.*, 13, 585–587, doi:10.1103/PhysRevLett.13.585.
- Haberman, R. (2004), *Applied Partial Differential Equations*, 4 ed., 769 pp., Pearson Prentice Hall, Upper Saddle River, NJ, United States.
- Habersack, H. M. (2001), Radio-tracking gravel particles in a large braided river in New Zealand: A field test of the stochastic theory of bed load transport proposed by Einstein, *Hydrol. Process.*, 15(3), 377–391, doi:10.1002/hyp.147.
- Hadamard, J. S. (1923), *Lectures on Cauchy's problem in linear partial differential equations*, 316 pp., Yale University Press, New Haven, CT, United States.

- Hager, W. H. (2003), Fargue, founder of experimental river engineering, *J. Hydraul. Res.*, 41(3), 227–233, doi:10.1080/00221680309499967.
- Hall, A. R. (1954), *The Scientific Revolution 1500–1800. The Formation of the Modern Scientific Attitude.*, 390 pp., Longmans, London, United Kingdom.
- Hamming, R. (1962), *Numerical Methods for Scientists and Engineers*, McGraw-Hill, New York, NY, United States.
- Haque, M. I., and K. Mahmood (1983), Analytical determination of form friction factor, *J. Hydraul. Eng.*, 109(4), 590–610, doi:10.1061/(ASCE)0733-9429(1983)109:4(590).
- Harari, Y. N. (2016), *Homo deus: A brief history of tomorrow*, 440 pp., Harvill Secker, London, United Kingdom.
- Harlow, F. H., and A. A. Amsden (1975), Numerical calculation of multiphase fluid flow, *J. Comput. Phys.*, 17(1), 19–52, doi:10.1016/0021-9991(75)90061-3.
- Harten, A. (1983), High resolution schemes for hyperbolic conservation laws, *J. Comput. Phys.*, 49(3), 357–393, doi:10.1016/0021-9991(83)90136-5.
- Harten, A. (1984), On a class of high resolution total-variation-stable finite-difference schemes, *SIAM J. Numer. Anal.*, 21(1), 1–23, doi:10.1137/0721001.
- Harten, A., P. D. Lax, and B. van Leer (1983), On upstream differencing and Godunov-type schemes for hyperbolic conservation laws, *SIAM Rev.*, 25(1), 35–61, doi:10.1137/1025002.
- Haschenburger, J. (2013), Tracing river gravels: Insights into dispersion from a long-term field experiment, *Geomorphology*, 200, 121–131, doi:10.1016/j.geomorph.2013.03.033.
- Haschenburger, J. K. (2011), The rate of fluvial gravel dispersion, *Geophys. Res. Lett.*, 38(24), L24403, doi:10.1029/2011GL049928.
- Hass, R. (2000), *What Light Can Do: Essays on Art, Imagination, and the Natural World*, 496 pp., Ecco, New York, NY, United States.
- Hassan, M. A., and M. Church (1994), Vertical mixing of coarse particles in gravel bed rivers: A kinematic model, *Water Resour. Res.*, 30(4), 1173–1185, doi:10.1029/93WR03351.
- Hassan, M. A., M. Church, and A. P. Schick (1991), Distance of movement of coarse particles in gravel bed streams, *Water Resour. Res.*, 27(4), 503–511, doi:10.1029/90WR02762.
- Hassan, M. A., A. P. Schick, and P. A. Shaw (1999), The transport of gravel in an ephemeral sandbed river, *Earth Surf. Process. Landf.*, 24(7), 623–640, doi:10.1002/(SICI)1096-9837(199907)24:7 < 623::AID-ESP978 > 3.0.CO;2-2.
- Havlin, S., and D. Ben-Avraham (1987), Diffusion in disordered media, *Adv. Phys.*, 36(6), 695–798, doi:10.1080/00018738700101072.

- Heller, V. (2011), Scale effects in physical hydraulic engineering models, *J. Hydraul. Res.*, 49(3), 293–306, doi:10.1080/00221686.2011.578914.
- von Helmholtz, H. (1868), Über discontinuierliche Flüssigkeits-Bewegungen, *Monatsberichte der Königlich Preussische Akademie der Wissenschaften zu Berlin*, 23, 215–228, (in German).
- Hewitt, E., and R. E. Hewitt (1979), The Gibbs-Wilbraham phenomenon: An episode in Fourier analysis, *Arch. Hist. Exact Sci.*, 21(2), 129–160, doi:10.1007/BF00330404.
- Heyman, J., P. Bohorquez, and C. Ancey (2016), Entrainment, motion, and deposition of coarse particles transported by water over a sloping mobile bed, *J. Geophys. Res., Earth Surface*, 121(10), 1931–1952, doi:10.1002/2015JF003672.
- Higgs, P. W. (1964), Broken symmetries and the masses of gauge bosons, *Phys. Rev. Lett.*, 13, 508–509, doi:10.1103/PhysRevLett.13.508.
- Hill, K. M., L. DellAngelo, and M. M. Meerschaert (2010), Heavy-tailed travel distance in gravel bed transport: An exploratory enquiry, *J. Geophys. Res., Earth Surface*, 115(F2), F00A14, doi:10.1029/2009JF001276.
- Hirano, M. (1971), River bed degradation with armoring, *Proc. Jpn. Soc. Civ. Eng.*, 195, 55–65, doi:10.2208/jscej1969.1971.195_55.
- Hoey, T. B., and R. I. Ferguson (1994), Numerical simulation of downstream fining by selective transport in gravel bed rivers: Model development and illustration, *Water Resour. Res.*, 30(7), 2251–2260, doi:10.1029/94WR00556.
- Holley, E. R. (1971), Transverse mixing in rivers, *Tech. Rep. S132*, Delft Hydraulics Laboratory, Delft, the Netherlands, 96 pp.
- van Houweninge, G., and A. de Graauw (1982), The closure of tidal basins, *Coastal Eng.*, 6(4), 331 – 360, doi:10.1016/0378-3839(82)90006-0.
- Hovda, S. (2017), Gibbs-like phenomenon inherent in a lumped element model of a rod, *Adv. Mech. Eng.*, 9(8), 1–12, doi:10.1177/1687814017713703.
- Hu, C., and Y. Hui (1996a), Bed-load transport. I: Mechanical characteristics, *J. Hydraul. Eng.*, 122(5), 245–254, doi:10.1061/(ASCE)0733-9429(1996)122:5(245).
- Hu, C., and Y. Hui (1996b), Bed-load transport. II: Stochastic characteristics, *J. Hydraul. Eng.*, 122(5), 255–261, doi:10.1061/(ASCE)0733-9429(1996)122:5(255).
- Ikeda, H., and F. Iseya (1986), Longitudinal sorting process in heterogeneous sediment transportation, *Proc. 30th Japanese Conference on Hydraulics*, 30, 217–222, doi:10.2208/prohe1975.30.217, (in Japanese).
- Ikeda, S., and T. Nishimura (1985), Bed topography in bends of sand-silt rivers, *J. Hydraul. Eng.*, 111(11), 1397–1410, doi:10.1061/(ASCE)0733-9429(1985)111:11(1397).

- Ikeda, S., and T. Nishimura (1986), Flow and bed profile in meandering sand-silt rivers, *J. Hydraul. Eng.*, 112(7), 562–579, doi:10.1061/(ASCE)0733-9429(1986)112:7(562).
- Ikeda, S., G. Parker, and K. Sawai (1981), Bend theory of river meanders. Part 1. Linear development, *J. Fluid Mech.*, 112, 363–377, doi:10.1017/S0022112081000451.
- Isaacson, E., and B. Temple (1992), Nonlinear resonance in systems of conservation laws, *SIAM J. Appl. Math.*, 52(5), 1260–1278, doi:10.1137/0152073.
- Isaacson, E., J. J. Stoker, and A. Troesch (1954), Numerical solution of flood prediction and river regulation problems, *Tech. Rep. II IMN-NYU 205*, New York University Institute for Mathematics and Mechanics, New York, NY, United States, 47 pp.
- Iseya, F., and H. Ikeda (1987), Pulsations in bedload transport rates induced by a longitudinal sediment sorting: A flume study using sand and gravel mixtures, *Geografiska Annaler: Series A, Physical Geography*, 69(1), 15–27, doi:10.1080/04353676.1987.11880193.
- Ivrii, V. Y., and V. M. Petkov (1974), Necessary conditions for the Cauchy problem for non-strictly hyperbolic equations to be well-posed, *Russ. Math. Surv.*, 29(5), 1–70.
- Iwasaki, T., J. Nelson, Y. Shimizu, and G. Parker (2017), Numerical simulation of large-scale bed load particle tracer advection-dispersion in rivers with free bars, *J. Geophys. Res., Earth Surface*, 122(4), 847–874, doi:10.1002/2016JF003951, 2016JF003951.
- Jagers, B. (2003), Modelling planform changes of braided rivers, Ph.D. thesis, University of Twente, Enschede, the Netherlands.
- Jain, S. C. (1992), Note on lag in bedload discharge, *J. Hydraul. Eng.*, 118(6), 904–917, doi:10.1061/(ASCE)0733-9429(1992)118:6(904).
- Javernick, L., D. M. Hicks, R. Measures, B. Caruso, and J. Brasington (2016), Numerical modelling of braided rivers with structure-from-motion-derived terrain models, *River Res. Appl.*, 32(5), 1071–1081, doi:10.1002/rra.2918.
- Javernick, L., M. Redolfi, and W. Bertoldi (2018), Evaluation of a numerical model's ability to predict bed load transport observed in braided river experiments, *Adv. Water Resour.*, 115, 207–218, doi:10.1016/j.advwatres.2018.03.012.
- Jeffreys, H. (1925), The flow of water in an inclined channel of rectangular section, *The London, Edinburgh, and Dublin Philosophical Magazine and Journal of Science*, 49(293), 793–807, doi:10.1080/14786442508634662.
- Jerolmack, D. J., and D. Mohrig (2005), A unified model for subaqueous bed form dynamics, *Water Resour. Res.*, 41(12), W12421, doi:10.1029/2005WR004329.
- Jiang, G.-S., and C.-W. Shu (1996), Efficient implementation of Weighted ENO schemes, *J. Comput. Phys.*, 126(1), 202–228, doi:10.1006/jcph.1996.0130.
- Jiménez, J. (2018), Coherent structures in wall-bounded turbulence, *J. Fluid Mech.*, 842, P1, doi:10.1017/jfm.2018.144.

- Johannesson, H., and G. Parker (1989), Secondary flow in mildly sinuous channel, *J. Hydraul. Eng.*, 115(3), 289–308, doi:10.1061/(ASCE)0733-9429(1989)115:3(289).
- Johnson, J. W. (1942), The importance of considering sidewall friction in bed-load investigations, *Civil Engineering*, 12, 329–332.
- Jop, P., Y. Forterre, and O. Pouliquen (2005), Crucial role of sidewalls in granular surface flows: Consequences for the rheology, *J. Fluid Mech.*, 541, 167–192, doi:10.1017/S0022112005005987.
- Jop, P., Y. Forterre, and O. Pouliquen (2006), A constitutive law for dense granular flows, *Nature*, 441, 727–730, doi:10.1038/nature04801.
- Joseph, D., and J. Saut (1990), Short-wave instabilities and ill-posed initial-value problems, *Theor. Comput. Fluid Mech.*, 1(4), 191–227, doi:10.1007/BF00418002.
- Kabanikhin, S. I. (2008), Definitions and examples of inverse and ill-posed problems, *J. Inv. Ill-Posed Problems*, 16, 317–357, doi:10.1515/JIIP.2008.019.
- Kalinske, A. A. (1947), Movement of sediment as bed load in rivers, *EOS, Trans. Am. Geophys. Union*, 28(4), 615–620, doi:10.1029/TR028i004p00615.
- Kalkwijk, J. P. T., and R. Booij (1986), Adaptation of secondary flow in nearly-horizontal flow, *J. Hydraul. Res.*, 24(1), 19–37, doi:10.1080/00221688609499330.
- Kalkwijk, J. P. T., and H. J. de Vriend (1980), Computation of the flow in shallow river bends, *J. Hydraul. Res.*, 18(4), 327–342, doi:10.1080/00221688009499539.
- Karim, M. F., F. M. Holly, and J. F. Kennedy (1983), Bed armouring procedures in IAL-LUVIAL and application to the Missouri River, *Tech. Rep. 269*, Iowa Institute for Hydraulic Research, University of Iowa, Iowa City, IA, United States.
- Kelvin, W. T. (1871), Hydrokinetic solutions and observations, *Philos. Mag.*, 42(281), 362–377, doi:10.1080/14786447108640585.
- Kennedy, J. F. (1963), The mechanics of dunes and antidunes in erodible-bed channels, *J. Fluid Mech.*, 16(4), 521–544, doi:10.1017/S0022112063000975.
- van Kessel, T., J. Vanlede, and J. de Kok (2011a), Development of a mud transport model for the Scheldt estuary, *Cont. Shelf Res.*, 31(10, Supplement), S165–S181, doi:10.1016/j.csr.2010.12.006.
- van Kessel, T., H. Winterwerp, B. van Prooijen, M. van Ledden, and W. Borst (2011b), Modelling the seasonal dynamics of SPM with a simple algorithm for the buffering of fines in a sandy seabed, *Cont. Shelf Res.*, 31(10, Supplement), S124–S134, doi:10.1016/j.csr.2010.04.008.
- Kitanidis, P. K., and J. F. Kennedy (1984), Secondary current and river-meander formation, *J. Fluid Mech.*, 144, 217–229, doi:10.1017/S0022112084001580.

- Kleinhans, M., A. Wilbers, A. de Swaaf, and J. van den Berg (2002), Sediment supply-limited bedforms in sand-gravel bed rivers, *J. Sediment. Res.*, 72(5), 629–640, doi:10.1306/030702720629.
- Knowles, J. K., and E. Sternberg (1975), On the ellipticity of the equations of nonlinear elastostatics for a special material, *J. Elast.*, 5(3), 341–361, doi:10.1007/BF00126996.
- Knowles, J. K., and E. Sternberg (1976), On the failure of ellipticity of the equations for finite elastostatic plane strain, *Arch. Ration. Mech. Anal.*, 63(4), 321–336, doi:10.1007/BF00279991.
- Koch, F. G., and C. Flokstra (1981), Bed level computations for curved alluvial channels, in *Proc. 19th IAHR World Congress, 2–7 February, New Delhi, India*.
- Komar, P. D. (1987a), Selective gravel entrainment and the empirical evaluation of flow competence, *Sedimentology*, 34(6), 1165–1176, doi:10.1111/j.1365-3091.1987.tb00599.x.
- Komar, P. D. (1987b), Selective grain entrainment by a current from a bed of mixed sizes: A reanalysis, *J. Sediment. Petrol.*, 57(2), 203–211.
- Kuhnle, R. A. (1993), Incipient motion of sand-gravel sediment mixtures, *J. Hydraul. Eng.*, 119(12), 1400–1415, doi:10.1061/(ASCE)0733-9429(1993)119:12(1400).
- Kuhnle, R. A., and J. B. Southard (1988), Bed load transport fluctuations in a gravel bed laboratory channel, *Water Resour. Res.*, 24(2), 247–260, doi:10.1029/WR024i002p00247.
- Kumbaro, A., and M. Ndjinga (2011), Influence of interfacial pressure term on the hyperbolicity of a general multifluid model, *J. Comput. Multiphase Flows*, 3(3), 177–195, doi:10.1260/1757-482X.3.3.177.
- Kutta, W. (1901), Beitrag zur näherungsweise Integration totaler Differentialgleichungen, *Z. Math. Phys.*, 46, 435–453, (in German).
- Kyong, O. B., and W. S. Il (2016), On the methods for determining the transverse dispersion coefficient in river mixing, *Adv. Water Resour.*, 90, 1–9, doi:10.1016/j.advwatres.2016.01.009.
- Lajeunesse, E., L. Malverti, and F. Charru (2010), Bed load transport in turbulent flow at the grain scale: Experiments and modeling, *J. Geophys. Res., Earth Surface*, 115(F4), F04001, doi:10.1029/2009JF001628.
- Lajeunesse, E., O. Devauchelle, M. Houssais, and G. Seizilles (2013), Tracer dispersion in bedload transport, *Adv. Geosci.*, 37, 1–6, doi:10.5194/adgeo-37-1-2013.
- Lajeunesse, E., O. Devauchelle, F. Lachaussée, and P. Claudin (2017), Bedload transport in laboratory rivers: The erosion-deposition model, in *Gravel-Bed Rivers: Process and Disasters*, edited by D. Tsutsumi and J. B. Laronne, chap. 15, pp. 415–438, Wiley-Blackwell, Hoboken, NJ, United States, doi:10.1002/9781118971437.ch15.

- Lajeunesse, E., O. Devauchelle, and F. James (2018), Advection and dispersion of bed load tracers, *Earth Surf. Dyn.*, 6(2), 389–399, doi:10.5194/esurf-6-389-2018.
- Lanzoni, S., and M. Tubino (1999), Grain sorting and bar instability, *J. Fluid Mech.*, 393, 149–174, doi:10.1017/S0022112099005583.
- Lanzoni, S., A. Siviglia, A. Frascati, and G. Seminara (2006), Long waves in erodible channels and morphodynamic influence, *Water Resour. Res.*, 42(6), doi:10.1029/2006WR004916.
- Laplace, P. S. (1814), *Essai philosophique sur les probabilités*, 96 pp., Courcier, Paris, France, (in French).
- Latteux, B. (1995), Techniques for long-term morphological simulation under tidal action, *Mar. Geol.*, 126(126), 129–141, doi:10.1016/0025-3227(95)00069-B.
- Lawrence, G. A. (1990), On the hydraulics of Boussinesq and non-Boussinesq two-layer flows, *J. Fluid Mech.*, 215, 457–480, doi:10.1017/S0022112090002713.
- Lax, P. D. (1957), Asymptotic solutions of oscillatory initial value problems, *Duke Math. J.*, 24(4), 627–646, doi:10.1215/S0012-7094-57-02471-7.
- Lax, P. D. (1958), Differential equations, difference equations and matrix theory, *Commun. Pure Appl. Math.*, 11(2), 175–194, doi:10.1002/cpa.3160110203.
- Lax, P. D. (1980), On the notion of hyperbolicity, *Commun. Pure Appl. Math.*, 33(3), 395–397.
- van Ledden, M. (2003), Sand-mud segregation in estuaries and tidal basins, Ph.D. thesis, Delft University of Technology, Delft, the Netherlands.
- van Ledden, M., Z.-B. Wang, H. Winterwerp, and H. de Vriend (2004a), Sand–mud morphodynamics in a short tidal basin, *Ocean Dyn.*, 54(3), 385–391, doi:10.1007/s10236-003-0050-y.
- van Ledden, M., W. G. M. van Kesteren, and J. C. Winterwerp (2004b), A conceptual framework for the erosion behaviour of sand-mud mixtures, *Cont. Shelf Res.*, 24(1), 1–11, doi:10.1016/j.csr.2003.09.002.
- Lee, H.-Y., and A. J. Odgaard (1986), Simulation of bed armoring in alluvial channels, *J. Hydraul. Eng.*, 112(9), 794–801, doi:10.1061/(ASCE)0733-9429(1986)112:9(794).
- Lee, M. M. (2006), Acheloös Peplaphoros: A lost statuette of a River God in feminine dress, *Hesperia: The Journal of the American School of Classical Studies at Athens*, 75(3), 317–325.
- van Leer, B., W.-T. Lee, and P. L. Roe (1991), Characteristic time-stepping or local preconditioning of the Euler equations, *Tech. Rep. 1991-1552*, AIAA, Washington, DC, United States, 260–282 pp.

- Legleiter, C. J., and P. C. Kyriakidis (2006), Forward and inverse transformations between Cartesian and channel-fitted coordinate systems for meandering rivers, *Math. Geol.*, 38(8), 927–958, doi:10.1007/s11004-006-9056-6.
- Lesser, G., J. Roelvink, J. van Kester, and G. Stelling (2004), Development and validation of a three-dimensional morphological model, *Coastal Eng.*, 51(8–9), 883–915, doi:10.1016/j.coastaleng.2004.07.014.
- LeVeque, R. J. (2004), *Finite Volume Methods for Hyperbolic Problems*, no. 31 in Cambridge Texts in Applied Mathematics, Cambridge University Press, Cambridge, United Kingdom, doi:10.1017/CBO9780511791253.
- Lien, H. C., T. Y. Hsieh, J. C. Yang, and K. C. Yeh (1999), Bend-flow simulation using 2D depth-averaged model, *J. Hydraul. Eng.*, 125(10), 1097–1108, doi:10.1061/(ASCE)0733-9429(1999)125:10(1097).
- Liska, R., L. Margolin, and B. Wendroff (1995), Nonhydrostatic two-layer models of incompressible flow, *Comput. Math. Appl.*, 29(9), 25–37, doi:10.1016/0898-1221(95)00035-W.
- Liu, T.-P. (1987), Nonlinear resonance for quasilinear hyperbolic equation, *J. Math. Phys.*, 28(11), 2593–2602, doi:10.1063/1.527751.
- Liu, X.-D., S. Osher, and T. Chan (1994), Weighted essentially non-oscillatory schemes, *J. Comput. Phys.*, 115(1), 200–212, doi:10.1006/jcph.1994.1187.
- Long, R. R. (1956), Long waves in a two-fluid system, *J. Meteor.*, 13(1), 70–74, doi:10.1175/1520-0469(1956)013 < 0070:LWIATF > 2.o.CO;2.
- Long, W., J. T. Kirby, and Z. Shao (2008), A numerical scheme for morphological bed level calculations, *Coastal Eng.*, 55(2), 167–180, doi:10.1016/j.coastaleng.2007.09.009.
- Lorentz, H. (1926), *Verslag van de commissie Lorentz*, Algemene Landsdrukkerij, 's-Gravenhage, the Netherlands, (in Dutch).
- Lorenz, E. N. (1963), Deterministic nonperiodic flow, *J. Atmos. Sci.*, 20(2), 130–141, doi:10.1175/1520-0469(1963)020 < 0130:DNF > 2.o.CO;2.
- Love, E., and W. Rider (2013), On the convergence of finite difference methods for PDE under temporal refinement, *Comput. Math. Appl.*, 66(1), 33–40, doi:10.1016/j.camwa.2013.04.019.
- Luu, X. L., H. Takebayashi, and S. Egashira (2004), Characteristics of sediment sorting predicted by two different exchange layer models, *Jap. Soc. Fluid Mech.*, A225, 248–249.
- Luu, X. L., S. Egashira, and H. Takebayashi (2006), A new treatment of the exchange layer thickness to evaluate sediment sorting and armoring, *J. Appl. Mech.*, 9, 1025–1030, doi:10.2208/journalam.9.1025.

- Lyczkowski, R. W., D. Gidaspow, C. W. Solbrig, and E. D. Hughes (1978), Characteristics and stability analyses of transient one-dimensional two-phase flow equations and their finite difference approximations, *Nucl. Sci. Eng.*, 66(3), 378–396, doi:10.13182/NSE78-4.
- Lyn, D. A. (1987), Unsteady sediment transport modeling, *J. Hydraul. Eng.*, 113(1), 1–15, doi:10.1061/(ASCE)0733-9429(1987)113:1(1).
- Lyn, D. A., and M. Altinakar (2002), St. Venant-Exner equations for near-critical and transcritical flows, *J. Hydraul. Eng.*, 128(6), 579–587, doi:10.1061/(ASCE)0733-9429(2002)128:6(579).
- Lyn, D. A., and P. Goodwin (1987), Stability of a general Preissmann scheme, *J. Hydraul. Eng.*, 113(1), 16–28, doi:10.1061/(ASCE)0733-9429(1987)113:1(16).
- Malmon, D., T. Dunne, and S. Reneau (2003), Stochastic theory of particle trajectories through alluvial valley floors, *J. Geol.*, 111(5), 525–542, doi:10.1086/376764.
- Martin, L. R., K. P. Purohit, and D. J. Jerolmack (2014), Sedimentary bed evolution as a mean-reverting random walk: Implications for tracer statistics, *Geophys. Res. Lett.*, 41(17), 6152–6159, doi:10.1002/2014GL060525.
- Martin, R. L., D. J. Jerolmack, and R. Schumer (2012), The physical basis for anomalous diffusion in bed load transport, *J. Geophys. Res., Earth Surface*, 117(F1), F01018, doi:10.1029/2011JF002075.
- Mays, L. W. (2010), A brief history of roman water technology, in *Ancient Water Technologies*, edited by L. W. Mays, chap. 7, pp. 115–137, Springer, Dordrecht, the Netherlands, doi:10.1007/978-90-481-8632-7_7.
- Mazure, J. P. (1963), Hydraulic research for the Zuiderzeeworks, in *Selected Aspects of Hydraulic Engineering. Liber Amicorum dedicated to Johannes Theodoor Thijsse, on occasion of his retirement as professor*, edited by A. A. van Douwen, pp. 119–150, Delft University of Technology, Delft, the Netherlands.
- Metzler, R., and J. Klafter (2000), The random walk's guide to anomalous diffusion: A fractional dynamics approach, *Phys. Rep.*, 339(1), 1–77, doi:10.1016/S0370-1573(00)00070-3.
- Meyer-Peter, E., and R. Müller (1948), Formulas for bed-load transport, in *Proc. 2nd IAHR World Congress, 6–9 June, Stockholm, Sweden*, pp. 39–64.
- Miłosz, C. (1988), *The collected poems, 1931–1987*, Ecco, New York, NY, United States.
- Misri, R. L., R. J. Garde, and K. G. R. Raju (1984), Bed load transport of coarse nonuniform sediment, *J. Hydraul. Eng.*, 110(3), 312–328, doi:10.1061/(ASCE)0733-9429(1984)110:3(312).
- Mizohata, S. (1961), Some remarks on the Cauchy problem, *J. Math. Kyoto Univ.*, 1(1), 109–127, doi:10.1215/kjm/1250525109.

- Morris, P. H., and D. J. Williams (1996), Relative celerities of mobile bed flows with finite solids concentrations, *J. Hydraul. Eng.*, 122, doi:10.1061/(ASCE)0733-9429(1996)122:6(311).
- Mosselman, E. (2005), Basic equations for sediment transport in CFD for fluvial morphodynamics, in *Computational Fluid Dynamics: Applications in Environmental Hydraulics*, edited by P. D. Bates, S. N. Lane, and R. I. Ferguson, chap. 4, pp. 71–89, John Wiley & Sons, Chichester, United Kingdom.
- Mosselman, E., and K. Sloff (2007), The importance of floods for bed topography and bed sediment composition: numerical modelling of Rhine bifurcation at Pannerden, in *Gravel-Bed Rivers VI: From Process Understanding to River Restoration, Developments in Earth Surface Processes*, vol. 11, edited by H. Habersack, H. Piégay, and M. Rinaldi, chap. 7, pp. 161–179, Elsevier, doi:https://doi.org/10.1016/S0928-2025(07)11124-X.
- Mosselman, E., K. Sloff, and S. van Vuren (2008), Different sediment mixtures at constant flow conditions can produce the same celerity of bed disturbances, in *Proceedings of the 4th International Conference on Fluvial Hydraulics (River Flow), 3-5 September, Cesme, Izmir, Turkey*, vol. 2, edited by M. Altınakar, M. A. Kokpınar, İsmail Aydın, Şevket Cokgor, and S. Kirgoz, pp. 1373–1377, Kubaba Congress Department and Travel Services, Ankara, Turkey.
- Murray, A. B. (2007), Reducing model complexity for explanation and prediction, *Geomorphology*, 90(3-4), 178–191, doi:10.1016/j.geomorph.2006.10.020.
- Murray, A. B., and C. Paola (1994), A cellular model of braided rivers, *Nature*, 371(54), 54–57, doi:10.1038/371054a0.
- Murray, A. B., and C. Paola (1997), Properties of a cellular braided-stream model, *Earth Surf. Process. Landf.*, 22(11), 1001–1025, doi:10.1002/(SICI)1096-9837(199711)22:11<1001::AID-ESP798>3.0.CO;2-O.
- Murray, J. D. (1965), On the mathematics of fluidization. Part 1. Fundamental equations and wave propagation, *J. Fluid Mech.*, 21(3), 465–493, doi:10.1017/S0022112065000277.
- Na Ranong, C., J. Hapke, and W. Roetzel (2010), Numerical calculation of the transient behaviour of two pure cross-flow heat exchangers coupled by a circulating flow stream, *Heat Mass Transfer.*, 46(10), 1069–1075, doi:10.1007/s00231-010-0681-8.
- Nakagawa, H., and T. Tsujimoto (1979), Characteristic of sediment transport process on duned beds analyzed by stochastic approach, *Bull. Disas. Prev. Res. Inst. Kyoto Univ.*, 29(261), 45–63.
- Nakagawa, H., and T. Tsujimoto (1980a), Sand bed instability due to bed load motion, *J. Hydraulics Div.*, 106, 2029–2051.
- Nakagawa, H., and T. Tsujimoto (1980b), Stochastic study on origin of small scale bed forms related to probabilistic characteristics of bed load movements, in *Proc. 3rd International Symposium on Stochastic Hydraulics, 5-7 August, Tokyo, Japan*, pp. 359–370.

- Naqshband, S., J. S. Ribberink, D. Hurther, and S. J. M. H. Hulscher (2014), Bed load and suspended load contributions to migrating sand dunes in equilibrium, *J. Geophys. Res., Earth Surface*, 119(5), 1043–1063, doi:10.1002/2013JF003043.
- Needham, D. J. (1990), Wave hierarchies in alluvial river flows, *Geophys. Astrophys. Fluid Dyn.*, 51(1-4), 167–194, doi:10.1080/03091929008219855.
- Nezu, I., and H. Nakagawa (1984), Cellular secondary currents in straight conduit, *J. Hydraul. Eng.*, 110(2), 173–193, doi:10.1061/(ASCE)0733-9429(1984)110:2(173).
- Niño, Y., M. García, and L. Ayala (1994), Gravel saltation: 1. Experiments, *Water Resour. Res.*, 30(6), 1907–1914, doi:10.1029/94WR00533.
- van Niekerk, A., K. R. Vogel, R. L. Slingerland, and J. S. Bridge (1992), Routing of heterogeneous sediments over movable bed: Model development, *J. Hydraul. Eng.*, 118(2), 246–262, doi:10.1061/(ASCE)0733-9429(1992)118:2(246).
- Nieuwstadt, F. T., B. J. Boersma, and J. Westerweel (2016), *Turbulence*, 284 pp., Springer, Switzerland.
- Nikora, V., H. Habersack, T. Huber, and I. McEwan (2002), On bed particle diffusion in gravel bed flows under weak bed load transport, *Water Resour. Res.*, 38(6), 1081, doi:10.1029/2001WR000513.
- Nikuradse, J. (1930), Untersuchungen über turbulente Strömungen in nicht kreisförmigen Rohren, *Ingenieur-Archiv*, 1(3), 306–332, doi:10.1007/BF02079937, (in German).
- Nikuradse, J. (1933), Strömungsgesetze in rauhen Rohren, *VDI-Forschungsheft 361. Beilage zu "Forschung auf dem Gebiete des Ingenieurwesens" Ausgabe B Band 4.*, (in German).
- Olesen, K. W. (1982), Influence of secondary flow on meandering rivers, *Tech. Rep. 1-82*, Laboratory of Fluid Mechanics, Faculty of Civil Engineering and Geosciences, Delft University of Technology, Delft, the Netherlands, 67 pp.
- Orrú, C., A. Blom, V. Chavarrías, V. Ferrara, and G. Stecca (2016a), A new technique for measuring the bed surface texture during flow and application to a degradational sand-gravel laboratory experiment, *Water Resour. Res.*, 52(9), 7005–7022, doi:10.1002/2016WR018938.
- Orrú, C., A. Blom, and W. S. J. Uijttewaal (2016b), Armor breakup and reformation in a degradational laboratory experiment, *Earth Surf. Dyn.*, 4(2), 461–470, doi:10.5194/esurf-4-461-2016.
- Ortega y Gasset, J. (1937), *La rebelión de las masas*, Austral, Buenos Aires, Argentina, (in Spanish).
- Ottevanger, W., K. Blanckaert, W. S. J. Uijttewaal, and H. J. de Vriend (2013), Meander dynamics: A reduced-order nonlinear model without curvature restrictions for flow and bed morphology, *J. Geophys. Res., Earth Surface*, 118(2), 1118–1131, doi:10.1002/jgrf.20080.

- Ottevanger, W., S. Giri, and K. Sloff (2015), Sustainable Fairway Rhinedelta II, *Tech. Rep. 1209175-000*, Deltares, Delft, the Netherlands.
- Ouwehand, C. (1958), Some notes on the god Susa-no-o, *Monumenta Nipponica*, 14(3-4), 384-407, doi:10.2307/2382776.
- Paine, T. (1776), *The American Crisis*, Pennsylvania Journal.
- Paola, C. (2000), Quantitative models of sedimentary basin filling, *Sedimentology*, 47(s1), 121-178, doi:10.1046/j.1365-3091.2000.00006.x.
- Paola, C., and M. Leeder (2011), Environmental dynamics: Simplicity versus complexity, *Nature*, 469, 38-39, doi:10.1038/469038a.
- Paola, C., and V. R. Voller (2005), A generalized Exner equation for sediment mass balance, *J. Geophys. Res., Earth Surface*, 110(F4), F04014, doi:10.1029/2004JF000274.
- Paola, C., P. L. Heller, and C. L. Angevine (1992), The large-scale dynamics of grain-size variation in alluvial basins, 1: Theory, *Basin Res.*, 4(2), 73-90, doi:10.1111/j.1365-2117.1992.tb00145.x.
- Park, I., and S. C. Jain (1987), Numerical simulation of degradation of alluvial channel beds, *J. Hydraul. Eng.*, 113(7), 845-859, doi:10.1061/(ASCE)0733-9429(1987)113:7(845).
- Parker, G. (1976), On the cause and characteristic scales of meandering and braiding in rivers, *J. Fluid Mech.*, 76(3), 457-480, doi:10.1017/S0022112076000748.
- Parker, G. (1978), Self-formed straight rivers with equilibrium banks and mobile bed. Part 1. The sand-silt river, *J. Fluid Mech.*, 89(1), 109-125, doi:10.1017/S0022112078002499.
- Parker, G. (1990), Surface-based bedload transport relation for gravel rivers, *J. Hydraul. Res.*, 28(4), 417-436, doi:10.1080/00221689009499058.
- Parker, G. (1991), Selective sorting and abrasion of river gravel. I: Theory, *J. Hydraul. Eng.*, 117(2), 131-147, doi:10.1061/(ASCE)0733-9429(1991)117:2(131).
- Parker, G. (2008), Transport of gravel and sediment mixtures, in *Sedimentation Engineering*, edited by M. Garcia, chap. 3, pp. 165-251, America Society of Civil Engineers, doi:10.1061/9780784408148.ch03.
- Parker, G., and E. D. Andrews (1985), Sorting of bed load sediment by flow in meander bends, *Water Resour. Res.*, 21(9), 1361-1373, doi:10.1029/WR0211009p01361.
- Parker, G., and P. C. Klingeman (1982), On why gravel bed streams are paved, *Water Resour. Res.*, 18(5), 1409-1423, doi:10.1029/WR0181005p01409.
- Parker, G., and A. J. Sutherland (1990), Fluvial armor, *J. Hydraul. Res.*, 28(5), 529-544, doi:10.1080/00221689009499044.
- Parker, G., and P. Wilcock (1993), Sediment feed and recirculating flumes: Fundamental difference, *J. Hydraul. Eng.*, 119(11), 1192-1204, doi:10.1061/(ASCE)0733-9429(1993)119:11(1192).

- Parker, G., P. C. Klingeman, and D. G. McLean (1982), Bedload and size distribution in paved gravel-bed streams, *J. Hydraulics Div.*, 108(4), 544–571.
- Parker, G., C. Paola, and S. Leclair (2000), Probabilistic Exner sediment continuity equation for mixtures with no active layer, *J. Hydraul. Eng.*, 126(11), 818–826, doi:10.1061/(ASCE)0733-9429(2000)126:11(818).
- Parker, G., G. Seminara, and L. Solari (2003), Bed load at low Shields stress on arbitrarily sloping beds: Alternative entrainment formulation, *Water Resour. Res.*, 39(7), 1183, doi:10.1029/2001WR001253.
- Pelanti, M., F. Bouchut, and A. Mangeney (2008), A Roe-type scheme for two-phase shallow granular flows over variable topography, *ESAIM: Mathematical Modelling and Numerical Analysis*, 42(5), 851–885, doi:10.1051/m2an:2008029.
- Pelosi, A., G. Parker, R. Schumer, and H.-B. Ma (2014), Exner-based master equation for transport and dispersion of river pebble tracers: Derivation, asymptotic forms, and quantification of nonlocal vertical dispersion, *J. Geophys. Res., Earth Surface*, 119(9), 1818–1832, doi:10.1002/2014JF003130.
- Pelosi, A., R. Schumer, G. Parker, and R. I. Ferguson (2016), The cause of advective slowdown of tracer pebbles in rivers: Implementation of Exner-based Master Equation for coevolving streamwise and vertical dispersion, *J. Geophys. Res., Earth Surface*, 121(3), 623–637, doi:10.1002/2015JF003497.
- Petts, G., M. Thoms, K. Brittan, and B. Atkin (1989), A freeze-coring technique applied to pollution by fine sediments in gravel-bed rivers, *Sci. Total Environ.*, 84, 259–272, doi:10.1016/0048-9697(89)90388-4.
- Phillips, B. C., and A. J. Sutherland (1989), Spatial lag effects in bed load sediment transport, *J. Hydraul. Res.*, 27(1), 115–133, doi:10.1080/00221688909499247.
- Phillips, B. C., and A. J. Sutherland (1990), Temporal lag effect in bed load sediment transport, *J. Hydraul. Res.*, 28(1), 5–23, doi:10.1080/00221689009499144.
- Plows, W. H. (1968), Some numerical results for two-dimensional steady laminar Bénard convection, *Phys. Fluids*, 11(8), 1593–1599, doi:10.1063/1.1692166.
- Poole, S. (2016), *Rethink: The Surprising History of New Ideas*, 352 pp., Scribner, New York, NY, United States.
- van Prooijen, B. C., and W. S. J. Uijttewaal (2002), A linear approach for the evolution of coherent structures in shallow mixing layers, *Phys. Fluids*, 14(12), 4105–4114, doi:10.1063/1.1514660.
- Pyrce, R. S., and P. E. Ashmore (2003), The relation between particle path length distributions and channel morphology in gravel-bed streams: A synthesis, *Geomorphology*, 56(1), 167–187, doi:10.1016/S0169-555X(03)00077-1.

- Qian, H., Z. Cao, H. Liu, and G. Pender (2016), Numerical modelling of alternate bar formation, development and sediment sorting in straight channels, *Earth Surf. Process. Landf.*, 42(7), 555–574, doi:10.1002/esp.3988.
- Rahuel, J., F. Holly, J. Chollet, P. Belleudy, and G. Yang (1989), Modeling of riverbed evolution for bedload sediment mixtures, *J. Hydraul. Eng.*, 115(11), 1521–1542, doi:10.1061/(ASCE)0733-9429(1989)115:11(1521).
- Ramshaw, J. D., and J. A. Trapp (1978), Characteristics, stability, and short-wavelength phenomena in two-phase flow equation systems, *Nucl. Sci. Eng.*, 66(1), 93–102, doi:10.13182/NSE78-A15191.
- Ranasinghe, R., C. Swinkels, A. Lujendijk, D. Roelvink, J. Bosboom, M. Stive, and D. Walstra (2011), Morphodynamic upscaling with the MORFAC approach: Dependencies and sensitivities, *Coastal Eng.*, 58(8), 806–811, doi:10.1016/j.coastaleng.2011.03.010.
- Rathbun, R. E., V. C. Kennedy, and J. K. Culbertson (1971), Transport and dispersion of fluorescent tracer particles for the flat-bed condition, Rio Grande conveyance channel, near Bernardo, New Mexico, *US Geological Survey Professional Paper 562-I*, US Government Printing Office, Washington, DC, United States, 263 pp.
- Recking, A., P. Frey, A. Paquier, and P. Belleudy (2009), An experimental investigation of mechanisms involved in bed load sheet production and migration, *J. Geophys. Res., Earth Surface*, 114(F3), F03010, doi:10.1029/2008JF000990.
- Ribberink, J. S. (1987), Mathematical modelling of one-dimensional morphological changes in rivers with non-uniform sediment, Ph.D. thesis, Delft University of Technology, Delft, the Netherlands.
- van Rijn, L. C. (1984), Sediment transport, part I: Bed load transport, *J. Hydraul. Eng.*, 110(10), 1431–1456, doi:10.1061/(ASCE)0733-9429(1984)110:10(1431).
- Rodrigues, L., and K. Zumbrun (2016), Periodic-coefficient damping estimates, and stability of large-amplitude roll waves in inclined thin film flow, *SIAM J. Math. Anal.*, 48(1), 268–280, doi:10.1137/15M1016242.
- Roelvink, J. (2006), Coastal morphodynamic evolution techniques, *Coastal Eng.*, 53(2–3), 277–287, doi:10.1016/j.coastaleng.2005.10.015.
- Roseberry, J. C., M. W. Schmeckle, and D. J. Furbish (2012), A probabilistic description of the bed load sediment flux: 2. Particle activity and motions, *J. Geophys. Res., Earth Surface*, 117(F3), F03032, doi:10.1029/2012JF002353.
- Roy, C. J. (2005), Review of code and solution verification procedures for computational simulation, *J. Comput. Phys.*, 205(1), 131–156, doi:10.1016/j.jcp.2004.10.036.
- Rozovskii, I. L. (1957), *Flow of water in bends in open channels*, 233 pp., Academy of Sciences of the Ukrainian SSR, (in English translated by Y. Prushansky in 1961).

- Runge, C. (1895), Ueber die numerische Auflösung von Differentialgleichungen, *Mathematische Annalen*, 46(2), 167–178, doi:10.1007/BF01446807, (in German).
- Saint-Venant, A. J. C. B. (1871), Théorie du mouvement non permanent des eaux, avec application aux crues des rivières et à l'introduction des marées dans leur lit, *Comptes Rendus des séances de l'Académie des Sciences*, 73, 237–240, (in French).
- Sarno, L., A. Carravetta, R. Martino, M. Papa, and Y.-C. Tai (2017), Some considerations on numerical schemes for treating hyperbolicity issues in two-layer models, *Adv. Water Resour.*, 100(Supplement C), 183–198, doi:10.1016/j.advwatres.2016.12.014.
- Savary, C., and Y. Zech (2007), Boundary conditions in a two-layer geomorphological model. Application to a hydraulic jump over a mobile bed, *J. Hydraul. Res.*, 45(3), 316–332, doi:10.1080/00221686.2007.9521766.
- Sayre, W. W., and D. W. Hubbell (1965), Transport and dispersion of labeled bed material North Loup River, Nebraska, *US Geological Survey Professional Paper 433-C*, US Government Printing Office, Washington, DC, United States, 48 pp.
- Schielen, R., A. Doelman, and H. E. de Swart (1993), On the nonlinear dynamics of free bars in straight channels, *J. Fluid Mech.*, 252, 325–356, doi:10.1017/S0022112093003787.
- Schmidt, K.-H., and P. Ergenzinger (1992), Bedload entrainment, travel lengths, step lengths, rest periods—studied with passive (iron, magnetic) and active (radio) tracer techniques, *Earth Surf. Process. Landf.*, 17(2), 147–165, doi:10.1002/esp.3290170204.
- Schumer, R., and D. J. Jerolmack (2009), Real and apparent changes in sediment deposition rates through time, *J. Geophys. Res., Earth Surface*, 114(F3), F00A06, doi:10.1029/2009JF001266.
- Sekine, M., and H. Kikkawa (1992), Mechanics of saltating grains. II, *J. Hydraul. Eng.*, 118(4), 536–558, doi:10.1061/(ASCE)0733-9429(1992)118:4(536).
- Seminara, G. (2006), Meanders, *J. Fluid Mech.*, 554, 271–297, doi:10.1017/S0022112006008925.
- Seminara, G., and M. Tubino (1989), Alternate bars and meandering, in *River Meandering*, edited by S. Ikeda and G. Parker, chap. 10, pp. 267–320, AGU, Washington, DC, United States, doi:10.1029/WM012p0267.
- Seminara, G., M. Colombini, and G. Parker (1996), Nearly pure sorting waves and formation of bedload sheets, *J. Fluid Mech.*, 312, 253–278, doi:10.1017/S0022112096001991.
- Seminara, G., L. Solari, and G. Parker (2002), Bed load at low Shields stress on arbitrarily sloping beds: Failure of the Bagnold hypothesis, *Water Resour. Res.*, 38(11), 1249, doi:10.1029/2001WR000681.
- Shields, A. (1936), Anwendung der Ähnlichkeitsmechanik und Turbulenzforschung auf die Geschiebebewegung, Ph.D. thesis, Versuchsanstalt für Wasserbau und Schiffbau, 26, Berlin, Germany, (in German).

- Shimizu, Y., S. Giri, S. Yamaguchi, and J. Nelson (2009), Numerical simulation of dune-flat bed transition and stage-discharge relationship with hysteresis effect, *Water Resour. Res.*, 45(4), W04429, doi:10.1029/2008WR006830.
- Sieben, A. (1994), Notes on the mathematical modelling of alluvial mountain rivers with graded sediment, *Tech. Rep. 94-3*, Faculty of Civil Engineering and Geosciences, Delft University of Technology, Delft, the Netherlands, 134 pp.
- Sieben, J. (1997), Modelling of hydraulics and morphology in mountain rivers, Ph.D. thesis, Delft University of Technology, Delft, the Netherlands.
- Sieben, J. (1999), A theoretical analysis of discontinuous flow with mobile bed, *J. Hydraul. Res.*, 37(2), 199–212, doi:10.1080/00221689909498306.
- Simons, D. B., and M. L. Albertson (1963), Uniform water conveyance channels in alluvial materials, *Transaction ASCE*, 128, 65–105.
- Siviglia, A., G. Stecca, and A. Blom (2017), Modeling of mixed-sediment morphodynamics in gravel bed rivers using the active layer approach: Insights from mathematical and numerical analysis, in *Gravel-Bed Rivers: Process and Disasters*, edited by D. Tsutsumi and J. Laronne, chap. 26, pp. 703–728, Wiley-Blackwell, Hoboken, NJ, United States, doi:10.1002/9781118971437.ch26.
- Sloff, K., and E. Mosselman (2012), Bifurcation modelling in a meandering gravel-sand bed river, *Earth Surf. Process. Landf.*, 37(14), 1556–1566, doi:10.1002/esp.3305.
- Smith, J. D., and S. R. McLean (1977), Spatially averaged flow over a wavy surface, *J. Geophys. Res.*, 82(12), 1735–1746, doi:10.1029/JCo82i012p01735.
- Soh, W. Y., and S. A. Berger (1984), Laminar entrance flow in a curved pipe, *J. Fluid Mech.*, 148, 109–135, doi:10.1017/S0022112084002275.
- Solari, L., and G. Parker (2000), The curious case of mobility reversal in sediment mixtures, *J. Hydraul. Eng.*, 126(3), 185–197, doi:10.1061/(ASCE)0733-9429(2000)126:3(185).
- Sonke, J. E., D. J. Furbish, and V. J. M. Salters (2003), Dispersion effects of laminar flow and spray chamber volume in capillary electrophoresis-inductively coupled plasma-mass spectrometry: a numerical and experimental approach, *J. Chromatogr. A*, 1015(1), 205–218, doi:10.1016/S0021-9673(03)01210-X.
- Spinewine, B., V. Guinot, S. Soares Frazão, and Y. Zech (2011), Solution properties and approximate Riemann solvers for two-layer shallow flow models, *Comput. Fluids*, 44(1), 202–220, doi:10.1016/j.compfluid.2011.01.001.
- Stecca, G., A. Siviglia, and A. Blom (2014), Mathematical analysis of the Saint-Venant-Hirano model for mixed-sediment morphodynamics, *Water Resour. Res.*, 50(10), 7563–7589, doi:10.1002/2014WR015251.
- Stecca, G., A. Siviglia, and A. Blom (2016), An accurate numerical solution to the Saint-Venant-Hirano model for mixed-sediment morphodynamics in rivers, *Adv. Water Resour.*, 93, Part A, 39–61, doi:10.1016/j.advwatres.2015.05.022.

- Sternberg, H. (1875), Untersuchungen über Längen- und Querprofil geschiefbeführender Flüsse, *Zeitschrift für Bauwesen*, 25, 483–506, (in German).
- Stevens, M. A. (1988), Discussion of “Unsteady sediment transport modeling” by Dennis A. Lyn (January, 1987, Vol. 113, No. 1), *J. Hydraul. Eng.*, 114(8), 954–956, doi:10.1061/(ASCE)0733-9429(1988)114:8(954).
- Stewart, H. B. (1979), Stability of two-phase flow calculation using two-fluid models, *J. Comput. Phys.*, 33(2), 259–270, doi:10.1016/0021-9991(79)90020-2.
- Stewart, H. B., and B. Wendroff (1984), Two-phase flow: Models and methods, *J. Comput. Phys.*, 56(3), 363–409, doi:10.1016/0021-9991(84)90103-7.
- Strikwerda, J. (2004), *Finite Difference Schemes and Partial Differential Equations*, 2 ed., 427 pp., Society for Industrial and Applied Mathematics, Philadelphia, PA, United States, doi:10.1137/1.9780898717938.
- Stuhmiller, J. (1977), The influence of interfacial pressure forces on the character of two-phase flow model equations, *Int. J. Multiphase Flow*, 3(6), 551–560, doi:10.1016/0301-9322(77)90029-5.
- Sumer, B. M., and M. Bakioglu (1984), On the formation of ripples on an erodible bed, *J. Fluid Mech.*, 144, 177–190, doi:10.1017/S0022112084001567.
- Suzuki, K. (1976), On the propagation of a disturbance in the bed composition of an open channel, *Tech. Rep. R 1976/09/L*, Laboratory of Fluid Mechanics, Faculty of Civil Engineering and Geosciences, Delft University of Technology, Delft, the Netherlands, 41 pp.
- Talmon, A. M., N. Struiksmā, and M. C. L. M. V. Mierlo (1995), Laboratory measurements of the direction of sediment transport on transverse alluvial-bed slopes, *J. Hydraul. Res.*, 33(4), 495–517, doi:10.1080/00221689509498657.
- Talstra, H. (2011), Large-scale turbulence structures in shallow separating flows, Ph.D. thesis, Delft University of Technology, Delft, the Netherlands.
- Tan, W. Y. (1992), *Shallow Water Hydrodynamics: Mathematical Theory and Numerical Solution for a Two-dimensional System of Shallow-water Equations*, Elsevier Oceanography Series, vol. 55, 1 ed., 433 pp., Elsevier, Amsterdam, the Netherlands.
- Thomson, J. (1876), On the origin of windings of rivers in alluvial plains, with remarks on the flow of water round bends in pipes, *Proc. Roy. Soc. London*, 25(171-178), 5–8, doi:10.1098/rsp1.1876.0004.
- Tiselj, I., and S. Petelin (1997), Modelling of two-phase flow with second-order accurate scheme, *J. Comput. Phys.*, 136(2), 503–521, doi:10.1006/jcph.1997.5778.
- Toro, E. F. (2001), *Shock-capturing methods for free-surface shallow flows*, 326 pp., John Wiley & Sons, Hoboken, NJ, United States.

- Toro, E. F. (2009), *Riemann Solvers and Numerical Methods for Fluid Dynamics*, 3 ed., 724 pp., Springer-Verlag Berlin-Heidelberg, Heidelberg, Germany, doi:10.1007/b79761.
- Toro, E. F., B. Thornber, Q. Zhang, A. Scoz, and C. Contarino (2018), A computational model for the dynamics of cerebrospinal fluid in the spinal subarachnoid space, *J. Biomech. Eng.*, doi:10.1115/1.4041551.
- Toro-Escobar, C. M., C. Paola, and G. Parker (1996), Transfer function for the deposition of poorly sorted gravel in response to streambed aggradation, *J. Hydraul. Res.*, 34(1), 35–53, doi:10.1080/00221689609498763.
- Travis, J. R., F. H. Harlow, and A. A. Amsden (1976), Numerical calculation of two-phase flows, *Nucl. Sci. Eng.*, 61(1), 1–10, doi:10.13182/NSE76-A28455.
- Tsujimoto, T. (1989a), Formation of alternate longitudinal sorting as an instability of fluvial bed-surface composition, *Doboku Gakkai Ronbunshu*, 411, 143–150, doi:10.2208/jscej.1989.411_143, (in Japanese).
- Tsujimoto, T. (1989b), Longitudinal stripes of sorting due to cellular secondary currents, *J. Hydrosoci. Hydraul. Eng.*, 7(1), 23–34.
- Tsujimoto, T. (1989c), Formation of longitudinal stripes due to lateral sorting by cellular secondary currents, in *Proc. 33rd Japanese Conference on Hydraulics*, vol. 33, pp. 403–408, doi:10.2208/prohe1975.33.403, (in Japanese).
- Tsujimoto, T. (1990), Instability of longitudinal distribution of fluvial bed-surface composition, *J. Hydrosoci. Hydraul. Eng.*, 7(2), 69–80.
- Tsujimoto, T., and K. Motohashi (1989), Formation mechanism and predominant wave length of alternate longitudinal sorting on a stream bed composed of sand and gravel, in *Proc. 33rd Japanese Conference on Hydraulics*, vol. 33, pp. 409–414, doi:10.2208/prohe1975.33.409, (in Japanese).
- Turkel, E. (1987), Preconditioned methods for solving the incompressible and low speed compressible equations, *J. Comput. Phys.*, 72(2), 277–298, doi:10.1016/0021-9991(87)90084-2.
- Turkel, E. (1993), Review of preconditioning methods for fluid dynamics, *Appl. Numer. Math.*, 12(1), 257–284, doi:10.1016/0168-9274(93)90122-8.
- Turkel, E. (1999), Preconditioning techniques in computational fluid dynamics, *Annu. Rev. Fluid Mech.*, 31(1), 385–416, doi:10.1146/annurev.fluid.31.1.385.
- Vargas-Luna, A. (2016), Role of vegetation in river bank accretion, Ph.D. thesis, Delft University of Technology, Delft, the Netherlands.
- Vargas-Luna, A., A. Crosato, and W. S. J. Uijttewaal (2014), Effects of vegetation on flow and sediment transport: Comparative analyses and validation of predicting models, *Earth Surf. Process. Landf.*, 40(2), 157–176, doi:10.1002/esp.3633.

- Västilä, K., and J. Järvelä (2014), Modeling the flow resistance of woody vegetation using physically based properties of the foliage and stem, *Water Resour. Res.*, 50(1), 229–245, doi:10.1002/2013WR013819.
- Veprek, R. G., S. Steiger, and B. Witzigmann (2007), Ellipticity and the spurious solution problem of k-p envelope equations, *Phys. Rev. B*, 76, 165320, doi:10.1103/PhysRevB.76.165320.
- Verwer, J. G., and J. M. Sanz-Serna (1984), Convergence of method of lines approximations to partial differential equations, *Computing*, 33(3), 297–313, doi:10.1007/BF02242274.
- Vetsch, D., D. Ehrbar, S. Peter, P. Russelot, C. Volz, L. Vonwiller, R. Faeh, D. Farshi, R. Mueller, and R. Veprek (2006), *BASEMENT, Basic Simulation Environment for Computation of Environmental Flow and Natural Hazard Simulation, software manual.*, Laboratory of Hydraulics, Hydrology and Glaciology (VAW), Eidgenössische Technische Hochschule Zürich, Zürich, Switzerland.
- Villaret, C., J.-M. Hervouet, R. Kopmann, U. Merkel, and A. G. Davies (2013), Morphodynamic modeling using the Telemac finite-element system, *Computers & Geosciences*, 53, 105–113, doi:10.1016/j.cageo.2011.10.004.
- da Vinci, L. (ca. 1478–1518), *The notebook of Leonardo da Vinci*, (translated by Jean Paul Richter in 1888).
- Viparelli, E., O. E. Sequeiros, A. Cantelli, P. R. Wilcock, and G. Parker (2010), River morphodynamics with creation/consumption of grain size stratigraphy 2: Numerical model, *J. Hydraul. Res.*, 48(6), 727–741, doi:10.1080/00221686.2010.526759.
- Viparelli, E., R. R. H. Moreira, and A. Blom (2017), Modelling stratigraphy-based GBR morphodynamics., in *Gravel-Bed Rivers: Process and Disasters*, edited by D. Tsutsumi and J. Laronne, chap. 23, pp. 609–637, Wiley-Blackwell, Hoboken, NJ, United States, doi:10.1002/9781118971437.ch23.
- Voepel, H., R. Schumer, and M. A. Hassan (2013), Sediment residence time distributions: Theory and application from bed elevation measurements, *J. Geophys. Res., Earth Surface*, 118(4), 2557–2567, doi:10.1002/jgrf.20151.
- Vogel, K. R., A. van Niekerk, R. L. Slingerland, and J. S. Bridge (1992), Routing of heterogeneous sediments over movable bed: Model verification, *J. Hydraul. Eng.*, 118(2), 263–279, doi:10.1061/(ASCE)0733-9429(1992)118:2(263).
- Vreugdenhil, C. B. (1994), *Numerical Methods for Shallow-Water Flow*, 262 pp., Springer, Dordrecht, the Netherlands, doi:10.1007/978-94-015-8354-1.
- Vreugdenhil, K., G. Alberts, and P. van Gelder (2001), Een eeuw wiskunde en werkelijkheid waterloopkunde, *Nieuw Archief voor Wiskunde*, 3, 266–276, (in Dutch).
- de Vriend, H. J. (1977), A mathematical model of steady flow in curved shallow channels, *J. Hydraul. Res.*, 15(1), 37–54, doi:10.1080/00221687709499748.

- de Vriend, H. J. (1981), Steady flow in shallow channel bends, Ph.D. thesis, Delft University of Technology, Delft, the Netherlands.
- de Vries, M. (1965), Considerations about non-steady bed load transport in open channels, *Tech. Rep. 36*, Delft Hydraulics Laboratory, Delft, the Netherlands, 10 pp.
- de Vries, M. (1973), River-bed variations - aggradation and degradation, *Tech. Rep. 107*, Delft Hydraulics Laboratory, Delft, the Netherlands, 21 pp.
- Walshe, M. (1995), *The Long Discourses of the Buddha: A Translation of the Digha Nikaya*, 648 pp., Wisdom Publications, Somerville, MA, United States.
- Warrier, S. (2014), *Kamandalu: The Seven Sacred Rivers of Hinduism*, 280 pp., Mayur University, London, United Kingdom.
- Whiting, P. J., W. E. Dietrich, L. B. Leopold, T. G. Drake, and R. L. Shreve (1988), Bedload sheets in heterogeneous sediment, *Geology*, 16(2), 105–108, doi:10.1130/0091-7613(1988)016<0105:BSIHS>2.3.CO;2.
- Wilbraham, H. (1848), On a certain periodic function, *The Cambridge and Dublin Mathematical Journal*, 3, 198–201.
- Wilcock, P. R., and J. C. Crowe (2003), Surface-based transport model for mixed-size sediment, *J. Hydraul. Eng.*, 129(2), 120–128, doi:10.1061/(ASCE)0733-9429(2003)129:2(120).
- Williams, R. D., R. Measures, D. M. Hicks, and J. Brasington (2016), Assessment of a numerical model to reproduce event-scale erosion and deposition distributions in a braided river, *Water Resour. Res.*, 52(8), 6621–6642, doi:10.1002/2015WR018491.
- Wong, M., and G. Parker (2006a), Reanalysis and correction of bed-load relation of Meyer-Peter and Müller using their own database, *J. Hydraul. Eng.*, 132(11), 1159–1168, doi:10.1061/(ASCE)0733-9429(2006)132:11(1159).
- Wong, M., and G. Parker (2006b), One-dimensional modeling of bed evolution in a gravel bed river subject to a cycled flood hydrograph, *J. Geophys. Res., Earth Surface*, 111(F3), F03018, doi:10.1029/2006JF000478.
- Woodhouse, M. J., A. R. Thornton, C. G. Johnson, B. P. Kokelaar, and J. M. N. T. Gray (2012), Segregation-induced fingering instabilities in granular free-surface flows, *J. Fluid Mech.*, 709, 543–580, doi:10.1017/jfm.2012.348.
- Wright, S., and G. Parker (2004), Flow resistance and suspended load in sand-bed rivers: Simplified stratification model, *J. Hydraul. Eng.*, 130(8), 796–805, doi:10.1061/(ASCE)0733-9429(2004)130:8(796).
- Wu, W. (2004), Depth-averaged two-dimensional numerical modeling of unsteady flow and nonuniform sediment transport in open channels, *J. Hydraul. Eng.*, 130(10), 1013–1024, doi:10.1061/(ASCE)0733-9429(2004)130:10(1013).

- Wu, W. (2007), *Computational River Dynamics*, 494 pp., Taylor & Francis, London, United Kingdom.
- Wu, W., S. S. Wang, and Y. Jia (2000), Nonuniform sediment transport in alluvial rivers, *J. Hydraul. Res.*, 38(6), 427–434, doi:10.1080/00221680009498296.
- Wu, Z., E. Foufoula-Georgiou, G. Parker, A. Singh, X. Fu, and G. Wang (2019), Analytical solution for anomalous diffusion of bedload tracers gradually undergoing burial, *J. Geophys. Res., Earth Surface*, 124(1), 21–37, doi:10.1029/2018JF004654.
- Yalin, M. S. (1964), Geometrical properties of sand wave, *J. Hydraulics Div.*, 90(5), 105–119.
- Yatsu, E. (1955), On the longitudinal profile of the graded river, *EOS, Trans. Am. Geophys. Union*, 36(4), 655–663.
- Yee, H., R. Warming, and A. Harten (1985), Implicit total variation diminishing (TVD) schemes for steady-state calculations, *J. Comput. Phys.*, 57(3), 327–360, doi:10.1016/0021-9991(85)90183-4.
- Yubero-Ferrero, F. (1998), El universo poético de Claudio Rodríguez, Ph.D. thesis, Faculty of Filology, Complutense University of Madrid, Madrid, Spain, (in Spanish).
- Zanotti, A. L., C. G. Méndez, N. M. Nigro, and M. Storti (2007), A preconditioning mass matrix to avoid the ill-posed two-fluid model, *J. Appl. Mech.*, 74(4), 732–740, doi:doi:10.1115/1.2711224.
- Zanré, D. D. L., and D. J. Needham (1994), On the hyperbolic nature of the equations of alluvial river hydraulics and the equivalence of stable and energy dissipating shocks, *Geophys. Astrophys. Fluid Dyn.*, 76, 193–222, doi:10.1080/03091929408203665.
- Zhang, H., and R. Kahawita (1987), Nonlinear model for aggradation in alluvial channels, *J. Hydraul. Eng.*, 113(3), 353–369, doi:10.1061/(ASCE)0733-9429(1987)113:3(353).
- Zhang, H., and R. Kahawita (1990), Linear hyperbolic model for alluvial channels, *J. Hydraul. Eng.*, 116(4), 478–493, doi:10.1061/(ASCE)0733-9429(1990)116:4(478).
- Zima, W., M. Nowak-Ochoń, and P. Ochoń (2015), Simulation of fluid heating in combustion chamber waterwalls of boilers for supercritical steam parameters, *Energy*, 92, 117–127, doi:10.1016/j.energy.2015.02.111.

Epilogue

At the beginning of the Ph.D. I read *Phaedo* and I took the following paragraph as a driver for the rest of the project:

[Socrates to Simmias]

Then he [a person] will do this [come closest to the knowledge of the reality of all other things] most perfectly who approaches the object with thought alone, without associating any sight with his thought, or dragging in any sense perception with his reasoning, but who, using pure thought alone, tries to track down each reality pure and by itself, freeing himself as far as possible from eyes and ears, and in a word, from the whole body, because the body confuses the soul and does not allow it to acquire truth and wisdom whenever it is associated with it. Will not that man reach reality, Simmias, if anyone does?

Plato, Phaedo

By the end of the Ph.D. I read the *Pensées* and I encountered the following paragraph:

The world is a good judge of things, for it is in natural ignorance, which is man's true state. The sciences have two extremes which meet. The first is the pure natural ignorance in which all men find themselves at birth. The other extreme is that reached by great intellects, who, having run through all that men can know, find they know nothing, and come back again to that same ignorance from which they set out; but this is a learned ignorance which is conscious of itself. Those between the two, who have departed from natural ignorance and not been able to reach the other, have some smattering of this vain knowledge and pretend to be wise. These trouble the world and are bad judges of everything. The people and the wise constitute the world; these despise it, and are despised. They judge badly of everything, and the world judges rightly of them.

Blaise Pascal, Pensées

I do not completely agree with Pascal, as I feel ignorant and I do not think I have “run through all that man can know” (which is evident from the long list of recommendations for further research in Chapter 7). Yet, Pascal's *pensée* is a good reminder of the risk of thinking that Socratic reality is achievable: bad judgment of everything.

The reader that has accompanied me during this journey will realize that this journey is not finished, and that we are condemned to remain ignorant for the rest of our lives. Let's try to at least make good judgment with the mere knowledge we gained.

Acknowledgements

The alarm goes off and I quickly stop it. I don't want to wake them up. I look to the right and they are there. Peacefully sleeping my two Elisas. Life would have no meaning, or at least a completely different one, without you, Elisa.

I stand for a second below the door lintel with my bike enjoying the silence in the street, the cold, the darkness. I feel very lucky riding to the lab and think about Carlos, who is also riding at this moment, far from here. I wonder about the influence you exert on me. It is difficult to quantify it, but I am sure it is huge. It is time for me to thank you for teaching me everything about the orthic triangle.

Jose Manuel may be also be riding to work. He is the only one going by bike when there is a meter of snow in Toronto. Your approach to life makes me think a great deal since the first time I saw you in a MMC exam. Thanks for that tortilla while conducting the MSc thesis experiment overnight: "Llegará el fin del mundo y nos pillaré con la boca llena".

Going by bike is a great pleasure and I remember the trips with Joan and Villagrasa. Joan's ability to feel the third derivative when he is angry at me ("don't accelerate too fast!"), and Villagrasa's ability to break parts of the bike I didn't even know that existed, made life something wonderful. Villagrasa, thanks for all the coffee knowledge and for introducing me to the power of \LaTeX . My *alma mater* made possible to share experiences and learn from a large group of people such as Javi, Diana, Ocho, Isaac, Andrea...

Thanks to Minne I am the most efficient of all my friends. Thanks for showing me the power of reducing your drag when going by bike. Even more, thanks for teaching me to go by bike again. Even further, thanks because I feel I have always been in the Netherlands when being with you and Nici. Will Nici be in the lab today? I hope so. You completely change the atmosphere, the day improves dramatically. Thanks Nici. Your goodness is contagious.

The lab is empty. After some time I hear Jaap: "Koud, eh?!". The technicians of the lab

are indispensable. Rob, Hans, Arno, Pieter, Frank, Ruben, and overseeing everything, Sander. No one ever said to me "this is not possible".

I hear loud music from a car in the distance. The music gets louder as the car approaches. The music stops and whistling starts. Bram has arrived, and with him his happiness and enthusiasm. I had no idea one could do a PhD before I met you. You have not only opened the box of knowledge, but also pushed me into it. It is difficult to thank you enough for such a thing. I like when you enter my office in a rush with a big smile. Thanks for explaining me the difference between researchers of type 1 and 2 and push me to be of the 2-type.

Yorick arrives. It is finally time for coffee and fixing the lab screen issue. I wonder how many times have we done this routine. You make me feel at home. Thanks for, together with Rebecca, taking care of me when I am alone and showing me Spitsbergen.

Wim enters the lab and joins the coffee with Yorick and Bram. I pay attention, he will say a *stelling* at some point that will keep me thinking for the rest of the day. Your broad interest, sharp mind, and coherence in life makes me greatly enjoy discussing everything with you, from Smagorinsky to Brexit. Thank you for, among others, giving me the opportunity of being in this laboratory.

People start arriving. Lodewijk enters with a smile, "*hola holaaa*", grabs a paper cup, hits it twice against the table, fills it with water after letting pass 50 ml, and drinks. This ritual keeps surprising me. We start discussing about the latest Matlab trick, continue with the CO₂ footprint of tea, and end up talking about a bicycle storage place we have to build. Thanks for such a great company and opening my eyes to estuaries.

"Hey Stuart, how are you?", "Not bad". The internal energy entering the lab with you may contradict the first law of thermodynamics. Thanks for such a positive attitude and for all the dinners together. Life in the lab is much better with you.

I hear she is coming, I feel it. We have been orbiting each like a binary star system. Liselot, you are an intrinsic part of my project and personal development. I have discussed with you all I have done. You are the only one that knows everything I have done until the last detail. Thanks for being that critical mind on the other side of the lab that understands what I am saying even when I do not understand it myself. I will miss discussing research with you. I will also miss going to conferences and coding Elv with you. It is with pleasure that I accept the label of being the "binary bastards". Thank you.

Thomas and Renate send a message: "Are you in for climbing or a bike trip this weekend?". Beers afterward are implicit. Traveling with you is really nice. You are inside this group of people that make me feel I have always been in the Netherlands. Thank you very much.

And there she is, alpha and omega. The main reason I am now here, writing this acknowledgments. You tirelessly taught and teach me to write and to delete, to do science, to read and comment, to care about things I didn't care, to present in public, to make a poster, to teach and guide students, to create and grade exams. In one word: everything. You have had to read terrible manuscripts and with infinite patience you carefully read and comment it all. This acknowledgments section is going to be the first text I have written in the last years that you have not read (usually several times) before submitting. Now I always have this voice inside me that says "how will she say this?". I apologize for the first version of every document I gave you. I am extremely thankful to you for teaching me with so much care. Thanks for protecting me when necessary (sometimes also from myself). Thanks for pushing me to the limits. We think differently in several things, including research topics, and this sometimes led to frustration, lack of understanding, and friction. In hindsight I see this as a necessary step to grow up. Thanks for making me to grow up. "We would not struggle if we would not care about each other". If you are reading this, it means that we

managed. Thanks, Astrid.

A student comes searching for Andrés to do a MSc thesis with him. I explain, sadly, that unfortunately he is 9000 km from Delft. We had a great time sharing office. "Un tintico?". Thanks Andrés and Paola for the fantastic time spent together.

It is a bit sad to think about the people with whom I shared office at some point but continued their careers far from here. Thanks Dirk. Thanks James for all the English questions that you patiently (with some British humor) answered. "There is a word I don't know how to pronounce correctly" I ask, "Only one?" he replies. Pieter, you make my day when you come to visit the lab. Thanks for all the whiskey knowledge and the deep conversations on the origin of time, conscience, momentum, and beyond. I am looking forward for the next time you knock on the window when I think you are across the Atlantic. Thanks Gu, for introducing me to the world of eigenvalues and FORTRAN. Thanks for thoroughly reading and checking every single document I send you with great detail on the math.

We go outside to have lunch and I have great fun remembering skiing stories with Marco. Thanks for providing the necessary momentum to conduct several of the activities we have done and the music to all events. Irene (1 and 2), María, Merel, Cynthia, Zeinab, Gonzalo, Ana, the lab improves when you are there. All details matter. It improves with Irene's laugh, with María's conversations about how things are in Galiza ("añade la parroquia a la dirección postal!"), with Zeinab never missing a "good morning" and "good bye", with Merel's decisiveness to make the lab a better place, ... Thanks because a thesis is less individualistic than we all think it is.

The lunch discussion continues afterward with Jakob. I could discuss for hours with you. Thanks for showing me the world with a different prism and sharpen my arguments. We were not successful in programing a robot (actually we were very unsuccessful) but it was a great experience to work with you.

Erik Hendriks comes back from Deltares. This thesis started with a problem modelling the experiments of my MSc thesis. And my MSc thesis started as a continuation of your BSc thesis. By the transitive relation, this is your thesis! Thanks for bringing your good vibes to the lab.

Meles, Matt, Clàudia, make rivers great again! Michelle, thanks for the best present Silke will ever receive in her life.

I look to the left and I see Jill. I look more to the left and I see a chaotic drawer. Jill, thanks for allowing a bit of chaos in the office and make me feel better by contributing to it. It is great to have you in the office.

I get an email from Juan Pedro with the latest news about some problems in the Ebro River. You brought me to the Netherlands, put me in contact with who is now my Promotor, supervised my MSc thesis, made sure I presented my Final Project, and even economically supported a few of the first months in the Netherlands after the first year. Moreover, you motivated me to study rivers. I will never be able to thank you enough for all these things you have unselfishly done for me.

This week is my turn. I have a good difficult word for you, Erik Mosselman. I hope you don't know the origin. Thanks because, what for you are simple coffee conversations, for me it is an insane amount of knowledge I really like to learn. From the tomb of Louis XVII to the actual reasons a project was carried on. Thank you very much.

I send an email to Willem with a question about preallocating a variable in bott3d.f90. I get an answer back in a minute and the reminder to commit my changes. Thanks for unceasingly answering all my Delft3D questions.

Kees appears. I know your time is very limited and, for this reason, I thank you for so enthusiastically explaining me all river related issues that are going on around the world.

I take a deep breath when I receive an email from Ralph. I know it is going to be full of very tough questions that will keep me thinking for a week. Or maybe it comes with a paper attached with more Greek than Latin characters. Thank you for

these emails and the insight they provide. Thanks for making this entire project to happen. Thanks for your genuine interest in solving the problem of ill-posedness. Chapter 3 would not exist if you would have not been willing to implement the check-routine in Delft3D. Thanks. Thank you for making me realize that a linear world is just the first (boring) step, and that it gets much more interesting once you get out it.

The phone rings. Only Otti calls to my office. In the time to take the phone all the computational power of my mind is searching for a missing form or email that I should have filled or replied. Trembling, I take the phone. Everything is in order. She wants to make sure that all my paperwork is well done, the rooms for the short course are booked, and I correctly got all the information I needed. Thanks Otti for being so patience with me. You oil the gears of this department.

Ioannis sends an email and a picture with Theofili. The first two years in Delft were very nice thanks in part to you. Thanks for adopting me at your house *ad infinitum*. It is a pity that you are far from here. Thanks for your companionship.

I have a Skype call with Nunzio. What was meant to be a short discussion ends up being a 2 hour 40 minutes long conversation that enlightens me. Thank you for so selflessly and disinterestedly invest time an effort in improving my research.

As I go home, I get a message from Herrando inviting me to go visit him in Basel in a few weeks. Thank you for all these years of friendship. I feel very lucky every time you send me a message.

Eric Penya, Paco, Tomás, Jose, Dani, Gemma, Timo, Mauri, Laia, Mihoko, Ramón, Xancó, De Miguel. This thesis has nothing to do with judo, but I think I am greatly moulded and influenced by it. Thanks because this character imprint that made the thesis possible would have not been possible without you.

My brother and Dovi send a picture and ask how is Silke doing. Thanks Dani and Dovi for all the

love, attention, and care that you are able to convey in the distance. Thanks, mother, for bringing me until here. And thanks, Sergio, for helping my brother, my mother, and me. You have done much more than you think. I would have liked to finish my thesis at the age of 21, like Heisenberg, for one reason only: my grandfather to read it. I am certain he would have been the only one reading it top to down. Thanks for the engineering background. And thanks, Luci, for cementing the family.

A picture of a perfectly shaped *croqueta* pops up. Thanks Elisa Pascual, for the love with which you treat me. Thanks Juan for, among others, the support you provided in conducting the Final Project. Thanks Javier, Guillermo, and Miriam, for making me feel glad to have joined this family. The moral support I got directly and indirectly helped in conducting the PhD.

I get home and my Elisás (wife and daughter) open the door. I think about Agustín Mora Valero, my wife's great grandfather, who in the exile was only thinking about seeing his Elisás (wife and daughter) again, and his memoirs finish when he manages, as if that was the only objective in life. I will follow your example. The font of this acknowledgments is a tribute to your memoirs.

Delft, 2nd January 2019.

Appendices

A

Supplementary material to Chapter 2

*If we are too young our judgement is impaired,
just as it is if we are too old.
Thinking too little about things or thinking too much
both make us obstinate and fanatical.*

Blaise Pascal, Pensées, 381.

*No man ever steps in the same river twice,
for it's not the same river and he's not the same man.*

Heraclitus

This appendix provides the supplementary material to Chapter 2 “Ill-posedness in modeling mixed sediment river morphodynamics”. The appendix is organized as follows. The flow and active layer equations are presented in Sections A.1 and A.2, respectively. In Section A.3 we present the closure relations to compute the sediment transport rate. In Section A.4 we present the equations of the steady vertically continuous model consisting of two size fractions. In Section A.5 we conduct a perturbation analysis to show that the mathematical character of a system of equations is determined by the eigenvalues of the system matrix. In Section A.6 we show the effect of the aggradational flux to the substrate on the extent of the elliptic domain. In Section A.7 we present the results of the numerical analysis for all simulations conducted to analyze the consequences of ill-posedness. In Section A.8 we prove that considering an unsteady active layer thickness increases the likelihood of the active layer model becoming ill-posed.

A.1. Flow Equations

The water phase is mathematically described by the *Saint-Venant* equations (*Saint-Venant*, 1871) in which mass conservation is represented by the continuity equation:

$$\frac{\partial h}{\partial t} + \frac{\partial q}{\partial x} = 0, \quad (\text{A.1})$$

where t [s] denotes the time coordinate, x [m] the streamwise coordinate, and $q = uh$ [m^2/s] the water discharge per unit width. The balance of streamwise momentum is represented by:

$$\frac{\partial q}{\partial t} + \frac{\partial(q^2/h + gh^2/2)}{\partial x} + gh \frac{\partial \eta}{\partial x} = -ghS_f, \quad (\text{A.2})$$

where η [m] denotes the bed elevation and S_f [–] the friction slope.

Considering steady flow, the conservation of water mass, Equation (A.1), reduces to a spatially constant discharge, and the conservation of momentum, Equation (A.2), to the backwater equation:

$$\frac{\partial h}{\partial x} = \frac{-1}{1 - \text{Fr}^2} \frac{\partial \eta}{\partial x} - \frac{S_f}{1 - \text{Fr}^2}. \quad (\text{A.3})$$

A.2. Active Layer Equations

The conservation of the total amount of sediment in the bed is represented by the *Exner* equation (*Exner*, 1920):

$$\frac{\partial \eta}{\partial t} + \frac{\partial q_b}{\partial x} = 0, \quad (\text{A.4})$$

where q_b [m^2/s] is the sediment transport rate per unit width multiplied by $1/(1-p)$ where p [–] is the bed porosity (i.e., the sediment transport rate q_b accounts for pores). For simplicity, mechanisms such as subsidence and uplift, compaction and dilation of sediment are neglected in the above equation (*Paola and Voller*, 2005). Of special relevance is the implicit assumption that the temporal change of the storage of sediment within the water column and its effects on bed elevation are negligible (*Park and Jain*, 1987; *Stevens*, 1988; *Correia et al.*, 1992; *Morris and Williams*, 1996). We consider that there is no lag

between changes in bottom bed shear stress (*Bell and Sutherland, 1983; Jain, 1992*). Worded differently, the sediment transport rate is at capacity and adapts instantaneously to the flow field. Thus, the sediment transport rate does not require a constitutive equation and is treated as a closure relation.

Assuming constant porosity and density, the active layer equation describes the conservation of mass of grain size fraction k in the active layer (*Hirano, 1971*):

$$\frac{\partial M_{ak}}{\partial t} + f_k^I \frac{\partial(\eta - L_a)}{\partial t} + \frac{\partial q_{bk}}{\partial x} = 0, \quad (\text{A.5})$$

where M_{ak} [m] is the volume of sediment of size fraction k in the active layer per unit of bed area, f_k^I [–] is the volume fraction content of size fraction k at the interface between the active layer and the substrate ($f_k^I \in [0, 1]$), L_a [m] is the active layer thickness, and q_{bk} [m²/s] is the sediment transport rate per unit width of size fraction k multiplied by $1/(1-p)$. The addition of the sediment transport rate for each size fraction equals the total amount of sediment in transport including pores:

$$q_b = \sum_{k=1}^N q_{bk}. \quad (\text{A.6})$$

Assuming constant porosity and density, mass conservation of sediment of size fraction k in the substrate is expressed by:

$$\frac{\partial M_{sk}}{\partial t} - f_k^I \frac{\partial(\eta - L_a)}{\partial t} = 0, \quad (\text{A.7})$$

where M_{sk} [m] is the sediment volume of size fraction k in the substrate per unit of bed area.

The volume of sediment per unit of bed area in the active layer and the substrate are defined as:

$$M_{ak} = F_{ak} L_a, \quad M_{sk} = \int_{\eta_0}^{\eta - L_a} f_{sk}(z) dz, \quad (\text{A.8})$$

where F_{ak} [–] is the volume fraction content of size fraction k in the active layer ($F_{ak} \in [0, 1]$), $f_{sk}(z)$ [–] is the volume fraction content of size fraction k in the substrate at elevation z [m] ($f_{sk}(z) \in [0, 1]$), and η_0 [m] is the time invariant datum for bed elevation. The volume fraction contents are constrained by the equations:

$$\sum_{k=1}^N f_k^I = 1, \quad \sum_{k=1}^N F_{ak} = 1, \quad \sum_{k=1}^N f_{sk}(z) = 1. \quad (\text{A.9})$$

Thus, the volume of sediment per unit of bed area is constrained by the equations:

$$\sum_{k=1}^N M_{ak} = L_a, \quad \sum_{k=1}^N M_{sk} = \eta - L_a - \eta_0. \quad (\text{A.10})$$

The summation of N active layer equations yields the *Exner* equation (*Ribberink, 1987; Parker et al., 2000*), as the active layer equation, (A.5), represents fractional mass

conservation of sediment and the *Exner* equation, (A.4), represent the conservation of the total amount of sediment. Thus, to consider N active layer equations is equivalent to considering $N - 1$ active layer equations and the *Exner* equation. We here choose for the second option, as in this way the conservation of sediment mass per size fraction can be considered as an extension of the unisize model.

The substrate equation, (A.7), is a linear combination of the *Exner* equation, (A.4), and the active layer equation, (A.5), which means that the substrate equation does not play a role in the mathematical behavior of the system and can be treated in a decoupled manner.

A.3. Sediment Transport Closure Relation

The sediment transport rate of size fraction k per unit width (including pores), q_{bk} , is expressed as the product of the volume fraction content of size fraction k at the bed surface (F_{bk} [—]) and the sediment transport capacity Q_{bk} [m^2/s] which is the sediment transport we would obtain if the bed was formed by unisize sediment yet including hiding effects (*Deigaard and Fredsøe, 1978; Ribberink, 1987; Armanini, 1995*):

$$q_{bk} = F_{bk} Q_{bk}. \quad (\text{A.11})$$

The sediment transport capacity is the product of a nondimensional sediment transport rate (q_{bk}^* [—]) and the parameter $\sqrt{g R d_k^3}$ (*Einstein, 1950*):

$$Q_{bk} = q_{bk}^* \frac{\sqrt{g R d_k^3}}{1 - p}, \quad (\text{A.12})$$

where we account for the volume of pores multiplying by $1 - p$. $R = \rho_s / \rho_w - 1$ [—] is the submerged specific gravity, $\rho_s = 2650 \text{ kg/m}^3$ the sediment density, and $\rho_w = 1000 \text{ kg/m}^3$ the water density. The volume fraction content of size fraction k at the bed surface is constrained by the condition:

$$\sum_{k=1}^N F_{bk} = 1. \quad (\text{A.13})$$

In the active layer model the volume fraction content of size fraction k at the bed surface is considered to be equal to the volume fraction content in the active layer ($F_{bk} = F_{ak}$). In the vertically continuous model developed by *Viparelli et al. (2017)*, it is considered equal to the integral of the volume fraction content of size fraction k in the bed sediment weighted by the elevation's exposure to the flow:

$$F_{bk} = \int_{-\infty}^{+\infty} f_k(y) p_e(y) dy. \quad (\text{A.14})$$

The sediment transport rate q_{bk}^* is related to the mean characteristics of the flow. Here we consider a generalized form of the *Meyer-Peter and Müller (1948)* transport relation, which estimates sediment transport as a power function of the excess bed shear (Equation 2.6). The nondimensional bed shear stress of size fraction k or *Shields (1936)* parameter is computed as $\theta_k = C_f \mu^2 / (g R d_k)$ [—].

A commonly used hiding relation is the one due to *Egiazaroff* (1965):

$$\xi_k = \left(\frac{\log_{10}(19)}{\log_{10}\left(19 \frac{d_k}{D_m}\right)} \right)^2, \quad (\text{A.15})$$

where D_m [m] is a characteristic mean grain size of the mixture obtained as an average of the grains in movement and in the bed surface. In practical terms, D_m is computed as the arithmetic mean (e.g., *Wu et al.*, 2000), geometric mean (e.g., *Bettes and Frangipane*, 2003) or the median grain size (e.g., *Van Niekerk et al.*, 1992; *Kleinbans et al.*, 2002) of the bed surface sediment. A simpler expression was developed by *Parker et al.* (1982):

$$\xi_k = \left(\frac{D_m}{d_k} \right)^b, \quad (\text{A.16})$$

where the characteristic mean grain size is the median grain size (D_{50}) of the subpavement sediment (below an armor layer) (*Parker et al.*, 1982) or the geometric mean of the surface sediment (*Parker*, 1990).

If the nondimensional parameter b is equal to 0, there is no hiding effect and each grain size behaves independently of each other. If $b = 1$, the sediment transport of each size fraction is independent of its grain size (for $B = 1.5$), thus only depends on its presence at the surface (F_{bk}). *Buffington and Montgomery* (1997) made an inventory of values of b spanning between 0.32 and 1.25. A value of $b > 1$ implies reverse mobility (*Solari and Parker*, 2000).

Here, we compute the characteristic mean grain size, D_m , as the geometric mean:

$$D_m = d_{\text{ref}} 2^{\sum_{k=1}^N F_{bk} \log_2\left(\frac{d_k}{d_{\text{ref}}}\right)}, \quad (\text{A.17})$$

where $d_{\text{ref}} = 1$ mm is a reference grain size that makes the grain size on ϕ -scale nondimensional.

A.4. System of Equations of the Steady Vertically Continuous Model Consisting of Two Size Fractions

The vector of dependent variables (\mathbf{Q}_{vcS2}) is:

$$\mathbf{Q}_{\text{vcS2}} = [\eta, f_1]^T, \quad (\text{A.18})$$

the vector of source terms is:

$$\mathbf{S}_{\text{vcS2}} = -S_f \frac{u\psi}{1-Fr^2} \left[1, \frac{p_c}{P_c} g_1 \right]^T, \quad (\text{A.19})$$

and the system matrix is:

$$\mathbf{A}_{\text{vcS2}} = u \begin{bmatrix} \frac{\psi}{1-Fr^2} & \frac{1}{P_c} X_1 \\ \frac{\psi}{1-Fr^2} \frac{p_c}{P_c} g_1 & X_1 \frac{1}{P_c} m_{1,1} \end{bmatrix}. \quad (\text{A.20})$$

Parameters g_1 , X_1 , $m_{1,1}$, and $d_{1,1}$ are the equivalent of parameters γ_1 , χ_1 , $\mu_{1,1}$, and $\delta_{1,1}$ in the active layer model (Section 2.3.1):

$$g_1 = c_1 - \varphi_1, \quad (\text{A.21})$$

$$\varphi_1 = -\frac{1}{p_c} \frac{\partial f_1 p_c}{\partial y}, \quad (\text{A.22})$$

$$X_1 = \frac{p_c}{u} \frac{\partial q_b}{\partial f_1}, \quad (\text{A.23})$$

$$m_{1,1} = \delta_{1,1} - \varphi_1, \quad (\text{A.24})$$

$$\delta_{1,1} = \frac{p_c}{u X_1} \frac{\partial q_{b1}}{\partial f_1}. \quad (\text{A.25})$$

The eigenvalues of the system matrix, Equation (A.20), nondimensionalized dividing by the flow velocity, are:

$$\lambda_{\text{vcS2}i} = \frac{1}{2} \left[\lambda_b + \lambda_{\text{sc1}} \pm \sqrt{\Delta_{\text{vcS2}}} \right] \quad \text{for } i = 1, 2, \quad (\text{A.26})$$

where the discriminant is:

$$\Delta_{\text{vcS2}} = (\lambda_b - \lambda_{\text{sc1}})^2 + 4\lambda_b \lambda_{\text{sc1}} \frac{g_1}{m_{1,1}}. \quad (\text{A.27})$$

We define λ_{sc1} as the nondimensional sorting celerity of the vertically continuous model, as the equivalent of the sorting celerity in the active layer model in Equation (2.28):

$$\lambda_{\text{sc1}} = \frac{X_1 m_{1,1}}{p_c}. \quad (\text{A.28})$$

A.5. Perturbation Analysis

In this section we conduct a perturbation analysis of the one-dimensional quasi-linear non-conservative form of the advection equation:

$$\frac{\partial \mathbf{Q}}{\partial t} + \mathbf{A} \frac{\partial \mathbf{Q}}{\partial x} = \mathbf{S}. \quad (\text{A.29})$$

We consider a reference state of dependent variables \mathbf{Q}_0 which is a solution of Equation (A.29) and a small perturbation to the state \mathbf{Q}' so that $\mathbf{Q} = \mathbf{Q}_0 + \mathbf{Q}'$. The reference state is that of steady uniform straight flow over a flat sloping bed composed of an arbitrary uniform grain size distribution. Linearizing and using the fact that \mathbf{Q}_0 is a solution we obtain the system of equations of the perturbations:

$$\frac{\partial \mathbf{Q}'}{\partial t} + \mathbf{A}_0 \frac{\partial \mathbf{Q}'}{\partial x} + \mathbf{B}_0 \mathbf{Q}' = \mathbf{0}, \quad (\text{A.30})$$

where \mathbf{A}_0 is the system matrix of the unperturbed state (Equation (2.11) for the case of the general active layer model) and \mathbf{B}_0 is the matrix containing the linearized friction terms and the linear terms of the reference solution. For the general active layer model this is equal to:

$$\mathbf{B}_0 = \begin{bmatrix} 0 & 0 & 0 & 0 & 0 \\ \frac{C_t q_0^2}{b_0^2} & -2\frac{C_t q_0}{b_0^2} & 0 & 0 & 0 \\ 0 & 0 & 0 & 0 & 0 \\ 0 & 0 & 0 & 0 & 0 \\ \cdots & \cdots & \cdots & \cdots & \cdots \\ 0 & 0 & 0 & 0 & 0 \end{bmatrix}. \quad (\text{A.31})$$

Assuming a wave-type perturbation, $\mathbf{Q}' = \hat{\mathbf{Q}}(t)e^{ik_w x}$, where i is the imaginary unit and k_w is the wave number of the perturbation, we obtain:

$$\frac{\partial \hat{\mathbf{Q}}(t)}{\partial t} = -ik_w \left(\mathbf{A}_0 - \frac{\mathbf{B}_0}{ik_w} \right) \hat{\mathbf{Q}}(t). \quad (\text{A.32})$$

Using the properties of the eigenvalues we obtain the ordinary differential equation:

$$\frac{d\Phi}{dt} = -ik_w \lambda \Phi, \quad (\text{A.33})$$

where Φ and λ are an eigenvector and eigenvalue of matrix $\mathbf{A}_0 - \frac{\mathbf{B}_0}{ik_w}$, respectively. The perturbed solution grows exponentially with a factor $-ik_w \lambda t$. Thus, large wave numbers grow fastest. Note that friction matters in the characterization of the model. However, for large wave numbers the effect of friction vanishes. Thus, we can neglect friction in the analysis since we are interested in the perturbations that grow fastest.

A.6. Effect of Grain Size Distribution of the Aggradational Flux to the Substrate on the Elliptic Domain

In this appendix we assess the effect of the contribution of the bed load to the aggradational flux to the substrate on the elliptic domain of the active layer model assuming quasi-steady flow and two sediment fractions.

According to *Hoey and Ferguson* (1994), under aggradational conditions the sediment at the interface (f_k^I) is a combination of the sediment transport rate and the active layer sediment (Section 2.2.4). As such, the volume fraction content of the sediment transferred to the substrate can be written as:

$$f_k^I = \alpha F_{ak} + (1 - \alpha) p_k = \alpha (F_{ak} - p_k) + p_k, \quad (\text{A.34})$$

where $\alpha \in [0, 1]$ is a nondimensional parameter and $p_k \in [0, 1]$ is the fraction of sediment k in transport:

$$p_k = \frac{F_{ak} Q_{bk}}{\sum_{l=1}^N F_{al} Q_{bl}}. \quad (\text{A.35})$$

A

We now substitute Equation (A.34) in the discriminant of the eigenvalues of the two-fractions active layer model assuming steady flow, Equation (2.26):

$$\begin{aligned} \Delta_{\text{aIS}_2}(\alpha) = & \left[\frac{1}{uL_a} (Q_{b1} - Q_{b2})(F_{a1} - p_1) \right]^2 \alpha^2 \\ & + \frac{2}{uL_a} (Q_{b1} - Q_{b2})(F_{a1} - p_1) \left[\frac{1}{uL_a} (Q_{b1} - Q_{b2}) p_1 - \frac{Q_{b1}}{uL_a} - \frac{\psi}{1 - \text{Fr}^2} \right] \alpha \\ & + \frac{1}{uL_a} (Q_{b1} - Q_{b2}) p_1 \left[\frac{1}{uL_a} (Q_{b1} - Q_{b2}) p_1 - 2 \left(\frac{Q_{b1}}{uL_a} - \frac{\psi}{1 - \text{Fr}^2} \right) \right] \\ & + \frac{\psi}{1 - \text{Fr}^2} \left[\frac{\psi}{1 - \text{Fr}^2} + \frac{2}{uL_a} (2c_1(Q_{b1} - Q_{b2}) - Q_{b1}) \right] + \left(\frac{Q_{b1}}{uL_a} \right)^2, \end{aligned} \quad (\text{A.36})$$

which is a second degree equation on α .

For simplicity we rewrite Equation (A.36) as $a\alpha^2 + b\alpha + c$. The fact that $a > 0$ proves that the parabola is concave (direct because it is a power 2). A value of $-b/2a < 0$ implies that the discriminant increases with an increasing value of α :

$$\begin{aligned} \frac{-b}{2a} < 0 \Rightarrow b > 0 \Rightarrow & \frac{1}{uL_a} (Q_{b1} - Q_{b2}) p_1 - \frac{Q_{b1}}{uL_a} - \frac{\psi}{1 - \text{Fr}^2} < 0 \Rightarrow \\ & \frac{1}{uL_a} [Q_{b1}(p_1 - 1) - Q_{b2}p_1] - \frac{\psi}{1 - \text{Fr}^2} < 0, \end{aligned} \quad (\text{A.37})$$

which is always true. In the derivation we have used that:

$$Q_{b1} < Q_{b2} \text{ and } F_{a1} < p_1. \quad (\text{A.38})$$

Thus, a larger contribution of the active layer sediment decreases the likelihood that the model becomes elliptic.

We investigate the limit of the effect of α in the elliptic domain. To this end we consider the parameter settings in which the likelihood of ellipticity is higher under aggradational conditions: $\alpha = 0$ (the sediment transferred to the substrate has the same grain size distribution as the bed load), and $\xi_k = 1 \forall k$ (the sediment transport relation is as grain size selective as possible, Section 2.2.4). In this case the volume fraction content of fine sediment at the interface (f_1^I) can be written as:

$$f_1^I = \frac{F_{a1}}{F_{a1} + F_{a2}P}, \quad (\text{A.39})$$

where the nondimensional parameter $P \in (0, 1)$ is defined as:

$$P = \frac{Q_{b2}}{Q_{b1}} = \left(\frac{d_2(\theta_2 - \theta_c)}{d_1(\theta_1 - \theta_c)} \right)^{3/2}. \quad (\text{A.40})$$

The parameter c_1 , Equation (2.21), can be written as:

$$c_1 = \frac{F_{a1}}{F_{a1} + F_{a2}G}, \quad (\text{A.41})$$

where the nondimensional parameter $G \in (0, 1)$ is defined as:

$$G = \left(\frac{d_2(\theta_2 - \theta_c)}{d_1(\theta_1 - \theta_c)} \right)^{1/2}, \quad (\text{A.42})$$

thus, γ_1 (Equation (2.20)), can be written as:

$$\gamma_1 = \frac{F_{a1}F_{a2}(P - G)}{(F_{a1} + F_{a2}G)(F_{a1} + F_{a2}P)}. \quad (\text{A.43})$$

Note that $\gamma_1 < 0$ which implies that the model can be elliptic. Yet, γ_1 tends to 0 (thus minimizing the likelihood of ellipticity) for both a very fine or coarse active layer ($F_{a2} \rightarrow 0$ or $F_{a1} \rightarrow 0$) and also for a large or small effective Shields stress ($\theta - \theta_c \rightarrow \theta$ or $\theta - \theta_c \rightarrow 0$). Moreover, P and G have the same order of magnitude so its difference is small. This fact yields a small absolute value of γ_1 (close to zero) in comparison with a degradational case into a fine substrate in which the parameter γ_1 can be as negative as $-f_1^1$ (Stecca *et al.*, 2014).

A.7. Results of all Simulations of the Sensitivity Analysis

In this section we present the results of all simulations of Section 2.5.2. For clarity reasons, Figure 2.5a shows the simulations with a horizontal discretization length (Δx) equal to 0.1 m and a thickness of the substrate layers equal to 0.01 m and 0.10 m. Here Figure A.1a presents the results of all simulations. The intermediate values of the bookkeeping layer thickness follows the trend explained in Section 2.5.2. An increase in the bookkeeping layer thickness slightly increases the maximum amplitude of the oscillations in the solution. Similarly, Figure 2.5c shows the results for those simulations with a thickness of the bookkeeping layers (Δz) equal to 0.01 m only. Here Figure A.1c presents the results of all simulations. A thinly discretized domain causes oscillations to achieve its maximum amplitude value more upstream than if a coarse domain is used.

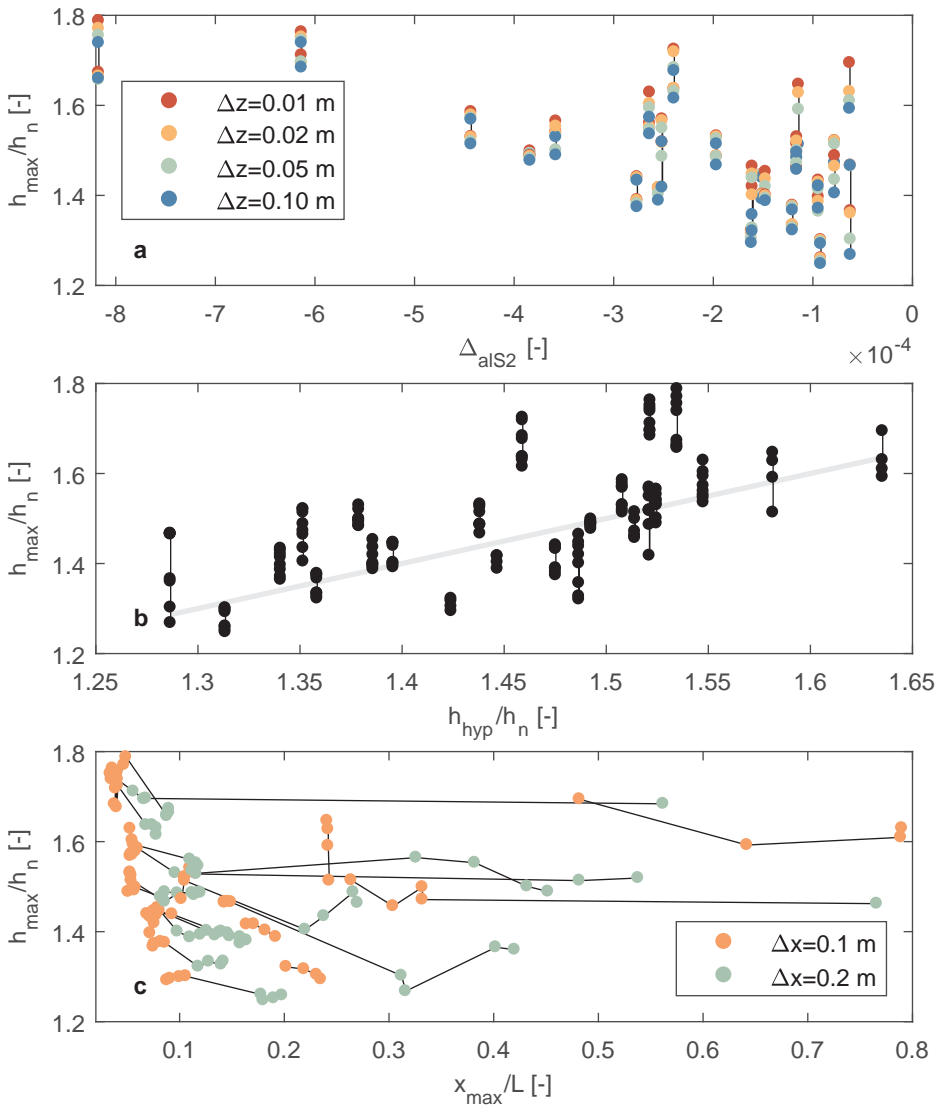


Figure A.1: Maximum flow depth h_{\max} (nondimensionalized by the normal flow depth h_n) that develops as a consequence of ellipticity. In (a) the maximum flow depth is plotted against the discriminant Δ_{als2} , Equation 2.26, for a thickness of the bookkeeping layers (Δz) equal to 0.01 m (red dots), 0.02 m (orange dots), 0.05 m (green dots), and 0.10 m (blue dots). The vertical black lines connect two simulations in which all parameters but Δz are the same. In (b) the maximum flow depth is plotted against the *hyperbolic flow depth* (h_{hyp}) nondimensionalized with the normal flow depth. Each black dot is the result of a simulation. The black lines connect simulations with the same physical parameters and the grey line shows the perfect agreement. In (c) the maximum flow depth is plotted against the distance from upstream at which the maximum flow depth occurs (x_{\max}) nondimensionalized with the length of the domain (L) for a horizontal discretization length equal to 0.1 m (orange dots) and 0.2 m (green dots). The black lines connect two simulations in which all parameters but Δx are the same.

A.8. Implications of an Unsteady Active Layer Thickness in the Ill-posed Domain

In this appendix we analyze the implications of considering that the active layer thickness varies as a function of the flow depth in a two-fractions case assuming negligible hiding. The assumption of negligible hiding allows for obtaining a simple expression of the derivative of the sediment transport with respect to the volume of sediment in the active layer (Stecca *et al.*, 2014):

$$\frac{\partial q_{bk}}{\partial M_{al}} = \begin{cases} \frac{Q_{bk}}{L_a} & \text{for } 1 \leq k = l \leq N-1 \\ 0 & \text{for } k \neq l \end{cases}, \quad (\text{A.44})$$

and:

$$\frac{\partial q_b}{\partial M_{al}} = \frac{Q_{bl} - Q_{bN}}{L_a}, \quad (\text{A.45})$$

The implications of this assumption are studied in Section 2.4.1.

The derivative of the sediment transport rate with respect to the active layer thickness is:

$$\frac{\partial q_{bk}}{\partial L_a} = -\frac{q_{bk}}{L_a} \quad \text{for } 1 \leq k \leq N-1, \quad (\text{A.46})$$

and:

$$\frac{\partial q_b}{\partial L_a} = -\frac{q_b - Q_{bN}}{L_a}. \quad (\text{A.47})$$

The two-fractions active layer model considering a variable active layer thickness has 5 dependent variables. We obtain the nondimensional characteristic polynomial ($p(\lambda)$) of the model by equating the determinant of the system matrix (Equation 2.11) to zero and dividing it by u^5 :

$$p(\lambda) = \lambda n(\lambda), \quad (\text{A.48})$$

which implies that the roots of p are the roots of n and 0 where:

$$n(\lambda) = m(\lambda) - d(\lambda), \quad (\text{A.49})$$

being m a fourth order polynomial and d a first order polynomial:

$$m(\lambda) = m_c(\lambda) + m_v(\lambda), \quad (\text{A.50})$$

and

$$d(\lambda) = d_c(\lambda) + d_v(\lambda), \quad (\text{A.51})$$

where

$$d_c(\lambda) = \gamma_1 \frac{\psi}{Fr^2} \frac{Q_{b1} - Q_{b2}}{uL_a} (\lambda - 1), \quad (\text{A.52})$$

$$d_v(\lambda) = \beta f_1^I \frac{1}{Fr^2} \frac{Q_{b1} - Q_{b2}}{uL_a} \left(\lambda - \frac{F_{a1}}{f_1^I} \lambda_{s1} \right), \quad (\text{A.53})$$

$$m_c(\lambda) = (\lambda - \lambda_{s1}) V(\lambda), \quad (\text{A.54})$$

$$m_v(\lambda) = (\lambda - \lambda_{s1}) \beta F_{a1} \frac{Q_{b1} - Q_{b2}}{uL_a} \frac{1}{Fr^2}, \quad (\text{A.55})$$

where the parameter β is defined as:

$$\beta = a_L b_L h^{b_L - 1}, \quad (\text{A.56})$$

and $V(\lambda)$ refers to the Saint-Venant-Exner characteristic polynomial:

$$V(\lambda) = \frac{\psi}{Fr^2} (1 - \lambda) + \lambda \left((\lambda - 1)^2 - \frac{1}{Fr^2} \right). \quad (\text{A.57})$$

λ_{s1} is the sorting celerity defined in Equation (2.28). Assuming negligible hiding we obtain:

$$\lambda_{s1} = \frac{Q_{b1}(1 - f_1^I) + f_1^I Q_{b2}}{uL_a}. \quad (\text{A.58})$$

The subscript v indicates that the term is only present if we consider a variable active layer thickness while the subscript c indicates that the term in question is also obtained if the active layer thickness is constant.

Note that in aggradational conditions or in degradational conditions into a substrate coarser than the active layer the slope of d is positive and its root (d_0) is larger than λ_{s1} since $\lambda_{s1} < 1$.

A sufficient condition that guarantees that the polynomial n has four real roots (the system thus being hyperbolic) is that the slope of a line with the same root as d that crosses m at $x = 0$ has a larger slope than d . This is mathematically written as:

$$d' < \frac{-m(0)}{d_0} \Rightarrow \frac{\psi \frac{uL_a}{Q_{b1} - Q_{b2}} + \beta F_{a1} \frac{\lambda_{s1} uL_a}{(Q_{b1} - Q_{b2})\gamma_1}}{\psi \frac{uL_a}{Q_{b1} - Q_{b2}} + \beta F_{a1}} < \frac{\lambda_{s1} uL_a}{(Q_{b1} - Q_{b2})\gamma_1}, \quad (\text{A.59})$$

where the apostrophe indicates a derivative and the subscript 0 indicates the root. Inequality (A.59) is true provided that:

$$1 < \frac{\lambda_{s1} uL_a}{(Q_{b1} - Q_{b2})\gamma_1} = \frac{Q_{b1}(1 - f_1^I) + f_1^I Q_{b2}}{(Q_{b1} - Q_{b2})\gamma_1}. \quad (\text{A.60})$$

We know that Inequality (A.60) is true since:

$$\gamma_1 < 1 - f_1^I < \frac{Q_{b1}(1 - f_1^I) + f_1^I Q_{b2}}{(Q_{b1} - Q_{b2})} \Rightarrow 1 < \frac{1 - f_1^I}{\gamma_1} < \frac{Q_{b1}(1 - f_1^I) + f_1^I Q_{b2}}{(Q_{b1} - Q_{b2})\gamma_1}, \quad (\text{A.61})$$

where the first condition was proven by *Stecca et al.* (2014).

Thus, in aggradational conditions or in degradational conditions into a substrate coarser than the active layer, the system of equations formed by the unsteady flow equations in combination with the active layer model for two sediment size fractions considering an unsteady active layer thickness proportional to dune height is hyperbolic.

In degradational conditions into a substrate finer than the active layer the line d_v always has a positive slope and its root is smaller than λ_{s1} since $F_{a1} < f_1^1$ by definition. If the root of d_v is smaller than the intersection between d_c and m , d_v is positive in the domain where d_c intersects m and thus $d > d_c$. In degradational conditions into a substrate finer than the active layer, the volume fraction content of fine sediment in the active layer is small ($F_{a1} \ll 1$). Thus, we assume that m does not appreciably change by considering $\beta \neq 0$. Worded differently, we assume $m \approx m_c$. Using this assumption, with respect to a situation where the effects of variable active layer thickness are not considered ($d_v = 0$), a variable active layer thickness increases the likelihood that the model is elliptic.

Thus,

1. if $\lambda_{s1} < \lambda_b$, the root of d_v is smaller than the intersection between d_c and m_v , and a variable active layer thickness increases the likelihood that the model is elliptic.
2. if $\lambda_{s1} > \lambda_b$ but $\lambda_{s1}F_{a1}/f_1^1 < \lambda_b$, the root of d_v is smaller than the intersection between d_c and m_v , and a variable active layer thickness increases the likelihood that the model is elliptic.

To study the relative importance of the cases in which $\lambda_b < \lambda_{s1}F_{a1}/f_1^1$ we study a case where the characteristic grain sizes of the fine and coarse sediment are equal to 0.001 m and 0.01 m, the nondimensional friction coefficient equals 0.01, and the sediment transport rate is computed using the *Meyer-Peter and Müller (1948)* transport relation. We vary the flow velocity between 0.5 m/s to 5 m/s, the flow depth between 0.5 m to 5 m, and the volume fraction content in the active layer and at the interface between 0 to 1. We analyze the cases which provide subcritical flow and degradation into a fine substrate obtaining 39.253.500 cases. The active layer thickness is set a function of the flow depth using Equation (2.2) with parameters $a_L = 0.2 \text{ m}^{0.1}$ and $b_L = 0.9$.

In Figure A.2 we plot the parameter $\lambda_{s1} - \lambda_b$ with respect to $\frac{F_{a1}}{f_1^1} \lambda_{s1} - \lambda_b$ for all situations. Note that the majority of cases fall into the domain in which considering an unsteady active layer thickness increases the likelihood of obtaining an ill-posed model. The green dots mark those cases which are hyperbolic. Red dots identify elliptic cases, and blue dots mark those situations which are elliptic if the active layer is considered unsteady only. We do not find a case in which the model is hyperbolic if the active layer is unsteady but elliptic if it is constant.

Based on the histograms we note that although a variable active layer thickness increases the domain of ill-posedness, the main cause of ill-posedness is due to the active layer model itself and not to the unsteady active layer thickness.

The assumption that m does not appreciably change by considering $\beta \neq 0$ is sustained by the fact that in none of the considered cases, a situation that is hyperbolic for a constant active layer thickness becomes elliptic for a variable active layer thickness.

A

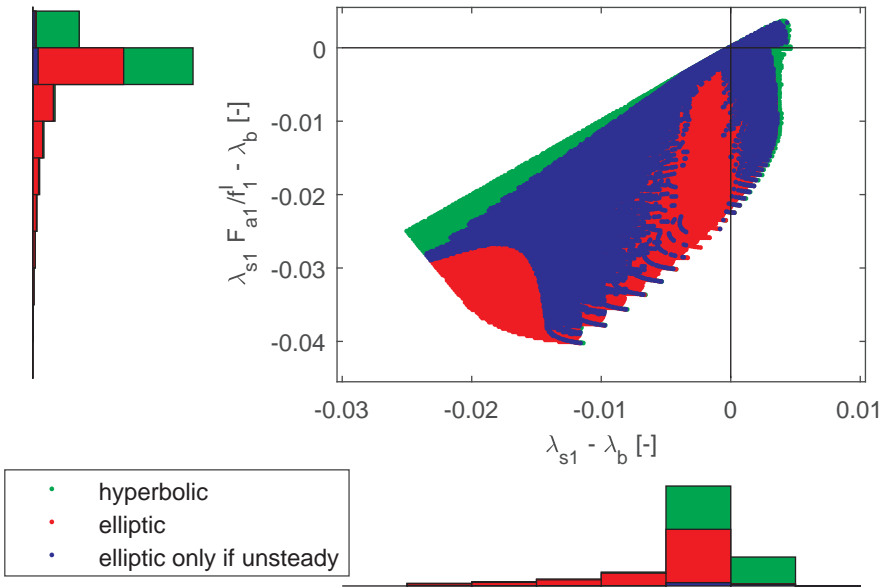


Figure A.2: Parameter $\lambda_{s1} - \lambda_b$ with respect to $\frac{E_{a1}}{f_1} \lambda_{s1} - \lambda_b$ for 39.253.500 cases. The majority of cases fall into the domain in which we prove that an unsteady active layer thickness increases the likelihood of the model being elliptic. In the remaining cases an unsteady active layer thickness also increases the likelihood although we do not prove it. Nevertheless, only a small percentage of cases become elliptic strictly due to the unsteady active layer thickness.

B

Supplementary material to Chapter 3

*Who do you look up the most?
People who think for themselves and spread joy in the world.*

Olle Eksell

Antes de hablar del agua hay que haberla contemplado mucho.

Claudio Rodríguez (see e.g. Yubero-Ferrero (1998))

This appendix provides the supplementary material to Chapter 3 “Ill-posedness in modelling 2D morphodynamic problems: Effect of bed slope and secondary flow”. In Section B.1 we explain the limitations of the eddy viscosity coefficient derived by *Elder* (1959). In Section B.2 we present the closure relations to compute the sediment transport rate. We prove that the two-dimensional morphodynamic model presented in Section 3.2 may be ill-posed due to not accounting for diffusion in the equation modelling the transport of the secondary flow intensity (Section B.3) and due to not accounting for the effect of the bed slope on the sediment transport direction under unisize conditions (Section B.4). In Section B.5 we present the details of the computation of the domain in which the model accounting for mixed-size sediment is well-posed regarding the effect of the bed slope.

B.1. Eddy Viscosity

In general terms, given the anisotropy of the flow field, the diffusion tensor has non-diagonal terms and the diagonal terms are not equal (i.e., the diffusion coefficient in the streamwise direction ν_s is different than in the transverse direction ν_n). The non-diagonal terms become significant close to corners (*Fischer*, 1973) but far from corners the diagonal terms dominate. *Elder* (1959) derived an eddy viscosity coefficient in the streamwise and lateral direction assuming a logarithmic profile for the primary flow:

$$\nu_s = \left(\frac{0.4041}{\chi^3} + \frac{1}{6}\chi \right) hu^*, \quad (\text{B.1})$$

$$\nu_n = \frac{1}{6}\chi hu^*. \quad (\text{B.2})$$

Elder neglected the effect of the viscous sublayer, which causes his analytical expression to be a lower limit of the diffusion coefficient (*Fischer*, 1967).

Several researchers (e.g. *Erdogan and Chatwin*, 1967; *Simons and Albertson*, 1963; *Fischer*, 1969; *Holley*, 1971; *Fischer*, 1973; *Kyong and Il*, 2016) propose values for the diffusion coefficient that are significantly larger than the one derived by *Elder* (1959). These values are used, for instance, by *Parker* (1978); *Ikedo and Nishimura* (1985) and *Van Prooijen and Uijtewaal* (2002). These values of the diffusion coefficient are derived from experimental measurements and implicitly account for the enhanced momentum redistribution due to secondary flow that we account for by means of the dispersive stresses.

In numerical simulations resolving the secondary flow, the diffusion coefficients derived by *Elder* (1959) are valid if the grid is of the order of magnitude of the flow depth (assuming that the relevant turbulent processes scale with the flow depth). Otherwise the numerical grid filters out significant two-dimensional turbulent motions that need to be accounted for in the closure model (*Talstra*, 2011). In our numerical runs the grid cell size is always smaller than the flow depth.

B.2. Magnitude of the Sediment Transport Rate

The module of the specific sediment transport rate of size fraction k , q_{bk} [m^2/s], has a direction given by the angle φ_{sk} [rad]:

$$(q_{b_{xk}}, q_{b_{yk}}) = q_{bk} (\cos \varphi_{sk}, \sin \varphi_{sk}). \quad (\text{B.3})$$

The magnitude of the sediment transport rate is equal to:

$$q_{bk} = F_{ak} \frac{\sqrt{g R d_k^3}}{1 - p} q_{bk}^* \tag{B.4}$$

where p is the porosity and $q_{bk}^* [-]$ is a nondimensional sediment transport rate (*Einstein*, 1950) dependent on the *Shields* (1936) stress:

$$\theta_k = \frac{C_f \left(\frac{Q}{b}\right)^2}{g R d_k} \tag{B.5}$$

The parameter $R = \rho_s / \rho_w - 1 [-]$ is the submerged sediment density, $\rho_s = 2650 \text{ kg/m}^3$ is the sediment density and $\rho_w = 1000 \text{ kg/m}^3$ is the water density. To compute the nondimensional sediment transport rate we use a fractional form (*Blom et al.*, 2016, 2017b) of the relation proposed by *Engelund and Hansen* (1967) neglecting form drag:

$$q_{bk}^* = \frac{0.05}{C_f} \theta_k^{5/2} \tag{B.6}$$

and the relation including a nondimensional critical shear stress $\theta_c [-]$ proposed by *Ashida and Michiue* (1971):

$$q_{bk}^* = 17 (\theta_k - \xi_k \theta_c) \left(\sqrt{\theta_k} - \sqrt{\xi_k \theta_c} \right) \tag{B.7}$$

The parameter $\xi_k [-]$ is the hiding factor that accounts for the fact that fine sediment in a mixture hides behind larger grains and a coarse sediment in a mixture is more exposed than in unisize coarse sediment (*Einstein*, 1950). *Ashida and Michiue* (1971) proposes $\theta_c = 0.05$ and the relation:

$$\xi_k = \begin{cases} 0.843 \left(\frac{d_k}{D_m}\right)^{-1} & \text{for } \frac{d_k}{D_m} \leq 0.4 \\ \left(\frac{\log_{10}(19)}{\log_{10}(19 \frac{d_k}{D_m})}\right)^2 & \text{for } \frac{d_k}{D_m} > 0.4 \end{cases} \tag{B.8}$$

where D_m is a characteristic mean grain size of the sediment mixture.

B.3. Proof of Ill-posedness Due to Secondary Flow without Diffusion

In this section we prove that the model based on the Shallow Water Equations accounting for secondary flow without diffusion is ill-posed.

The system of equations is composed of the first four rows and columns of the full system of equations in Equation (3.24). Neglecting diffusive processes matrices \mathbf{D}_{x0} and \mathbf{D}_{y0} are equal to 0. As we are interested in the short-wave domain, friction can be neglected. The resulting matrix \mathbf{M}_0 of the linearised eigenvalue problem (Equation (3.33)) is:

$$\mathbf{M}_0 = \mathbf{A}_{x0} k_{wx} + \mathbf{A}_{y0} k_{wy} \tag{B.9}$$

We compute the fourth order characteristic polynomial of matrix \mathbf{M}_0 . The roots of the characteristic polynomial are the eigenvalues (i.e., the angular frequencies ω in Equation (3.31)). The discriminant of a fourth order polynomial $p(\omega) = p_4\omega^4 + p_3\omega^3 + p_2\omega^2 + p_1\omega + p_0 = 0$ is equal to (Beeler *et al.*, 1972):

$$\begin{aligned} \Delta_4 = & (p_1^2 p_2^2 p_3^2 - 4p_1^3 p_3^3 - 4p_1^2 p_2^3 p_4 + 18p_1^3 p_2 p_3 p_4 - 27p_1^4 p_4^2 + 256p_0^3 p_4^3) \\ & + p_0(-4p_2^3 p_3^2 + 18p_1 p_2 p_3^3 + 16p_2^4 p_4 - 80p_1 p_2^2 p_3 p_4 - 6p_1^2 p_3^2 p_4 + 144p_1^2 p_2 p_4^2) \\ & + p_0^2(-27p_3^4 + 144p_2 p_3^2 p_4 - 128p_2^2 p_4^2 - 192p_1 p_3 p_4^2). \end{aligned} \quad (\text{B.10})$$

We find that the discriminant of the characteristic polynomial is:

$$\Delta_4 = \frac{16gb^2 T^2 \beta_u}{L_1} k_{\text{wx}}^2 (k_{\text{wx}}^2 - k_{\text{wy}}^2), \quad (\text{B.11})$$

where $\beta_u = \beta^* q_x^2 / b^2$ and:

$$T = L_{1g} \left[L_1 g (k_{\text{wx}}^2 + k_{\text{wy}}^2)^2 + \beta_u (6k_{\text{wx}}^2 k_{\text{wy}}^2 - 2k_{\text{wx}}^4) \right] + \beta_u^2 k_{\text{wx}}^4. \quad (\text{B.12})$$

As the coefficients of the characteristic polynomial $p(\omega)$ are all real, a positive discriminant indicates that either all the roots are real or all the roots are complex. A negative discriminant indicates that there are two real and two complex roots. The complex roots come in pairs of complex conjugates. For this reason, if the discriminant is negative there exist an eigenvalue with a positive imaginary component. As the discriminant is negative for $k_{\text{wx}} < k_{\text{wy}}$ independently from the wave number, there exists always a region of growth. This implies that the model is ill-posed.

B.4. Proof of Ill-posedness Due to Lack of Bed Slope Effect under Unisize Conditions

In this section we prove that the model based on the Shallow Water Equations without accounting for the effect of secondary flow in combination with the Exner (1920) equation to model bed elevation changes is ill-posed if the effect of the bed slope on the direction of the sediment transport is not taken into consideration.

The system of equations is composed of the first three and the fifth rows and columns of the system of equations in Equation (3.24). Neglecting diffusive processes in the momentum equations and the effect of the bed slope, matrices \mathbf{D}_{x0} and \mathbf{D}_{y0} are equal to $\mathbf{0}$. The system of equations has 4 unknowns (h , q_x , q_y , and η). The unknowns are coupled meaning that a change in bed elevation influences the flow and vice versa. The celerity of perturbations associated with the flow variables (i.e., h , q_x , and q_y) are orders of magnitude larger than the celerity of perturbations in bed elevation if the Froude number is sufficiently small ($\text{Fr} \lesssim 0.7$ (De Vries, 1965, 1973; Lyn and Altinakar, 2002)). Under this condition we can decouple the system and consider steady flow to study the propagation of perturbations in bed elevation (i.e., quasi-steady flow assumption (De Vries, 1965; Cao and Carling, 2002a; Colombini and Stocchino, 2005)). In this manner we reduce the

number of unknowns to one (η), which means that there is only one eigenvalue (ω). We obtain ω equating to 0 the determinant of matrix:

$$\mathbf{R} = \begin{bmatrix} 0 & 0 & 0 & 0 \\ 0 & 0 & 0 & 0 \\ 0 & 0 & 0 & 0 \\ 0 & 0 & 0 & \omega \end{bmatrix} - \mathbf{M}_0 \quad (\text{B.13})$$

The growth rate (the imaginary part of ω) is:

$$\omega_i = \frac{q_b C_f k_{wx}^2}{k_{wx}^2 \omega_2^2 + \omega_1^2} \left(\omega_3 + (n-1) k_{wy}^4 \right), \quad (\text{B.14})$$

where ω_1 , ω_2 , and ω_3 are second degree polynomials on k_{wy} :

$$\omega_1 = C_f \left[(1 - 4\text{Fr}^2) k_{wx}^2 + 2k_{wy}^2 \right], \quad (\text{B.15})$$

$$\omega_2 = b_1 + (1 - \text{Fr}^2) k_{wx}^2 + k_{wy}^2, \quad (\text{B.16})$$

$$\omega_3 = -3\text{Fr}^2 n k_{wx}^4 - b_1 n k_{wx}^2 + \left[n(2 - \text{Fr}^2) - (2 + \text{Fr}^2) \right] k_{wx}^2 k_{wy}^2 + b_1 (n-3) k_{wy}^2, \quad (\text{B.17})$$

where b_1 is:

$$b_1 = \frac{3C_f^2 \text{Fr}^2}{h^2}. \quad (\text{B.18})$$

Parameter n is the degree of non-linearity of the sediment transport relation (*Mosselman et al., 2008*):

$$n = \frac{Q}{q_b} \frac{\partial q_b}{\partial Q}, \quad (\text{B.19})$$

which is larger than 1. For instance, $n = 5$ in the relation developed by *Engelund and Hansen (1967)* and $n > 3$ in the one by *Meyer-Peter and Müller (1948)*. In general $n > 3$ for the sediment transport relation to be physically realistic (*Mosselman, 2005*).

For k_{wy} tending to infinity, parameter ω_3 becomes negligible with respect to $(n-1)k_{wy}^4$. As all other terms in Equation (B.14) are positive, for a large wave number the growth rate is positive which implies that the model is ill-posed.

B.5. Well-Posed Domain under Mixed-Size Sediment Conditions

In this section we show that the Shallow Water Equations in combination with the active layer model (*Hirano, 1971*) used to account for mixed-size sediment morphodynamics may yield an ill-posed model depending on the closure relation used to account for the effect of the bed slope on the sediment transport direction.

We consider a model with two sediment size fractions. The system of equations is composed of the first three, the fifth and the sixth rows and columns of the full system

of equations in Equation (3.24). We neglect diffusive processes in the momentum equations. The system of equations has 5 unknowns (b , q_x , q_y , η , and M_{a1}). We consider that the Froude number is sufficiently small such that the quasi-steady approximation is valid (Appendix B.4) and we assume that the celerity associated with changes in the grain size distribution of the bed surface are of the same order of magnitude as the celerity of bed elevation changes (Ribberink, 1987; Sieben, 1997; Stecca et al., 2016). Under these conditions it is valid to decouple the system and consider steady flow to study the propagation of perturbations in bed elevation and bed surface grain size distribution. In this manner we reduce the number of unknowns to two (η and M_{a1}), which means that there are two angular frequencies to find. We obtain ω equating to 0 the determinant of matrix:

$$\mathbf{R} = \begin{bmatrix} 0 & 0 & 0 & 0 & 0 \\ 0 & 0 & 0 & 0 & 0 \\ 0 & 0 & 0 & 0 & 0 \\ 0 & 0 & 0 & \omega & 0 \\ 0 & 0 & 0 & 0 & \omega \end{bmatrix} - \mathbf{M}_0 \quad (\text{B.20})$$

We define a set of physically meaningful parameters useful to simplify the expression of the growth rate. Subscripts k and l refer to the grain size fraction while the subscript j refers to the direction (i.e., x and y). The parameters are a generalization of the parameters used by Stecca et al. (2014) and Chavarrias et al. (2018a) to the x and y direction.

Parameter ψ_j [–] represents the sediment transport intensity (e.g. De Vries, 1965; Lyn and Altinakar, 2002; Stecca et al., 2014) and ranges between 0 (no sediment transport) and $\mathcal{O}(10^{-2})$ (high sediment discharge):

$$\psi_j = \frac{\partial q_{bj}}{\partial q_j}. \quad (\text{B.21})$$

Parameter $c_{jk} \in [0, 1]$ [–] represents the sediment transport intensity of fraction k relative to the total sediment transport intensity:

$$c_{jk} = \frac{1}{\psi_j} \frac{\partial q_{bjk}}{\partial q_j}. \quad (\text{B.22})$$

Parameter γ_{jk} [–] represents the sediment transport intensity of fraction k relative to the fraction content of sediment of fraction k at the interface between the active layer and the substrate:

$$\gamma_{jk} = c_{jk} - f_k^1, \quad (\text{B.23})$$

Parameter χ_{jk} [–] represents the nondimensional rate of change of the total sediment transport rate with respect to the change of volume of sediment of size fraction k in the active layer:

$$\chi_{jk} = \frac{1}{u_j} \frac{\partial q_{bj}}{\partial M_{ak}}. \quad (\text{B.24})$$

Parameter $d_{jk,l}$ [–] represents the nondimensional rate of change of the sediment transport rate of size fraction l with respect to the volume of sediment of size fraction k in the active layer:

$$d_{jk,l} = \frac{1}{u_j \chi_{jk}} \frac{\partial q_{bjl}}{\partial M_{ak}}. \quad (\text{B.25})$$

Parameter $\mu_{jk,l}$ [–] represents the rate of change of the sediment transport rate with respect to the volume of sediment in the active layer relative to the fraction content of sediment of fraction k at the interface between the active layer and the substrate:

$$\mu_{jk,l} = d_{jk,l} - f_k^1. \quad (\text{B.26})$$

Parameter $R_j < 0$ [m^2/s] represents the effect of the bed slope on the direction of the sediment transport rate:

$$R_j = \frac{\partial q_{bj}}{\partial s_j}, \quad (\text{B.27})$$

where $s_j = \partial \eta / \partial j$. Parameter r_{jk} [–] represents the effect of the bed slope on the direction of the sediment transport rate of fraction k relative to the total effect:

$$r_{jk} = \frac{1}{R_j} \frac{\partial q_{bjk}}{\partial s_j}. \quad (\text{B.28})$$

Parameter l_{jk} [–] represents the effect of the bed slope on the direction of the sediment transport rate of fraction k relative to the fraction content of sediment at the interface between the active layer and the substrate:

$$l_{jk} = r_{jk} - f_k^1. \quad (\text{B.29})$$

The largest of the two growth rates (i.e., the largest imaginary part of the two eigenvalues ω of the system) is:

$$\omega_i = \frac{1}{2} \left(\frac{\sqrt{2}}{2} \sqrt{f_1} - \sqrt{f_2} \right), \quad (\text{B.30})$$

where:

$$f_1 = \sqrt{m_1^2 + m_2} - m_1, \quad (\text{B.31})$$

and:

$$f_2 = R_y^2 k_{wy}^4. \quad (\text{B.32})$$

When parameter f_1 is larger than $2f_2$, $\omega_i > 0$ and perturbations grow. Parameter f_1 becomes large with respect to f_2 when parameter m_2 becomes large with respect to m_1 where:

$$m_1 = k_{wx}^2 u^2 a_3 - f_2, \quad (\text{B.33})$$

and:

$$m_2 = 4k_{wx}^2 u^2 f_2 o^2. \quad (\text{B.34})$$

Focusing on the bed slope effect, for a given value of f_2 (i.e., a given value of R_y), parameter m_2 becomes large with respect to m_1 when parameter o becomes large, where:

$$o = a_1 + 2\chi_{x1}(r_{y1} - d_{x1,1}). \quad (\text{B.35})$$

Thus, the growth rate of perturbations is prone to be positive when the absolute value of $r_{y1} - d_{x1,1}$ increases. The parameters a_m for $m = 1, 2, 3$ are:

$$a_1 = e_x + e_y + \chi_{x1}\mu_{x1,1}, \quad (\text{B.36})$$

$$a_2 = \gamma_{x1}e_x + \gamma_{y1}e_y - \mu_{x1,1}e_x - \mu_{x1,1}e_y, \quad (\text{B.37})$$

$$a_3 = a_1^2 + 4\chi_{x1}a_2. \quad (\text{B.38})$$

The parameters e_j for $j = x, y$ are:

$$e_x = \psi_x \frac{k_{wx}^2}{(1 - \text{Fr}^2)k_{wx}^2 + k_{wy}^2}, \quad (\text{B.39})$$

$$e_y = \psi_y \frac{k_{wy}^2}{(1 - \text{Fr}^2)k_{wx}^2 + k_{wy}^2}. \quad (\text{B.40})$$

We compute the limit of the growth rate (Equation (B.30)) for k_{wx} and k_{wy} tending to infinity:

$$\omega_i^{\text{lim}} = \alpha_1 (r_{y1} - d_{x1,1})^2 + \alpha_2 (r_{y1} - d_{x1,1}) + \alpha_3, \quad (\text{B.41})$$

where:

$$\alpha_1 = \frac{-u^2\chi_{x1}}{R_y}\chi_{x1}, \quad \alpha_2 = \frac{-u^2\chi_{x1}}{R_y}a_1^{\text{lim}}, \quad \alpha_3 = \frac{u^2\chi_{x1}}{R_y}a_2^{\text{lim}}, \quad (\text{B.42})$$

where the superscript lim indicates that these are the limit values and:

$$e_x^{\text{lim}} = \frac{\psi_x}{2 - \text{Fr}^2}, \quad (\text{B.43})$$

$$e_y^{\text{lim}} = \frac{\psi_y}{2 - \text{Fr}^2}. \quad (\text{B.44})$$

As $R_y < 0$ and $\chi_{x1} > 0$, the mathematical character of the system of equations is given by the sign of the second degree polynomial with variable $(r_{y1} - d_{x1,1})$. The fact that $\alpha_1 > 0$ (the factor of the squared term) indicates that the model is well-posed when $r_{y1}^- < r_{y1} < r_{y1}^+$ where:

$$r_{y1}^\pm = \frac{1}{2\chi_{x1}} \left(-a_1^{\text{lim}} \pm \sqrt{a_1^{\text{lim}^2} + 4\chi_{x1}a_2^{\text{lim}}} \right) + d_{x1,1}. \quad (\text{B.45})$$

C

Supplementary material to Chapter 4

*To argue with a person who has renounced the use of reason
is like administering medicine to the dead.*

Paine (1776)

Chance is the name we give to what we choose to ignore.

Voltaire (see e.g. Jiménez (2018))

This appendix provides the supplementary material to Chapter 4 “A regularization strategy for modelling mixed-sediment river morphodynamics”. The document is organized as follows. In Section C.1 we present the model equations. In Section C.2 we study the possible values of the regularization parameters by imposing that the regularized active layer model is mass conservative. The parameters of the experiment conducted by *Ribberink* (1987) are shown in Section C.3. In Section C.4 we show that the eigenvalues of the regularized active layer model are always positive. This guarantees that the regularized model is well-posed. In Section C.5 we describe the numerical technique used in solving the system of equations. In Section C.6 we describe the preparatory laboratory experiments. These experiments are used to calibrate the friction coefficient, estimate a reasonable value of the active layer thickness, study the initial condition of the laboratory experiments conducted under conditions in which the active layer model is ill-posed, and select a sediment transport relation. In Section C.7 we calibrate the numerical model applied to reproduce the laboratory experiments. In Section C.8 we derive the celerity at which tracer sediment propagates downstream, which is useful to select the thickness of the active layer.

C.1. Model Equations

In this section we present the system of equations for modeling mixed-sediment river morphodynamics. In Section C.1.1 we present the flow equations. In Section C.1.2 we present the active layer model (*Hirano*, 1971). A simplified active layer model is presented in Section C.1.3. In Section C.1.4 we show the closure relations. In Section C.1.5 we present the system of equations in matrix-vector formulation.

C.1.1. Flow Equations

We consider a one-dimensional mixture of water and sediment flowing over a mobile bed. A set of partial differential equations that accounts for the interactions between sediment and water is found by applying mass and momentum conservation principles for the mixture of sediment and water (e.g., *Garegnani et al.*, 2011; *Greco et al.*, 2012). The complete system of equations reduces to the Saint-Venant-Exner model (i.e., clear water approximation) under low sediment concentrations ($c = q_b/q < 0.006$, where q_b [m^2/s] and q [m^2/s] are the sediment transport rate and flow discharge per unit width, respectively (e.g., *Garegnani et al.*, 2011, 2013)). In the remaining we will assume that the clear water approximation is valid.

The flow is modeled using the *Saint-Venant* (1871) equations:

$$\frac{\partial h}{\partial t} + \frac{\partial q}{\partial x} = 0, \quad (\text{C.1})$$

$$\frac{\partial q}{\partial t} + \frac{\partial(q^2/h + gh^2/2)}{\partial x} + gh \frac{\partial \eta}{\partial x} = -ghS_f, \quad (\text{C.2})$$

where t [s] denotes the time coordinate, x [m] the streamwise coordinate, h [m] the flow depth, g [m/s^2] the acceleration due to gravity, η [m] the bed elevation, and S_f [–] the friction slope.

The flow equations can be further simplified assuming steady flow. Under this condition the conservation of water mass and momentum reduce to a spatially constant discharge, and the backwater equation:

$$\frac{\partial h}{\partial x} = \frac{-1}{1 - Fr^2} \frac{\partial \eta}{\partial x} - \frac{S_f}{1 - Fr^2}, \quad (C.3)$$

where $Fr = q/\sqrt{gb^3}$ is the Froude number.

C.1.2. Active Layer Model

To model changes in bed elevation we assume that the sediment transport rate adapts instantaneously to changes in bed shear stress. Spatial and/or temporal adaptation to capacity load (*Bell and Sutherland, 1983; Phillips and Sutherland, 1989, 1990*) is not considered. Neglecting mechanisms such as subsidence and uplift (*Paola and Voller, 2005*), and assuming a constant bed porosity, we obtain the *Exner (1920)* equation:

$$\frac{\partial \eta}{\partial t} + \frac{\partial q_b}{\partial x} = 0, \quad (C.4)$$

where for simplicity the sediment transport rate includes the pores.

The sediment phase is composed of a mixture of N non-cohesive sediment size fractions. Each fraction is characterized by a grain size d_k [m] where k is an index identifying a size fraction. The total sediment transport rate per unit width is the sum of the sediment transport rate of size fraction k , q_{bk} [m²/s]:

$$q_b = \sum_{k=1}^N q_{bk}. \quad (C.5)$$

The conservation of the volume of sediment of size fraction k in the active layer per unit of bed area ($M_{ak} = F_{ak}L_a$ [m]) is expressed mathematically as (*Hirano, 1971*):

$$\frac{\partial M_{ak}}{\partial t} + f_k^I \frac{\partial (\eta - L_a)}{\partial t} + \frac{\partial q_{bk}}{\partial x} = 0 \quad \text{for } 1 \leq k \leq N-1, \quad (C.6)$$

where $F_{ak} \in [0, 1]$ [-] is the volume fraction content of size fraction k in the active layer, $f_k^I \in [0, 1]$ [-] is the volume fraction content of size fraction k at the interface between the active layer and the substrate, and L_a [m] is the active layer thickness. By definition,

$$\sum_{k=1}^N F_{ak} = 1, \quad \sum_{k=1}^N f_k^I = 1. \quad (C.7)$$

From the first constrain in Equation (C.7) one obtains the change of the volume of sediment in the active layer of the N th grain size with time.

The system is complete with an equation for the conservation of mass in the substrate. Yet, this equation is linearly dependent on the *Exner (1920)* and *Hirano (1971)* equations which implies that it does not play a role in the mathematical character of the system (*Stecca et al., 2014; Chavarrías et al., 2018a*).

C.1.3. Simplified Active Layer Model

To simplify the system of equations we replace the $N - 1$ equations that account for the change in bed surface volume fraction content of the N fractions by one equation that models the average grain size following the approach of *Ribberink* (1987). We multiply each regularized active layer equation by its characteristic grain size and we add all the equations:

$$\alpha \frac{\partial D_{\text{ma}}}{\partial t} - \frac{D_{\text{m}}^{\text{I}}}{L_{\text{a}}} \frac{\partial q_{\text{b}}}{\partial x} + \frac{1}{L_{\text{a}}} \sum_{k=1}^N d_k \frac{\partial q_{\text{bk}}}{\partial x} = 0 \quad (\text{C.8})$$

where $D_{\text{ma}} = \sum_{k=1}^N d_k F_{\text{ak}}$ [m] is the mean grain size of the sediment in the active layer and $D_{\text{m}}^{\text{I}} = \sum_{k=1}^N d_k f_k^{\text{I}}$ [m] is the mean grain size of the sediment at the interface between the active layer and the substrate. The mean grain size is computed arithmetically as it is a necessary step to obtain an approximate equation. Yet, we consider that the mean grain size is better approximated assuming the grain size distribution to be logarithmically distributed.

We write the sediment transport rate q_{bk} as a function of the flow depth h and the mean grain size of the sediment in the active layer D_{ma} such that:

$$\frac{\partial q_{\text{bk}}}{\partial x} = \frac{\partial q_{\text{bk}}}{\partial h} \frac{\partial h}{\partial x} + \frac{\partial q_{\text{bk}}}{\partial D_{\text{ma}}} \frac{\partial D_{\text{ma}}}{\partial x}. \quad (\text{C.9})$$

We use that:

$$D_{\text{ma}} = \sum_{k=1}^N d_k F_{\text{ak}} = d_N + \frac{1}{L_{\text{a}}} \sum_{k=1}^{N-1} M_{\text{ak}} (d_k - d_N), \quad (\text{C.10})$$

where we have used the constrain that $\sum_{k=1}^N F_{\text{ak}} = 1$. Thus,

$$\frac{\partial q_{\text{bk}}}{\partial D_{\text{ma}}} = \sum_{l=1}^{N-1} \frac{\partial q_{\text{bk}}}{\partial M_{\text{al}}} \frac{\partial M_{\text{al}}}{\partial D_{\text{ma}}} = L_{\text{a}} \sum_{l=1}^{N-1} \frac{1}{d_l - d_N} \frac{\partial q_{\text{bk}}}{\partial M_{\text{al}}}, \quad (\text{C.11})$$

where we have used that:

$$\frac{\partial M_{\text{al}}}{\partial D_{\text{ma}}} = \frac{L_{\text{a}}}{d_l - d_N}. \quad (\text{C.12})$$

We substitute the backwater equation (Eq. C.3) in the *Exner* (1920) equation (Eq. C.4) and the equation of the mean grain size (Eq. C.8) to obtain the final set of equations:

$$\frac{\partial \eta}{\partial t} - \frac{1}{1 - \text{Fr}^2} \frac{\partial q_{\text{b}}}{\partial h} \frac{\partial \eta}{\partial x} + \frac{\partial q_{\text{b}}}{\partial D_{\text{ma}}} \frac{\partial D_{\text{ma}}}{\partial x} = \frac{1}{1 - \text{Fr}^2} \frac{\partial q_{\text{b}}}{\partial h} S_{\text{f}}, \quad (\text{C.13})$$

$$\begin{aligned} & \alpha \frac{\partial D_{\text{ma}}}{\partial t} + \frac{1}{L_{\text{a}}} \frac{1}{1 - \text{Fr}^2} \left[D_{\text{m}}^{\text{I}} \frac{\partial q_{\text{b}}}{\partial h} - \sum_{k=1}^N d_k \frac{\partial q_{\text{bk}}}{\partial h} \right] \frac{\partial \eta}{\partial x} \\ & - \frac{1}{L_{\text{a}}} \left[D_{\text{m}}^{\text{I}} \frac{\partial q_{\text{b}}}{\partial D_{\text{ma}}} - \sum_{k=1}^N d_k \frac{\partial q_{\text{bk}}}{\partial D_{\text{ma}}} \right] \frac{\partial D_{\text{ma}}}{\partial x} = \\ & = \frac{-1}{L_{\text{a}} (1 - \text{Fr}^2)} \left[D_{\text{m}}^{\text{I}} \frac{\partial q_{\text{b}}}{\partial h} - \sum_{k=1}^N d_k \frac{\partial q_{\text{bk}}}{\partial h} \right] S_{\text{f}}. \end{aligned} \quad (\text{C.14})$$

C.1.4. Closure Relations

To close the system of equations we provide closure relations for the friction term, the sediment transport rate, and the flux between the active layer and the substrate.

We adopt the following Chézy closure relation for the friction term:

$$S_f = \frac{C_f u^2}{gh}, \quad (\text{C.15})$$

where C_f [–] is a nondimensional friction coefficient that we assume to be constant (i.e., independent of the flow or bed properties), and $u = q/h$ [m/s] is the mean flow velocity.

The sediment transport rate of size fraction k per unit width is assumed to be the product of a nondimensional sediment transport rate (q_{bk}^* [–]) and the bed surface fraction content. The latter we assume equal to the active layer volume fraction content. The *Einstein* (1950) parameter ($\sqrt{gRd_k^3}$) scales the nondimensional quantity such that:

$$q_{bk} = F_{ak} \frac{\sqrt{gRd_k^3}}{1-p} q_{bk}^*, \quad (\text{C.16})$$

where $R = \rho_s/\rho_w - 1$ [–] is the submerged specific gravity, $\rho_s = 2650 \text{ kg/m}^3$ the sediment density, and $\rho_w = 1000 \text{ kg/m}^3$ the water density. The sediment transport rate q_{bk} includes the volume of pores. The nondimensional sediment transport rate is assumed to be a function of the nondimensional bed shear stress, θ_k (*Shields*, 1936):

$$\theta_k = \frac{C_{fb} u^2}{gRd_k}, \quad (\text{C.17})$$

where C_{fb} [–] is the skin friction coefficient.

The nondimensional sediment transport rate is computed using a sediment transport relation such as the one proposed by *Ashida and Michiue* (1971):

$$q_{bk}^* = 17(\theta_k - \xi_k \theta_c) \left(\sqrt{\theta_k} - \sqrt{\xi_k \theta_c} \right). \quad (\text{C.18})$$

The parameter ξ_k [–] is the hiding function:

$$\xi_k = \begin{cases} 0.843 \left(\frac{d_k}{D_m} \right)^{-1} & \text{for } \frac{d_k}{D_m} \leq 0.4 \\ \left(\frac{\log_{10}(19)}{\log_{10}(19 \frac{d_k}{D_m})} \right)^2 & \text{for } \frac{d_k}{D_m} > 0.4 \end{cases}, \quad (\text{C.19})$$

where D_m is a characteristic mean grain size of the sediment mixture. *Ashida and Michiue* (1971) propose $\theta_c = 0.05$.

Under degradational conditions we assume that the volume fraction content of sediment at the interface between the active layer and the substrate is equal to the sediment in the top part of the substrate. Under aggradational conditions the sediment in the active layer is assumed to be transferred to the substrate (*Hirano*, 1971):

$$f_k^I = \begin{cases} f_{sk}(z = \eta - L_a) & \text{if } \frac{\partial(\eta - L_a)}{\partial t} < 0 \\ F_{ak} & \text{if } \frac{\partial(\eta - L_a)}{\partial t} > 0 \end{cases}. \quad (\text{C.20})$$

Other formulations include those of *Hoey and Ferguson* (1994).

C.1.5. Matrix Formulation

In this section we present the matrix-vector form (Equation (2.9)) of the active layer model in combination with the unsteady flow equations (Stecca *et al.*, 2014) and assuming steady flow (Chavarrías *et al.*, 2018a) as well as the simplified morphodynamic model.

The vector of dependent variables (\mathbf{Q}_u), system matrix (\mathbf{A}_u), and vector of source terms (\mathbf{S}_u) of the fully unsteady system is (Stecca *et al.*, 2014):

$$\mathbf{Q}_u = [h, q, \eta, [M_{ak}]]^T, \quad (\text{C.21})$$

$$\mathbf{A}_u = \begin{bmatrix} 0 & 1 & 0 & 0 \\ gh - \left(\frac{q}{h}\right)^2 & \frac{2q}{h} & gh & 0 \\ \frac{\partial q_b}{\partial h} & \frac{\partial q_b}{\partial q} & 0 & \left[\frac{\partial q_b}{\partial M_{al}}\right] \\ \left[\frac{\partial q_{bk}}{\partial h} - f_k^I \frac{\partial q_b}{\partial h}\right] & \left[\frac{\partial q_{bk}}{\partial q} - f_k^I \frac{\partial q_b}{\partial q}\right] & 0 & \left[\frac{\partial q_{bk}}{\partial M_{al}} - f_k^I \frac{\partial q_b}{\partial M_{al}}\right] \end{bmatrix}, \quad (\text{C.22})$$

$$\mathbf{S}_u = [0, -ghS_f, 0, 0]^T. \quad (\text{C.23})$$

The preconditioning matrix is in this case:

$$\mathbf{M}_u = \begin{bmatrix} 1 & 0 & 0 & & & \\ 0 & 1 & 0 & & & 0 \\ 0 & 0 & \beta & & & \\ & & & \beta\alpha_1 & & \\ & & & & \ddots & \\ 0 & & & & & \beta\alpha_{N-1} \end{bmatrix}. \quad (\text{C.24})$$

Assuming steady flow, the vector of dependent variables (\mathbf{Q}_s), system matrix (\mathbf{A}_s), and vector of source term (\mathbf{S}_s) are equal to (Chavarrías *et al.*, 2018a):

$$\mathbf{Q}_s = [\eta, [M_{ak}]]^T, \quad (\text{C.25})$$

$$\mathbf{A}_s = \begin{bmatrix} -\frac{1}{1-\text{Fr}^2} \frac{\partial q_b}{\partial h} & & \left[\frac{\partial q_b}{\partial M_{al}}\right] \\ \left[-\frac{1}{1-\text{Fr}^2} \left(\frac{\partial q_{bk}}{\partial h} - f_k^I \frac{\partial q_b}{\partial h}\right)\right] & & \left[\frac{\partial q_{bk}}{\partial M_{al}} - f_k^I \frac{\partial q_b}{\partial M_{al}}\right] \end{bmatrix}, \quad (\text{C.26})$$

$$\mathbf{S}_s = \left[\frac{S_f}{1-\text{Fr}^2} \frac{\partial q_b}{\partial h}, \left[\frac{S_f}{1-\text{Fr}^2} \left(\frac{\partial q_{bk}}{\partial h} - f_k^I \frac{\partial q_b}{\partial h} \right) \right] \right]^T. \quad (\text{C.27})$$

The preconditioning matrix assuming steady flow is:

$$\mathbf{M}_s = \beta \begin{bmatrix} 1 & & 0 & & \\ & \alpha_1 & & & \\ & & \ddots & & \\ 0 & & & & \alpha_{N-1} \end{bmatrix}. \quad (\text{C.28})$$

The nondimensional approximated bed and sorting celerities are (De Vries, 1965; Chavarrías *et al.*, 2018a):

$$\lambda_b = \frac{\psi}{1-\text{Fr}^2}, \quad (\text{C.29})$$

$$\lambda_{s1} = \chi_1 \mu_{1,1}, \quad (\text{C.30})$$

where the parameters are (Stecca et al., 2014; Chavarrías et al., 2018a):

$$\psi = \frac{\partial q_b}{\partial q}, \quad (\text{C.31})$$

$$\gamma_k = c_k - f_k^I, \quad (\text{C.32})$$

$$c_k = \frac{1}{\psi} \frac{\partial q_{bk}}{\partial q}, \quad (\text{C.33})$$

$$\chi_l = \frac{1}{u} \frac{\partial q_b}{\partial M_{al}}, \quad (\text{C.34})$$

$$\mu_{l,k} = d_{l,k} - f_k^I, \quad (\text{C.35})$$

$$d_{l,k} = \frac{1}{u \chi_l} \frac{\partial q_{bk}}{\partial M_{al}}. \quad (\text{C.36})$$

In the simplified morphodynamic model (Section C.1.3), the vector of dependent variables (\mathbf{Q}_m), system matrix (\mathbf{A}_m), and vector of source term (\mathbf{S}_m) are:

$$\mathbf{Q}_m = [\eta, D_{ma}]^T, \quad (\text{C.37})$$

$$\mathbf{A}_m = u \begin{bmatrix} -\frac{1}{1-\text{Fr}^2} \frac{\partial q_b}{\partial h} & \frac{\partial q_b}{\partial D_{ma}} \\ \frac{1}{L_a} \frac{1}{1-\text{Fr}^2} \left(D_m^I \frac{\partial q_b}{\partial h} - \sum_{k=1}^N d_k \frac{\partial q_{bk}}{\partial h} \right) & -\frac{1}{L_a} \left(D_m^I \frac{\partial q_b}{\partial D_{ma}} - \sum_{k=1}^N d_k \frac{\partial q_{bk}}{\partial D_{ma}} \right) \end{bmatrix}, \quad (\text{C.38})$$

$$\mathbf{S}_m = \frac{S_f}{1-\text{Fr}^2} \left[\frac{\partial q_b}{\partial h}, \frac{-1}{L_a} \left(D_m^I \frac{\partial q_b}{\partial h} - \sum_{k=1}^N d_k \frac{\partial q_{bk}}{\partial h} \right) \right]^T. \quad (\text{C.39})$$

The preconditioning matrix is:

$$\mathbf{M}_m = \beta \begin{bmatrix} 1 & 0 \\ 0 & \alpha \end{bmatrix}. \quad (\text{C.40})$$

The parameters are:

$$\lambda_m = \chi_m \mu_m, \quad (\text{C.41})$$

$$\gamma_m = c_m - f_m^I, \quad (\text{C.42})$$

$$c_m = \frac{1}{\psi L_a} \sum_{k=1}^N d_k \frac{\partial q_{bk}}{\partial q}, \quad (\text{C.43})$$

$$f_m^I = \frac{D_m^I}{L_a}, \quad (\text{C.44})$$

$$\chi_m = \frac{1}{u} \frac{\partial q_b}{\partial D_{ma}}, \quad (\text{C.45})$$

$$\mu_m = d_m - f_m^I, \quad (\text{C.46})$$

$$d_m = \frac{1}{u \chi_m L_a} \sum_{k=1}^N d_k \frac{\partial q_{bk}}{\partial D_{ma}}. \quad (\text{C.47})$$

C.2. Mass Conservation of the Modified System

Mass conservation of the modified system of equations (Section 4.3.1) is guaranteed if the sum of the N modified active layer equations is equal to the modified *Exner* (1920) equation. As we already substituted the *Exner* (1920) equation in the active layer equation, the addition of the N modified active layer equations must yield an identity:

$$\begin{aligned} \sum_{k=1}^N \beta \alpha_k \frac{\partial M_{ak}}{\partial t} + \sum_{k=1}^N f_k^I \beta \frac{\partial (\eta - L_a)}{\partial t} + \sum_{k=1}^N \frac{\partial q_{bk}}{\partial x} = 0 \Rightarrow \\ \beta \frac{\partial L_a}{\partial t} \left(\sum_{k=1}^N \alpha_k F_{ak} - 1 \right) + \beta L_a \sum_{k=1}^N \left(\alpha_k \frac{\partial F_{ak}}{\partial t} \right) = 0. \end{aligned} \quad (\text{C.48})$$

To allow for morphodynamic changes the parameter β must be different than 0. This yields a multiplicity of cumbersome closure relations for α_k relating the temporal change of the active layer thickness to those of the volume fraction contents at the bed surface. We choose to simplify the problem assuming that $\alpha_k = \alpha \forall k$ so that we obtain:

$$\beta \frac{\partial L_a}{\partial t} (\alpha - 1) = 0. \quad (\text{C.49})$$

Given that $\alpha \neq 1$ to recover the well-posedness of the system of equation, the active layer thickness must be constant to conserve mass in the modified system of equations.

C.3. Parameters of the Numerical Simulation of the Thought Experiment

In this section we provide the details of our numerical simulation of the thought experiment conducted by *Ribberink* (1987). The thought experiment is based on the laboratory Experiment E8-E9 conducted by *Ribberink* (1987). The only difference is that in the thought experiment the substrate is finer than in the laboratory experiment.

The domain is 30 m long and it is discretized into 0.01 m long cells. The simulation time is 120 h. The total and skin friction coefficient are equal to 0.0117. The sediment mixture is composed of two sediment sizes equal to 0.78 mm and 1.29 mm. The flow discharge per unit width is constant and equal to 0.0803 m²/s. The downstream water level is constant and such that initially the bed is in equilibrium. The upstream sediment load is initially equal to 5.64 × 10⁻⁶ m²/s and it is composed of 50% of the fine fraction. During the first 30 h the fraction of fine sediment linearly decreases to 0. The total amount of sediment decreases to 95% of the initial value. The active layer thickness is equal to 0.02 m. The initial volume fraction content of fine sediment in the substrate is 0.6.

It is not fully clear to the authors which sediment transport relation and which parameters *Ribberink* (1987) used in the simulation of the thought experiment using the two-layer model. We have inferred that he used the relation developed by *Meyer-Peter and Müller* (1948) with the hiding function by *Egiazaroff* (1965) with the calibrated parameters $A = 15.85$, $B = 1.5$, and $\theta_c = 0.0307$. The mean grain size is computed arithmetically. We calibrate the ripple factor (a constant multiplying the *Shields* (1936) stress) such that the bed slope and volume fraction content of fine sediment are as close as possible to

the reported values. We obtain that for a ripple factor equal to 0.3169 the bed slope is 1.65×10^{-3} (the same as *Ribberink* (1987) reported) and the volume fraction content of fine sediment in the active layer is equal to 0.409 (*Ribberink* (1987) reported a value equal to 0.43).

C.4. Proof of Positive Regularized Eigenvalues

In this section we prove that the eigenvalues of the regularized active layer model consisting of $\alpha > 1$ and $\beta = 1$ are always positive.

The eigenvalues are (Equation (4.11)):

$$\lambda_k = \frac{u}{2} \left(\lambda_b + \frac{\lambda_{s1}}{\alpha_c} \right) \quad \text{for } k = 1, 2, \quad (\text{C.50})$$

and the value of α_c that regularizes the system of equations is (Equation (C.51)):

$$\alpha_c = \frac{\lambda_{s1}}{\lambda_b} \left(1 - 2 \frac{\gamma_1}{\mu_{1,1}} \pm 2 \sqrt{\frac{\gamma_1}{\mu_{1,1}} \left(\frac{\gamma_1}{\mu_{1,1}} - 1 \right)} \right). \quad (\text{C.51})$$

Substituting Equation (C.51) in Equation (C.50) we obtain:

$$\lambda_k = \frac{u \lambda_b}{2} \left(1 + \frac{1}{1 - 2 \frac{\gamma_1}{\mu_{1,1}} \pm 2 \sqrt{\frac{\gamma_1}{\mu_{1,1}} \left(\frac{\gamma_1}{\mu_{1,1}} - 1 \right)}} \right) \quad \text{for } k = 1, 2. \quad (\text{C.52})$$

The two eigenvalues are equal (i.e., $\lambda_1 = \lambda_2$) and the sign of the square root term is chosen such that that $\alpha_c > 1$. The symbols are defined in Appendix C.1.5.

If $\lambda_{s1} > 0$, the fact that $\alpha_c > 1$ implies that the square root term is positive (see Equation (C.51)). Moreover, as $\alpha_c > 0$ the following inequality holds:

$$1 - 2 \frac{\gamma_1}{\mu_{1,1}} + 2 \sqrt{\frac{\gamma_1}{\mu_{1,1}} \left(\frac{\gamma_1}{\mu_{1,1}} - 1 \right)} > 0. \quad (\text{C.53})$$

The above inequality implies that $\lambda_k > 0$ (see Equation (C.52)).

If $\lambda_{s1} < 0$, the fact that $\alpha_c > 1$ implies that the square root term is negative (see Equation (C.51)). Moreover, as $\alpha_c > 0$ the following inequality holds:

$$1 - 2 \frac{\gamma_1}{\mu_{1,1}} - 2 \sqrt{\frac{\gamma_1}{\mu_{1,1}} \left(\frac{\gamma_1}{\mu_{1,1}} - 1 \right)} < 0. \quad (\text{C.54})$$

The eigenvalues are positive if and only if:

$$1 + \frac{1}{1 - 2\frac{\gamma_1}{\mu_{1,1}} - 2\sqrt{\frac{\gamma_1}{\mu_{1,1}}\left(\frac{\gamma_1}{\mu_{1,1}} - 1\right)}} > 0 \implies$$

$$-\frac{\gamma_1}{\mu_{1,1}} < \sqrt{\frac{\gamma_1}{\mu_{1,1}}\left(\frac{\gamma_1}{\mu_{1,1}} - 1\right)}. \quad (\text{C.55})$$

The discriminant Δ (Equation (4.7)) is negative for $\alpha = 1$, as the problem is ill-posed if we do not regularize it. This implies that the sign of λ_{s1} is opposite to the sign of $2\gamma_1/\mu_{1,1} - 1$, as $\lambda_b > 0$. For this reason $\gamma_1/\mu_{1,1} > 1/2$ and Inequality (C.55) is true.

Thus, the regularization strategy based on $\alpha > 1$ and $\beta = 1$ always yields positive eigenvalues.

C.5. Numerical Solution of the System of Equations

We have developed the code Elv to numerically solve the system of equations that models river morphodynamic processes. In this section we present the details of the numerical technique. In Section C.5.1 we present the model equations. In Section C.5.2 we describe the procedure to solve the system of equations. The discretized flow, bed elevation, substrate, and bed surface equations are shown in Sections C.5.3, C.5.4, C.5.5, and C.5.6, respectively.

C.5.1. Model Equations

The model accounts for one-dimensional river morphodynamic processes on a domain of length L [m] over time T [s]. The cross section is assumed rectangular and wide with respect to the flow depth, such that the hydraulic radius is assumed equal to the flow depth. The flow is assumed to be steady. Under these conditions, mass and momentum conservation of water flow reduce to the backwater equation:

$$\frac{\partial h}{\partial x} = \frac{-1}{1 - \text{Fr}^2} \frac{\partial \eta}{\partial x} - \frac{S_f}{1 - \text{Fr}^2}, \quad (\text{C.56})$$

where x [m] denotes the streamwise coordinate, h [m] the flow depth, η [m] the bed elevation, S_f [–] the friction slope, $\text{Fr} = q/\sqrt{g h^3}$ the Froude number, g [m/s²] the acceleration due to gravity, and q [m²/s] the flow discharge per unit width.

The bed is assumed to be alluvial and composed of a mixture of N non-cohesive size fractions with characteristic size d_k [m] for $1 \leq k \leq N$. Bed elevation changes are modelled using the *Exner* (1920) equation:

$$\frac{\partial \eta}{\partial t} + \frac{\partial q_b}{\partial x} = 0, \quad (\text{C.57})$$

where t [s] denotes the time coordinate and q_b [m²/s] the sediment transport rate per unit width (including pores). The sediment transport rate results from the addition of the

sediment transport rate of each size fraction such that $q_b = \sum_{k=1}^N q_{bk}$, where q_{bk} [m²/s] is the sediment transport rate of size fraction k per unit width (including pores).

Changes in grain size distribution at the bed surface are modelled by means of the modified active layer equation:

$$\alpha \frac{\partial M_{ak}}{\partial t} + f_k^I \frac{\partial(\eta - L_a)}{\partial t} + \frac{\partial q_{bk}}{\partial x} = 0 \quad \text{for } 1 \leq k \leq N-1, \quad (\text{C.58})$$

where α [-] denotes the regularization parameter, $M_{ak} = F_{ak} L_a$ [m] the volume of sediment of size fraction k in the active layer per unit of bed area, $F_{ak} \in [0, 1]$ [-] is the volume fraction content of sediment of size fraction k in the active layer, $f_k^I \in [0, 1]$ [-] is the volume fraction content of sediment of size fraction k at the interface between the active layer and the substrate, and L_a [m] is the active layer thickness.

Mass conservation of sediment of size fraction k in the substrate is expressed by:

$$\frac{\partial M_{sk}}{\partial t} - f_k^I \frac{\partial(\eta - L_a)}{\partial t} = 0 \quad \text{for } 1 \leq k \leq N-1, \quad (\text{C.59})$$

where M_{sk} [m] is the volume of sediment of size fraction k in the substrate per unit of bed area.

The friction slope and the sediment transport rate depend on the local properties of the flow and the bed surface. Worded differently, S_f and q_{bk} are functions of h , q , and M_{ak} for $1 \leq k \leq N-1$. These functions are presented in Section C.1.4.

The parameters of the model include the acceleration due to gravity g , the active layer thickness L_a , the nondimensional friction coefficient C_f [-], the skin-related nondimensional friction coefficient C_{fb} [-], the water and sediment densities ρ_w [kg/m³] and ρ_s [kg/m³], and the parameters of the sediment transport relation (see Section C.1.4).

The boundary conditions are the the flow discharge, q , the sediment transport rate of size fraction k at the upstream end of the domain, q_{bk0} , and the downstream water elevation η_{wL} . The initial condition consists of the bed elevation η_0 , the volume of sediment in the active layer M_{ak0} for $1 \leq k \leq N-1$, and in the substrate M_{sk0} for $1 \leq k \leq N-1$ at the initial time t_0 .

We refer to Appendix C.1 for a description of the assumptions underlying the model equations.

C.5.2. Solution Procedure

In this section we detail the procedure followed in solving the model equations. The domain L is discretized using cells of equal length Δx [m]. The equation are solved in a decoupled form. This assumes a weak interaction between the equations (Section 4.3.5) and allows, at each time step, to solve Equations (C.56)-(C.59) in series. Worded differently, all equations are solved assuming all variables to be constant during one time step. All variables are computed at cell centers and the boundary conditions are imposed at the edges of the first and last cells.

The workflow is as follows. First, the input is checked for errors and inconsistencies and memory is allocated for all variables. Starting from the initial condition, the flow depth is updated (Section C.5.3). Second, the sediment transport rate is computed.

Using the sediment transport rate, the bed elevation is updated (Section C.5.4). Subsequently, the substrate is updated, which allows for computing the volume fraction content of sediment at the interface between the active layer and the substrate (Section C.5.5). If the regularization strategy is applied, the mathematical character of the model (i.e., well-posed or ill-posed) at each node is obtained. This implies computing an algebraic relation for a case with two sediment size fractions and solving an eigenvalue problem for more than two sediment size fractions (*Chavarrías et al.*, 2018a). Subsequently, the value of the regularization parameter α at each ill-posed node is computed (Section 4.3.2). Using parameter α (or $\alpha = 1$ for the case in which the regularization strategy is not applied), the volume of sediment of each size fraction k in the active layer is updated (Section C.5.6). At this point, all dependent variables have been computed. The celerities (i.e., the system eigenvalues) are computed (Equation (4.11)), which allows for computing the time step of the next loop iteration given a predefined maximum CFL number. The variables are checked for inconsistencies and, if required, are saved. This last step finishes the loop iteration, which starts again by computing the flow depth given the new bed elevation and grain size distribution. The loop finishes once the final time T is reached. The workflow is shown in Figure C.1.

C.5.3. Flow Solver

We have implemented a steady and an unsteady solver in Elv. For the case of steady flow, as we assume here, the flow is represented by one Ordinary Differential Equation, as the bed level is assumed to remain constant such that there is only one independent variable (i.e., the streamwise coordinate x). The user can choose between a first-order and fourth-order solver. Moreover, the user can choose to solve the backwater equation in its flow depth or in its energy form. Here we describe the standard fourth-order Runge-Kutta method (*Runge* (1895); *Kutta* (1901), see e.g. *Butcher* (1996); *Butcher and Wanner* (1996)) used to solve the backwater equation (Equation (C.56)) in its flow depth form.

The bed elevation η , flow discharge per unit width q , and nondimensional friction coefficient C_f are known at the center of each cell. Given the flow depth at the center of cell n , h_n , we compute the flow depth at the center of the cell immediately upstream (i.e., h_{n-1}):

$$h_{n-1} = h_n - \frac{1}{6} (R_{1_n} + 2R_{2_n} + 2R_{3_n} + R_{4_n}), \quad (\text{C.60})$$

where:

$$R_{1_n} = \Delta x \left. \frac{dh}{dx} \right|_{h=h_n, n}, \quad (\text{C.61})$$

$$R_{2_n} = \Delta x \left. \frac{dh}{dx} \right|_{h=h_n+0.5R_{1_n}, n}, \quad (\text{C.62})$$

$$R_{3_n} = \Delta x \left. \frac{dh}{dx} \right|_{h=h_n+0.5R_{2_n}, n}, \quad (\text{C.63})$$

$$R_{4_n} = \Delta x \left. \frac{dh}{dx} \right|_{h=h_n+R_{3_n}, n}, \quad (\text{C.64})$$

where:

$$\frac{db}{dx} = \frac{s_n - C_f Fr^2}{1 - Fr^2}, \quad (C.65)$$

where:

$$Fr^2 = \frac{q^2}{g b^3}, \quad (C.66)$$

$$s_n = \frac{\eta_n - \eta_{n-1}}{\Delta x}. \quad (C.67)$$

The computation of the flow depth at the cell center of the most downstream cell (i.e., the first computation) takes into consideration that the boundary condition is at $\Delta x/2$ distance from the cell center and linearly extrapolates the bed slope between the last two cells.

C.5.4. Bed Elevation Solver

We apply the Method Of Lines (e.g., *Carver and Hinds, 1978; Verwer and Sanz-Serna, 1984; LeVeque, 2004; Toro, 2009*) in solving the Partial Differential Equation representing changes in bed elevation (i.e., the *Exner (1920)* equation (Eq. (C.57))). The divergence of the sediment transport rate at the cell edges is computed using first order upwind differences. The time integration is conducted using a forward Euler scheme. This strategy, often referred in literature as a Forward in Time and Backward in Space (FTBS) scheme (e.g., *Sonke et al., 2003; Long et al., 2008; Na Ranong et al., 2010; Esfahanian et al., 2013; Zima et al., 2015*), is first-order accurate in both space and time and widely applied in solving transport equations.

Our numerical method is finite difference, not spectral, and hence does not suffer from overshoots and undershoots caused by the spectral reconstruction of data around a discontinuity (i.e., Gibbs phenomenon (*Wilbraham, 1848; Gibbs, 1898, 1899; Hewitt and Hewitt, 1979*)). The numerical technique could cause oscillations in the vicinity of shock waves because of numerical instability (i.e., Gibbs-like phenomenon (*Liu et al., 1994; Biondini and Trogdon, 2017; Hovda, 2017*)). All numerical schemes of order larger than 1 suffer from such a problem (*Godunov, 1959, 1999*) and the adoption of techniques to avoid them, such as TVD methods (*Harten, 1983, 1984; Yee et al., 1985*) and WENO reconstructions (*Liu et al., 1994; Jiang and Shu, 1996*), are mandatory. In our case, we use a first-order method that is proven to be monotone (i.e., stable at shocks) (Section C.6).

Given the sediment transport rate and the bed elevation at the center of each cell n at time m (i.e., $q_{b_n}^m$ and η_n^m), we compute the bed elevation at the center of cell n at time $m + 1$ as:

$$\eta_n^{m+1} = \eta_n^m - \frac{\Delta t}{\Delta x} (q_{b_{n-1}}^m - q_{b_n}^m). \quad (C.68)$$

The boundary condition is applied at the upstream edge of the most upstream cell.

C.5.5. Substrate Solver

The substrate is discretized into N_s layers of thickness L_{s_l} such that $M_{sk} = \sum_{l=1}^{N_s} m_{sk_l}$, where index $l = 1, \dots, N_s$ refers to the substrate layers from top to down and m_{sk_l} is the

volume of sediment of size fraction k per unit of bed area in layer l of the substrate. The lower elevation of the substrate is fixed and must always be lower than the interface between the active layer and the substrate.

Under aggradational conditions, sediment is transferred from the bed surface to the substrate and the thickness of the top substrate layer increases. When the thickness of the top substrate layer exceeds a predefined value, a new layer is created. In this case, if the number of substrate layers exceeds N_s , the lowermost two layer are combined into one single layer such that eventually the total number of substrate layers does not exceed N_s .

Under degradational conditions, sediment is transferred from the substrate to the active layer. When degradation occurs on only the top substrate layer, the thickness of this layer decreases. When degradation occurs over more than one substrate layer, the thickness of the topmost layer(s) becomes equal to 0 and degradation continues on the first substrate layer with nonzero thickness.

In solving each of the $N-1$ substrate equations (Equation (C.59)), we apply a forward Euler scheme. Given the volume of sediment of size fraction k in the substrate per unit of bed area at the cell center of each cell n at time m ($M_{sk_n}^m$), the bed elevation at the center of each cell n at times m and $m+1$ (η_n^m and η_n^{m+1}), and the active layer thickness at the center of each cell n at times m and $m+1$ ($L_{a_n}^m$ and $L_{a_n}^{m+1}$), we compute the volume of sediment of size fraction k in the substrate per unit of bed area at the cell center of each cell n at time $m+1$ ($M_{sk_n}^{m+1}$) as:

$$M_{sk_n}^{m+1} = M_{sk_n}^m + f_{k_n}^{I^m} (\eta_n^{m+1} - \eta_n^m + L_{a_n}^m - L_{a_n}^{m+1}). \quad (\text{C.69})$$

The volume fraction content of sediment at the interface between the active layer and the substrate ($f_{k_n}^{I^m}$) depends on whether the interface between the active layer and the substrate lowers or increases its elevation:

$$f_{k_n}^{I^m} = \begin{cases} f_{sk_{n\text{top}}}^m & \text{if } \eta_n^{m+1} - \eta_n^m + L_{a_n}^m - L_{a_n}^{m+1} < 0 \\ F_{ak_n}^m & \text{if } \eta_n^{m+1} - \eta_n^m + L_{a_n}^m - L_{a_n}^{m+1} > 0 \end{cases}, \quad (\text{C.70})$$

where $F_{ak_n}^m = M_{ak_n}^m / L_{a_n}^m$ is the volume fraction content of sediment of size fraction k in the active layer and $f_{sk_{n\text{top}}}^m$ is the volume fraction content of sediment of size fraction k at the top part of the substrate. The top part of the substrate contains the substrate cells in which degradation takes place. If degradation occurs on only the top layer of the substrate $f_{sk_{n\text{top}}}^m = f_{sk_{n_1}}^m$. If degradation consumes the entire first substrate layer and part of the second layer, the volume fraction content at the interface between the active layer and the substrate is a weighted average of the sediment in both layers. This approach guarantees mass conservation of the substrate sediment.

C.5.6. Active Layer Solver

The $N-1$ active layer equations (Equation (C.58)) must be solved using the same scheme as the *Exner* (1920) equation (Section C.5.4) to preserve mass.

Given the volume of sediment of size fraction k in the active layer per unit of bed area at the center of each cell n at time m ($M_{sk_n}^m$), the bed elevation at the center of each cell n at times m and $m + 1$ (η_n^m and η_n^{m+1}), the active layer thickness at the center of each cell n at times m and $m + 1$ ($L_{a_n}^m$ and $L_{a_n}^{m+1}$), and the sediment transport rate of size fraction k at the center of each cell n at time m ($q_{bk_n}^m$), we compute the volume of sediment of size fraction k in the active layer per unit of bed area at the center of each cell n at time $m + 1$ ($M_{sk_n}^{m+1}$) as:

$$M_{sk_n}^{m+1} = M_{sk_n}^m - \frac{1}{\alpha} \left[f_{k_n}^{I^m} (\eta_n^{m+1} - \eta_n^m + L_{a_n}^m - L_{a_n}^{m+1}) + \frac{\Delta t}{\Delta x} (q_{bk_{n-1}}^m - q_{bk_n}^m) \right]. \quad (\text{C.71})$$

The volume fraction content of sediment at the interface between the active layer and the substrate is obtained from solving the substrate equation (Section C.5.5). The regularization parameter α is equal to 1 for the active layer model and it is computed following the methodology explained in Section 4.3.2 when applying the regularization strategy.

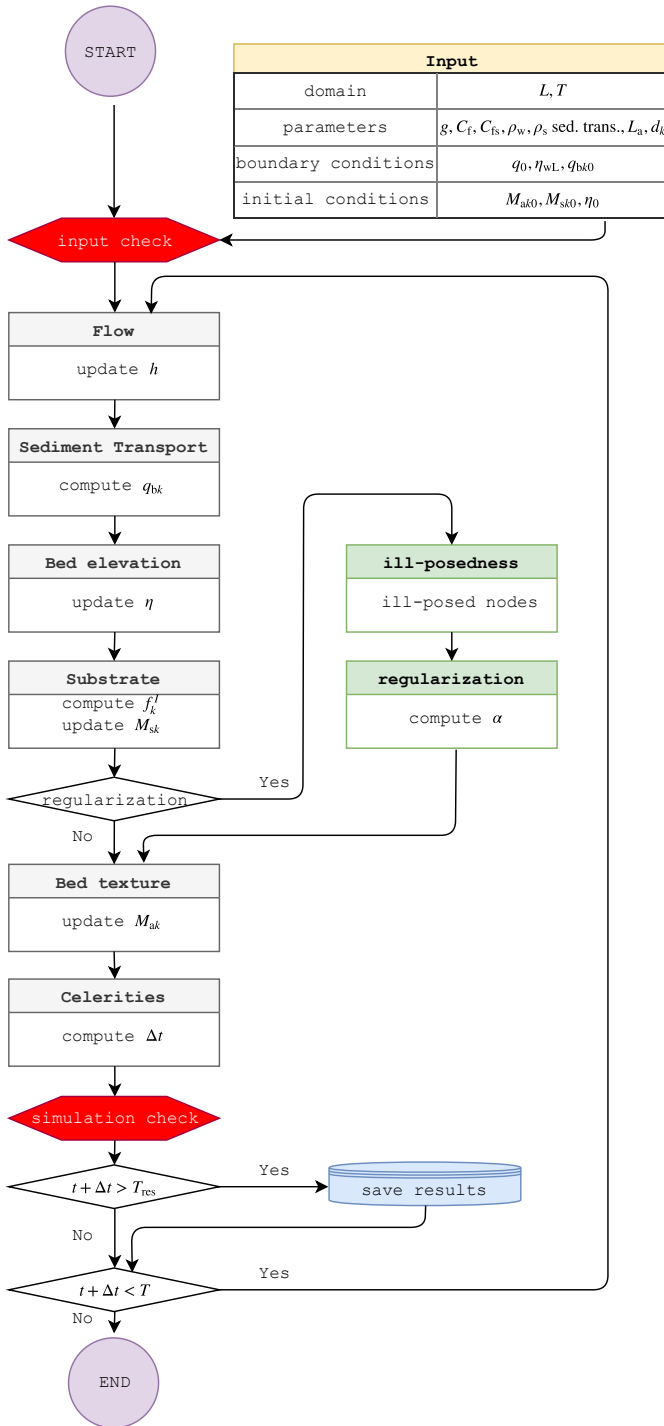


Figure C.1: Elv flowchart.

C.6. Preparatory Experiments

In this section we describe 4 preparatory experiments (P₁, P₂, P₃ and P₄) conducted: (1) to calibrate the friction coefficient, (2) to select a sediment transport relation, (3) to select a value for the active layer thickness, and (4) to estimate the equilibrium conditions in which we start the experiments conducted under conditions in which the active layer model is ill-posed (i.e., Experiments I₁, I₂, I₃, and I₄, Section 4.4).

In Experiments P₁ and P₂ we feed coarse and fine sediment, respectively. The experiments are run under equilibrium conditions. In these experiments we measure the sediment transport rate and profiles of bed and water elevation. The conditions of Experiment P₁ are equal to the initial condition of Experiments I₁, I₂, I₃, and I₄. In the latter experiments degradational conditions are imposed decreasing the level of the downstream weir. Yet, the lowering rate is sufficiently small such that the degradational conditions do not significantly differ from the conditions of Experiment P₁. Experiment P₃ is equal to P₁ except for the fact that we feed tracer sediment to study its propagation under equilibrium conditions. The aim of Experiment P₄ is to study the same degradational conditions imposed in Experiments I₁, I₂, I₃, and I₄ except for the fact that we use unisize sediment. The sediment in the patch is tracer sediment rather than fine sediment. In Experiments P₃ and P₄ we measured the surface volume fraction content of tracer sediment (Table C.1).

Experiment	Sediment	Tracer	Conditions	Measurements
P ₁	coarse	no	Equilibrium	water and bed elev., sed. trans.
P ₂	fine	no	Equilibrium	water and bed elev., sed. trans.
P ₃	coarse	yes	Equilibrium	tracer content
P ₄	coarse	yes	Degradational	tracer content

Table C.1: Preparatory experiments.

Table C.2 summarizes the main parameters of Experiments P₁ and P₂. The granular roughness ($d_{\text{rel}} = \frac{d_k}{\beta}$) is smaller than 0.05, which implies that flow is *deep* in the sense that individual grains do not affect bed friction (e.g. *Ferguson*, 2007; *Church*, 2013, 2015). The flow Reynolds number ($\text{Re} = \frac{q}{\nu}$, where $\nu = 1 \times 10^{-6} \text{ m}^2/\text{s}$ is the kinematic viscosity of water) is far above 500, which implies that the flow is fully turbulent (e.g. *Allen*, 1985; *Lajeunesse et al.*, 2010). The particle Reynolds number ($\text{Re}^* = \frac{u^* d_k}{\nu}$, where u^* [m/s] is the shear velocity) is above 300 for Experiment P₁, which indicates the lack of a viscous sublayer (i.e., rough wall) (e.g. *Shields*, 1936; *Lajeunesse et al.*, 2010; *Nieuwstadt et al.*, 2016). In Experiment P₂, the fact that $\text{Re}^* = 101$ indicates that the viscous sublayer may not be negligible in this case. The Rouse number ($\text{Ro} = \frac{V_s}{\alpha u^*}$, where V_s [m/s] is the settling velocity and $\alpha = 0.41$ [–] is the von Kármán constant) is larger than 7, which implies that, as observed, sediment is transported as bed load predominantly (e.g. *Dade and Friend*, 1998). The Stokes number ($\text{St} = \frac{\text{Re}_s \rho_s}{9 \rho_w}$, where $\text{Re}_s = \frac{V_s d_k}{\nu}$ is the settling Reynolds number) is far above 1 and the sediment concentration $c = q_b/q$ is below 6×10^{-3} . This implies that the fluid and particles move in a quasi-autonomous way (i.e., they do not affect each other)

and that the concentration of sediment does not need to be accounted for in the equations for the conservation of water mass and momentum (i.e., clear water approximation *Garegnani et al.* (2011, 2013); *Heyman et al.* (2016)).

We assume the particle settling velocity to be given by $V_s = \sqrt{Rgd_k}$ which neglects the weak dependency of the drag coefficient on the Reynolds number (*Lajeunesse et al.*, 2010). To obtain the bed friction coefficient C_{fb} we correct the total friction coefficient C_f for side wall friction with the method developed by *Johnson* (1942) (see *Guo*, 2015).

We conclude that in the experiments conducted under conditions in which the active layer model is ill-posed we can assume that the flow is fully turbulent, deep (single grains do not affect bed friction), and rough (lack of viscous sublayer). Moreover, sediment is mainly transported as bed load and in a small enough concentration such that the clear water approximation holds.

	P1	P2
Q [m ³ /s]	0.060	0.045
s [–]	3.6×10^{-3}	1.8×10^{-3}
h [m]	0.187	0.174
d_{rel} [–]	0.029	0.012
q [m ² /s]	0.15	0.11
Fr [–]	0.59	0.49
u [m/s]	0.799	0.647
θ [–]	0.061	0.067
u^* [m/s]	0.073	0.048
C_f [–]	0.0104	0.0074
C_{fb} [–]	0.0084	0.0055
Re^* [–]	403	101
Re_s [–]	1600	390
Re [–]	1.5×10^5	1.1×10^5
Ro [–]	10	9
St [–]	480	110
\bar{q}_b [g/min]	400	80
σ_{q_b} [g/min]	190	30
c [–]	4.2×10^{-5}	1.1×10^{-5}

Table C.2: Mean parameters of Experiments P1 and P2.

In both Experiments P1 and P2 the mean value of the measured sediment transport rate at the downstream end (\bar{q}_b) is slightly smaller than the feed rate. This indicates that statistical equilibrium conditions (i.e., conditions where the mean supply rate equals the mean transport rate) are not achieved. The difficulty of achieving those conditions arise from the large variability of the sediment transport rate with time (σ_{q_b} and Figure C.2). Yet, we consider that we were in conditions sufficiently close to equilibrium as we did not measure significant aggradation or degradation.

The bed was covered by low relief bedforms, which were two or three grain sizes high

and approximately 2 m long.

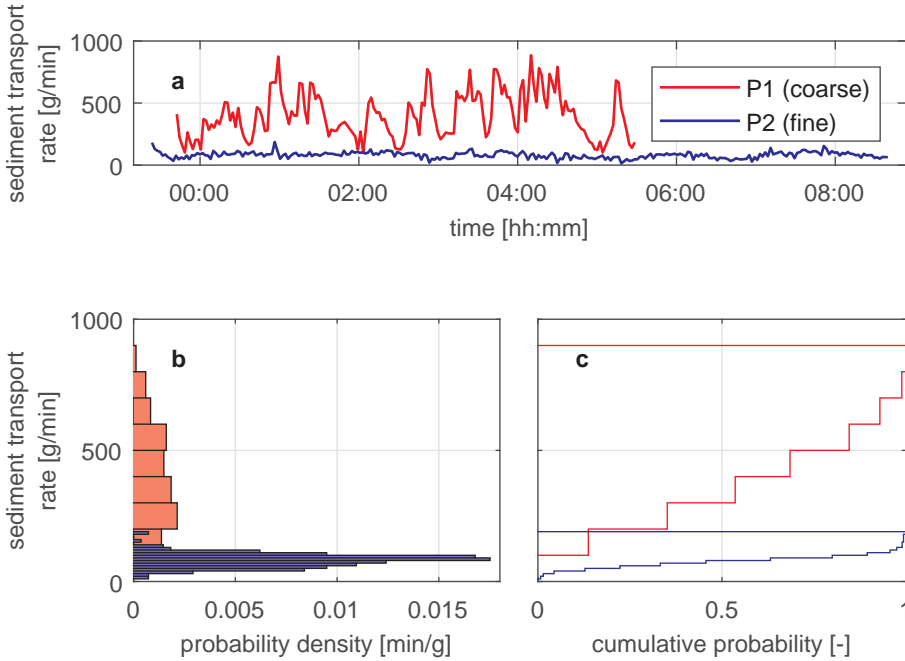


Figure C.2: Measured sediment transport rate in the equilibrium experiments with coarse sediment (P1, red) and fine sediment (P2, blue): (a) time series, (b) probability density, and (c) cumulative probability.

The probability distribution of bed elevation (Figure C.3) indicates that a reasonable value for the active layer thickness is 0.01 m, corresponding to the elevation with a probability of exposure below approximately 5% (Ribberink, 1987; Blom, 2008). This value is also in accordance with 1–3 times D_{90} as proposed by, for instance, Hirano (1971), Hoey and Ferguson (1994), and Seminara et al. (1996).

Experiment P3 is the same as Experiment P1 except for the fact that the feed sediment has a different color than the initial bed sediment. This allows us to measure the surface fraction content of tracer material at the downstream end of the flume as a function of time (Figure C.4).

The fed tracer sediment travels downstream mainly through the migration of incipient dunes (Carling, 1999; Carling et al., 2005). Some individual particles travel at a faster speed and reach the downstream end of the flume more quickly. The incipient dunes entrain non-tracer substrate sediment, which decreases the tracer content of the bed surface sediment. This vertical sediment mixing also induces tracer sediment to be deposited (and temporarily stored) at relatively low elevations of the bed, which creates a top layer of tracer sediment of a certain thickness (2 to 3 times D_{90}). The temporary storage of tracer sediment at low elevations slows down the propagation of the (tracer) sediment and increases the variation of the time needed for particles to reach the downstream end of the flume (Ribberink, 1987; Blom et al., 2003). The tracer content of the bed surface

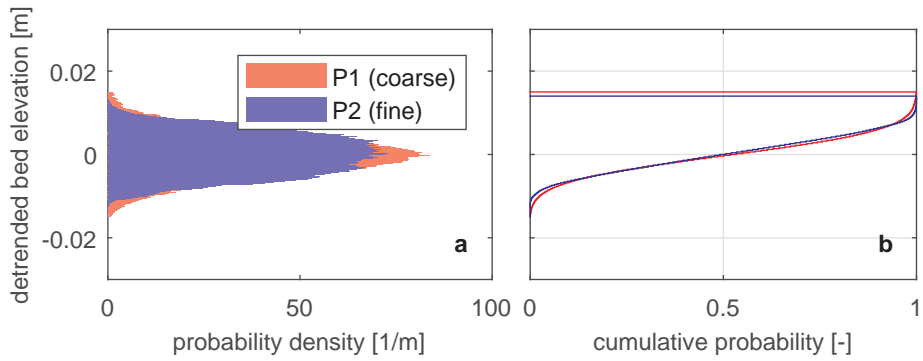


Figure C.3: Measured bed elevation in the preparatory experiments with coarse sediment (P1, red) and fine sediment (P2, blue): (a) probability density and (b) cumulative probability.

sediment stops increasing once the top layer is so thick that the incipient dunes no longer entrain non-tracer substrate sediment.

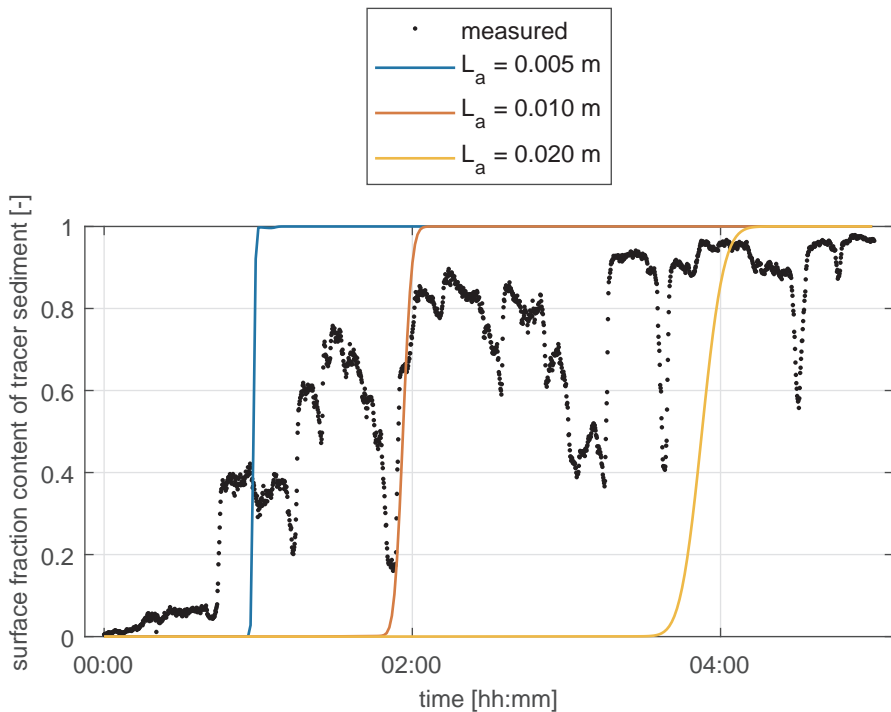


Figure C.4: Surface fraction content of tracer sediment at $x = 9.17$ m: measured (black dots), and predicted values using an active layer thickness equal to 0.005 m, 0.010 m, and 0.020 m (lines).

Experiment P₄ is equal to Experiment I₁ (Section 4.4.1) except for the fact that the sediment in the patch is tracer sediment rather than fine sediment. In the bedform troughs, substrate sediment is entrained, which causes a periodic entrainment of tracer sediment at the location of the patch (Figure C.5a). Downstream from the patch, the oscillating behavior diffuses as tracer and non-tracer sediment is mixed and reworked. The more downstream, the less pronounced are the changes in volume fraction content of tracer sediment (Figure C.5b).

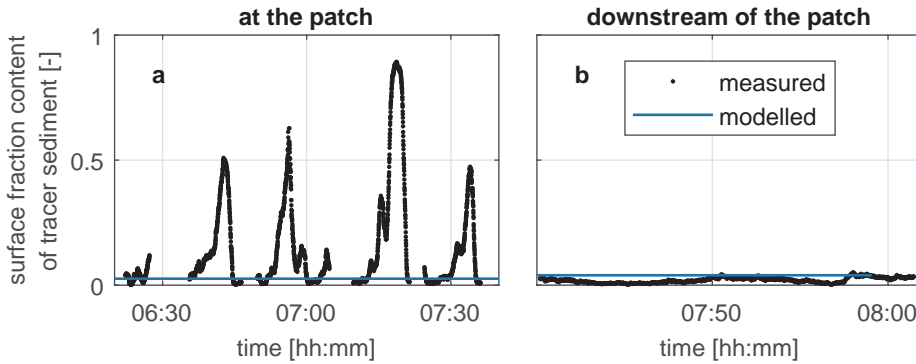


Figure C.5: Surface fraction content of tracer sediment with time (a) at the center of the patch $x = 4.95$ m, and (b) downstream of the patch $x = 9.15$ m.

C.7. Calibration of the Numerical Model

In this section we select a sediment transport relation and calibrate the value of the active layer thickness for modeling of the experiments.

Assuming that Experiments P₁ and P₂ are in equilibrium, we compute a time-average bed shear stress based on the mean bed slope computed individually for each bed elevation profile. Based on the time-average values of the measured sediment transport rate at the downstream end we compute the nondimensional sediment transport rate q_b^* (Section C.1.4) and we compare our measurements to the values predicted using the sediment transport relations by *Meyer-Peter and Müller (1948)*, *Fernandez-Luque and Van Beek (1976)*, *Engelund and Hansen (1967)*, *Ashida and Michiue (1972)*, and *Wilcock and Crowe (2003)* (Figure C.6).

All sediment transport relations predict the sediment transport rates of the coarse and the fine size fractions reasonably well. We choose to apply the sediment transport relation by *Ashida and Michiue (1972)* in our analysis. We have verified that the choice of the sediment transport relation does not affect the conclusions of our analysis.

We model Experiment P₃ (feed of unisize tracer sediment under equilibrium conditions) using different values of the active layer thickness to estimate a suitable value. The cell size is equal to 0.01 m. As the active layer model does not capture the phenomena related to small scale variability in bed elevation (Section 4.3.1), it predicts that the tracer sediment propagates downstream as a front (i.e., a step or Heaviside function). Worded differently, downstream of the tracer front the volume fraction content of tracer sediment

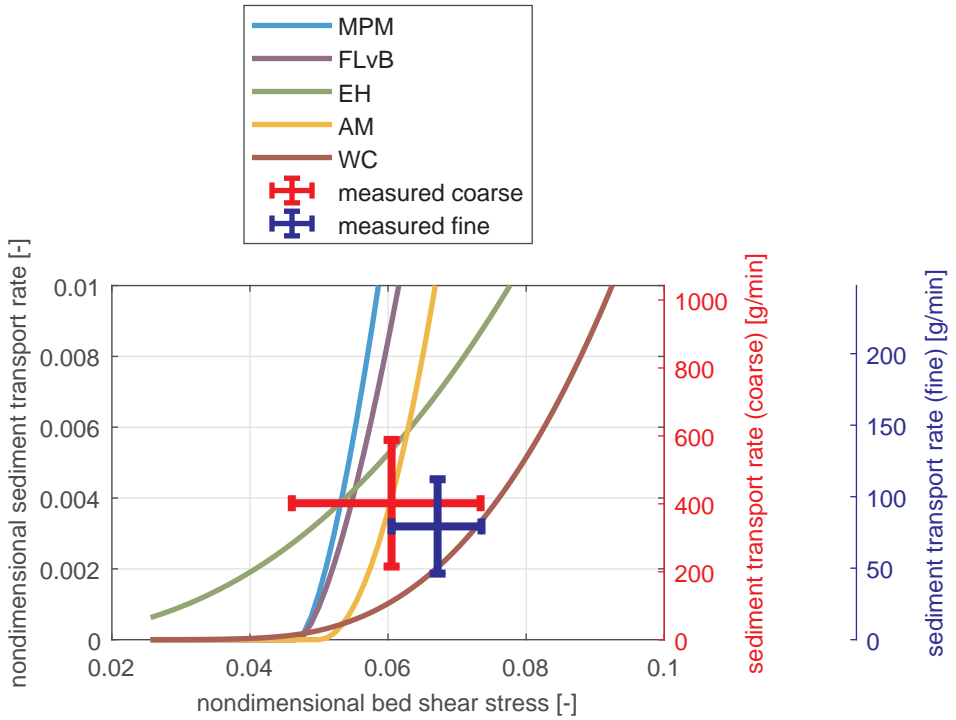


Figure C.6: Comparison between the measured (error bars) and predicted (lines) sediment transport rate using the closure relations by *Meyer-Peter and Müller (1948)* (MPM), *Fernandez-Luque and Van Beek (1976)* (FLvB), *Engelund and Hansen (1967)* (EH), *Ashida and Michiue (1972)*, and *Wilcock and Crowe (2003)* (WC). The error bars are one standard deviation long in each direction.

is 0 and it is 1 upstream of it. The speed at which the front travels is inversely related to the active layer thickness (Section C.8). The results show that an active layer thickness equal to 0.01 m seems reasonable (Figure C.4), which is consistent with the value for the active layer thickness obtained from the bed elevation profiles (Section C.6).

In numerical results, the discontinuous nature of the tracer front is not exactly preserved due to spurious numerical diffusion (Figure C.4). We have verified that the observed diffusive behavior is only numerical performing test with a finer mesh, as it reduces numerical diffusion.

We model Experiment P₄ using the calibrated friction coefficient, sediment transport relation, and active layer thickness. The active layer model predicts a constant entrainment of substrate sediment with time (Figure C.5a). This is because the active layer model does not capture the measured periodic entrainment of substrate sediment due to fluctuations in bed elevation. There is a slight increase in the surface content of tracer sediment with streamwise position along the patch. Downstream of the patch, the entrainment of non-tracer sediment causes a decrease in the content of tracer sediment with streamwise direction. At the downstream end of the flume, where the influence of the periodic

tracer entrainment is negligible, the active layer model reasonably well captures the mean behavior (Figure C.5b).

C.8. Predicted Propagation Speed of Tracer Sediment under Normal Flow Conditions

In this section we derive the celerity at which the active layer model predicts tracer sediment to propagate downstream under normal flow conditions.

The active layer equation for a tracer fraction reads:

$$\frac{\partial M_{a1}}{\partial t} + f_1^I \frac{\partial(\eta - L_a)}{\partial t} + \frac{\partial q_{b1}}{\partial x} = 0, \quad (C.72)$$

where the subscript 1 indicates the tracer fraction. Symbols are explained in Section C.5.1. Under normal flow conditions, the bed elevation remains constant with time because there is no streamwise imbalance in the total sediment transport rate, as the tracer has the same transport capacity as the non-tracer sediment. We assume a constant active layer thickness such that:

$$\frac{\partial M_{a1}}{\partial t} + \frac{\partial q_{b1}}{\partial x} = 0. \quad (C.73)$$

Applying the chain rule to the sediment transport relation we obtain:

$$\frac{\partial M_{a1}}{\partial t} + \frac{\partial q_{b1}}{\partial h} \frac{\partial h}{\partial x} + \frac{\partial q_{b1}}{\partial q} \frac{\partial q}{\partial x} + \frac{\partial q_{b1}}{\partial M_{a1}} \frac{\partial M_{a1}}{\partial x} = 0. \quad (C.74)$$

Under normal flow conditions there are neither gradients in flow depth nor discharge. Thus, we write:

$$\frac{\partial M_{a1}}{\partial t} + \frac{\partial q_{b1}}{\partial M_{a1}} \frac{\partial M_{a1}}{\partial x} = 0. \quad (C.75)$$

Equation (C.75) is an advection equation with characteristic speed:

$$c_{t1} = \frac{\partial q_{b1}}{\partial M_{a1}} = \frac{q_b}{L_a}. \quad (C.76)$$

Note the inverse proportionality between the propagation celerity of tracer sediment and the active layer thickness. From a physical point of view, this can be understood from the fact that a thicker active layer is associated with larger oscillations in bed elevation, and larger oscillations in bed elevation are associated with a slower adaptation of sorting processes (*Blom et al.*, 2008).

D

Supplementary material to Chapter 5

*Had I been present at the Creation,
I would have given some useful hints
for the better ordering of the universe.*

King Alfonso X “el Sabio” (“the Learned”) of Castile

*The water you touch in a river is the last of that which has passed,
and the first of that which is coming. Thus it is with time present.*

Da Vinci (ca. 1478–1518)

This appendix provides the supplementary material to Chapter 5 “A well-posed alternative to the Hirano active layer model for mixed-size sediment rivers”. Section D.1 presents the linearized SILKE model. In Section D.2 we derive the eigenvalues of the model and prove that (1) there exists a different time scale between the “fast” and “slow” eigenvalues, (2) that the model presents an instability mechanisms, and (3) that the model is well-posed. In Section D.3 we present the details of the derivation of the advection diffusion equation describing tracer sediment propagation. Section D.4 presents the conditions of the experiment by *Chavarrías et al.* (2019a). Section D.5 presents the conditions of the experiment by *Sayre and Hubbell* (1965) and the procedure to select a closure relation for the sediment transport rate under equilibrium conditions. Section D.6 presents the conditions of the experiment by *Blom et al.* (2003).

D

D.1. Matrices of the Linear Model

In this section we recast the perturbed system into matrix-vector form which is necessary to study the stability of the model and its well-posedness.

The reference state is obtained imposing equilibrium conditions. The reference bed slope is equal to the friction slope (i.e., $\frac{\partial \eta}{\partial x}|_0 = -S_{f0}$). The grain size distribution is uniform and arbitrary ($M_{ak0} = \text{ct.} \forall k \in \{1, N-1\}$, where ct. means a constant which satisfies the condition in Equation (5.6)). The particle activity is in equilibrium with the arbitrary grain size distribution. For this reason, imposing that the erosional rate is equal to the deposition rate we obtain that $\Gamma_{k0} = F_{ak} L_a \frac{\hat{E}_k}{\hat{D}_k} \forall k \in \{1, N-1\}$ and $\Gamma_{N0} = (1 - \sum_{k=1}^{N-1} F_{ak}) L_a \frac{\hat{E}_N}{\hat{D}_N}$.

We write the system of equations as:

$$\frac{\partial \mathbf{Q}'}{\partial t} + \mathbf{K}_0 \frac{\partial^2 \mathbf{Q}'}{\partial x^2} + \mathbf{A}_0 \frac{\partial \mathbf{Q}'}{\partial x} + \mathbf{B}_0 \mathbf{Q}' = 0. \quad (\text{D.1})$$

The vector of dependent variables is:

$$\mathbf{Q}' = [\eta', \underbrace{[\Gamma'_k]}_{N-1}, \Gamma'_N, \underbrace{[M'_{ak}]}_{N-1}]^T, \quad (\text{D.2})$$

The diffusion matrix is:

$$\mathbf{K}_0 = \begin{bmatrix} 0 & 0 & 0 & 0 \\ 0 & [-x_k \delta_{i,j}] & 0 & 0 \\ 0 & 0 & -x_N & 0 \\ 0 & 0 & 0 & 0 \end{bmatrix}. \quad (\text{D.3})$$

The matrix of gradient terms is:

$$\mathbf{A}_0 = \begin{bmatrix} 0 & 0 & 0 & 0 \\ [-\Gamma_k \frac{1}{1-\Gamma^2} \frac{\partial v_{pk}}{\partial b}] & [v_{pk} \delta_{i,j}] & 0 & 0 \\ -\Gamma_N \frac{1}{1-\Gamma^2} \frac{\partial v_{pN}}{\partial b} & 0 & v_{pN} & 0 \\ 0 & 0 & 0 & 0 \end{bmatrix}. \quad (\text{D.4})$$

The matrix of linear terms is:

$$\mathbf{B}_0 = \begin{bmatrix} 0 & \left[-\frac{1}{1-p} \hat{D}_l \right] & -\frac{1}{1-p} \hat{D}_N & \left[\frac{1}{1-p} (\hat{E}_l - \hat{E}_N) \right] \\ 0 & \left[\hat{D}_k \delta_{i,j} \right] & 0 & \left[-\hat{E}_k \delta_{i-1,j-3} \right] \\ 0 & 0 & \hat{D}_N & \left[\hat{E}_N \right] \\ 0 & \left[\frac{1}{1-p} (\hat{D}_l f_k^l - \delta_{k,l} \hat{D}_k) \right] & \left[\frac{1}{1-p} (\hat{D}_N f_k^l - \delta_{k,l} \hat{D}_k) \right] & \left[\frac{1}{1-p} (-f_k^l (\hat{E}_l - \hat{E}_N) + \delta_{k,l} \hat{E}_k) \right] \end{bmatrix}. \quad (\text{D.5})$$

To avoid an excess of notation, we do not mark that the variables in the matrices are evaluated at the reference state. The symbol $\delta_{i,j}$ represents the Dirac function.

For a case with two sediment size fractions the vector of dependent variables is:

$$\mathbf{Q}'_2 = [\eta', \Gamma'_1, \Gamma'_2, M'_{a1}]^T. \quad (\text{D.6})$$

The diffusion matrix is:

$$\mathbf{K}_{0_2} = \begin{bmatrix} 0 & 0 & 0 & 0 \\ 0 & -\chi_1 & 0 & 0 \\ 0 & 0 & -\chi_2 & 0 \\ 0 & 0 & 0 & 0 \end{bmatrix}. \quad (\text{D.7})$$

The matrix of gradient terms is:

$$\mathbf{A}_{0_2} = \begin{bmatrix} 0 & 0 & 0 & 0 \\ -\Gamma_1 \frac{1}{1-p} \frac{\partial v_{p1}}{\partial b} & v_{p1} & 0 & 0 \\ -\Gamma_2 \frac{1}{1-p} \frac{\partial v_{p2}}{\partial b} & 0 & v_{p2} & 0 \\ 0 & 0 & 0 & 0 \end{bmatrix}. \quad (\text{D.8})$$

The matrix of linear terms is:

$$\mathbf{B}_{0_2} = \begin{bmatrix} 0 & -\frac{1}{1-p} \hat{D}_1 & -\frac{1}{1-p} \hat{D}_2 & \frac{1}{1-p} (\hat{E}_1 - \hat{E}_2) \\ 0 & \hat{D}_1 & 0 & -\hat{E}_1 \\ 0 & 0 & \hat{D}_2 & \hat{E}_2 \\ 0 & \frac{1}{1-p} (\hat{D}_1 f_1^l - \hat{D}_1) & \frac{1}{1-p} \hat{D}_2 f_1^l & \frac{1}{1-p} (-f_1^l (\hat{E}_1 - \hat{E}_2) + \hat{E}_1) \end{bmatrix}. \quad (\text{D.9})$$

D.2. Eigenvalues of the Linear Model

In this section we study the order of magnitude of the eigenvalues of a case considering two sediment size fractions without diffusion. The fact that there are two different time scales, one associated with changes in bed elevation and bed surface texture, and a second one associated with changes in particle activity, allows us to decouple the problem. Studying the limit for a wave number tending to infinity we prove that our model is well-posed.

First we study the relative growth rate of perturbations associated with the different processes of the model. To this end we compute the characteristic polynomial of the system equating to zero the determinant $\det(\mathbf{M} - \omega \mathbf{1}) = 0$:

$$\omega^4 + c_3 \omega^3 + c_2 \omega^2 + c_1 \omega + c_0 = 0, \quad (\text{D.10})$$



where:

$$c_3 = -\zeta_1 - \zeta_2 + e_3 \frac{1}{1-p} i, \quad (\text{D.11})$$

$$c_2 = \zeta_1 \zeta_2 - e_3 \frac{1}{1-p} (\zeta_1 + \zeta_2) i - \frac{1}{1-p} (a_1 v_{p1} k_w + e_1 \hat{D}_1 i + a_2 v_{p2} k_w + e_2 \hat{D}_2 i) i, \quad (\text{D.12})$$

$$c_1 = \frac{1}{1-p} \left(v_{p1} v_{p2} k_w^2 (a_1 + a_2 + e_3) i + v_{p1} k_w \left(\hat{D}_2 (a_1 + e_1) + \hat{E}_2 a_1 \frac{1}{1-p} \right) + v_{p2} k_w \left(\hat{D}_1 (a_2 + e_2) + \hat{E}_1 a_2 \frac{1}{1-p} \right) \right), \quad (\text{D.13})$$

$$c_0 = -\left(\frac{1}{1-p} \right)^2 v_{p1} v_{p2} k_w^2 (a_1 \hat{E}_2 + a_2 \hat{E}_1), \quad (\text{D.14})$$

where:

$$\zeta_1 = v_{p1} k_w - \hat{D}_1 i, \quad (\text{D.15})$$

$$\zeta_2 = v_{p2} k_w - \hat{D}_2 i, \quad (\text{D.16})$$

$$e_1 = \hat{E}_1 (1 - f_1^I), \quad (\text{D.17})$$

$$e_2 = \hat{E}_2 f_1^I, \quad (\text{D.18})$$

$$e_3 = e_1 + e_2, \quad (\text{D.19})$$

$$a_1 = -F_{a1} L_a \frac{\hat{E}_1}{v_{p1}} \nu, \quad (\text{D.20})$$

$$a_2 = -(1 - F_{a1}) L_a \frac{\hat{E}_2}{v_{p2}} \nu, \quad (\text{D.21})$$

$$\nu = \frac{1}{1 - \text{Fr}^2} \frac{\partial v_{pk}}{\partial h}. \quad (\text{D.22})$$

The parameter ν is independent from the grain size because the derivative is independent from the grain size:

$$\frac{\partial v_{pk}}{\partial h} = 11.5 \sqrt{C_f \frac{u}{h}}, \quad (\text{D.23})$$

where we have assumed negligible hiding and the relation for the particle velocity developed by *Fernandez-Luque and Van Beek* (1976).

In our domain of interest the wave number of the perturbations is of order 1 or larger (equivalent to perturbations of the order of tens of meters or smaller). In this case, the real part of the parameters ζ_1 and ζ_2 scale with the particle velocity. The imaginary part

(\hat{D}_k) also scales with the particle velocity. This can be seen from the fact that $v_{pk}/\hat{D}_k = 0.0035/d_k$ (Section 5.2.2). The maximum order of parameters e_1 , e_2 , and e_3 , is that of the capacity entrainment rate (\hat{E}_k) . The capacity entrainment rate is significantly smaller than the particle velocity, which can be seen from the fact that $v_{pk}/\hat{E}_k = 575L_a f(\theta_k)$, where $f(\theta_k)$ is of order 1. Applying a similar analysis, we find that parameters a_1 and a_2 are also significantly smaller than the particle velocity. Hence, it is appropriate to discern between fast variables scaling with the particle velocity and slow variables.

To obtain an approximate solution of the eigenvalues we expand the eigenvalues in terms of an asymptotic power series $\omega = \omega^f + \epsilon\omega^s$ where ϵ is a parameter an order of magnitude smaller than the particle velocity and the superscript f and s indicate the fast and slow variables. Substituting the expansion in the characteristic polynomial (Equation (D.10)) and equating terms of equal order of magnitude we obtain the characteristic polynomial at first order:

$$\omega^f + (-\zeta_1 - \zeta_2)\omega^f + \zeta_1\zeta_2\omega^f = 0. \quad (\text{D.24})$$

Two solutions of Equation (D.24) are equal to 0, which is consistent with the assumption of different orders of magnitude of the eigenvalues. The other 2 solutions are $\omega_1^f = \zeta_1$ and $\omega_2^f = \zeta_2$. These are the eigenvalues associated to changes in particle activity.

At first order, the characteristic polynomial is:

$$b_2\omega^s + b_1\omega^s + c_0 = 0, \quad (\text{D.25})$$

where:

$$b_2 = \zeta_1\zeta_2, \quad (\text{D.26})$$

$$b_1 = \frac{1}{1-p} \left(\zeta_1(-e_2\hat{D}_2 + a_2v_{p2}k_w i) + \zeta_2(-e_1\hat{D}_1 + a_1v_{p1}k_w i) + e_3\zeta_1\zeta_2 i \right). \quad (\text{D.27})$$

The two solutions of Equation (D.25) are:

$$\omega^s = \frac{-b_1}{2b_2} \pm \frac{1}{2b_2} \sqrt{b_1^2 - 4b_2c_0}. \quad (\text{D.28})$$

The imaginary part of $-b_1/2b_2$ is negative. Hence growth of perturbations of the slow variables (i.e., a positive imaginary part of ω^s) is only possible if the imaginary part of the square root of the discriminant is positive. The discriminant can be written as a fourth order polynomial as a function of the wave number:

$$b_1^2 - 4b_2c_0 = \alpha_4k_w^4 + \alpha_3k_w^3 + \alpha_2k_w^2, \quad (\text{D.29})$$

where α_k are parameters depending on b_1 , b_2 , and c_0 . Parameter α_3 is purely imaginary and parameter α_2 is real. For this reason, for long waves (i.e., small values of k_w) the imaginary part of the discriminant is negligible. Under this condition, $\alpha_2 > 0$ implies

that the imaginary part of ω^s is only due to $-b_1/2b_2$ and hence negative. If $\alpha_2 < 0$ the imaginary part of ω^s may be positive. The parameter α_2 can be written as:

$$\alpha_2 = \beta_1 + \beta_2 + \beta_3 \Psi, \quad (\text{D.30})$$

where $\beta_1 > 0$, $\beta_2 > 0$, and $\beta_3 > 0$ are parameters depending on b_1 , b_2 , and c_0 and Ψ is given by Equation (5.27). Summarizing, only if $\Psi < 0$ perturbations can grow.

To prove that the model considering two sediment size fractions and no diffusion is well-posed, we compute the limit of the eigenvalues that are solution to Equation (D.25) for the wave number tending to infinity:

$$\omega_{1\text{lim}}^s = -i \frac{1}{2(1-p)} H_1, \quad (\text{D.31})$$

$$\omega_{2\text{lim}}^s = -i \frac{1}{2(1-p)} H_2, \quad (\text{D.32})$$

where:

$$H_1 = p_1 + e_3 + a_1 + a_2, \quad (\text{D.33})$$

$$H_2 = -p_1 + e_3 + a_1 + a_2, \quad (\text{D.34})$$

where:

$$p_1 = \sqrt{e_3^3 + (a_1 + a_2)^2 + 2e_3(a_1 r_1 + a_2 r_2)}, \quad (\text{D.35})$$

$$r_1 = \left(1 - \frac{2\hat{E}_2}{e_3} \right), \quad (\text{D.36})$$

$$r_2 = \left(-1 - \frac{2f_1^1(\hat{E}_1 - \hat{E}_2)}{e_3} \right). \quad (\text{D.37})$$

The subscript *lim* indicates that the parameter is the one in the limit for the wave number tending to infinity. Parameters a_1 , a_2 , and e_3 are real and positive, and parameters r_1 and r_2 are real and smaller than 1. If the term in the square root of p_1 is positive, the angular frequency is a negative pure imaginary number as $p_1 < e_3 + a_1 + a_2$. On the contrary, if the term in the square root is negative, it does not contribute to the growth rate, as it is a real number and the growth rate is negative. In summary, the growth rate of perturbations for both fast and slow variables is negative for a wave number tending to infinity. Thus, the model is well-posed.

D.3. Advection-Diffusion Behavior at Long Time Scales

In this section we present the details of the analysis of the SILKE model as regards to I tracer propagation in the “long” time scale (Section 5.3.4).

The system of equations modelling unisize tracer sediment propagation is:

$$(1-p)\frac{\partial \eta}{\partial t} = D - E, \quad (\text{D.38})$$

$$(1-p)\frac{\partial M_{a1}}{\partial t} + (1-p)f_1^1 \frac{\partial \eta}{\partial t} = D_1 - E_1, \quad (\text{D.39})$$

$$\frac{\partial \Gamma_1}{\partial t} + \frac{\partial v_p \Gamma_1}{\partial x} - \frac{\partial^2 x \Gamma_1}{\partial x^2} = E_1 - D_1, \quad (\text{D.40})$$

$$\frac{\partial \Gamma_2}{\partial t} + \frac{\partial v_p \Gamma_2}{\partial x} - \frac{\partial^2 x \Gamma_2}{\partial x^2} = E_2 - D_2, \quad (\text{D.41})$$

where, subscript 1 identifies the tracer sediment. Note that as the properties of the tracer sediment are equal as those of the parent material, the particle velocity, diffusivity, capacity of entrainment and deposition are also equivalent. Due to the equilibrium conditions (i.e., $\partial \eta / \partial t = 0$) we obtain:

$$D = E \implies \Gamma_T \hat{D} = L_a \hat{E}_1, \quad (\text{D.42})$$

where we have defined $\Gamma_T = \Gamma_1 + \Gamma_2$ [m] as the total amount of active sediment. In Equation (D.42) we observe that Γ_T remains constant with time. We write Equation (D.39) as:

$$\frac{\partial F_{a1}}{\partial t} = -\frac{1}{1-p} \frac{\Gamma_T}{L_a} \hat{D} (F_{a1} - F_{\Gamma_1}), \quad (\text{D.43})$$

where we define $F_{\Gamma_1} = \Gamma_1 / \Gamma_T$ [-] as the fraction of active tracer sediment. We write Equation (D.40) as:

$$\frac{\partial F_{\Gamma_1}}{\partial t} + v_p \frac{\partial F_{\Gamma_1}}{\partial x} - x \frac{\partial^2 F_{\Gamma_1}}{\partial x^2} = \hat{D} (F_{a1} - F_{\Gamma_1}), \quad (\text{D.44})$$

where we have used that the particle velocity and diffusivity do not vary in space as the flow is uniform.

We introduce the variables:

$$c = \frac{M_{a1} + \Gamma_1}{L_a + \Gamma_T} = \frac{F_{a1} L_a + F_{\Gamma_1} \Gamma_T}{L_a + \Gamma_T}, \quad (\text{D.45})$$

$$\delta = F_{a1} - F_{\Gamma_1}. \quad (\text{D.46})$$

Change of variables yields:

$$\begin{aligned} & \frac{\partial c}{\partial t} + v_p \frac{\Gamma_T}{L_a + \Gamma_T} \frac{\partial c}{\partial x} - x \frac{\Gamma_T}{L_a + \Gamma_T} \frac{\partial^2 c}{\partial x^2} = \\ & v_p \frac{L_a \Gamma_T}{(L_a + \Gamma_T)^2} \frac{\partial \delta}{\partial x} - x \frac{L_a \Gamma_T}{(L_a + \Gamma_T)^2} \frac{\partial^2 \delta}{\partial x^2} - \frac{p}{1-p} \hat{D} \frac{\Gamma_T}{L_a + \Gamma_T} \delta, \end{aligned} \quad (\text{D.47})$$

$$\begin{aligned} \frac{\partial \delta}{\partial t} + v_p \frac{L_a}{L_a + \Gamma_T} \frac{\partial \delta}{\partial x} - x \frac{L_a}{L_a + \Gamma_T} \frac{\partial^2 \delta}{\partial x^2} = \\ v_p \frac{\partial c}{\partial x} - x \frac{\partial^2 c}{\partial x^2} - \hat{D} \left(\frac{1}{1-p} \frac{\Gamma_T}{L_a} + 1 \right) \delta. \end{aligned} \quad (\text{D.48})$$

We seek an approximation of the system of equations in terms of the asymptotic power series:

$$c = c_0 + \epsilon c_1 + \dots, \quad (\text{D.49})$$

$$\delta = \epsilon \delta_1 + \epsilon^2 \delta_2 + \dots. \quad (\text{D.50})$$

We see that we cannot use a naive approximation, as in this case δ would disappear from the problem. For this reason we introduce the slow variables $T = \epsilon t$ and $X = \epsilon x$. The derivatives are:

$$\frac{\partial c}{\partial T} = \frac{\partial c}{\partial t} \frac{\partial t}{\partial T} = \frac{1}{\epsilon} \frac{\partial c}{\partial t}, \quad (\text{D.51})$$

$$\frac{\partial c}{\partial X} = \frac{\partial c}{\partial x} \frac{\partial x}{\partial X} = \frac{1}{\epsilon} \frac{\partial c}{\partial x}, \quad (\text{D.52})$$

$$\frac{\partial^2 c}{\partial X^2} = \frac{1}{\epsilon^2} \frac{\partial^2 c}{\partial x^2}. \quad (\text{D.53})$$

Substituting the expansions, the problem is rewritten as:

$$\begin{aligned} \epsilon \frac{\partial (c_0 + \epsilon c_1)}{\partial T} + v_p \frac{\Gamma_T}{L_a + \Gamma_T} \epsilon \frac{\partial (c_0 + \epsilon c_1)}{\partial X} - x \frac{\Gamma_T}{L_a + \Gamma_T} \epsilon^2 \frac{\partial^2 (c_0 + \epsilon c_1)}{\partial X^2} = \\ v_p \frac{L_a \Gamma_T}{(L_a + \Gamma_T)^2} \epsilon \frac{\partial (\epsilon \delta_1 + \epsilon^2 \delta_2)}{\partial X} - x \frac{L_a \Gamma_T}{(L_a + \Gamma_T)^2} \epsilon^2 \frac{\partial^2 (\epsilon \delta_1 + \epsilon^2 \delta_2)}{\partial X^2} \\ - \frac{p}{1-p} \hat{D} \frac{\Gamma_T}{L_a + \Gamma_T} (\epsilon \delta_1 + \epsilon^2 \delta_2), \end{aligned} \quad (\text{D.54})$$

$$\begin{aligned} \epsilon \frac{\partial (\epsilon \delta_1 + \epsilon^2 \delta_2)}{\partial T} + v_p \frac{L_a}{L_a + \Gamma_T} \epsilon \frac{\partial (\epsilon \delta_1 + \epsilon^2 \delta_2)}{\partial X} - x \frac{L_a}{L_a + \Gamma_T} \epsilon^2 \frac{\partial^2 (\epsilon \delta_1 + \epsilon^2 \delta_2)}{\partial X^2} = \\ v_p \epsilon \frac{\partial (c_0 + \epsilon c_1)}{\partial X} - x \epsilon^2 \frac{\partial^2 (c_0 + \epsilon c_1)}{\partial X^2} - \hat{D} \left(\frac{1}{1-p} \frac{\Gamma_T}{L_a} + 1 \right) (\epsilon \delta_1 + \epsilon^2 \delta_2). \end{aligned} \quad (\text{D.55})$$

We obtain a problem at order ϵ :

$$\frac{\partial c_0}{\partial T} + v_p \frac{\Gamma_T}{L_a + \Gamma_T} \frac{\partial c_0}{\partial X} = -\frac{p}{1-p} \hat{D} \frac{\Gamma_T}{L_a + \Gamma_T} \delta_1, \quad (\text{D.56})$$

$$0 = v_p \frac{\partial c_0}{\partial X} - \hat{D} \left(\frac{1}{1-p} \frac{\Gamma_T}{L_a} + 1 \right) \delta_1, \quad (\text{D.57})$$

and a problem at order ϵ^2 :

$$\frac{\partial c_1}{\partial T} + v_p \frac{\Gamma_T}{L_a + \Gamma_T} \frac{\partial c_1}{\partial X} - x \frac{\Gamma_T}{L_a + \Gamma_T} \frac{\partial^2 c_0}{\partial X^2} = v_p \frac{L_a \Gamma_T}{(L_a + \Gamma_T)^2} \frac{\partial \delta_1}{\partial X} - \frac{p}{1-p} \hat{D} \frac{\Gamma_T}{L_a + \Gamma_T} \delta_2, \quad (\text{D.58})$$

$$\frac{\partial \delta_1}{\partial T} + v_p \frac{L_a}{L_a + \Gamma_T} \frac{\partial \delta_1}{\partial X} = v_p \frac{\partial c_1}{\partial X} - x \frac{\partial^2 c_0}{\partial X^2} - \hat{D} \left(\frac{1}{1-p} \frac{\Gamma_T}{L_a} + 1 \right) \delta_2. \quad (\text{D.59})$$

From Equation (D.57) we obtain:

$$\frac{\partial \delta_1}{\partial X} = \frac{v_p}{\hat{D} \left(\frac{1}{1-p} \frac{\Gamma_T}{L_a} + 1 \right)} \frac{\partial^2 c_0}{\partial X^2}. \quad (\text{D.60})$$

Substituting in Equations (D.56) and (D.58) we obtain:

$$\frac{\partial c_0}{\partial T} + v_p \frac{\Gamma_T}{L_a + \Gamma_T} \left[1 + \frac{p}{\frac{1}{1-p} \frac{\Gamma_T}{L_a} + 1} \right] \frac{\partial c_0}{\partial X} = 0, \quad (\text{D.61})$$

$$\begin{aligned} \frac{\partial c_1}{\partial T} + v_p \frac{\Gamma_T}{L_a + \Gamma_T} \frac{\partial c_1}{\partial X} - \frac{\Gamma_T}{L_a + \Gamma_T} \left[x + v_p^2 \frac{L_a}{L_a + \Gamma_T} \frac{1}{\hat{D} \left(\frac{1}{1-p} \frac{\Gamma_T}{L_a} + 1 \right)} \right] \frac{\partial^2 c_0}{\partial X^2} = \\ - \hat{D} \frac{\Gamma_T}{L_a + \Gamma_T} \frac{p}{1-p} \delta_2. \end{aligned} \quad (\text{D.62})$$

We multiply Equation (D.62) by ϵ and we add the result to Equation (D.61). Substituting back to the original dependent variables, at first order the result is:

$$\frac{\partial c_0}{\partial t} + v_p \frac{\Gamma_T}{(1-p)L_a + \Gamma_T} \frac{\partial c_0}{\partial x} - \frac{\Gamma_T}{L_a + \Gamma_T} \left[x + \frac{v_p^2}{\hat{D}} \left(\frac{L_a}{L_a + \Gamma_T} \right) \left(\frac{(1-p)L_a}{(1-p)L_a + \Gamma_T} \right) \right] \frac{\partial^2 c_0}{\partial x^2} = 0. \quad (\text{D.63})$$

D.4. Conditions of the Experiment by Chavarrías et al. (2019)

In this section we summarize the parameters of the experiment conducted by *Chavarrías et al. (2019a)*. The bed was initially flat, with a constant slope, and composed of sediment painted red color. The same sediment was fed upstream at a constant rate. A constant flow rate and downstream water level were imposed. After a steady pattern of bed forms was established and equilibrium conditions were satisfied, unpainted (tracer) sediment was fed at the upstream end. Using a submerged camera situated at the downstream end of the flume (9.17 m downstream from the feeding location) allowed measuring the combined content of tracer sediment (at the bed surface and in transport) over time until the bed surface was composed mainly of tracer sediment (after approximately 5 h). The main parameters of the experiment are shown in Table D.1.

h [m]	u [m/s]	Fr [-]	q_{b0} [m ² /s]	C_f [-]	C_{fb} [-]	d_1 [m]
0.187	0.799	0.59	7.86×10^{-6}	0.0104	0.0084	0.0055

Table D.1: Main parameters of the experiment conducted by *Chavarrías et al.* (2019a) of unisize tracer propagation under equilibrium conditions. Parameter q_{b0} is the sediment feed rate.

D.5. Conditions, Results, and Model Calibration of the Experiment by Sayre and Hubbell (1965)

Sayre and Hubbell (1965) conducted an experiment to evaluate the risk of nuclear disposal in rivers. To this end, they added 18 kg of radioactively-labeled sand along an approximately 17 m wide stretch of the North Loup River (Nebraska, US). They tracked the propagation of the tracer sediment during approximately 12 days (287.4 h) by means of a scintillation detector, covering a distance of about 550 m. They took 11 longitudinal profiles on the right and left-hand side of the river and 2 along the centerline. The minimum and maximum sizes of the bed sediment were equal to 0.088 mm and 9.424 mm, respectively, with a geometric mean grain size equal to 0.315 mm. They discretized the sediment mixture in 11 characteristic grain sizes. The tracer sediment had a narrower grain size distribution. The minimum and maximum sizes were 0.175 mm and 0.500 mm and it was selected to have a mean grain size similar to the bed material and to be transported as bed load. The flow conditions did not significantly vary during the measurement campaign and it is reasonable to assume that normal flow prevailed. The time-averaged values of the hydraulic parameters are presented in Table D.2. *Sayre and Hubbell* (1965) report that the bed was covered with dunes between 0.30 m and 0.46 m height and based on core samples they found that the average maximum depth at which tracer was found was 0.44 m below the bed surface.

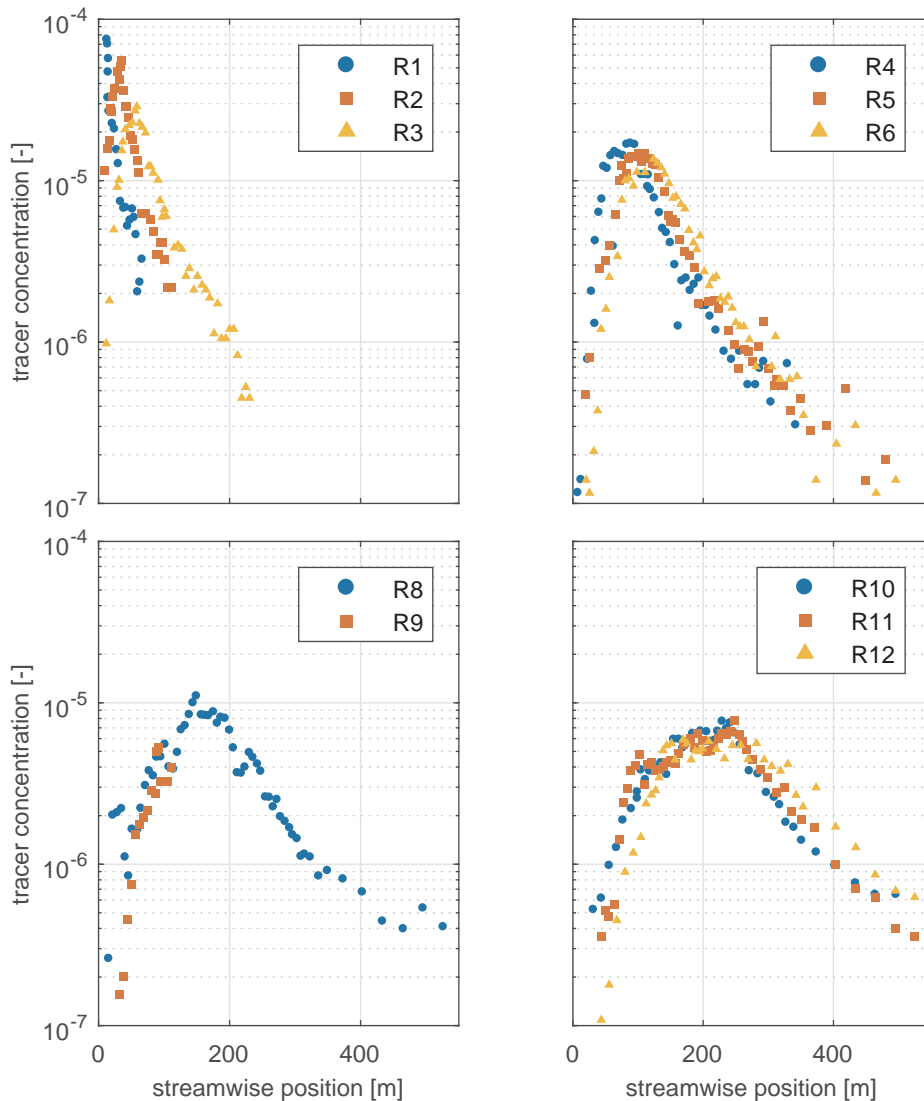
h [m]	u [m/s]	Fr [-]	q_{b0} [m ² /s]	C_f [-]	C_{fb} [-]
0.63	0.69	0.28	7.09×10^{-5}	0.0107	0.0049

Table D.2: Main parameters of the field campaign conducted by *Sayre and Hubbell* (1965). The skin friction coefficient is derived using the predictor by *Engelund and Hansen* (1967).

Sayre and Hubbell (1965) explain that the left-hand side measurements are less representative of the general dispersion behavior because a significant amount of tracer was captured in a deep trough near the upstream location for several days. Later it was re-entrained and part of it caught up with the sediment at the downstream part of the domain. For this reason we focus on the measurements that *Sayre and Hubbell* (1965) did on the right-hand side of the river (Figure D.1). According to *Sayre and Hubbell* (1965), the last measurement on the right-hand side unaffected by the later re-entrainment of sediment from the left-hand side was the one done 117.7 h after placing the tracer sediment (Table D.3).

The measured concentration at the downstream tail decreases linearly in logarithmic

scale, which indicates the possibility of anomalous diffusion. This observation is valid for all measurements. In assessing the possibility of anomalous diffusion it would be beneficial to know the confidence interval of the measured data. This is important as the difference between the concentration at the tails and at center spans two orders of magnitude and the measurement error increases for the small concentrations at the tails. This makes difficult to judge whether data shows anomalous diffusion or not.



D

Figure D.1: Tracer concentration measured *Sayre and Hubbell (1965)* for all profiles taken along the right-hand side of the river. See Table D.3 for the time after dosing at which each profile was taken.

profile	R1	R2	R3	R4	R5	R6	R8	R9	R10	R11	R12
time [h]	3.2	22.2	44.2	70.9	96.2	117.7	170.1	196	216.5	241.6	287.4

Table D.3: Time after dosing at which concentrations were measured.

D *Sayre and Hubbell* (1965) estimate the bed load transport rate of the size fractions comprised between 0.225 mm and 0.420 mm to be 171 ton/day. This is equivalent to $4.48 \times 10^{-5} \text{ m}^2/\text{s}$ (without including pores). The estimate is based on the measured average propagation celerity of the tracer sediment they placed in the river bed. We consider the bed surface grain size distribution reported by *Sayre and Hubbell* (1965) discretized using 11 characteristic grain sizes. Based on the bed surface grain size distribution and the mean flow parameters (Table D.2), we compute the sediment transport rate using several closure relations varying the skin friction coefficient (C_{fb}). In Figure D.2 we plot the sum of the sediment transport rate of the two fractions comprising the range estimated by *Sayre and Hubbell* (1965). Based on the mean surface grain size, bed shear stress, and geometry of the dunes reported by *Sayre and Hubbell* (1965), we compute the skin friction coefficient predicted using different closure relations (Figure D.2). We find that the sediment transport relation by *Ashida and Michiue* (1971) in combination with the skin friction predictor by *Engelund and Hansen* (1967) performs best, with an error of only 3%.

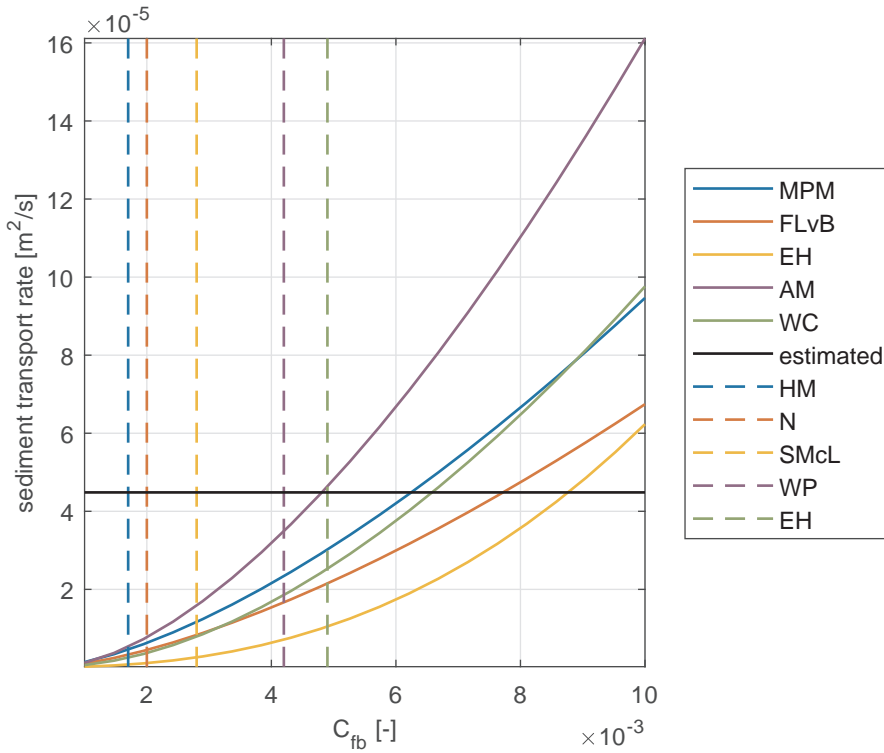


Figure D.2: Sediment transport rate in the range of the tracer sediment predicted using the relations by Meyer-Peter and Müller (1948) with Egiazaroff (1965) to account for hiding (MPM), Fernandez-Luque and Van Beek (1976) with Egiazaroff (1965) to account for hiding (FLvB), Engelund and Hansen (1967) (EH), Ashida and Michiue (1971) (AM), and Wilcock and Crowe (2003) (WC). The value estimated by Sayre and Hubbell (1965) is shown in black. The vertical dashed lines indicate the value of the skin friction as predicted using the relations by Haque and Mahmood (1983) (HM), Nikwadse (1933) (N), Smith and McLean (1977) (SMcL), Wright and Parker (2004) (WP), and Engelund and Hansen (1967) (EH).

D.6. Conditions of the Experiment by Blom et al. (2003)

In this section we present the initial and final conditions of Experiment B2 conducted by Blom et al. (2003) (Table D.4). The characteristic grain sizes of the trimodal mixture where equal to 0.68 mm, 2.1 mm, and 5.7 mm.

D

variable	initial	final
h [m]	0.155	0.389
u [m/s]	0.63	0.69
S_f [–]	1.9×10^{-3}	2.2×10^{-3}
H [m]	0.018	0.122
C_{fb} [–]	0.0032	0.0069
q_b [m ² /s]	1.79×10^{-5}	4.45×10^{-5}
F_{b1} [–]	0.34	0.90
F_{b2} [–]	0.54	0.05
F_{a1} [–]	0.50	0.88
F_{a2} [–]	0.43	0.07

Table D.4: Main parameters of the experiment conducted by *Blom et al.* (2003). The symbols not defined previously are the mean dune height (H), and the fraction of the sediment transport rate of size fraction k (F_{bk}). We derive the skin friction coefficient by correcting the total friction reported by *Blom* (2008) for (1) flume wall friction using the method by *Johnson* (1942) (see e.g. *Guo* (2015)), and (2) form drag using the method by *Smith and McLean* (1977). The values for the volume fraction content of sediment in the active layer are derived integrating the measured vertical grain size distribution profiles. The subscripts 1 and 2 correspond to the fine and medium size fractions, respectively.

List of Figures

1.1	Proserpina dam, Mérida (Spain). Picture by Alonso de Mendoza (CC BY-SA4.0).	2
1.2	Relief of Sobek in the temple of Kom Ombo (Egypt). Picture by Hedwig Storch (CC BY-SA3.0).	3
1.3	Picture of the scale model of the Dutch Rhine-Meuse branches built by the <i>Waterloopkundig Laboratorium</i> in the centre of Delft in 1950. The model was built in the Schuttersveld and the picture was taken from Het Raam. The church on the top right corner is the Lutherse Kerk (also known as Saint George’s Chapel) and the windmill on the top left is Molen de Roos. Flow goes from bottom to top. The right-hand branch is the Lek. The second branch starting to count from the right is the Waal. The third one is the Meuse. The upstream boundary is approximately at Wijk bij Duurstede and Tiel. The Biesbosch is visible in the centre of the domain on the left. Picture courtesy of Deltares.	4
1.4	Numerical discretization of the Wadden Sea to compute the tide after closure of the Zuiderzee by the Afsluitdijk (the straight line on the bottom part of domains 2c and 4). The subplot on the right indicates the nodes and the channels that divide the domain. The general plot shows the area represented by each channel. Some channels are subdivided (e.g. 1a, 1b, and 1c) as the properties along the channel change significantly although there is no connection (node) with another channel. This image is reproduced from the original in <i>Lorentz</i> (1926).	5
1.5	Predicted water level and water discharge division after closure of the Zuiderzee for the conditions of the storm of 1894. The figure presents the prediction for the conditions on the 23 rd of December of 1894 between 3 and 4 am. Water level values (in centimeters) are underlined. Water flow direction is shown using arrows and discharge values (in cubic meters per second) are on the arrows. This image is reproduced from the original in <i>Lorentz</i> (1926).	6
1.6	Morphodynamic simulation of the Bovenrijn between Emmerich (Germany), Rhine-kilometer 852.3, and the bifurcation near Pannerden (the Netherlands), Rhine-kilometer 866.0 (<i>Ottevanger et al.</i> , 2015). The Rhine bridge at Emmerich is seen in the lower right-hand corner. The flow discharge is equal to 2251 m ³ /s. The simulation is made using Delft3D. Data represents the river in 2015. Satellite data from Google Earth®	7

1.7 Solutions of the model representing the propagation of waves on a string. In panel **a** we show the model sketch. The transparent string represents the equilibrium solution. The solutions in panels **b-c** are found considering $\gamma = 1 \text{ m}^2/\text{s}^2$ and imposing an initial conditions. In panels **d-e** we consider $\gamma = -1 \text{ m}^2/\text{s}^2$ and we impose an initial condition. In panels **f-g**, we consider a value of $\gamma = -1 \text{ m}^2/\text{s}^2$ and we impose a future condition at $\tau = 0.6 \text{ s}$. The value of k is equal to 10 rad/m in panels **b, d, and f** and it is equal to 20 rad/m in panels **c, e, and g**. 9

2.1 Schematic of the effect of a perturbation in bed elevation in (a) a unisize sediment case and (b) a mixed sediment case. In the latter case, a perturbation in bed elevation introduces another wave, which is mainly related to the bed surface grain size distribution. Yet, each wave perturbs the flow, bed elevation, and bed surface grain size distribution. The arrows indicate the direction of propagation of the perturbations under subcritical flow conditions. The words “water”, “bed”, and “sorting” refer to a perturbation in water flow, bed level, and surface grain size distribution, respectively. 19

2.2 Representation of the main variables of the active layer model (Hirano, 1971) and the vertically continuous model proposed by Viparelli et al. (2017). 21

2.3 Discriminant Δ_{alS_2} , Equation 2.26, as a function of: (a) the hiding relation for the fine fraction ξ_1 , (b) the prefactor of the sediment transport formula A , (c) the power B , and (d) the critical Shields stress θ_c . The blue line is obtained varying the parameters from the reference state using the Meyer-Peter and Müller (1948) (MPM) sediment transport relation. The red line is obtained using the Engelund and Hansen (1967) (EH) relation. The yellow line is obtained by varying the characteristic grain size of the fine fraction using the hiding relation by Egiazaroff (1965), Equation (A.15), in combination with the MPM relation, the purple line by varying the coefficient b of the power law function by Parker et al. (1982), Equation (2.7), in combination with the MPM relation. The dots represent the reference situation described in Table 2.2. Note that there is a different reference situation depending on the sediment transport relation. 30

2.4 Discriminant Δ_{alS_2} , Equation 2.26, as a function of (a) the active layer thickness L_a , (b) the hiding function of the fine fraction ξ_1 , and (c) the morphological factor M_f . Numerical solutions of (d) Simulation 1, (e) Simulation 2, (f) Simulation 3, and (g) Simulation 4. See Table 2.3 for the parameters definition. 34

- 2.5 Maximum flow depth h_{\max} (nondimensionalized by the normal flow depth h_n) that develops as a consequence of ellipticity. In (a) the maximum flow depth is plotted against the discriminant Δ_{als_2} for a horizontal discretization length (Δx) equal to 0.1 m and for a thickness of the bookkeeping layers (Δz) equal to 0.01 m (red dots) and 0.10 m (blue dots). The vertical black lines connect two simulations in which all parameters but Δz are the same. In (b) the maximum flow depth is plotted against the *hyperbolic flow depth* (h_{hyp}) nondimensionalized with the normal flow depth. Each black dot is the result of a simulation. The black lines connect simulations with the same physical parameters and the grey line is the perfect agreement. In (c) the maximum flow depth is plotted against the distance from upstream at which the maximum flow depth occurs (x_{\max}) nondimensionalized with the length of the domain (L) for a thickness of the bookkeeping layers (Δz) equal to 0.01 m and for a horizontal discretization length equal to 0.1 m (orange dots) and 0.2 m (green dots). The black lines connect two simulations in which all parameters but Δx are the same. 37
- 2.6 Grain size stratification at the end of: (a) Simulation 1, (b) Simulation 5, (c) Simulation 6, and (d) Simulation 7. The substrate of the ill-posed simulations coarsens unrealistically. 38
- 2.7 Results of an ill-posed simulation with 3 grain size fractions under degradational conditions into a substrate coarser than the active layer: (a) bed elevation at selected times, (b) surface mean grain size with time, and (c) grain size stratification at the end of the simulation. 40
- 2.8 Ill-posed domain for degradational cases in which the sediment mixture is discretized into (a) two and (b) three size fractions as a function of the Froude number (Fr) and the difference between the mean grain size of the sediment in the active layer (D_{ma}) and at the interface between the active layer and the substrate (D_{ml}). When the mixture is discretized into three size fractions the model may be ill-posed under degradational conditions into a substrate coarser than the active layer. 41
- 3.1 Growth rate of perturbations added to the reference case (tables 3.1 and 3.2) as a function of the wave number and the wavelength: (a)-(b) iSWE, $Fr < 2$ (Case I1, well-posed), (c)-(d) iSHE+Exner (Case B1, well-posed), and (e)-(f) iSWE, $Fr > 2$ (Case I2, ill-posed). The subplots in the two columns show the same information but highlight the behaviour for large wave numbers (left column) and for large wavelengths (right column). Red and green indicates growth and decay of perturbations, respectively. . 58
- 3.2 Simulated bed elevation (surface) and mean grain size at the bed surface (colour) of a well-posed case (left column, H1, table 3.3) and an ill-posed case (right column, H2, table 3.3). In each row we present the results for varying cell size. The colour of the $x - y$ plane shows the result of the routine that checks whether the conditions at each node yield a well-posed (green) or an ill-posed (red) model. 62

- 3.3 Growth rate of perturbations added to the reference case (tables 3.1 and 3.4) as a function of the wave number and the wavelength: (a)-(b) without secondary flow (Case S1, well-posed), (c)-(d) accounting for secondary flow with diffusion (Case S2, well-posed), and (e)-(f) accounting for secondary flow without diffusion (Case S3, ill-posed). The subplots in the two columns show the same information but highlight the behaviour for large wave numbers (left column) and for large wavelengths (right column). Red and green indicates growth and decay of perturbations, respectively. 64
- 3.4 Wavelength of the shortest perturbation with positive growth rate (l_{wm}) relative to the flow depth (h) as a function of the Froude number (Fr) and the diffusion coefficient (ν) relative to the diffusion coefficient according to Elder (1959) (ν_E). Different flow conditions are studied varying the flow depth between 0.2 m and 1.5 m from the reference case (table 3.1). The cyan markers indicate the conditions of three numerical simulations with different values of the diffusion coefficient (Section 3.5.1). The arrow next to the diamond marker indicates that the value lies outside the figure. Red (green) colours indicate that the shortest wave length with positive growth rate are smaller (larger) than the flow depth. 66
- 3.5 Growth rate of perturbations added to the reference case (tables 3.1 and 3.5) as a function of the wave number and the wavelength: (a)-(b) Case B2 (ill-posed), (c)-(d) Case B3 (well-posed), (e)-(f) Case B4 (ill-posed), and (g)-(h) Case B5 (ill-posed). The subplots in the two columns show the same information but highlight the behaviour for large wave numbers (left column) and for large wavelengths (right column). Red and green indicates growth and decay of perturbations, respectively. 69
- 3.6 Domain of ill-posedness due to the bed slope effect under mixed-size sediment conditions: as a function of the ratio between fine and coarse sediment (a), the Froude number (b), and the volume fraction content of fine sediment in the active layer (c). The bed slope effect is measured by g_{s1}/A_s and the range of parameters is obtained by varying B_s (Equation (3.23)). The range of values of d_1/d_2 is obtained by varying d_2 . The range of values of the Froude number is obtained by varying u . The volume fraction content of fine sediment at the interface between the active layer and the substrate is kept equal to the volume fraction content of fine sediment in the active layer. The conditions represent unisize sediment when $d_1/d_2 = 1$, $F_{a1} = 0$, or $F_{a1} = 1$ 70
- 3.7 Flow depth at the end of the simulations: (a) without accounting for secondary flow (Case S1), (b) setting $\nu = \nu_E$ (Case S2), (c) setting $\nu = 0$ (Case S3), (d) setting $\nu = 100\nu_E$, and (e) setting $\nu = \nu_E$ using a coarser numerical grid (Case S2). The colour map is adjusted for each case and centred around the initial and equilibrium value ($h = 1$ m). 72

- 3.8 Flow depth at the end of the simulations of: (a) Case B₁, (b) Case B₂; and volume fraction content of fine sediment in the active layer: (c) Case B₃, (d) Case B₄, (e) Case B₅. The colour map is adjusted for each case and centred around the initial and equilibrium value. 73
- 3.9 Conditions in which the flow model (top) and the morphodynamic model (bottom) is stable, unstable, or ill-posed. The code below the model type (e.g., S₁) indicates an example case of such a situation. See tables 3.2, 3.3, 3.4, and 3.5 for an explanation of the cases S₁₋₃, B₁₋₄, H₁₋₂, and I₂. * Parameter β_c denotes the critical width-to-depth ratio (*Engelund and Skovgaard, 1973; Colombini et al., 1987; Schielen et al., 1993*). 77
- 4.1 Maximum imaginary part of all the eigenvalues of the reference case (Table 4.1) as a function of α . In this case $\alpha_c = 16.1$ is the smallest value of $\alpha > 1$ that yields a well-posed model (i.e., all eigenvalues are real). 88
- 4.2 Comparison between (a) the steady and unsteady values of the regularization parameter α_c , and (b) the exact and approximate values for a 3 size fractions case. 89
- 4.3 Sketch of the flume set-up: (a) turbulence dissipator, (b) metal plate with glued sediment, (c) alluvial bed, (d) feeder, (e) sand trap, (f) sediment pump, (g) weir, (h) laser sensors for water and bed surface elevation, and (i) camera for measuring the bed surface grain size distribution. 92
- 4.4 Measured bed elevation before fine sediment of the patches is entrained showing the superposition of bedforms of two different length scales (Experiment I₄ at 1:51 h). 94
- 4.5 Sketch of the cyclic entrainment of substrate sediment: (a) bedforms formed out of coarse sediments only, (b) fine sediment from the patch is entrained in the trough of a bedform, (c) a degradational wave forms and travels downstream, (d) coarse sediment from upstream fills the pit left by the degradational wave. 94
- 4.6 Measured surface fraction content of coarse sediment as a function of time for various lengths of the patch L_p : at the center of the patch (a,c,e,g), and at the downstream end (b,d,f,h). Note that the streamwise location of the center of the patch varies for each experiment while the downstream position is the same for all cases ($x = 9.15$ m). 95
- 4.7 Detrended bed elevation as a function of time in Experiment (a) I₁, (b) I₂, (c) I₃, and (d) I₄. The dashed black lines indicate the boundaries of the patch. The bed elevation is detrended subtracting the bed slope of each profile individually, obtained fitting a first degree polynomial. 97
- 4.8 Probability density of detrended bed elevation: (a) upstream of the patch, (b) at the patch, (c) and downstream of the patch. 98

- 4.9 Bed elevation at $t = 300$ s predicted using the (a) active layer model (Hirano, 1971) and (b) regularized active layer model. Each of the 13 lines presents the results computed using a different cell size (ranging from 0.1 m down to 2.44×10^{-5} m, where darker colors represent smaller cell sizes). Panels (c) and (d) present the error at a certain time using a particular cell size (see Equation (4.13)) when using the active layer model and the regularized active layer model, respectively. In panels (b) and (d) only one line is visible, as it overlaps all other lines. 100
- 4.10 Comparison between measured data and regularized model results: Experiment I1 (a-d), Experiment I2 (e-h), Experiment I3 (i-l), and Experiment I4 (m-p). The first and second columns show the measured and predicted bed elevation with time, respectively. The vertical dashed lines indicate the position of the patch of fine sediment. The third and fourth columns present the surface fraction content of coarse sediment at the center of the patch of fine sediment and at the downstream end of the flume, respectively. 103
- 4.11 Bed elevation (a) and mean grain size at the bed surface (b) as a function of time predicted in Experiment I4 using the regularized active layer model using 2 and 3 sediment sizes. 104
- 4.12 Bed elevation (a) and mean grain size of the bed surface sediment (b) with time predicted for the thought experiment based on Experiment E8-E9 conducted by Ribberink (1987) using Ribberink's two-layer model and the regularized active layer model. The results of the two-layer model are extracted from Figure 7.9 of Ribberink (1987). 106
- 5.1 Sketch representing the main variables of the active layer model (Hirano, 1971) and the SILKE model. The figure is adapted from Figure 2 in Chavarrias et al. (2018a). 118
- 5.2 Separatrix between the growth domain (G) and decay domain (D) as a function of the wave number (k_w) and Ψ (Equation (5.27)). The wave number is nondimensionalized using the fine grain size. Parameter Ψ is relative to its minimum value $\Psi_{\min} = 1/\phi - 2V$. Each line represents a separatrix as a function of the ratio between: (a) the grain size of the fine fraction and the active layer thickness, and (b) the grain sizes. In (a) the active layer thickness is varied to obtain different conditions while in (b) we vary the grain size of the fine size fraction. The green markers represent the conditions of two numerical simulation under growth (circle) and decay (square) conditions. In the numerical simulations $d_1/L_a = 0.01$ and $d_1/d_2 = 0.2$, and the separatrix is highlighted using a dashed black line. 125
- 5.3 Detrended bed elevation (i.e., bed elevation subtracting the initial bed elevation) as a function of space and time for two numerical simulations run under conditions in which the linear model predicts: (a) growth of perturbations, and (b) decay of perturbations. 127

- 5.4 Bed surface fraction content of tracer sediment 9.17 m downstream from the feeding location. The black dots are measured data (*Chavarrías et al.*, 2019a) and the lines are the results of numerical simulations. The dash-dotted, dashed, and continuous lines present the results using the active layer model (*Hirano*, 1971), and the SILKE model with and without diffusion, respectively. The different colors represent a different active layer thickness. 132
- 5.5 Tracer concentration (accounting for the sediment in the active layer and in transport) along a reach of the North Loup River (Nebraska, US) 287.4 h after placing the tracer sediment. Results are computed using: (a) the active layer model under unisize conditions, (b) the active layer model under mixed-size conditions, (c) the SILKE model under unisize conditions, and (d) the SILKE model under mixed-size conditions. The dots represent the measured data by *Sayre and Hubbell* (1965) (profile 12R). The black lines indicate the total tracer concentration which is the sum over all tracer size fractions (i.e., d_1 , d_2 , and d_3) in the mixed-size sediment simulations. 135
- 5.6 Tracer concentration (accounting for the sediment in the active layer and in transport) along a reach of the North Loup River (Nebraska, US) 117.7 h after placing the tracer sediment. Results are computed considering: no diffusion (dotted blue line), a realistic amount of diffusion ($0.0022 \text{ m}^2/\text{s}$) (dashed red line), 100 times the realistic amount of diffusion (dash-dotted yellow line), and 1000 times the realistic amount of diffusion (continuous purple line). The dots represent the measured data by *Sayre and Hubbell* (1965) (profile 6R). 136
- 5.7 Bed elevation as a function of time in Experiment I4 conducted by *Chavarrías et al.* (2019a): (a) measured, (b) predicted using the active layer model (*Hirano*, 1971), (c) predicted using the regularized active layer model (*Chavarrías et al.*, 2019a), and (d) predicted using the SILKE model. Dashed lines indicate the position of the patch of fine sediment. 139
- 5.8 Surface volume fraction content of coarse sediment as a function of time in Experiment I4 conducted by *Chavarrías et al.* (2019a). Measured data is shown using black dots, results using the active layer model are shown using a blue line, the regularized model using a green dashed line, and the SILKE model using a dashed-dotted red line. 140
- 5.9 Volume fraction content of fine, medium, and coarse grain size fractions in the transported sediment as a function of time in Experiment B2 conducted by *Blom et al.* (2003). 142

- A.1 Maximum flow depth h_{\max} (nondimensionalized by the normal flow depth h_n) that develops as a consequence of ellipticity. In (a) the maximum flow depth is plotted against the discriminant Δ_{als2} , Equation 2.26, for a thickness of the bookkeeping layers (Δz) equal to 0.01 m (red dots), 0.02 m (orange dots), 0.05 m (green dots), and 0.10 m (blue dots). The vertical black lines connect two simulations in which all parameters but Δz are the same. In (b) the maximum flow depth is plotted against the *hyperbolic flow depth* (h_{hyp}) nondimensionalized with the normal flow depth. Each black dot is the result of a simulation. The black lines connect simulations with the same physical parameters and the grey line shows the perfect agreement. In (c) the maximum flow depth is plotted against the distance from upstream at which the maximum flow depth occurs (x_{\max}) nondimensionalized with the length of the domain (L) for a horizontal discretization length equal to 0.1 m (orange dots) and 0.2 m (green dots). The black lines connect two simulations in which all parameters but Δx are the same. 222
- A.2 Parameter $\lambda_{s1} - \lambda_b$ with respect to $\frac{E_{s1}}{J_1} \lambda_{s1} - \lambda_b$ for 39.253.500 cases. The majority of cases fall into the domain in which we prove that an unsteady active layer thickness increases the likelihood of the model being elliptic. In the remaining cases an unsteady active layer thickness also increases the likelihood although we do not prove it. Nevertheless, only a small percentage of cases become elliptic strictly due to the unsteady active layer thickness. 226
- C.1 Elv flowchart. 250
- C.2 Measured sediment transport rate in the equilibrium experiments with coarse sediment (P1, red) and fine sediment (P2, blue): (a) time series, (b) probability density, and (c) cumulative probability. 253
- C.3 Measured bed elevation in the preparatory experiments with coarse sediment (P1, red) and fine sediment (P2, blue): (a) probability density and (b) cumulative probability. 254
- C.4 Surface fraction content of tracer sediment at $x = 9.17$ m: measured (black dots), and predicted values using an active layer thickness equal to 0.005 m, 0.010 m, and 0.020 m (lines). 254
- C.5 Surface fraction content of tracer sediment with time (a) at the center of the patch $x = 4.95$ m, and (b) downstream of the patch $x = 9.15$ m. 255
- C.6 Comparison between the measured (error bars) and predicted (lines) sediment transport rate using the closure relations by *Meyer-Peter and Müller* (1948) (MPM), *Fernandez-Luque and Van Beek* (1976) (FLvB), *Engelund and Hansen* (1967) (EH), *Ashida and Michiue* (1972), and *Wilcock and Crowe* (2003) (WC). The error bars are one standard deviation long in each direction. 256

- D.1 Tracer concentration measured *Sayre and Hubbell* (1965) for all profiles taken along the right-hand side of the river. See Table D.3 for the time after dosing at which each profile was taken. 269
- D.2 Sediment transport rate in the range of the tracer sediment predicted using the relations by *Meyer-Peter and Müller* (1948) with *Egiazaroff* (1965) to account for hiding (MPM), *Fernandez-Luque and Van Beek* (1976) with *Egiazaroff* (1965) to account for hiding (FLvB), *Engelund and Hansen* (1967) (EH), *Ashida and Michiue* (1971) (AM), and *Wilcock and Crowe* (2003) (WC). The value estimated by *Sayre and Hubbell* (1965) is shown in black. The vertical dashed lines indicate the value of the skin friction as predicted using the relations by *Haque and Mahmood* (1983) (HM), *Nikuradse* (1933) (N), *Smith and McLean* (1977) (SMcL), *Wright and Parker* (2004) (WP), and *Engelund and Hansen* (1967) (EH). 271

List of Tables

2.1	Values of parameters in Equation (2.6) according to several authors.	23
2.2	Values of the reference case. For these values the active layer thickness can be seen as representative of plane bed conditions ($L_a \approx 2.5D_{90}$) as well as bedform dominated conditions ($L_a \approx a_L b^{b_L}$).	29
2.3	Overview of the simulations. Only the parameters that are different between simulations are shown.	33
2.4	Domain definition, boundary conditions, and numerical parameters. The symbols not defined in the text are: reach length (L), channel width (B), simulation time (T), lowering rate of the downstream water level (low. rate), horizontal discretization length (Δx), and time step (Δt).	33
2.5	Values of the physical and numerical parameters varied in the sensitivity analysis.	35
3.1	Reference state.	56
3.2	Cases of a stable well-posed model (I1), an unstable well-posed model (B1), and an ill-posed model (I2). Case I2 has the same parameter values as Case I1 but for the mean flow velocity which is equal to 6.30 m/s.	57
3.3	Cases showing the effect of grid cell size on the numerical solution of well-posed and ill-posed models.	59
3.4	Variations to the reference state (table 3.1) and results of the linear analysis with respect to secondary flow.	63
3.5	Variations to the reference state (table 3.1) and results of the linear analysis with respect to the effect of the bed slope on the sediment transport direction. EH and AM refer to the sediment transport relations by <i>Engelund and Hansen</i> (1967) and <i>Ashida and Michiue</i> (1971), respectively.	65
4.1	Reference values in the comparison of the value of α_c computed analytically and numerically.	88
4.2	Length (L_p) and position (initial x_{p0} and final x_{pf} coordinates) of the patch of fine sediment below the coarse bed surface.	92
4.3	Experimental conditions, where q denotes water discharge per unit width, s_0 initial bed slope, q_{b0} sediment feed rate per unit width, h flow depth, u mean flow velocity, and Fr is the Froude number.	93
5.1	Reference parameters for studying the domain in which perturbations grow or decay.	125
C.1	Preparatory experiments.	251

C.2	Mean parameters of Experiments P1 and P2.	252
D.1	Main parameters of the experiment conducted by <i>Chavarrías et al.</i> (2019a) of unisize tracer propagation under equilibrium conditions. Parameter q_{b0} is the sediment feed rate.	268
D.2	Main parameters of the field campaign conducted by <i>Sayre and Hubbell</i> (1965). The skin friction coefficient is derived using the predictor by <i>Engelund and Hansen</i> (1967).	268
D.3	Time after dosing at which concentrations where measured.	270
D.4	Main parameters of the experiment conducted by <i>Blom et al.</i> (2003). The symbols not defined previously are the mean dune height (H), and the fraction of the sediment transport rate of size fraction k (F_{bk}). We derive the skin friction coefficient by correcting the total friction reported by <i>Blom</i> (2008) for (1) flume wall friction using the method by <i>Johnson</i> (1942) (see e.g. <i>Guo</i> (2015)), and (2) form drag using the method by <i>Smith and McLean</i> (1977). The values for the volume fraction content of sediment in the active layer are derived integrating the measured vertical grain size distribution profiles. The subscripts 1 and 2 correspond to the fine and medium size fractions, respectively.	272

About the author

Víctor Chavarrías Borràs was born in Barcelona, Spain, on 22 March 1989. From 1993 to 2005 he attended Arrels school in Barcelona. The following two years he studied at Maristes La Immaculada (Barcelona), obtaining his baccalaureate in 2007. In that same year he started studying Civil Engineering (Ingeniería de Caminos, Canales y Puertos) at the Polytechnic University of Catalonia (UPC) in Barcelona. As an exchange student in the Delft University of Technology (TU Delft) in Delft, the Netherlands, he specialized in river engineering and conducted his MSc thesis (*tesina*) on the dynamics of mixed-size sediment on steep deltas. For one year he continued the research of his MSc thesis as an exchange researcher at TU Delft while conducting the Final Project to obtain the engineering degree. He spent a month in the University of South Carolina in Columbia, United States. After graduating in 2014, he started his Ph.D. research at TU Delft.



List of Publications

Journal Articles

First Author

- Chavarrías, V., L. Arkesteijn, and A. Blom (2019), A well-posed alternative to the Hirano active layer model for rivers with mixed-size sediment, *J. Geophys. Res., Earth Surface*, (in press).
- Chavarrías, V., R. Schielen, W. Ottevanger, and A. Blom, (2019), Ill posedness in modelling two-dimensional morphodynamic problems: Effects of bed slope and secondary flow, *J. Fluid Mech.*, 868, 461–500, doi:10.1017/jfm.2019.166.
- Chavarrías, V., G. Stecca, A. Siviglia, and A. Blom (2019), A regularization strategy for modeling mixed-sediment river morphodynamics, *Adv. Water Resour.*, 127, 291–309, doi:10.1016/j.advwatres.2019.04.001.
- Chavarrías, V., G. Stecca, and A. Blom (2018), Ill-posedness in modelling mixed-sediment river morphodynamics, *Adv. Water Resour.*, 114, 219–235, doi:10.1016/j.advwatres.2018.02.011.
- Chavarrías, V., A. Blom, C. Orrú, J. P. Martín Vide, and E. Viparelli, (2018), A sand-gravel Gilbert delta subject to base level change, *J. Geophys. Res., Earth Surface*, 123(5), 1160–1179, doi:10.1029/2017JF004428.

Co-author

- Arkesteijn, L., A. Blom, M. J. Czapiga, V. Chavarrías, and R. J. Labeur (2019), The quasi-equilibrium longitudinal profile in backwater reaches of the engineered alluvial river: A space-marching method, *J. Geophys. Res., Earth Surface*, (in press).
- Blom, A., V. Chavarrías, R. I. Ferguson, and E. Viparelli (2017), Advance, retreat, and halt of abrupt gravel-sand transitions in alluvial rivers, *Geophys. Res. Lett.*, 44(19), 9751–9760, doi:10.1002/2017GL074231.
- Blom, A., L. Arkesteijn, V. Chavarrías, and E. Viparelli (2017), The equilibrium alluvial river under variable flow and its channel-forming discharge, *J. Geophys. Res., Earth Surface*, 122(10), 1924–1948, doi:10.1002/2017JF004213.
- Blom, A., E. Viparelli, and V. Chavarrías (2016), The graded alluvial river: Profile concavity and downstream fining, *Geophys. Res. Lett.*, 43(12), 6285–6293, doi:10.1002/2016GL068898.

- Orrú, C., A. Blom, V. Chavarrías, V. Ferrara, and G. Stecca (2016), A new technique for measuring the bed surface texture during flow and application to a degradational sand-gravel laboratory experiment, *Water Resour. Res.*, 52, 7005–7022, doi:10.1002/2016WR018938.
- Orrú, C., V. Chavarrías, W. S. J. Uijtewaal, and A. Blom (2014), Image analysis for measuring the size stratification in sand-gravel laboratory experiments, *Earth Surf. Dyn.*, 2(1), 217–232, doi:10.5194/esurf-2-217-2014.

Conference Proceedings

First Author

- Chavarrías, V. and A. Blom (2019), Modelling degradational rivers, in *Proceedings of the NCR days, 31 January–1 February, Delft, the Netherlands*, edited by E. Stouthamer, H. Middelkoop, M. Kleinhans, M. van der Perk, and M. Straatsma, 43-2019, pp. 40–41, Netherlands Center for River studies.
- Chavarrías, V., G. Stecca, R. J. Labeur, and A. Blom (2018), A well-posed model for mixed-sediment river morphodynamics, in *River Flow, Proceedings of the 9th International Conference on Fluvial Hydraulics, 5–8 September, Lyon-Villeurbanne, France*, edited by A. Paquier and N. Rivière, 05060, EDP Sciences, doi:10.1051/e3sconf/20184005060.
- Chavarrías, V., W. Ottevanger, R. Schielen, and A. Blom (2018), Secondary flow and bed slope effects contributing to ill-posedness in river modelling, in *Proceedings of the NCR days, Delft, 8–9 February, the Netherlands*, edited by Y. H. K. D. Berends, I. Niesten, and E. Mosselman, 42-2018, pp. 84–85, Netherlands Center for River studies.
- Chavarrías, V., G. Stecca, R. J. Labeur, and A. Blom (2017), A strategy to avoid ill-posedness in mixed sediment morphodynamics, in *Proceedings of the 10th Symposium on River, Coastal and Estuarine Morphodynamics, 15–22 September, Trento-Padova, Italy*, edited by S. Lanzoni, M. Redolfi, and G. Zolezzi, p. 166.
- Chavarrías, V., W. Ottevanger, R. J. Labeur, and A. Blom (2017), Ill-posedness in modelling 2D river morphodynamics., in *Proceedings of the NCR days, 1–3 February, Wageningen, the Netherlands*, edited by A. J. F. Hoitink, T. V. de Ruijsscher, T. J. Geertsema, B. Makaske, J. Wallinga, J. H. J. Candel, and J. Poelman, 41-2017, pp. 74–76, Netherlands Center for River studies.
- Chavarrías, V., A. Blom, and G. Stecca (2016), Ill-posedness of the Saint-Venant-Hirano model, in *Proceedings of the 31st IUGG Conference on Mathematical Geophysics, 6–10 June, Paris, France*, p. 56.
- Chavarrías, V., G. Stecca, A. Siviglia, and A. Blom (2015), Ellipticity of the Saint-Venant-Hirano model for mixed-sediment river morphodynamics, in *Proceedings of the 9th Symposium on River, Coastal, and Estuarine Morphodynamics, 30 August–3 September, Iquitos, Perú*.

- Chavarrías, V., G. Stecca, A. Siviglia, R. J. Labeur, and A. Blom (2015), Limitations when modelling mixed-sediment river morphodynamics, in *Proceedings of the NCR days, 1–2 October, Nijmegen, the Netherlands*, edited by H. J. R. Lenders, F. P. L. Collas, G. W. Geerling, and R. S. E. W. Leuven, 39-2015, pp. 97–100, Netherlands Center for River studies.
- Chavarrías, V., E. Viparelli, and A. Blom (2014), Size stratification in a laboratory Gilbert delta due to a varying base level: Measurement, and numerical modelling., *Abstract EP53C-3669 presented at the 47th Fall Meeting of the AGU, 15–19 December, San Francisco, CA, United States*.
- Chavarrías, V., C. Orrú, E. Viparelli, J. P. Martín-Vide, and A. Blom (2014), Size stratification in a Gilbert delta due to a varying base level: flume experiments, in *Abstract 15595 presented at the EGU General Assembly, 27 April–2 May, Vienna, Austria*.
- Chavarrías, V., G. Stecca, E. Viparelli, and A. Blom (2014), Ellipticity in modelling mixed sediment river morphodynamics, in *Proceedings of the NCR days, 2–3 October, Enschede, the Netherlands*, edited by D. C. M. Augustijn and J. J. Warmink, 38-2014, pp. 25–26, Netherlands Centre for River studies.
- Chavarrías, V., A. Blom, C. Orrú, and E. Viparelli (2013), Laboratory experiment of a mixed-sediment gilbert delta under varying base level, in *Proceedings of the 8th Symposium on River, Coastal and Estuarine Morphodynamics, 9–13 June, Santander, Spain*, edited by G. Coco, B. Blanco, M. Olabarrieta, and R. Tinoco, p. 114, Universidad de Cantabria, Santander, Spain.
- Chavarrías, V., A. Blom, C. Orrú, E. Viparelli, and J. P. Martín-Vide (2013), Stream-wise variation in stratigraphy in a laboratory Gilbert delta in response to a varying base level, in *Proceedings of the NCR days, 3–4 October, Delft, the Netherlands*, edited by A. Crosato, 37-2013, pp. 3-5–3-6, Netherlands Center for River studies.

Co-author

- Blom, A., V. Chavarrías, and E. Viparelli (2017), The dynamics of a gravel-sand transition, in *Proceedings of the 10th Symposium on River, Coastal and Estuarine Morphodynamics, 15–22 September, Trento-Padova, Italy*, edited by S. Lanzoni, M. Redolfi, and G. Zolezzi, p. 158.
- Blom, A., L. Arkesteijn, V. Chavarrías, and E. Viparelli (2017), Response of the alluvial river through adjustment of the slope, surface texture, and width, *Abstract EP31E-06 presented at the 50th Fall Meeting of the AGU, 11–15 December, San Francisco, CA, United States*.
- Blom, A., E. Viparelli, and V. Chavarrías (2016), Equilibrium, quasi-equilibrium, and transient river longitudinal profiles, in *Proceedings of the 31st IUGG Conference on Mathematical Geophysics, 6–10 June, Paris, France*, p. 52.

- Blom, A., E. Viparelli, and V. Chavarrías (2015), Gravel wedge progradation in sand-gravel laboratory experiments: New insights on the gravel-sand transition, *Abstract EP13C-03 presented at the 48th Fall Meeting of the AGU, 14–18 December, San Francisco, CA, United States.*
- Blom, A., E. Viparelli, and V. Chavarrías (2015), The role of size-selective transport and abrasion in river profile concavity and downstream fining under alluvial and equilibrium conditions, *Abstract presented at the 8th Conference on Gravel Bed Rivers, 13–18 September, Kyoto-Takayama, Japan.*
- Blom, A., and V. Chavarrías (2014), An analytical solution to river profile concavity and downstream fining, *Abstract EP53C-3670 presented at the 47th Fall Meeting of the AGU, 15–19 December, San Francisco, CA, United States.*
- Orrú, C., V. Chavarrías, V. Ferrara, and A. Blom (2014), A laboratory experiment on the evolution of a sand-gravel reach under a lack of sediment supply, *Abstract EP52A-05 presented at the 47th Fall Meeting of the AGU, 15–19 December, San Francisco, CA, United States.*

Scientific Reports

- Chavarrías, V., W. Ottevanger, R. Schielen, and A. Blom (2018), Ill-posedness in 2D mixed sediment river morphodynamics, *Tech. Rep. RWS 4500268550, TUD 17363, Delft University of Technology, Delft, the Netherlands.*
- Chavarrías V., Ottevanger, W. (2016), Mathematical analysis of the well-posedness of the Hirano active layer concept in 2D models, *Tech. Rep. 1230044-000-ZWS-0035 Deltares, Delft, the Netherlands.*